EPIGENETIC MECHANISMS OF EU- AND HETEROCHROMATIN POSITIONING IN INTERPHASE NUCLEI

CONGDI SONG

MÜNCHEN 2015

EPIGENETIC MECHANISMS OF EU- AND HETEROCHROMATIN POSITIONING IN INTERPHASE NUCLEI

CONGDI SONG

an der Fakultät für Biologie
der Ludwig-Maximilians-Universität
München

vorgelegt von
Congdi Song
aus Hebei, China

München, den 22.07.2015

Erstgutachter: Prof. Dr. Heinrich Leonhardt

Zweitgutachter: Prof. Dr. Rainer Uhl

Tag der Abgabe: 22.07.2015

Tag der mündlichen Prüfung: 03.09.2015

Contents

Abstract

The spatial organization of the genome plays an important role in the regulation of nuclear functions, including transcriptional control. The two major classes of chromatin, transcriptionally active euchromatin and transcriptionally silent heterochromatin, have distinct spatial segregation in the nucleus. In conventional nuclei, heterochromatin underlies the nuclear envelope and abuts nucleolar periphery, whereas euchromatin localizes to the nuclear interior. Such chromatin arrangement is nearly universal among eukaryotes. The only known exception is found in rod photoreceptor cells of nocturnal mammals where, for optical reasons, eu- and heterochromatin invert their positions: heterochromatin is accumulated in the nuclear center and euchromatin forms a thin peripheral shell. Thus, rod nuclei have an inverted organization in comparison to the conventional nuclei. Recently, two mechanisms for tethering peripheral heterochromatin to the nuclear envelope, a lamin A/C-dependent (A-type) and LBR-dependent (B-type), were identified. In particular, it was shown that absence of both of them lead to the nuclear inversion. Still, our knowledge about the mechanisms of chromatin classes positioning in both conventional and inverted nuclei is very limited. In the present work I attempted to elucidate these mechanisms further.

First, I analyzed the distribution of epigenetic marks characteristic of eu- and heterochromatin as well as several chromatin associated proteins which might be involved in establishing the nuclear inversion in rods. For this purpose I used extensive immunoassays of mouse retina cryosections. I found that the major chromatin classes in both inverted and conventional nuclei possess the same histone modifications and that inversion in rod nuclei, as well as maintenance of peripheral heterochromatin in conventional nuclei, are not affected by a loss of the major silencing histone modifications, such as H3K9me2,3 and H4K20me2,3. My results show that conventional nuclear organization relies on strong redundancy of the epigenetic code and code writers, whereas nuclear inversion relies on the absence of specific code readers, A- and B-type heterochromatin tethers.

Second, I analyzed the functional distribution of the chromatin regulating protein, Methyl-CpG binding protein 2 (MECP2), in retina and other mouse tissues. I found that MECP2 is expressed at very high levels in all retinal neurons except in rods, and it is also present in almost all non-neural cell types, with the exception intestinal epithelial cells, erythropoietic cells, and hair matrix keratinocytes. I demonstrated that MECP2 is a marker of the differentiated state. In particular, I showed that the onset of its expression during retina development coincides with massive synapse formation. Surprisingly, I found that overall development of retina as well as the nuclear architecture and

distribution of major histone modifications were unaffected in MECP2-null mice. I also did not find a compensatory expression of other methyl-CpG binding proteins in cultured cells and various tissues upon MECP2 deletion.

Third, I sought to identify an interacting partner of lamins A/C in the A-type tether of the peripheral heterochromatin in mammalian cells. For this purpose, I screened wild type mouse tissues with antibodies against several inner nuclear envelope transmembrane proteins (INM proteins) and obtained a cell-type specific signature of the INM proteins expression for nearly twenty cell types in WT and Lmna-KO mice. I found that the two most prominent candidates were LEM-domain proteins LEM2 and emerin. To test their functional role in the A-type tether, I aimed at ectopic expression of both proteins together with lamin C in mouse rod cells. To this end, I have cloned these proteins and prepared vectors containing either single proteins or their combination with lamin C (LEM2 & lamin C; emerin & lamin C) under the rod-specific Nrl promoter. Conventional nuclear architecture of rod cells upon transgenic expression of one of the vectors would indicate a role of these INM proteins in the coordination of A-type lamins to maintain the peripheral heterochromatin. This study is still in progress.

1 Introduction

1.1 Epigenetic factors: chromatin level

Epigenetics refers to the heritable processes regulating gene expression without alteration of gene sequences, mainly achieved by chemical modifications. It involves several mechanisms, such as DNA methylation, post-translational histone modifications (PTMs), as well as RNA-based mechanisms. The control of eukaryotic gene expression is achieved by a complex regulatory network from three hierarchical levels: DNA sequence, chromatin structure and nuclear organization (Misteli, 2007; van Driel et al., 2003).

1.1.1 DNA methylation

In mammals DNA methylation occurs exclusively at the C5 position of cytosine residues as 5-methylcytosine (5mC) in the context of CpG dinucleotides. It is involved in normal mammalian genomic imprinting, X-chromosome inactivation and lineage-specific gene expression regulation (Bernstein et al., 2007; Illingworth and Bird, 2009; Li, 2002). DNA methylation of promoter regions causes a strong and heritable transcriptional inhibition of the corresponding genes (Bird, 2002). So far two modes of repression have been proposed. First, the methyl group can directly interfere with the transcription factor to bind their target sites (Becker et al., 1987). Second, the binding of the methyl-CpG binding proteins (MBPs) recruit repressive chromatin modifiers. However, DNA methylation occurring at gene bodies was positively correlated with transcription (Hellman and Chess, 2007; Rauch et al., 2009). The active X chromosome displays more than two times as much allele-specific methylation as inactive X chromsome, and the methylation is concentrated at gene bodies (Hellman and Chess, 2007).

DNA methylation marks are established and maintained by the DNA methyltransferases (DNMTs), which contain a highly conserved C-terminal catalytic domain, while the N-terminal regulatory domain shows striking differences. The de novo DNMTs, DNMT3a and DNMT3b, together with their catalytically inactive cofactor DNMT3L, are responsible for the establishment of methylation mark during differentiation (Jia et al., 2007; Okano et al., 1999; Okano et al., 1998). The obtained marks are maintained by maintenance methyltransferase DNMT1 through the cell cycle (Bacolla et al., 2001; Bacolla et al., 1999; Bestor et al., 1988; Pradhan et al., 1999). The occurred DNA methylation sites can be recognized by MBPs, including the methyl-CpG binding domain (MBD) family (Hendrich and Bird, 1998; Saito et al., 2002), the Kaiso protein family (Filion et al., 2006; Prokhortchouk et al., 2001) and the

ubiquitin-like plant homeodomain and RING finger domain-containing (UHRF) protein family (Unoki et al., 2004).

DNA methylation could be reversely removed by the ten-eleven translocation (TET) protein family, including TET1, TET2 and TET3. All members of the TET family contain a C-terminal 2-oxoglutarate (2OG) - and Fe (II)-dependent dioxygenase domain (DSBH), catalyzing the conversion of 5mC into 5 hydroxymethylcytosine (5hmC) in vitro and in vivo. 5hmC could be further oxidized to 5-formylcytosine (5fC) and 5-carboxylcytosine (5caC) (Ito et al., 2010; Kriaucionis and Heintz, 2009; Maiti and Drohat, 2011; Tahiliani et al., 2009). The products hmC, fC, caC could be subsequently removed by TDG or NEIL glycosylase and the BER pathway (Muller et al., 2014).

1.1.2 Histone modifications

Nucleosome builds up the fundamental unit of chromatin, which consists of an octamer of core histones, two copies of H3-H4 and H2A-H2B dimers, wrapped by 147 bp of DNA. The structure of histones is similar, each consisting of a globular, hydrophobic internal region and a highly conserved N-terminal histone tail, which extends beyond the nucleosome and where the post-translational modifications occur. These residues can be modified by different enzymes that can "write" or "erase" the modifications. Lysine residues can be acetylated or deacetylated, methylated or demethylated, or coupled to ubiquitin; arginine residues can be methylated or demethylated; and serine or threonine residues can be phosphorylated (Kouzarides, 2007; Peterson and Laniel, 2004).

Table 1. Activating and repressive histone posttranslational modifications.

Modification	Role in transcription	Modification site	
Acetylation	Activation	H2B	K6,K7,K16,K17*
		H3	K9, K14, K18, K56*
		H4	K5,K8,K12,K16*
Methylation	Activation	H3	K4me2, K4me3, K36me3, K79me2* K4me1, K79me1, K79me3, K9me1, K27me1**
		H4	K20me1**
Methylation	Repression	H3	K9me3, K27me3***
		H4	K20me3***

* Strahl and Allis, 2000; ** Balazs, 2011; *** Joshua C. Black 2012.

Histone PTMs "tailor" the degree of chromatin fibers compaction: the chromatin fibers tend to be less compact during transcription and replication. Correspondingly, PTMs, such

as acetylation occurs to "unravel" chromatin since it neutralizes the basic charge of lysine residues, decreasing the affinity for DNA. The chromatin fibers are more compact in transcriptionally silent regions and during mitosis (Schneider and Grosschedl, 2007). From the perspective of euchromatin and heterochromatin establishment and maintenance, lysine acetylation and methylation of H3K4 or H3K36 always correlates with transcriptionally active euchromatin (Berger, 2007). High level of H3K27me3 is the characteristic of the facultative heterochromatin (Cao et al., 2002). Strong enrichment of H3K9me3, H4K20me3 and H3K64me3 is associated with the constitutive heterochromatin (Daujat et al., 2009; Peters et al., 2002; Schotta et al., 2004) (Table 1). In particular, distinct chromatin marks are observed in pericentric heterochromatin, including DNA methylation, histone hypoacetylation, repressive histone modifications, such as H3K9 methylation, which contains a binding sites for the Heterochromatin protein 1 (HP1) family (Almouzni and Probst, 2011).

1.1.3 Chromatin binding proteins

The histone PTM marks and methylated CpG dinucleotide recruits non-histone proteins to chromatin, which mediates the downstream effects on chromatin compaction, e.g., H3K9me2/3 and methylated CpG recruits HP1/CBX1 (Kutateladze, 2011) and MECP2 (Brero et al., 2005), respectively. Spreading of heterochromatin features was shown to exploit a self-sustaining loop mechanism in which HP1 self-associates and interacts with the H3K9 HMTase, Suv39 h1/2, to add more H3K9me (Aagaard et al., 1999; Maison and Almouzni, 2004). HP1 also has the capacity to recruit de novo methyltransferase and directs DNA methylation to major satellite repeats at pericentric heterochromatin (Lehnertz et al., 2003).

MECP2 was firstly identified as a protein that binds specifically to methylated DNA (Lewis et al., 1992). Mutations of the MECP2 gene were found to be the cause of an autism spectrum disorder, Rett syndrome (Wan et al., 1999). MECP2 is characterized by a methyl binding domain (MBD) and a transcription repression domain (TRD). The unstructured aminoacidic sequence linking MBD and TRD domains is responsible for the interaction of MECP2 with LBR. The formation of the MECP2-LBR protein complex might partly explain the link of peripheral heterochromatin to inner membrane (Guarda et al., 2009). Moreover, by interacting with Sin3A and recruiting histone deacetylases, MECP2 represses transcription and thereby stabilizes and consolidates the heterochromatic state of DNA (Bird and Wolffe, 1999; Leonhardt and Cardoso, 2000). MECP2 has also been shown to be particularly concentrated at the pericentromeric heterochromatin (Lewis et al., 1992).

1.2 Epigenetic factors: genome packaging into the nucleus

Based on the results from extensive studies using microscopic approaches, and more recently molecular based methods, a detailed view of three-dimensional (3D) arrangement of chromosomes inside interphase nucleus emerged (Bickmore, 2013; Bickmore and van Steensel, 2013; Cook, 2010; Cremer and Cremer, 2001; Cremer and Cremer, 2010; Dekker et al., 2013; Gibcus and Dekker, 2013; Gilbert et al., 2005; Misteli, 2007).

1.2.1 Chromosome territories and their arrangement in the nucleus

Chromosomes occupy distinct territories (Chromosome Territories; CTs) in the interphase nucleus (Cremer and Cremer, 2010). The visualization of microirradiated DNA by 3H-thymidine incorporation (Cremer et al., 1982) or immunostaining with antibodies against UV-damaged DNA (Raith et al., 1984) provided the first indirect evidence of the existence of CTs. The direct visualization of individual CTs was enabled by in situ hybridization techniques in the mid 1980s (Manuelidis, 1985; Schardin et al., 1985). Fluorescence In Situ Hybridization (FISH) experiments revealed the nonrandom distribution of chromosomes depending on their size and gene density: large and gene-poor chromosomes tend to be located near the nuclear periphery, whereas small and gene-rich chromosomes are located more internally (Bolzer et al., 2005; Boyle et al., 2001; Cremer et al., 2003; Cremer and Cremer, 2001; Croft et al., 1999; Kreth et al., 2004) (Figure 1B)..
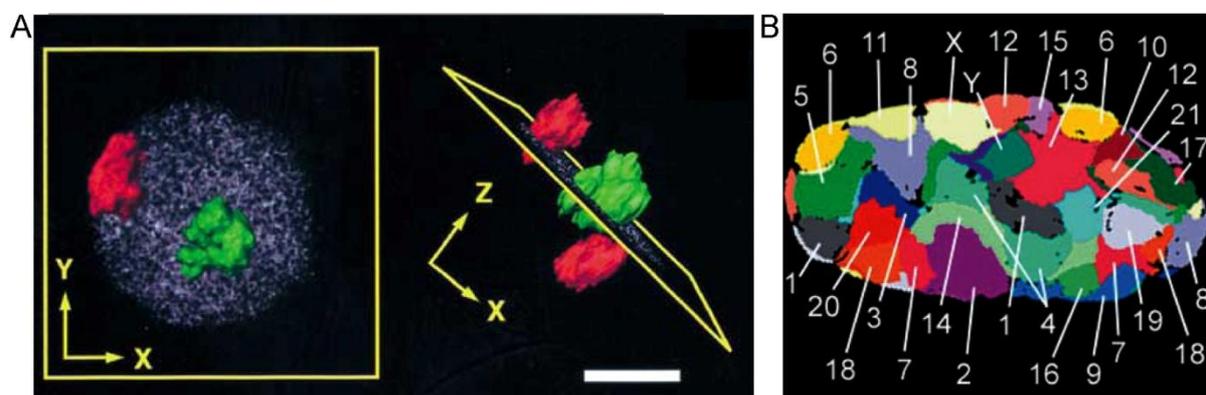

Figure 1. Chromosome territories revealed by two (A) and 24-color (B) FISH. A, 3D reconstruction of chromosome 18 (red) and 19 (green) territories after FISH with respective chromosome paints in the nucleus of G0 human lymphocytes. Chromosome 19 is located closer to the center of the nucleus, whereas chromosome 18 is preferentially located closer to the nuclear envelope, according to their gene-density. The mid-plane section of the nucleus is shown in magenta. Scale bar: 5 μm (adapted from Cremer & Cremer, 2001). B, False-colored chromosome territories in human G0 fibroblast nucleus (46, XY). Each chromosome paint was labeled with a different set of fluorochromes by combinatorial labeling which secured correct identification and classification of chromosomes using goldFISH software. The distribution of chromosomes is not random: large and gene-poor chromosomes tend to be located near the nuclear periphery, whereas the small and gene-rich chromosomes are located more internally (Adapted from Bolzer, 2005; Speicher and Carter, 2005).

Early evidence was based on the FISH studies on human chromosome 19 and 18, with the highest and lowest gene density, respectively. The chromosome 19 was found to be consistently localized in the interior of nuclei, not only in human lymphocyte, but also in other cell types. In contrast, chromosome 18 was found at the nuclear periphery (Cremer et al., 2003; Cremer and Cremer, 2001; Croft et al., 1999) (Figure 1A). Similar gene density correlated radial arrangements in the nuclei were shown for all human chromosomes (Boyle et al., 2001; Kreth et al., 2004)

The limitations of microscopic studies, which include the fluorescence sensitivity and the spatial resolution, make it difficult to obtain a comprehensive analysis of the three dimension (3D) folding of the genome, or to determine an entire chromosome organization at kilobase resolution. For example, with the standard fluorescence microscopy system the diffraction-limited spatial resolution is at the classic Abbé limit of ~0.2 µm. Recently, few new microscopic techniques were employed to increase the resolution, such as the application of three-dimensional structured illumination microscopy (3D-SIM) (Carlton, 2008; Schermelleh et al., 2008).

In the last decade, the development of Chromosome Conformation Capture (3C) technology, combined with computer simulations, has revolutionized the analysis of genome organization within the nucleus (Bau and Marti-Renom, 2011; Bohn and Heermann, 2010; Dekker et al., 2002; Fudenberg and Mirny, 2012; Hakim and Misteli, 2012; van Steensel and Dekker, 2010). Hi-C method, one of the modified 3C techniques, confirmed territorial organization of the interphase chromosome shown previously by FISH and microscopic studies. The average intrachromosomal contact probability, even at distances greater than 200 Mb, is always much higher than the contact probabilities between different chromosomes (interchromosomal contacts) (Figure 2A). Moreover, ratio of observed/expected interchromosomal contact probabilities shows that small, gene-rich chromosomes, including chromosomes 16, 17, 19, 20, 21, 22, preferentially interact with each other (Lieberman-Aiden et al., 2009) (Figure 2B).

The recent Hi-C studies have shown that chromosomes are composed of smaller domains, referred to as Topologically Associated Domains (TADs) (Figure 4B). TADs are contiguous chromosomal regions where the genomic interactions are strong within the regions but are sharply depleted on the boundaries. TADs comprise from several hundreds kb up to 1-2 Mb (Dixon et al., 2012; Nora et al., 2012; Sexton et al., 2012). Studies from multiple cell lines have revealed that TADs are to a large extent tissue invariant, leading to the proposal that TADs are fundamental architectural building blocks of chromosomes (Dekker et al., 2013; Gibcus and Dekker, 2013; Nora et al., 2013). Earlier microscopic studies identified so called chromosomal domains (or 1Mb replication domains), structurally defined chromatin entities of several hundred kb in size (the same length scale as TADs),

moving as a unit and persisting over at least several cell cycles (Cremer and Cremer, 2001; Markaki et al., 2010). It is tempting to speculate that chromosomal domains and TADs are the same entities, although direct proof for this is still lacking (Dekker, 2014).
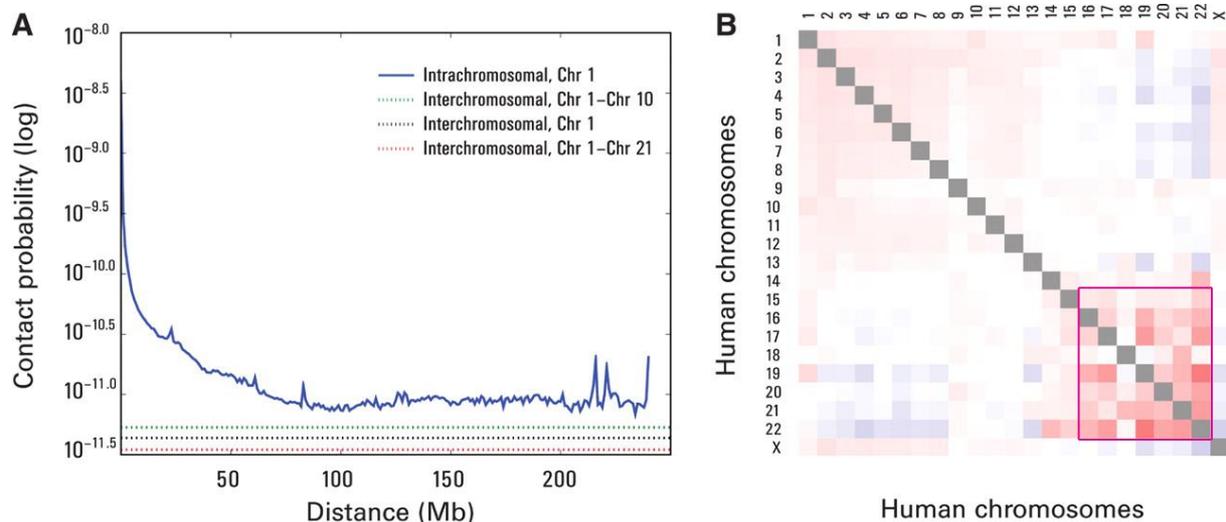

Figure 2. Chromosome territories (A) and their intranuclear distribution (B) revealed by Hi-C. A, Frequencies of interchromosomal interactions are significantly higher in comparison to intra-chromosomal interactions: loci within chromosome 1 homologue interact more frequently with each other (blue solid line) than with loci of another homologue of chromosome 1 (black dash line) or with loci on other chromosomes 10 or 21 (green and red dash lines, respectively). B, Observed/expected number of interchromosomal contacts between all pairs of human chromosomes in lymphoblastoid cells. The number ranges from 0.5 to 2, blue and red indicate depletion and enrichment, respectively. Small, gene-rich chromosomes tend to interact more frequently with each other than large gene-poor chromosomes, with exception to small but gene-poor chromosome 18. Both figures adapted from Erez Lieberman-Aiden et al (2009).

1.2.2 Chromosome territory dynamics

The CTs undergoes dynamic changes to meet the needs of development, differentiation, proliferation, or disease status. In addition to the relocation of individual region of chromosomes, repositioning of whole chromosome territory has also been observed during differentiation of the following cell types: ES cells (Dixon et al., 2015), T-cells (Kim et al., 2004), myoblasts (Gianakopoulos et al., 2011) and adipocytes (Kuroda et al., 2004). The nuclear architecture changes are observed during early development of different mammalian species, such as mouse, rabbit and cow (Koehler et al., 2010).

The global arrangement of CTs plays an important role in the regulation of nuclear functions, especially the transcriptional activities of genes within (Deng and Blobel, 2014). The genome-wide transcriptome is affected when CTs are repositioned via chromosome translocation (Harewood et al., 2010). Also, FISH assays demonstrated that a number of genes relocate away from the nuclear periphery upon transcriptional activation and towards the nuclear periphery upon transcriptional silencing (Kosak et al., 2002; Takizawa et al.,

2008; Williams et al., 2006). Such as, during thymocytes maturation the Dntt gene becomes silenced and relocates to loci of pericentromeric heterochromatin (Su et al., 2004). Notably, the proximity to the nuclear lamina is not sufficient to cause the transcriptional repression. Artificially targeting of chromatin to nuclear lamina cause either silencing or maintenance of the normal expression level (Finlan et al., 2008; Kumaran et al., 2008; Reddy et al., 2008). The effect of proximity to nuclear lamina on gene silencing might depend on the nature of the genes, their transcriptional status in the studied cell types, and the 3D structure of the chromosome regions flanking the genes in question (reviewed in (Joffe et al., 2010)).

1.2.3 Segregation of euchromatin and heterochromatin in the nucleus

Chromatin is traditionally classified to euchromatin and heterochromatin based on the differential compaction and spatial arrangement during interphase (Heitz, 1928). Euchromatin occupies the internal nuclear regions whereas heterochromatin is distributed along the nuclear envelope and around the nucleoli (for detailed information see 2.4) (Figure 3A). Euchromatin is decondensed, more accessible, characterized by gene richness and active transcription. In general, euchromatin replicates early in S-phase and is associated with the active epigenetic marks, such as histone acetylation, H3K4 methylation and H3K36 methylation. By contrast, heterochromatin is condensed, gene poor and predominately silent. Heterochromatin replicates late in S-phase (Dillon and Festenstein, 2002) (Figure 3B). In mammals, heterochromatin is characterized by high levels of H3K9me2/3, H4K20me2/3, deacetylated histone H4 and DNA methylation (Misteli, 2007).
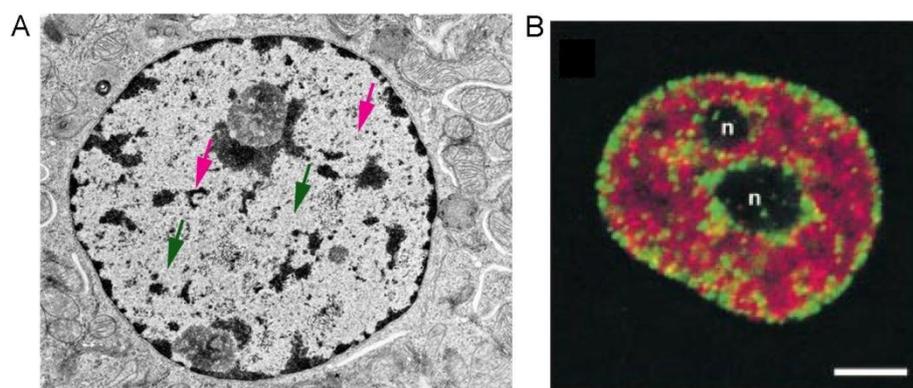
Figure 3. Segregation of euchromatin and heterochromatin in the nucleus observed on ultrastructural level (A) and after replication labeling (B). A, Transmission electron microscopy images of nucleus after standard contrasting procedure using uranyl acetate and lead citrate highlighting DNA and proteins. Heterochromatin lines the nuclear envelope and the nucleolus (magenta arrows), whereas euchromatin is distributed in the nuclear interior (green arrows). B, Sites of DNA replication in early (Cy3-dUTP, green) versus mid-late (Cy5-dUTP, red) S phase revealed by a "pulse-chase-pulse" experiment in mouse SH-EP N14 cells. Note that DNA replication during late S-phase takes place preferentially at the nuclear periphery and nucleolar periphery, whereas during

early S phase, it takes place in the interior of the nucleus with exception of the nucleoli (n). Scale bar: 5 µm (adapted from Schermelleh, 2001).

The compartmentalization of eu- and heterochromatin can be detected at a higher resolution and genome-wide scale with 3C-based methods. Based on the plaid pattern of the matrix obtained from Hi-C, each chromosome is divided into compartment A and B (Figure 4A). Greater interaction is found within each kind of compartment rather than between them (Dixon et al., 2012). When comparing the data obtained from Hi-C to known epigenetic features, compartment A correlates strongly with high gene densities, high expression, open state chromatin (positive correlation with H3K36me3 and strongly attenuated correlation with H3K27me3). The characteristics of A compartment identify it as euchromatin. The loci within compartment B exhibit stronger trend for interaction, which suggests that compartment B is packed more densely, indicating its heterochromatic nature (Lieberman-Aiden et al., 2009). Moreover, Rao and his collaborators zoomed in to the compartments (at higher resolution of 25 kb) and divided compartment A and B into two (A1 and A2) and four (B1, B2, B3 and B4) subcompartments, respectively, based on the high resolution Hi-C long-range contact patterns (Rao et al., 2014).
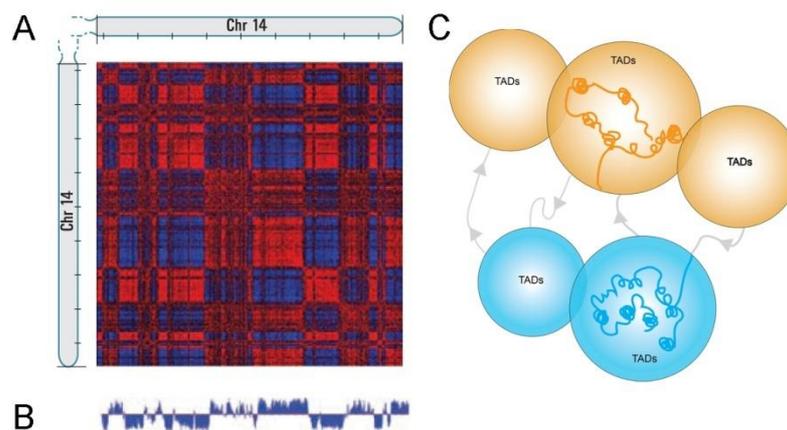
Figure 4. Segregation of euchromatin and heterochromatin in the nucleus observed by Hi-C. A, Matrix of intrachromosomal contact frequencies of human chromosome 14 after normalization and Pearson correlation. The plaid pattern indicates the presence of two compartments within the chromosome. B, PCA analysis to the matrix identifies A (red) and B (blue) compartments with more open and more close conformation, respectively. There are strong interactions within each compartment and weak interactions between A and B compartments. C, Schematics show that TADs, smaller structural units of chromosomes, belong to either A or B compartments (modified from Erez Lieberman-Aiden et al, 2009).

Compartmentalization of active (A) and inactive (B) chromatin domains is likely driven in part by the interaction of two domains with specific subnuclear structures. For instance, inactive chromatin domains are often found associated with the nuclear lamina (NL), which serves as a large anchoring platform for peripheral chromatin (Chubb et al., 2002; van Steensel and Dekker, 2010). Using DamID technique, an approach in which lamins (or

LAP1, emerin) are fused to a bacterial methyltransferase and the proximity to NL leads to A6 methylation of lamina-associated loci, it was shown that mammalian genome harbors about 1100-1400 Lamina-Associate Domains (LADs), which are characterized by low gene density and a general lack of transcription. LADs have the size from ~10kb to ~10Mb, and the overall amount of LADs cover nearly 40% of the genome (Guelen et al., 2008).

At least a fraction of LADs is recruited to NL via the Lamina-associated sequences (LASs), which are typically, however not globally, enriched in (GA) repeats. LASs are tethered to the NL by the complex formed by transcription repressor cKrox, histone deacetylase HDAC3 and INM protein LAP2β (Zullo et al., 2012). Although LADs are shown to interact with A- and B-type lamins (Collas et al., 2014; Kind and van Steensel, 2014; Meuleman et al., 2013), removal of essentially all lamins does not have any detectable effect on the genome-NL interaction in murine embryonic stem cells (Amendola and van Steensel, 2015). In lamin B1/B2 double knockout mES cells, overall LADs organization is largely retained from the perspective of both the number of LADs and the overall coverage (dKO vs wt: 38.4% vs 38.8%). Furthermore, no changes in LADs number were found when lamin A/C was reduced in lamin B1/B2 double knockout cells (Amendola and van Steensel, 2015).

During interphase, the genome-NL contacts are dynamic within a confined narrow zone (up to ~1μm). Kind and co-authors showed that LADs remained at the nuclear periphery are marked by H3K9me2, while LADs that relocated to the nuclear interior showed significantly less H3K9me2 (Kind et al., 2013). Similar dynamic is also observed when cells differentiate: some LADs may become associated with the NL, while others may lose their association with the nuclear periphery. These processes coincide with altered gene expression in a way that inactivated genes are found in new LADs and activated genes move to the nuclear interior. Thus LADs have significant cell-to-cell heterogeneity, and the NE serves as a cell-type specific anchoring platform where heterochromatic loci are tethered (Peric-Hupkes et al., 2010; Peric-Hupkes and van Steensel, 2010).

1.2.4 Inverted rod nuclei is a unique exception in vertebrates

As described above, most eukaryotic nuclei have conventional nuclear architecture during interphase, that is, heterochromatin is distributed along the nuclear envelope and around the nucleoli, whereas euchromatin occupies the internal nuclear regions (Figure 5B) (Solovei et al., 2009). The nuclei of mouse rod photoreceptor cells are characterized by the inverted distribution of chromatin: heterochromatin localizes in the nuclear center, whereas euchromatin lines the nuclear border (Figure 5C). All the mouse chromosomes are acrocentric and subpericentromeric major satellites of chromosomes aggregate to form the chromocenters (Figure 5A) (Guenatri et al., 2004; Joseph et al., 1989). In conventional nuclei, chromocenters adjoin both the nuclear envelope and the nucleoli. LINE-rich

facultative heterochromatin (fHC) lines the chromocenter, the nucleoli, and the nuclear envelope. SINE-rich euchromatin occupies the nuclear interior (Figure 5B). In rod cells there is one centrally located chromocenter, which is surrounded by a thick shell of facultative heterochromatin (LINE-rich) and thinner outer shell of euchromatin (SINE-rich). Centromeres and proximal telomeres fuse to 3-5 clusters at the surface of the chromocenter, while distal telomeres are found predominantly in the peripheral shell of euchromatin (Figure 5C) (Solovei et al., 2009).

Rod nuclei have conventional nuclear architecture at birth, which is characterized by the peripheral and the chromocenters-surrounding localization of L1-rich heterochromatin, whereas euchromatin localizes more internal. The process of nuclear architecture inversion is accompanied by chromocenter fusion: the median number decreases from 13 at P0 to 2 at P28 and concomitantly the median diameter increases from 1.2 µm to 2.8 µm. At P6, L1-rich heterochromatin begins to move away from the nuclear periphery and accumulates around the chromocenters. The relocalization of L1-rich hetrochromatin to chromocenters finished when examined at P14 and P21 (Solovei et al., 2009).
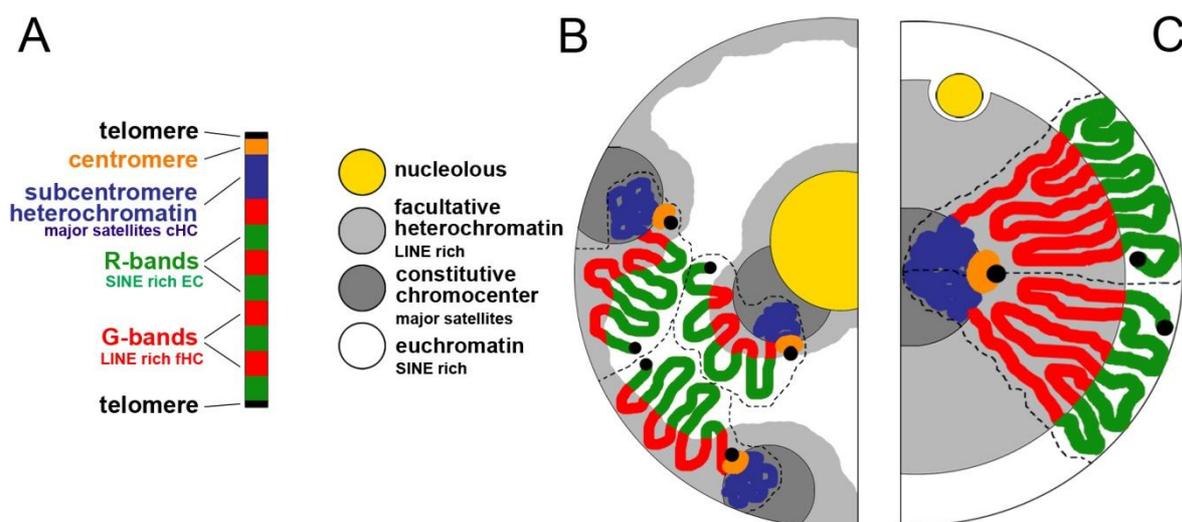
Figure 5. Schematics of chromosome subregions distribution on metaphase chromosome (A) and in interphase nuclei with the conventional (B) and inverted (C) nuclear architecture. A, In mammalian mitotic chromosomes gene-rich and gene-poor regions alternate as R- and G-bands, corresponding to early replicating and SINE-rich euchromatin and mid-late replicating LINE-rich facultative heterochromatin. Subcentromeric constitutive heterochromatin, comprised by satellite repeats, corresponds to C bands. B, In mouse nuclei with conventional nuclear architecture, euchromatin (white) localizes in the interior of the nucleus, whereas LINE-rich heterochromatin adjoins the nuclear border (light grey) and surrounds the chromocenter (dark grey). C, In nuclei of mouse rod photoreceptors chromatin is distributed in a concentric fashion: a single chromocenter (dark grey) localizes in the center of the nucleus and is surrounded by a shell of heterochromatin (light grey), which is in turn surrounded by a thin shell of euchromatin (white). In order to position eu- and heterochromosomal segments (green and red regions, respectively) into corresponding nuclear compartments, chromosomes are significantly folded between these two compartments (adapted from Solovei, 2009).

The inverted architecture was found exclusively in the rod cells of nocturnal mammals, and was shown to be related to nocturnal lifestyle. Direct measurements of light propagation through mouse rod cells proved that rod nuclei function as microlenses focusing light. Computer simulations demonstrated that columns of inverted nuclei do not scatter light, while columns of conventional nuclei scatter light strongly. These finding indicate that rod nuclei inversion is connected not to nuclear function but rather to retinal optics (Solovei et al., 2009).
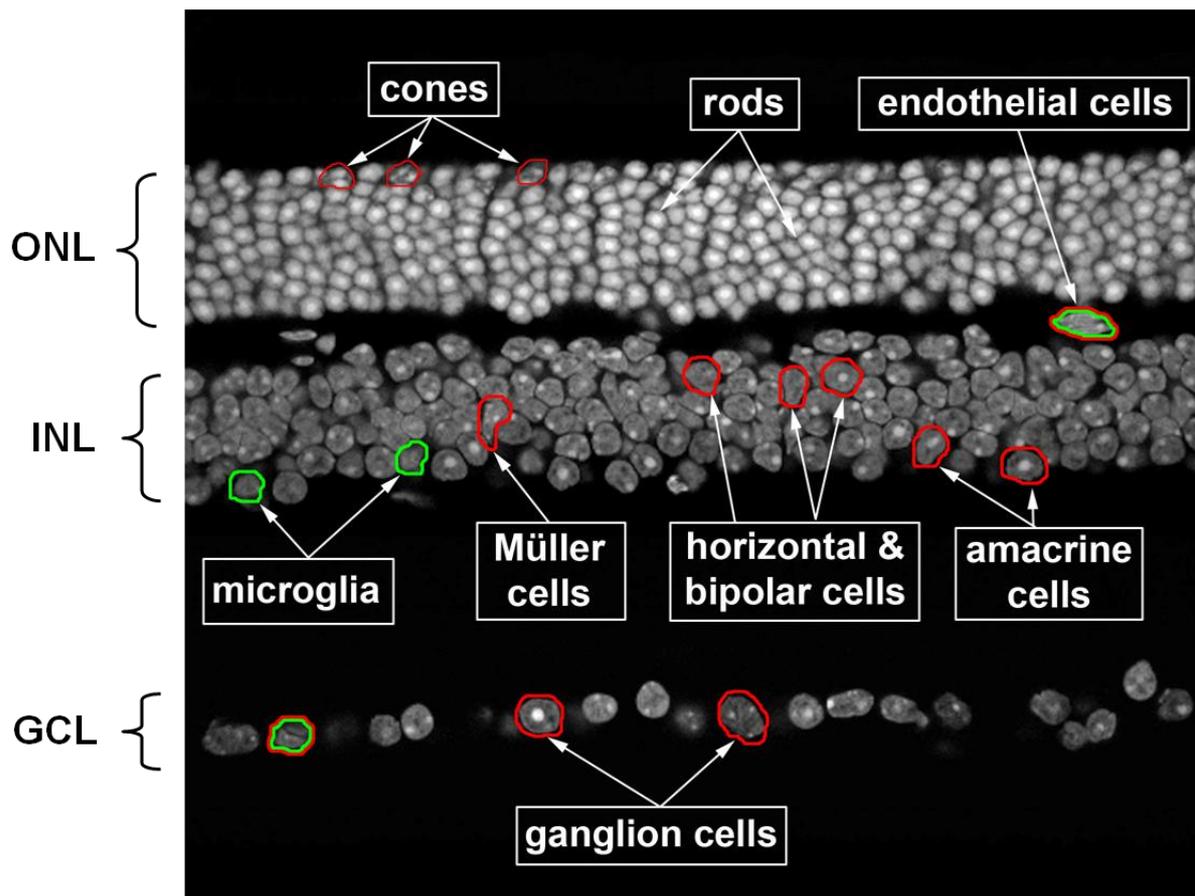
Figure 6. The cellular layers of mouse retina stained by DAPI. Retina is composed of three layers, outer nuclear layer (ONL), inner nuclear layer (INL) and ganglion cell layer (GCL). In mouse 97% of the photoreceptor cells are rod cells and cone cells comprise only 3% of photoreceptors. The INL comprises microglia, Muller cells, amacrine cells, horizontal and bipolar cells. GCL is mainly composed of ganglion cells. Endothelial cells of the retinal blood capillaries are found in the space between each two layers, including ONM and INM, INM and GCL.

Despite of their inverted organization, nuclei of rod photoreceptors are fully functionally active and have a very high transcriptional level (Siegert et al., 2012), which justifies using them as a model for studying the functional organization of the nucleus (Eberhart et al., 2013). Moreover, mouse retina represents a convenient model to study mechanisms of nuclear architecture. First, rod photoreceptors have clear separation of the three major chromatin classes, which allows comparing the distribution of histone modification marks

within different chromatin classes. Second, the results of histone mark distribution of rods can be compared to those of conventional nuclei found in other retinal cell types (Eberhart et al., 2012). Indeed, retina is a regularly structured tissue which consists of three distinct cell layers: DAPI image of mouse retina): outer nuclear layer (ONL), inner nuclear layer (INL) and ganglion cell layer (GCL). The major cell types in each layer can be easily identified even after only nuclear counterstaining with DAPI (Figure 6).

1.3 Roles of the nuclear envelope in the organization of the nuclear chromatin

The eukaryotic cell nucleus is enclosed by the nuclear envelope (NE). The NE includes two membranes, the inner nuclear membrane (INM) and the outer nuclear membrane (ONM), which are separated by the perinuclear lumenal space and joined at nuclear pore complexes (NPCs). Underneath the NE lies a mesh of the nuclear lamins, the major components of the nuclear lamina, which are connected to INM by more than 100 transmembrane proteins (Figure 7). NE defines nuclear integrity, positioning of the nucleus in cytoplasm, communication between cytoplasm and nucleoplasm as well as transporting of macromolecules, and organization of chromatin (Brachner and Foisner, 2011; Mellad et al., 2011; Shimi et al., 2011; Sosa et al., 2012; Starr and Fridolfsson, 2010). Below I focus on the roles of the NE in chromatin organization.

1.3.1 Lamins

Nuclear lamins are type V intermediate filaments and contain small N-terminal "head" domain, central α-helical rod domain and a large C-terminal "tail" domain. The rod domain is divided into four α-helical segments, coil 1a, coil 1b, coil 2a, coil 2b, separating by non-α-helical linker sequence (Fisher et al., 1986). The tail domains of all lamins contain a nuclear localization signal (NLS) and an Ig-fold domain (Dittmer and Misteli, 2011). The nuclear lamin proteins include A- and B-type lamins - A-type lamins, lamin A and C (as well as two rare varaints C2 and AΔ10), are splice variants of the same LMNA gene (Lehner et al., 1987; Rober et al., 1989; Stick and Hausen, 1985). B-type lamins, lamin B1 and lamin B2, are encoded by LMNB1 and LMNB2. In addition a splice variant of LMNB2, lamin B3 was identified in mouse spermatocyte (Furukawa and Hotta, 1993).

A- and B-type lamins have fundamentally different properties. First of all, they have different fates during mitosis: A-type lamins become soluble whereas B-type lamins stay associated with the NE vesicles, most possibly due to their different isoelectric points or CaaX-dependent isoprenylation. A-type lamins lose their isoprene moiety soon after incorporation into the lamina (Beck et al., 1990; Kilic et al., 1999; Weber et al., 1989), while B-type lamins are permanently isoprenylated (Gerace and Blobel, 1980; Hennekes and Nigg, 1994; Nigg et al., 1992; Stick et al., 1988). Secondly, expression pattern of lamins

differs: during development at least one B-type lamin is expressed in all cells, while A-type lamins are expressed later in development and in a differentiation-dependent and cell type-specific manner (Bestor et al., 1988; Dechat et al., 2010; Solovei et al., 2013).

Lamins can interact with chromatin either directly or through histones and other lamin-associated proteins, such as lamin B receptor (LBR), HP1, BAF, INM protein MAN1, emerin, LEM2 and several LAP2 isoforms (reviewed in (Maraldi et al., 2010; Wilson and Foisner, 2010)). Tethering of peripheral chromatin to the NL is visible in mammalian cells by electron microscopy (Belmont et al., 1993) and can be demonstrated biochemically (Guelen et al., 2008). Loss-of-function experiments in C. elegans and D. melanogaster reveal the changed chromatin organization in lamins null cells (Bao et al., 2007; Liu et al., 2000; Margalit et al., 2005a; Mattout et al., 2011). The changed chromatin organization can modulate gene expression by altering their accessibility to transcription factors (Bank and Gruenbaum, 2011; Milon et al., 2012).

1.3.2 Transmembrane proteins

1.3.2.1 LINC complexes link the nuclear interior to the cytoplasm

The INM and ONM possess different sets of transmembrane proteins (Schirmer and Foisner, 2007; Schirmer and Gerace, 2005). One well studied INM proteins are SUN proteins, which contain a conserved SUN domain (Sad1p, Unc-84). At the nucleoplasmic face of the INM, SUN1 was shown to bind directly to Lamin A. Despite the binding of SUN proteins to lamins, the localization of SUN proteins is not necessarily dependent on lamins in mammals, at lease in certain cell types, such as human UNC84A (Crisp et al., 2006; Haque et al., 2006; Hasan et al., 2006). At the perinuclear lumenal space, SUN proteins traverse the INM and bind to KASH (Klarsicht/ANC-1/SYNE homology) proteins which traverse ONM. At the cytoplasmic face of the ONM, KASH protein interacts with cytoskeletal components. Interaction of SUN and KASH proteins forms the so called LINC complexes (linker of the nucleoskeleton and cytoskeleton) (Figure 7) (Herrmann et al., 2007; Ketema et al., 2007).

In mammals there are four KASH proteins identified so far: the first, NESPRIN 1 (also known as SYNE1, MYNE1, and ENAPTIN) was found to be enriched in the NE of muscle nucleus clustered beneath the neuromuscular junction (NMJ) (Apel et al., 2000). The NESP1/SYNE1 gene encodes several splice isoforms, NESPRIN 1 Giant (NESP1G) is the largest one with the molecular weight of about 1000 kDa. The second, NESPRIN 2 (also known as SYNE2 and NUANCE) is transcribed from the SYNE2 gene which also encodes a large isoform NESP2G with molecular weight of 800 kDa. Both NESP1G and NESP2G have the same structure: N-terminal ABD, spectrin repeats (defining a high flexibility of molecule), and C-terminal KASH domain (Apel et al., 2000; Zhang et al., 2002; Zhang et al., 2001). The

third, NESPRIN 3 (NESP3) is also localized to ONM via the same mechanism. The fourth, NESP4 has only 42 kDa with a single spectrin repeat and somewhat degenerated KASH domain.

At the cytoplasmic face of the ONM, NESPRIN 1/2 Giant binds to Actin directly, NESPRIN 1/2 and NESPRIN 2/4 bind to microtubules via DYNEIN and KINESINE 1, respectively. NESPRIN 3 binds to intermediate filaments via PLECTIN (Figure 7) (Herrmann et al., 2007; Ketema et al., 2007; Mellad et al., 2011; Roux et al., 2009; Sosa et al., 2012; Starr and Fridolfsson, 2010). LINC has been found to be conserved from yeast to mammals and has essential roles in cell polarization, nuclear positioning and migration (Lei et al., 2009; Starr, 2009; Zhang et al., 2009). Mutations in proteins of LINC complexes causes laminopathies, in particular, EDMD (Emery-Dreifuss muscular dystrophy) can arise from mutations in different genes: EMD (which encodes EMERIN), LMNA (which encodes lamin A/C), SYNE1 (NESPRIN-1) or SYNE2 (NESPRIN-2). These proteins are interconnected, suggesting common mechanisms for development of laminopathies, and illustrating the importance of proper LINC complex functionality for healthy human development.

1.3.2.2 Transmembrane proteins and their involvement in the chromatin tethering

In mammals, there are over 100 different INM integrated proteins. In this chapter I will focus on eight transmembrane proteins (Figure 7, 8). LBR is the best characterized among them. N-terminus of LBR comprises two globular domains, one of them is Tudor domain, joined by a linker region. N-terminal faces to the nucleoplasm and interacts with DNA (directly bound to DNA via Tudor domain), B-type lamins, HP1, HA95 and chromatin (Duband-Goulet and Courvalin, 2000; Gajewski and Krohne, 1999; Holmer and Worman, 2001; Wagner et al., 2004). In vivo, LBR forms a complex with the core histones H3, H4 and linker histone HP1 (Polioudaki et al., 2001) (Figure 7,8) . LBR is involved in heterochromatin organization via the binding of LBR N-terminus to chromatin and histones. C-terminus of LBR is a short hydrophilic spanning region facing the nucleoplasm with unknown function (Hoffmann et al., 2002). The large middle part (212-583 aa of human LBR) is composed of eight putative transmembrane domains encompassing a conserved sterol reductase domain (Worman et al., 1990) (Figure 8). The first transmembrane domain is critical for the incorporation of LBR to the INM (Smith and Blobel, 1993). During cell cycle, LBR is found to play a central role in targeting the NE precursor membrane vesicles to the chromatin during NE assembly at the end of mitosis, by the interaction of N-terminal spanning region with importin β (Ma et al., 2007).

INM LEM-D proteins are defined by the presence of a common structural bihelical motif called the LEM domain. The name of LEM domain derives from the firstly identified proteins LAP2 (LAP2, lamina-associated polypeptide 2), EMERIN and MAN1 (Laguri et al., 2001; Lin

et al., 2000). Based on the domain organization, LEM-D proteins fall into three groups (Brachner and Foisner, 2011; Lee and Wilson, 2004; Wagner et al., 2010). Group I proteins contain N-terminal LEM domain and large nucleoplasmic domain, most of them have a single transmembrane domain at their C-terminus. Representatives of Group I include EMERIN and LAP2. Like Group I, Group II proteins also carry N-terminal LEM domains. Different from Group I proteins, they contain two internal transmembrane domains and C-terminal winged-helix MAN1/Scr1p/C-terminal (MSC) motif domains that directly bind DNA (Caputo et al., 2006). LEM2 and MAN1 are the representatives of Group II. Proteins of group III have internal LEM domains and multiple ankyrin groups, including ANKLE1 and ANKLE2. In contrast to other LEM-D proteins, Ankle1 shuttles between the nucleoplasm and cytoplasm (Brachner et al., 2012)(Brachner A, 2012), whereas Ankle2 localizes throughout the endoplasmic reticulum in human cells and at the NE in worms due to a transmembrane domain (Figure 7) (Asencio et al., 2012).

LEM-D proteins tether chromatin through different mechanisms. The shared LEM domain, an ~45-residue motif that folds as two α-helices (Laguri et al., 2001), binds a conserved metazoan chromatin protein BAF (Cai et al., 2001; Cai et al., 2007; Furukawa, 1999; Lee et al., 2001; Shimi et al., 2004; Shumaker et al., 2001). BAF was shown to interact with chromatin (Figure 7) (Margalit et al., 2007). Moreover, some LEM-D proteins have additional domains that directly bind DNA, or chromatin proteins. For example, LAP2 contains a second LEM-like domain that binds directly to DNA (Cai et al., 2001; Laguri et al., 2001); MAN1 and probably LEM2 bind DNA directly via the C-terminal winged helix MAN1/Scr1p/C-terminal domain (Caputo et al., 2006). LAP2β also binds chromatin protein HA95 (Martins et al., 2003). Furthermore, all identified LEM-D proteins bind either A- or B-type lamins, or both, directly (Brachner et al., 2005; Clements et al., 2000; Lee et al., 2001; Mansharamani and Wilson, 2005; Sakaki et al., 2001).

The interactions of LEM-D proteins, lamins, and BAF are strongly conserved between flies, nematodes and mammals, suggesting their fundamental roles in the nucleus, including anchoring chromatin to the NE (Wilson and Foisner, 2010). C. elegans contains three LEM-D proteins Ce-emerin, Ce-lem2 and Ce-Lem3. Double-knockdown of the former two LEM proteins causes embryonic lethality at the 100-cell stage. The phenotype includes more than 50% of the nuclei with abnormally condensed chromatin, anaphase bridges which appear as early as the first nuclear division, aneuploidy and failure of chromosome assembly after mitosis (Liu et al., 2003). Notably, down-regulation of either Ce-lamin (Margalit et al., 2005a) or BAF (Margalit et al., 2005b) causes the identical phenotype in C. elegans, strongly suggesting that LEM-D proteins, BAF and lamins are key components for maintenance of nuclear architecture.
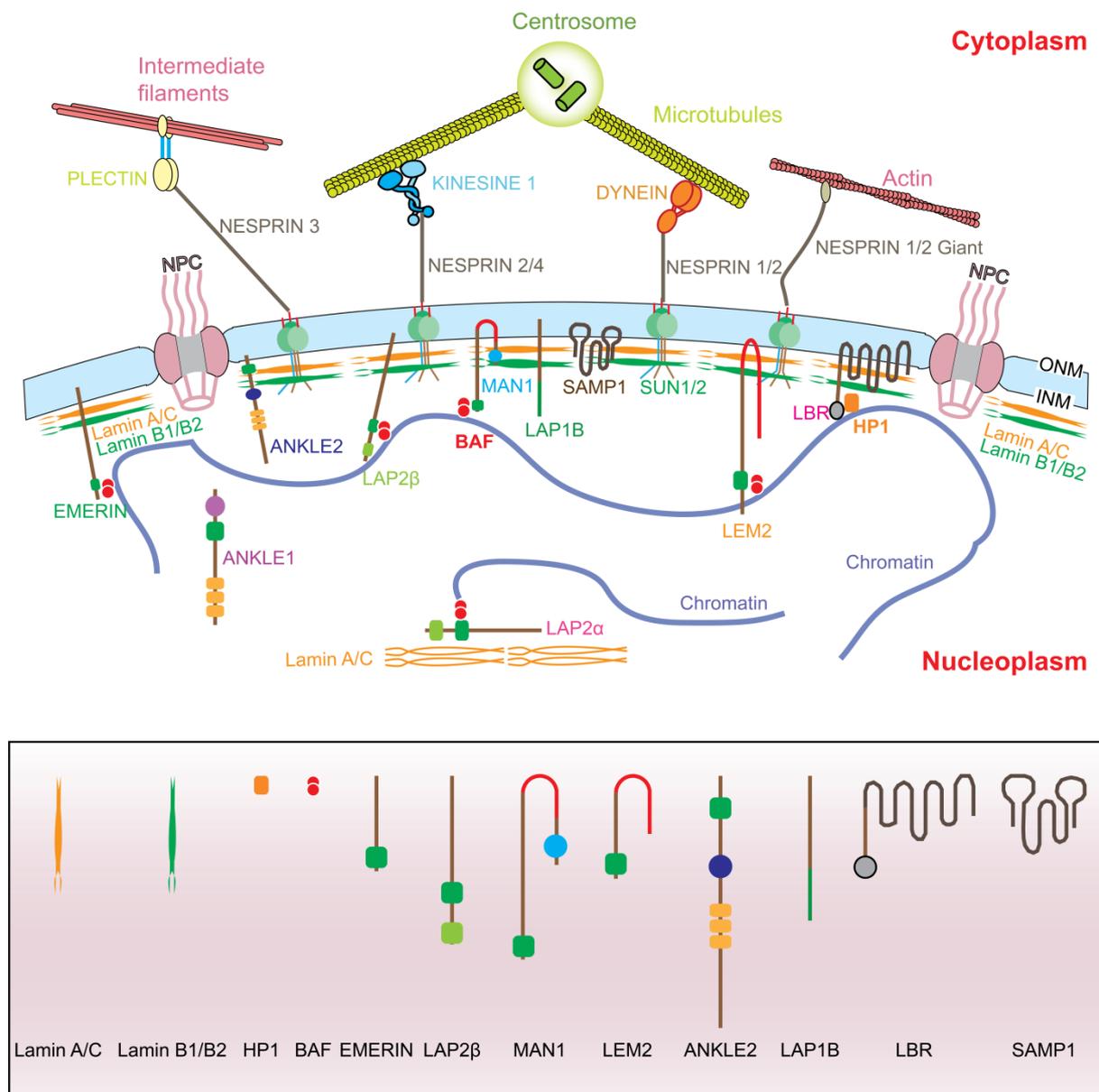
Figure 7. Schematics of the nuclear envelope proteins and interconnections between nuclear and cytoskeleton. Nuclear envelope is underlined by A- and B-type lamins. INM proteins, including LBR, EMERIN, LAP2β, MAN1, LEM2, SAMP1, and LAP1B, are anchored in the INM and connect to lamins. LBR and LEM-D proteins bind peripheral chromatin via the interaction with HP1 and BAF, respectively. SUN proteins, SUN1 and SUN2, are also anchored into INM and bind lamins, but they penetrate intermembrane space and interact with KASH domains of NESPRINS. NESPRINS are transmembrane proteins of the outer nuclear membrane and, in turn, interact with cytoskeleton filaments and microtubules. LAP2α is the only LEM-D protein which lacks the transmembrane domain and thus distributes throughout nucleoplasm, it interacts with soluble fraction of lamin A/C and chromatin.

LAP2α (Lamina-associated polypeptide 2α) is one of six splice variants of the mammalian LAP2 gene (originally termed TMPO) (Berger et al., 1996; Dechat et al., 1998; Furukawa et al., 1995; Harris et al., 1994). All LAP2 isoforms share the first 187 N-terminal residues (Dechat et al., 2000b) harboring the LEM domain (Brachner and Foisner, 2011), which binds

to the adaptor protein Barrier-to-autointegration factor (BAF) in a sequence-independent manner to mediate the interaction with chromatin (Figure 7,8) (Cai et al., 2001). The C-terminal domain of LAP2α differs considerably from that of other LAP2 isoforms: no transmembrane domain was found in LAP2α. Whereas most LAP2 isoforms are anchored in the INM via C-terminal transmembrane domain, LAP2α is uniformly distributed throughout the nucleoplasm (Dechat et al., 2004).

Moreover, unlike other LAP2 transmembrane proteins which primarily bind B-type lamins at the NL (Foisner and Gerace, 1993), LAP2α exclusively binds to A-type lamina via its unique C-terminal tail (Dechat et al., 2000a). LAP2α is crucial for the stabilization and the nuclear interior localization of the nucleoplasmic lamin A/C pool. In the cells and epithelial tissues derived from LAP2α-deficient mice, A-type lamins localize exclusively at the nuclear periphery and absent from the nuclear interior. Re-expression of LAP2α rescues the nuclear interior lamin A/C pool (Naetar et al., 2008). Both LAP2α (Dorner et al., 2006; Markiewicz et al., 2002) and A-type lamins (Mancini et al., 1994; Ozaki et al., 1994) bind pRb in vivo and in vitro, a major cell cycle regulator that represses the activity of E2F transcription factor and inhibits cell cycle progression (Hatakeyama and Weinberg, 1995). LAP2α and lamin A/C were found to negatively affect cell cycle progression and thus enhance cell cycle arrest in tissue progenitor cells of regenerating tissues. In LAP2α-deficient mice, the number of proliferating tissue progenitor cells increase significantly in skin, colon, skeletal muscle, and in the hematopoietic system (Gotic and Foisner, 2010; Gotic et al., 2010; Naetar and Foisner, 2009; Naetar et al., 2008).

LAP1 (Lamina-associated polypeptide 1) was first identified as polypeptide antigens recognized by a monoclonal antibody generated against rat liver NE protein extracts and was associated with lamina (Senior and Gerace, 1988). LAP1 has three proteins named LAP1A, LAP1B and LAP1C arising from splice variants (Foisner and Gerace, 1993). LAP1 has a single transmembrane segment, with N-terminus facing the nucleoplasm, C-terminus within the perinuclear space (Kondo et al., 2002). The luminal domain of LAP1 binds to torsinA, the mutation of torsinA gene causes the CNS specific disease DYT1 dystonia (Goodchild and Dauer, 2005). The amino-terminal domain of LAP1 binds to the nucleoplasmic proteins, such as PP1 (Santos et al., 2013), and the nucleoplasmic domains of other INM proteins (Shin et al., 2013) (Figure 8). The functional interaction of LAP1 with torsinA and emerin suggests that it may play a role in human disease DYT1 dystonia and EDMD (Emery-Dreifuss muscular dystrophy).

SAMP1 (spindle-associated membrane protein 1) is an inner nuclear membrane integral protein. It is conserved in metazoa and fission yeast, homologous to Net5 in rat (Schirmer and Gerace, 2005) and Ima1 in S. pombe (King et al., 2008). At the onset of mitosis most of SAMP1 dispersed out into the ER, similar to other transmembrane proteins. In addition, a

significant fraction of SAMP1 is specifically localized to the polar regions of the mitotic spindle during mitosis (Buch et al., 2009). N-terminus of SAMP1 has five hydrophobic segments; the first segment is a highly conserved cytoplasmic/nucleoplasmic loop containing four characteristic CxxC motifs, which are predicted to be organized into two zinc fingers. The rest four segments are transmembrane segments. The N-terminal cysteine-rich CxxC part of SAMP1 exposed to nucleoplasm and, although it is not transmembrane segment, is responsible for the NE targeting, especially the intact CxxC motif is needed for the NE targeting. The C-terminus is also exposed to nucleoplasm (Buch et al., 2009; Gudise et al., 2011). In Hela cells SAMP1 defines the correct localization of emerin and SUN1 to NE (Gudise et al., 2011) (Figure 8).

Table 2. Cell type or tissue specific expression of studied proteins and their implication into cellular processes or signaling pathways.

Protein	Cell type or tissue specific expression (literature)	Cell type specific expression (this study)	Implication in cellular process/signaling pathway
LBR	expressed in undifferentiated cells, renewed cells, several cell type of adult mice* (Solovei et al., 2013)		targeting NE membrane precursor vesicles to chromatin during NE reassembly (Ma et al., 2007)
LEM2	ubiquitous expression, much greater level in cardiac and skeletal muscle (Brachner et al., 2005; Chen et al., 2006)	absent in retinal neurons, hepatocyte and Kupffer cells, crypt cells of thin intestine and matrix keratinocytes of hair	ERK signaling (Huber et al., 2009)
MAN1		absent in crypt cells of small intestine and matrix cells of hair follicle	TGFbeta/BMP signaling (Bourgeois et al., 2013; Lin et al., 2005; Pan et al., 2005)
EMERIN	essentially express in all tissues (Tunnah et al., 2005)	very weak expression level in rod cells, and absent in hepatocyte of liver	ERK-signaling (Huber et al., 2009; Muchir et al., 2007), Wnt signaling (Markiewicz et al., 2006)
LAP2β	ubiquitious expression (Berk et al., 2013a; Ishijima et al., 1996)	absent in adult skeletal muscle, adult cardiac muscle and dermal papilla cells of the hair follicle	DNA replication (Martins et al., 2003; Martins et al., 2000)
LAP1B	ubiquitous expression pattern, abundant in differentiated adult tissues (Goodchild and Dauer, 2005; Kim et al., 2010; Santos et al., 2013; Shin et al., 2013)	absent in rod and other neuroretinal cells of retina, Purkinje and granular cells of cerebellum, absorptive and crypt cells of thin intestine and matrix keratinocytes of hair	
SAMP1	oocyte, fertilized eggs (Figueroa et al., 2010)	present only in neurons, muscles	Migration (Bone et al., 2014; Borrego-Pinto et al., 2012), centrosome orientation (Buch et al., 2009)
LAP2α	highest expressed in proliferating cells and down-regulated during cell cycle exist and differentiation (Gotic and Foisner, 2010; Markiewicz et al., 2002; Markiewicz et al., 2005; Naetar et al., 2008)	absent in Purkinje cells of cerebellum	retinoblastoma-E2F pathway (Berk et al., 2013a)

To be continued in next page

*Expression of LBR was detected in the following differentiated cell types of adult mice: microglia cells, lymphocytes, granulocytes, Kupffer cells, absorptive cells, podocytes, erythroblasts, megacaryocytes, smooth muscle cells and endothelia cells. The nuclei of adult hepatocytes, cardiomyocytes and myotubes retain a very low level of LBR.

Figure 8. Schematics of INM and LAP2α proteins. Black numbers indicate size of protein domains in amino acids (aa); magenta line indicate regions known to interact with specified proteins. References to the sources for first identification of the protein and the interacting partner proteins are indicated in the left and right column, respectively.

LAP2β
454 aa
Furukawa, et al,
1995

1-85
168-187
411-434

DNA
BAF
Lamin B (298-370 aa)

DNA: Furukawa, et al, 1997
Cai, et al, 2001
BAF: Shumaker, et al, 2001
Cai, et al, 2001
Lamin B: Furukawa, et al, 1998

LAP2α
693 aa
Harris, et al,
1995

1-85
168-187

DNA
BAF
Lamin A/C (615-693 aa)
chromosome association (188-692 aa)

DNA: Furukawa, et al, 1997
Cai, et al, 2001
BAF: Shumaker, et al, 2001
Cai, et al, 2001
Lamin A/C: Dechat, et al, 2000

LAP1B
584 aa
Kondo, et al, al
2002

346-368

EMERIN
TORSINA
TORSINB/TORSIN3

emerin: Shin, et al, 2013
TORSINA: Goodchild, et al, 2005
TORSINB/TORSIN3: Kim, et al,
2010

SAMP1
392 aa
Buch, et al,
2009

48-70
121-167
214-234 298-318 323-343 357-374

EMERIN/SUN1/Lamin A/C

emerin/SUN1/Lamin A/C: Gudise,
et al, 2011

Tudor   RS   globular II   LEM   LEM-like   TM   MSC   RRM   Zinc Finger
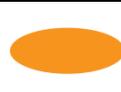
RS, arginine serine
TM, transmembrane
MSC, MAN1/Src1p/C-terminal
RRM, RNA-recognition motif

22

1.3.3 Two peripheral tethers of heterochromatin

Recently it was shown that the presence of either LBR or Lamin A/C is necessary for the maintenance of peripheral heterochromatin and conventional nuclear architecture. In particularly it was shown that the absence of LBR and Lamin A/C leads to the loss of peripheral heterochromatin in rod cells of nocturnal mammals, whereas other cell types express at least one of the two proteins and correspondingly, have conventional nuclear architecture. LBR directly binds heterochromatin at the nuclear periphery through interaction with HP1 (Holmer and Worman, 2001). Ectopic expression of LBR in rod cells under the rod-specific neural retina leucine zipper (Nrl) promoter of mice was sufficient to revert the chromatin organization into conventional one. On the other hand, LBR knockout caused inverted nuclear organization in cell types which do not express Lamin A/C in wild type mice.

Transgenic expression of lamin C in rod cells is not sufficient to revert the inverted nuclear architecture. The inability of LamC to tether peripheral heterochromatin indicates that LamA/C predominantly binds chromatin indirectly in vivo, perhaps via a complex with INM proteins (Solovei et al., 2013). In mammals, the role of Lamin A/C in peripheral heterochromatin tethering is still a subject of controversy. The evidence supporting binding of chromatin by Lamin A/C comes from the study of Hutchinson Gilford Progeria Syndrome (HGPS), a human disease caused by mutation of LMNA. In the human fibroblast from HGPS, loss of lamin A results in loss of peripheral heterochromatin, change in H3K27me3 distribution and global loss of the chromatin compartmentalization (McCord et al., 2013). While in another study no difference was found in wild type and Lamin A mutated cell lines (Kubben and Adriaens, 2012). Following-up studies are needed to clarify the exact mechanisms of Lamin A/C as peripheral heterochromatin tethers. In D. melanogaster, which only express B-type lamin (lamDm(0)), depletion of B-type lamin caused relocation away from the nuclear periphery and activation of testis specific genes (Shevelyov et al., 2009). B-type lamin is also essential for the peripheral localization and corresponding silence of the hunchback gene in differentiating drosophila neuroblasts (Kohwi et al., 2013). In C. elegans the introduced large heterochromatic repeats were located near the NL; depletion of the only lamin reversely detach the repeats from the NL (Towbin et al., 2010).

1.4 Aims of this PhD work

One of the prominent features of eukaryotes is spatial segregation of transcriptionally active euchromatin and transcriptionally silent heterochromatin in the nucleus, achieved by complicate hierarchical folding of the genome. The segregation is based on different epigenetic marks characteristic of the both chromatin classes and on nuclear elements, such as recently identified lamin A/C-dependent (A-type) and LBR-dependent (B-type) tethers of the heterochromatin to the nuclear envelope. Rod photoreceptors in mouse retina possess a very clear spatial separation of the two chromatin classes in their inverted nuclei and, hence, represent a convenient model to study different aspects of eu- and heterochromatin formation at the microscopic level. A general goal of the present work was to study further mechanisms of euchromatin and heterochromatin positioning in conventional and inverted mouse nuclei. The work comprises three major parts.

The first part focused on the analysis of epigenetic marks characteristic of eu- and heterochromatin in conventional and inverted nuclei of mouse retinal cells. I aimed to find epigenetic factors, such as histone modifications and chromatin-associated proteins, which might be involved in establishing the nuclear inversion in rods.

The second part of my work focused on characterization of cell-type specific and differentiation-dependent distribution of one of the proteins selectively binding to the methylated DNA, so called Methyl-CpG binding protein 2 (MECP2) in various mouse tissues. In particular, my goal was to study a functional role of MECP2 in retinal neurons during their differentiation by comparison of wild type (WT) and Mecp2 knock-out (KO) retinas.

The objective of the third part of my work was to uncover possible interacting partners of lamins A/C in the A-type tether of the peripheral heterochromatin. To identify likely proteins, I planed to assess cell-type specific expression of transmembrane proteins of the inner nuclear membrane, including LEM-D proteins, in a range of WT and Lmna-KO mouse tissues. I also aimed at cloning of selected candidates for further genetic engineering work, in particular, for transgenic mice generation.

2 Results

2.1 DNA methylation reader MECP2: cell type- and differentiation stage-specific protein distribution

Epigenetics & Chromatin

DNA methylation reader MECP2: cell type- and differentiation stage-specific protein distribution

Congdi Song[1], Yana Feodorova[1], Jacky Guy[2], Leo Peichl[3], Katharina Laurence Jost[4], Hiroshi Kimura[5],
Maria Cristina Cardoso[4], Adrian Bird[2], Heinrich Leonhardt[1], Boris Joffe[1^] and Irina Solovei[1*]

Abstract

Background: Methyl-CpG binding protein 2 (MECP2) is a protein that specifically binds methylated DNA, thus regulating transcription and chromatin organization. Mutations in the gene have been identified as the principal cause of Rett syndrome, a severe neurological disorder. Although the role of MECP2 has been extensively studied in nervous tissues, still very little is known about its function and cell type specific distribution in other tissues.

Results: Using immunostaining on tissue cryosections, we characterized the distribution of MECP2 in 60 cell types of 16 mouse neuronal and non-neuronal tissues. We show that MECP2 is expressed at a very high level in all retinal neurons except rod photoreceptors. The onset of its expression during retina development coincides with massive synapse formation. In contrast to astroglia, retinal microglial cells lack MECP2, similar to microglia in the brain, cerebellum, and spinal cord. MECP2 is also present in almost all non-neural cell types, with the exception of intestinal epithelial cells, erythropoietic cells, and hair matrix keratinocytes. Our study demonstrates the role of MECP2 as a marker of the differentiated state in all studied cells other than oocytes and spermatogenic cells. MECP2-deficient male ($Mecp2^{-/y}$) mice show no apparent defects in the morphology and development of the retina. The nuclear architecture of retinal neurons is also unaffected as the degree of chromocenter fusion and the distribution of major histone modifications do not differ between $Mecp2^{-/y}$ and $Mecp2^{wt}$ mice. Surprisingly, the absence of MECP2 is not compensated by other methyl-CpG binding proteins. On the contrary, their mRNA levels were downregulated in $Mecp2^{-/y}$ mice.

Conclusions: MECP2 is almost universally expressed in all studied cell types with few exceptions, including microglia. MECP2 deficiency does not change the nuclear architecture and epigenetic landscape of retinal cells despite the missing compensatory expression of other methyl-CpG binding proteins. Furthermore, retinal development and morphology are also preserved in $Mecp2$-null mice. Our study reveals the significance of MECP2 function in cell differentiation and sets the basis for future investigations in this direction.

Keywords: MECP2, MBD, Histone modifications, Nuclear architecture, Mouse retina, Retina development, Mouse tissues

Background

Methyl-CpG binding protein 2 (MECP2) was discovered as a protein that selectively binds methylated DNA [1]. Mutations of the *MECP2* gene were later identified as the principal causative factor for Rett syndrome, a severe progressive neurological disorder affecting almost exclusively females [2]. Mild loss of function mutations,

duplications, and expression level alterations has also been found in patients with a plethora of neurological and mental phenotypes [3-6]. In mice, deletion of the *Mecp2* gene causes symptoms similar to those of Rett syndrome even when the deletion is restricted to the brain [7-10], while expression of *Mecp2* rescues the Rett phenotype. More effective rescue was achieved through embryonic, compared to early postnatal expression [11-13], whereas targeted expression in postmitotic neurons resulted in asymptomatic mice [12,14]. *Mecp2* mutant mice exhibit abnormalities in the number of synapses [15], the morphology of neuronal processes [16,17], neuronal maturation [16], and the neurophysiological activity of these cells

* Correspondence: Irina.Solovei@lrz.uni-muenchen.de
^Deceased
[1]Department of Biology II, Center for Integrated Protein Science Munich (CIPSM), Ludwig Maximilians University Munich, Grosshadernerstrasse 2, 82152 Planegg-Martinsried, Germany
Full list of author information is available at the end of the article

[18,19]. These effects are associated with particular neuron types. For instance, brain stem GABA-ergic neurons are affected, but glycinergic ones are not [20]. Glutamatergic neurons of the brain and their synapses are also affected through the expression level of brain-derived neurotrophic factor (BDNF) [21] which is regulated by MECP2 in a neuronal activity-dependent manner [17,22,23].

The results listed above conform to the conclusion that MECP2 deficiency leads to subtle changes in the expression levels of genes causing diverse and widespread phenotypic changes [24]. There is growing evidence that both *Mecp2*-null astrocytes [25] and microglia [26] affect the dendritic morphology of neurons. Lack of MECP2 causes global histone H3 hyperacetylation in neurons [10,27], which can have different effects on transcription depending on which lysine residues are acetylated. It remains, however, unknown if global histone H3 acetylation levels increase exclusively in neurons or also take place in glia [10,21,27]. Factual data about the phenotypic changes in various tissues of *Mecp2*-null mice are currently insufficient and partially controversial.

In addition to its role in transcriptional regulation, MECP2 appears to be important for maintenance of the general chromatin organization. *Mecp2*-null brain shows a ca. 1.6-fold upregulation in spurious transcription of repetitive DNA, in particular L1 retrotransposons and pericentromeric satellites [27], which have been implicated in maintenance of the nuclear architecture and its formation during cell differentiation [28-30]. In all mouse cells, subcentromeric repetitive blocks, composed of major satellite repeat, form spherical bodies, so called chromocenters that are predominantly located at the nuclear periphery and adjacent to the nucleolus. Remarkably, mouse chromocenters are extremely enriched in MECP2 [1] and the same applies to clusters of human alphoid satellites, also often called chromocenters. There is growing evidence that DNA methylation and MECP2 binding to methylated DNA are pivotal for chromocenter formation and, therefore, the establishment of normal nuclear architecture [31-35]. MECP2 indeed seems to be required for chromocenter fusion during differentiation [8,32,36], although other methyl binding (MBD) proteins can compensate for its absence [31,33,35].

In order to provide better understanding of MECP2 function, we characterized the distribution of the protein in more than 60 cell types of 16 mouse neuronal and non-neuronal tissues by immunostaining. We show that MECP2 is expressed at a very high level in all retinal neurons except rod photoreceptors. The onset of its expression during retina development coincides with massive formation of the neural synapses. We also describe the distribution of MECP2 in other tissues at various stages of development and relate its increased expression to the terminal differentiation of cells. Mice lacking MECP2 show no apparent defects in the morphology and development of the retina, as well as in the nuclear architecture of retinal neurons. Finally, we show that the absence of MECP2 is not compensated by upregulation of other MBD proteins but rather causes their downregulation.

Results and discussion

We studied mouse tissues because the nuclei of all mouse cells have prominent chromocenters which are convenient for the microscopic approach. The main DNA sequence of chromocenters, major satellite repeat, is present on all autosomes, comprises ca. 10% of whole mouse DNA, contains ca. 50% of the CpG dinucleotides of the whole mouse genome [37], and was shown to bind MECP2 [1]. Therefore, chromocenters can serve as a sensitive indicator of MECP2 expression after immunostaining. To avoid interpretations which might depend only on chromocenters, in all relevant cases, we also studied rat tissues. In contrast to mouse, rat chromosomes do not have large blocks of pericentromeric repeats and therefore do not form noticeable chromocenters in interphase nuclei.

The standard methods of protein-level estimation, such as Western blot analysis routinely used for homogeneous cell cultures, are not really useful for native tissues containing various cell types. Therefore, our method of choice was MECP2 immunostaining on cryosections where we could distinguish different cell types using either histological criteria or cell-specific antibodies (Tables 1 and 2). To avoid false-positive and false-negative results after antibody staining, we used a robust and reliable method developed by us earlier [38,39]. This method allows quick comparison of immunostaining results in the same tissue after various fixation and antigen retrieval times. Polyclonal anti-MeCP2 antibodies, mostly used in the study, do not produce nuclear staining in fibroblasts derived from MECP2-deficient mice (Additional file 1A) and, when applied to Western blot, show expected enrichment of the protein in brain tissue derived from wild-type (WT) mice (Additional file 1B).

MECP2 in retinal cell types

The retina is an attractive model to study the role of MECP2 in a nerve center. Most of the retinal cell types can be recognized by their positions and by the shape of their nuclei; only in a few cases, identification requires cell type-specific immunostaining. Most of the mouse retinal cells express MECP2: their nuclei possess a weak or moderate staining of the nucleoplasm and a strong signal in chromocenters. In particular, all neurons in the ganglion cell layer (GCL), inner nuclear layer (INL), and cone photoreceptors in the outer nuclear layer (ONL) have very strong chromocenter staining and a weak nucleoplasm staining (Figure 1A).

Table 1 List of antibodies for cell type identification in retina and brain and for recognition of retinal structures

Antibody abbreviation	Antigen transmitter/protein	Recognized cells/structures	Source, catalogue number
ChAT	Choline acetyl transferase	Cholinergic amacrine cells	Millipore, AB144P
Calbindin	Calcium-binding protein 28 kD	Horizontal cells	SWANT, #300
GFAP	Glial fibrillary acidic protein	Astroglia	Sigma, G 3893
GABA	Gamma aminobutyric acid	Amacrine, horizontal cells	Sigma, A 2052
GABA-A α1	GABA receptor subunit α1	Bipolar, amacrine, and ganglion cell processes in IPL	Millipore, #06-868
GABA-C	GABA receptor subunit ρ1	Synapses in IPL	R. Enz, MPI for Brain Research, Frankfurt
GAT	GABA transporter	Presynaptic terminals	Abcam, ab426
GAD-65	Glutamic acid decarboxylase (GABA-synthesizing enzyme)	Amacrine, horizontal cells	Chemicon, MAB351R
GAD-67	Glutamic acid decarboxylase (GABA-synthesizing enzyme)	Amacrine, horizontal cells	Abcam, ab26116
GS	Glutamine synthetase	Müller cells (astroglia)	BD Biosciences, #610517
GluR3	Glutamate-gated ion channel (glutamate receptor 3)	Synapses in IPL and OPL	Santa Cruz, sc-7612
GlyT1	Glycine transporter 1	Amacrine cells	Chemicon, AB1770
Iba 1	Ionized calcium binding adaptor molecule 1	Microglia/macrophage	Wako, #019-19741
MAP2	Microtubule-associated protein 2	Neurons	Sigma, M1406
NR1C2	NMDA receptor 1 splice variant C2	IPL and OPL synapses	Chemicon, AB5050P
PKCα	Protein kinase C	Rod bipolar cells	Sigma, P 4334
PKA II β	Human protein kinase A, regulatory subunit II beta	Cone bipolar cells	BD Biosciences, #54720
PSD-95	Postsynaptic density protein 95	Photoreceptors (rods and cones) synapse marker	Dianova, MA1-046
SV2	Membrane of synaptic vesicles	General synapse marker	DSHB, SV2-a1
TH	Tyrosine hydroxylase	Dopaminergic amacrine cells	Immunostar, #22941
VGLUT1	Vesicular glutamate transporter 1	IPL and OPL synapses	Millipore, MAB5502
VGLUT3	Vesicular glutamate transporter 3	Amacrine cells	Millipore, AB5421
Znp-1 (Syt2)	Synaptotagmin II	Cone bipolar cells	Zebrafish International Resource Center, University of Oregon, Eugene, OR, Znp-1

Millipore (Billerica, MA, USA), Swant (Marly, Switzerland), Sigma-Aldrich (St. Louis, MO, USA), Abcam (Cambridge, UK), Chemicon (Billerica, USA), BD Biosciences (Franklin Lakes, NJ, USA), Santa Cruz (Dallas, TX, USA), Wako (Richmond, VA, USA), Dianova (Hamburg, Germany), DSHB (University of Iowa, IA, USA).

In contrast to other retinal cells, rod photoreceptor nuclei of nocturnal mammals possess a dramatically different pattern of chromatin distribution [30]. In these cells, a centrally positioned chromocenter is surrounded by a shell of LINE-rich heterochromatin, whereas euchromatin occupies the nuclear periphery. This nuclear organization is inverted in comparison to all other eukaryotic cells possessing conventional nuclear architecture with heterochromatin abutting the nuclear periphery and euchromatin located in the nuclear interior [28,30]. We have shown that the inverted nuclear architecture in rods has evolved as an adaptation to nocturnal vision: the heterochromatic cores of rod nuclei function as microlenses and reduce light scatter in ONL [30]. Unexpectedly, the nucleoplasm of the inverted rod nuclei is not stained by anti-MECP2 antibodies, and the central chromocenter is only weakly positive (Figure 1A).

In comparison to the multiple chromocenters characteristic of other mouse cell types, the single central chromocenter in mouse rods has a superior chromatin density, which is necessary for rod nuclei to function as microlenses

Table 2 List of antibodies for cell type identification in tissues other than the retina

| Cell type	Protein	Source, catalogue number
Smooth muscles	Calponin	Abcam, ab46794
Paneth cells	Lysozyme	Dako, A 0099
Enteroendocrine cells	Secretin	Santa Cruz, sc-26630
Goblet cells	Mucin-2	Santa Cruz, sc-15334
Satellite cells	Pax 7	DSHB

Dako (Troy, MI, USA).
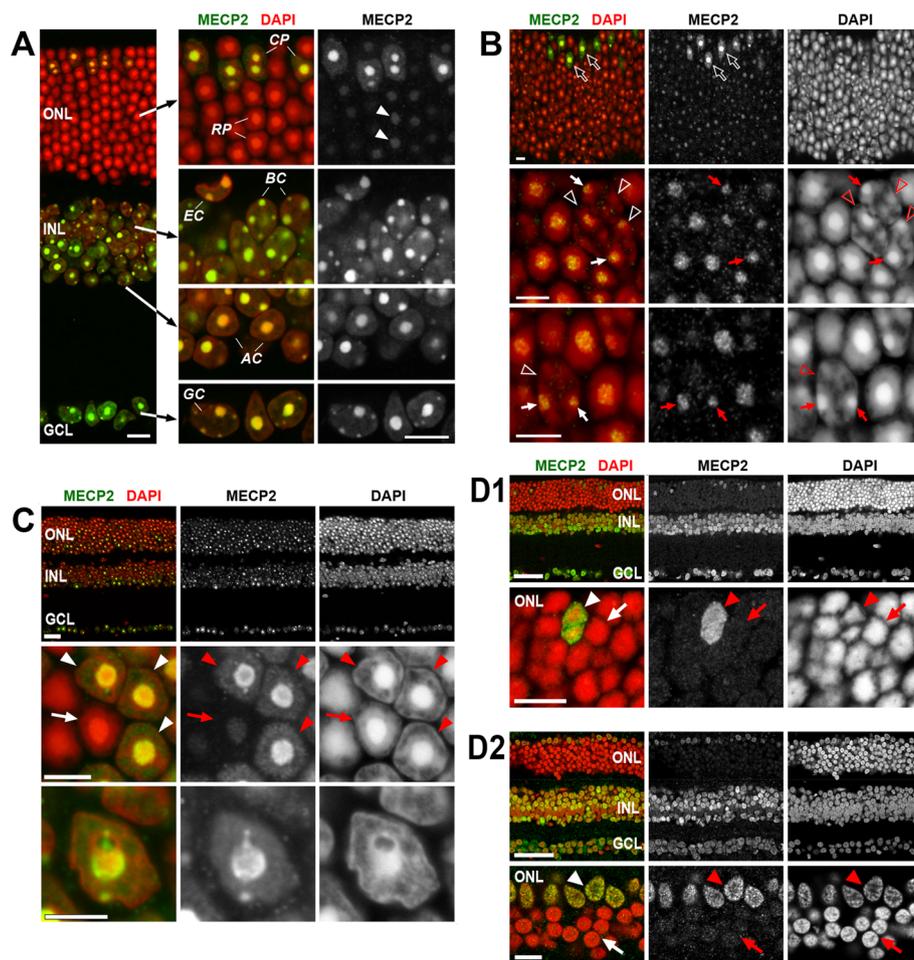
Figure 1 Distribution of MECP2 in the nuclei of retinal cells. (A) MECP2 is abundant in all retinal neurons: in the ganglion cell layer (GCL), inner nuclear cell layer (INL), in bipolar (BC) and amacrine (AC) cells. The signal is present throughout the whole nucleoplasm but is especially strong in chromocenters. In the ONL of adult mice, MECP2 produces a strong signal in cone photoreceptors (CP) whereas rod photoreceptors (RP) have very weak staining only noticeable in the chromocenters (*arrowheads*). **(B)** Restoration of conventional nuclear architecture in rod nuclei by *Lbr* expression in Lbr-TER mice does not increase MECP2 expression. In *Lbr*-expressing rods (three such nuclei are marked by *empty arrowheads*), there are multiple chromocenters adjacent to the nuclear periphery. These chromocenters (*arrows*) remain weakly MECP2-positive and with the staining intensity comparable to that of chromocenters in inverted nuclei not expressing *Lbr*. For comparison, bright staining of cone nuclei (*empty arrows*, left and middle upper panels) is shown. Note that all rods with multiple chromocenters adjacent to the nuclear periphery express *Lbr* (Solovei et al. [41]); LBR staining is not shown on this panel. **(C)** In R7E mice, rods de-differentiate, partially restore the conventional architecture of their nuclei, and lose their rod identity. This process is accompanied by increased expression of MECP2 which becomes abundant in chromocenters (three such nuclei are marked by *arrowheads*) and reaches the same level as in neuroretina (upper panel). For comparison, an unaltered rod nucleus is marked (*arrow*). **(D)** Retina of rat **(D1)** and macaque **(D2)**. Similarly to mice, MECP2 produces a bright signal in the GCL, INL, and cones (*arrowheads*) but is weak to undetectable in rod cells (*arrows*). Single confocal sections. Scale bars: (A) 10 μm; (B) 5 μm; (C) overview 25 μm, rods 5 μm; (D) overviews 50 μm, ONLs 10 μm.

[30]. This high chromatin compaction is obvious from recent electron microscopic studies (e.g., Figure two in [38] and Figure three panel a in [40]) and from the dramatic difference in immunostaining properties between rod chromocenters and chromocenters of other retinal neurons. As described in detail in the recent immunohistochemical studies [38-40], the chromocenter in rods requires much longer antigen retrieval in comparison to the neighboring cones and INL cells. Therefore, to rule out that weak MECP2 staining is caused by inaccessibility of chromocenter chromatin to the antibodies, we made use of transgenic mouse retinas in which rod cells ectopically express lamin B receptor (LBR). Rods expressing transgenic LBR acquire conventional nuclear architecture with euchromatin located to the nuclear interior and heterochromatin, including multiple chromocenters, located at the nuclear periphery. Chromocenters of these transgenic rods have apparently lower chromatin compaction and restore immunostaining ability typical for other retinal cells [41]. However, despite their reduced size and density, chromocenters in LBR-expressing rods remain as weakly MECP2-positive as the chromocenters of wild-type rods (Figure 1B).

The above observations are consistent with results of MECP2 staining in photoreceptors of R7E mice [42]. These transgenic mice specifically express CAG trinucleotide repeat encoding a polyglutamine stretch and represent a mouse model to study spinocerebellar ataxia type 7 (SCA7). In R7E mice, mature rods with inverted nuclei begin to de-differentiate in ca. 1-month-old animals, their nuclei partially restore a conventional nuclear architecture, and photoreceptors lose their rod identity [42]. MECP2 expression in R7E rods gradually increases in parallel to the de-differentiation, and at the age of 20 weeks, the MECP2 level in chromocenters reaches the level observed in the other neurons of the retina (Figure 1C).

Furthermore, we also tested for the presence of MECP2 in rods of two other mammalian species: (i) rat, a nocturnal mammal without chromocenters; and (ii) macaque, a diurnal primate with conventional nuclear architecture in rods. In both species, MECP2 was undetectable in rods, in a prominent difference to neuroretinal cells and cone photoreceptors where it produced a clear signal (Figure 1D). Taken together, the above data imply that weak expression of MECP2 is an intrinsic feature of rod photoreceptors.

The low level of MECP2 in rods can be tentatively connected to the relatively high level of linker histone H1c in rod cells described recently for mouse rod photoreceptors [43]. It has been shown that in the MECP2-rich neurons of the brain, approximately half of the linker histone H1 tends to be replaced by MECP2, and that in *Mecp2*-null mice, the H1 level in these neurons doubles [27]. Remarkably, triple KO mice deficient in linker H1c/H1e/H10 histone variants show significant increase of the rod nuclear diameter which was accompanied by decrease of the nuclear volume occupied by heterochromatin. These changes in the nuclear architecture were noticed only in rod nuclei [40]. The other way around, in de-differentiated rods of R7E mice, which demonstrate significantly reduced level of H1c [44,45], the expression of MECP2 increases (Figure 1C).

Microglial cells have no detectable MECP2

Non-neuronal cells of the retina—pigment epithelium, endothelial cells of blood vessels, and Müller cells (radial astroglia)—also expressed MECP2. The only exception was microglia where MECP2 was never detected by immunostaining (Figure 2A). Moreover, microglial cells, identified using anti-Iba1 antibodies, were negative for MECP2 staining not only in the retina but also in the brain, cerebellum and spinal cord (Figure 2A). In contrast, in astroglial cells (Figure 2B) and neurons (Figure 2C1, C2), nuclei are strongly positive after MECP2 staining. Absence of MECP2 in microglial cells revealed by immunostaining is especially intriguing in view of recent data on the involvement of microglial cells in the Rett phenotype [46] and questions the role of these cells in neuropathologic consequences of MECP2 deficiency. On the other hand, sensitivity of immunostaining is unquestionably lower than most of biochemical *in vitro* approaches, and therefore, one cannot wholly exclude that microglia cells express MECP2 at a level not detectable microscopically.

Retinas of *Mecp2*-null mice show no apparent defects

Absence of MECP2 impairs neuronal morphology and strongly affects functions of the brain [9]. The retina, as a compact and very regularly structured part of the CNS, represents an attractive model to study the possible effects of MECP2 on the nervous system development. Earlier, it was shown that in *Mecp2* knockout mice, decline in visual acuity, which was observed in late postnatal development, is caused by general silencing of the cortical circuitry [47]. However, major morphological characteristics of retinas in MECP2-deficient mice have not been yet reported. We dissected retinas of *Mecp2*$^{-/y}$ mice at different stages of retina maturation, at postnatal days P1, P7, P13, P30, and P53, and compared their histology to the retinas of wild-type littermates. We found that *Mecp2*$^{-/y}$ and WT retinas were not different with respect to the time of layer formation, thickness, and morphology of the layers at all five studied developmental stages (Additional file 2). In addition, we compared *Mecp2*$^{-/y}$ and *Mecp2*^{wt} retinas with respect to the distribution of various retinal markers. Twelve immunocytochemical markers specific for various amacrine, bipolar, ganglion, and horizontal cells, seven markers for inner plexiform layer (IPL) or/and outer plexiform layer (OPL), and markers for radial glia (Müller cells) and microglia (Table 1) were applied to retinas from adult *Mecp2*$^{-/y}$ and WT littermate mice. As shown in Figure 3A and Additional file 3, no noticeable differences in the distribution of certain neurons, synapses, and neurotransmitters were found between the two genotypes.

Nuclear architecture of neuronal nuclei in *Mecp2*-null mice is generally preserved

Since MECP2 is a methylation reader and apparently involved in heterochromatin formation [27,36], we checked whether its absence causes changes in the epigenetic landscape of rod and other retinal nuclei. We found that MECP2 deficiency did not have any microscopically visible effect on the presence and distribution of major histone modifications (Table 3). In *Mecp2*$^{-/y}$ mice, euchromatin marked by acetylated H3, H4, H3K9ac,me1, and H4K20ac, me1 was present in the nuclear interior of GCL and INL cells and in the outermost peripheral shell of rod nuclei, just as it was observed in WT mice (Figure 3B, Additional file 4). The presence of histone modifications H3K9me2,3 and H4K20me2,3, characteristic of heterochromatin, was restricted to the nuclear periphery and chromocenters
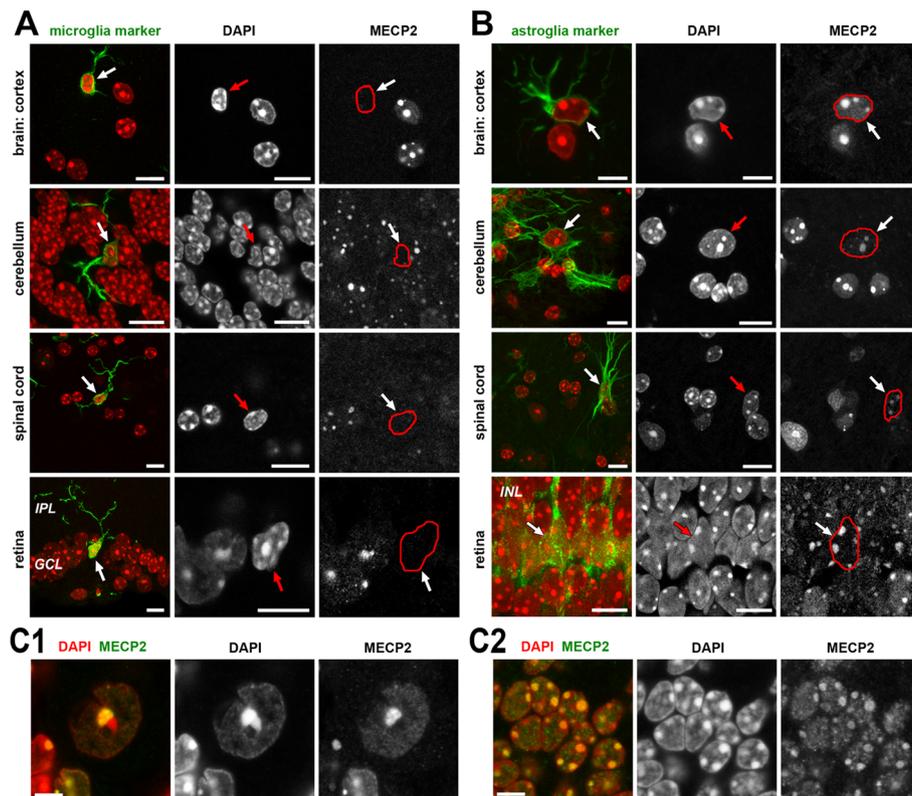
Figure 2 Microglial cells (A) have no detectable MECP2 compared to astroglia (B) and neurons (C). (A, **B)** MECP2 detection in brain cortex, cerebellum, spinal cord, and retina combined with microglial **(A)** and astroglial **(B)** cell type-specific staining. Overlays of 4',6-diamidino-2-phenylindole (DAPI) staining (*red*) with markers for microglia (Iba-1) and astroglia (GFAP) are shown in left columns as projections of short stacks. Middle and right columns show single optical sections (zoomed in) for DAPI and MECP2. Non-marked cells in the same images are predominantly neurons and strongly express MECP2. *Red outlines* in the right column images trace the shape of the nuclei of interest. **(C)** Neurons from cerebellum – Purkinje cells **(C1)** and granular cells **(C2)** demonstrate strong MECP2 staining in chromocenters and moderate staining of the nucleoplasm in a single confocal section. Scale bars: (A,B) 10 μm, (C) 5 μm.

of neuroretina cells and was also not different from the wild-type (Additional file 4; see also [38]).

Conversely, we checked whether erasing of the major heterochromatin hallmarks, H3K9me2,3 and H4K20me3, would prevent MECP2 binding. For this purpose, we studied retinas from mice lacking H4K20me3 due to deletion of Suv4-20 h2 and mice lacking both H4K20me3 and H3K9me3 due to deletion of Suv4-20 and Suv3-9 h1,2 methyltransferases. In mice of both genotypes, rod nuclei had the same morphology as the rod nuclei in the wild-type littermate controls [38]. We found that the pattern of MECP2 staining was not different between the retinal cells in the wild-type and knockout mice, suggesting that MECP2 binding to chromatin was not affected. Indeed, MECP2 was strongly expressed in neuroretina and cones, where it localizes mostly in chromocenters, and was almost undetectable in rods (Additional file 5). Recently, it was shown that deletion of Suv4-20 h2 influences chromatin organization in cultured cells, in particular, it increases the number of chromocenters in cultured fibroblasts derived from a *Suv3-9/Suv4-20 h* double knockout

mouse [48]. In contrast, double knockout of *Suv3-9* and *Suv4-20* affects neither rod nuclear morphology [38] nor MECP2 binding patterns (this study), suggesting that cells in a tissue context might have more redundancy in epigenetic mechanisms than cultured cells.

Although even a complete loss of MECP2 does not prevent chromocenter formation in mouse cells [8], observations on astroglial cells and neurons differentiated from embryonic stem cells *in vitro* showed that the number of chromocenters was significantly higher in MECP2-null cells compared to wild-type cells [36]. The other way around, ectopic expression of MECP2 induces clustering and fusion of chromocenters, a process which takes place during myotube differentiation [31]. These findings prompted us to assess rod chromocenter numbers in adult mice of both genotypes. Chromocenter fusion in nuclei of mouse rods is a slow process. A significant proportion of rods at ca. 1 month still have two or more chromocenters; their fusion in all rods is completed only at 2–2.5 months of age ([30,41]; c.f. Figure 3C2,C3). We scored cells with one
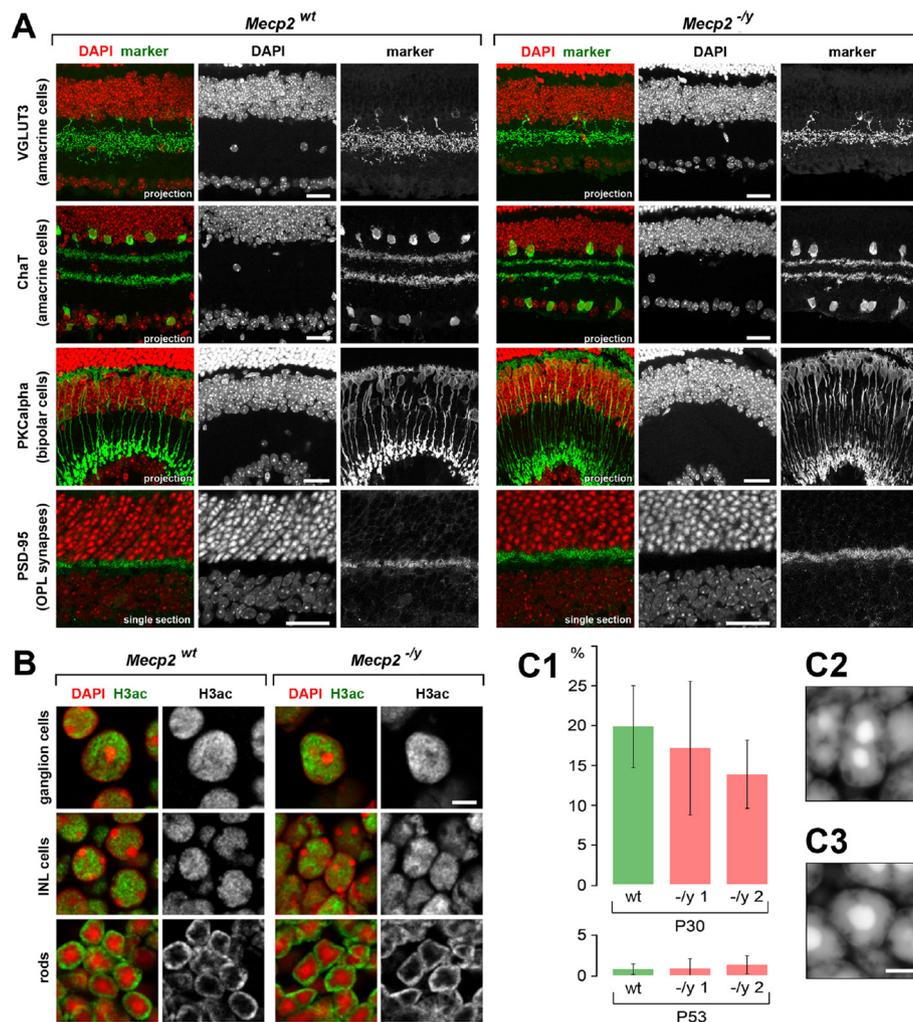
Figure 3 Retinas of *Mecp2*^{−/y} mice show no apparent defects. (A) Positioning of amacrine cells, rod bipolar cells, and photoreceptor synapses is similar in retinas of *Mecp2*^{−/y} and *Mecp2*^{lox/y} littermates. Other 14 markers for retinal cell types, synapses, and neurotransmitters are shown in Additional file 2. **(B)** Similar distribution of a histone modification typical of euchromatin (H3ac) in *Mecp2*^{−/y} and *Mecp2*^{wt} littermate retinas; nuclei with conventional (ganglion and INL cells) and inverted (rods) architecture are shown. **(C)** The proportions of rod nuclei with two or more chromocenters were scored in retinas of two *Mecp2*^{−/y} and one *Mecp2*^{wt} littermate at two age points, P30 and P53 **(C1)**. At P53, nearly all nuclei have a single chromocenter. Average proportions of rods with two or less chromocenters were not significantly different between the two genotypes. Errors bars are the 95% confidence intervals. Rod nuclei with two **(C2)** and one **(C3)** chromocenter. Scale bars: (A) 25 μm, (B) 5 μm, (C) 2 μm.

and two chromocenters in rod nuclei of *Mecp2*^{−/y} mice and their wild-type littermates at P30 and P53 (see the 'Methods' section for detailed description). The number of rods with two or more chromocenters in *Mecp2*^{−/y} mice of these ages was 15.5% at P30 and 1.2% at P53, which was not different from the wild-type (Figure 3C1).

In full agreement with our observations on rod cells, data obtained from cortical neurons in tissue sections and primary neuronal cultures indicate that chromocenter number is comparable between neurons from *Mecp2*^{−/y} and *Mecp2*^{+/y} mice [35]. Apparently, the difference in results obtained on cells in native tissues of *Mecp2*^{−/y} and *Mecp2*^{+/y} mice and on cultured cells derived from these mice [36] is

analogous to the observations on *Suv3-9/Suv4-20 h* double knockout cells and might be tentatively explained by compensatory mechanisms operating *in vivo* but not *in vitro*.

Almost all cell types in adult mammalian tissues express MECP2

The absence of MECP2 in microglia and its low level in rods raised the question of how common MECP2 is in various cell types. Data on MECP2 expression in different tissues are limited, and most reports are based on a bulk analysis of protein or RNA extracted from a whole tissue (e.g., [49,50]). Analyses of specific cell types are only occasional and predominantly concern neuronal tissues [49-51]. Therefore, we studied MECP2 distribution across

Table 3 List of antibodies for histone modification detection

Histone/residue	Modification	Source (catalogue number)
H3K9	Acetyl	HK (CMA310)
	Me1	HK (CMA316)
	Me2	HK (CMA317)
	Me3	HK (CMA318)
H4K20	Acetyl	HK (CMA420)
	Me1	HK (CMA421)
	Me2	HK (CMA422)
	Me3	HK (CMA423)
H3	Acetyl	Upstate (#06-599)
H4	Acetyl	Upstate (#06-866)

HK produced in the laboratory of Hiroshi Kimura, Osaka University (Osaka, Japan). Upstate (Lake Placid, NY, USA).

a number of mouse cell types. Cell identification was based either on histological criteria or, when needed, on cell type-specific immunostaining (for the list of antibodies used, see Table 2). Altogether, about 60 cell types were studied from 12 non-neuronal adult mouse tissues. In addition, epidermis and skeletal muscles were studied at five age points (P0, P2, P5, P9, and P14). The results of immunostaining are summarized in Figure 4A, and telling examples are shown in Figure 4B,C,D,E,F,G,H. We found that the majority of cell types express MECP2; those that do not are rather a minority. MECP2 is lacking in epithelial cells of the intestine and colon. In epidermis, the expression of MECP2 varies: it is absent or present at a hardly detectable level in keratinocytes of the trunk skin but is more abundant in lip epidermis cells, both basal and suprabasal. In the hair, proliferating matrix keratinocytes of the hair bulb lack MECP2 in clear difference to differentiated keratinocytes of hair shaft and hair root sheath where MECP2 produces a clear signal. MECP2 is also not expressed in the erythropoietic lineage, in contrast to other cells of the myeloid lineage and lymphocytes. A noteworthy exception are resident macrophages. As mentioned before, microglial cells in all studied nervous tissues do not express MECP2 at a detectable level (Figures 2A and 4A), whereas resident macrophages from other tissues, in particular, hepatic Kupffer cells, do express it (Figure 4A,H).

As MECP2 is primarily visible in the chromocenters of mouse cells, we studied MECP2 distribution in tissues of a species, which does not possess chromocenters in interphase nuclei. Rat chromosomes, in difference to mouse chromosomes, lack large blocks of pericentromeric satellite sequences, and consequently, rat nuclei have no clear chromocenters. Rat small intestine, skin with hairs, and skeletal and heart muscles were studied. Staining of these tissues confirmed that the gastrodermal epithelial and hair matrix cells in rat, similarly to mouse, lack MECP2,

whereas the nuclei of muscle cells (smooth, skeletal, and heart muscles) had a strong punctate MECP2 signal in the nucleoplasm (Figure 5). Our data support the notion that in addition to the functions in the nervous system that are associated with a major pathologic phenotype, MECP2 plays some important roles in almost all non-nervous tissues.

Involvement of MECP2 in chromatin regulation and maintenance of global nuclear architecture is well documented [27,52,53]. In particular, it is known that MECP2 plays a role in the regulation of transcription, being mostly a transcriptional repressor [54-56] and also an activator [54]. In the light of these findings, the fact that some cell types across different species are lacking MECP2 is intriguing and requires further analysis.

Expression of MECP2 increases during tissue development and terminal cell differentiation

There is a clear difference between MECP2 expression levels in tissues of different developmental stages. A telling example are fibroblasts of the dermal papilla in the hair bulb. These cells lack MECP2 at the late embryonic stages and in the first 2 days of postnatal development; the expression starts at P2 and continues afterwards (Figure 6D).

The expression of MECP2 in the retina starts at different times depending on the cell type. Remarkably, the onset of expression coincides with massive formation of synapses and, as a consequence, the formation of the IPL and OPL [57-59] (Figure 6A,B). In particular, MECP2 appears in the ganglion and amacrine cells at E17, when a clear gap appears between the GCL and INL + ONL anlage, marking the emerging IPL. Similarly, the MECP2 expression in the bipolar cells starts at P6 together with the formation of the gap between the INL and ONL, which develops into the OPL later. In rods, weak MECP2 expression starts after 2 weeks of postnatal development and remains weak thereafter (Figure 6A,C). Noteworthy, the onset of MECP2 expression roughly correlates with cell birthdays (the day of the last cell division; [60]) of the retinal neuronal cell types ($R_{Spearman} = 0.62$) and persists afterwards.

Initiation of MECP2 expression at late differentiation stages proved to be a general rule: undifferentiated or weakly differentiated cells (progenitors) do not express MECP2 or show a low expression level compared to the respective fully differentiated cells. In particular, matrix keratinocytes of the hair bulb do not express MECP2, the more differentiated keratinocytes of the hair shaft show a weak expression, and a stronger expression is observed in the keratinocytes at the root hair shaft. MECP2 is weak in satellite cells but abundant in the myotube nuclei (Figure 4A,F). The reverse situation occurs only in the gonads. In the ovaries, the follicle epithelium and the

A

tissue	cell type	staining intensity
brain	cortex neurons	+++
	astroglia	++
	microglia	-
cerebellum	Purkinje cells	+++
	granular cells	++
	Golgi cells	+++
	astroglia	+/++
spinal cord	neurons	+++
	astroglia	+/++
	microglia	-
retina	rod photoreceptors	+ w
	cone photoreceptors	+++
	neuroretina	+++
	Müller cells	++
	microglia	-
	pigment epithelium	+++
spleen	lymphocytes	+/++
	reticulocytes	+++
	late erythroblasts	-
	myeloblasts	-
	megakaryocytes	-
	spleen capsule cells	+++
liver	hepatocytes	+/++
	Kupffer cells	+++
	endothelial cells	+++
kidney	cells of collecting tubes	++
	cells of proximal and distal convoluted tubes	++
	cells of Henle's loop	++
	endothelial cells	+++
	cells of Bauman's capsule	++
	cells of kidney capsule	+++
small intestine	absorptive cells	-
	goblet cells	-
	enteroendocrine cells	-
	crypt regenerative cells	-
	Paneth cells	-
	smooth muscles	+++
colon	surface absorptive cells	-
	crypt goblet cells	-
	crypt regenerative cells	-
	smooth muscles	+++
heart muscles	cardiomyocytes	+++
	fibroblasts	+++
skeletal muscles *	nuclei of myotubes	+++ / +
	satellite cells **	++
trunk skin *	basal keratinocytes	+ w
	suprabasal keratinocytes	+ w
	dermal fibroblasts ***	+++
lips skin	basal keratinocytes	++
	suprabasal keratinocytes	++
hair *	dermal papilla ****	+++
	matrix keratinocytes	-
	hair shaft	+
	external root sheath	++
	connective tissue sheath	+++
testis	spermatogonia	-
	spermatocytes	-
	spermatids	-
	Sertoli cells	+++
	peritubular cells	+++
ovary	early oocytes	++
	late oocytes	-
	follicle epithelial cells	+++
	stromal cells	+++

Figure 4 Presence of MECP2 in different cell types of adult mouse tissues. (A) List of the studied tissues and cell types; the strength of MECP2 signal is shown by the number of plus signs (1 to 3). *Tissues studied at six developmental age points (P0, P2, P5, P9, and P14). **Satellite cells were negative at P0–P14. ***Dermal fibroblasts were negative at P0–P5. ****Fibroblasts of dermal papilla were negative at P0 and weakly positive at P2; see also Figure 5D. Examples of mouse tissues after MECP2 staining: intestine **(B, C)**, hair **(D)**, muscles **(E, F, G)**, and liver **(H)**. In **(C),** *empty arrows* point at MECP2-negative gastroepithelial cells in colon crypt; *empty arrowheads* point at positive smooth muscle nucleus beneath the gastrodermis. In **(D)**, *solid arrows* mark fibroblasts of the dermal papilla; *solid arrowheads* mark matrix keratinocytes of the hair bulb. For comparison of MECP2 staining in mouse and rat tissues, see Additional file 4. Single confocal sections. Scale bars: (B) 50 μm, (C, D) 10 μm, (E, F, G, H) 5 μm.

youngest oocytes express MECP2, whereas mature oocytes do not (Figure 7A). Sertoli cells and fibroblasts are MECP2 positive, whereas spermatogenic cells do not express MECP2 at any stage (Figure 7B). The absence of MECP2 immunostaining in mature gametes conforms to the known fact that zygotes, stem cells, and cells of young embryos [61-63] lack MECP2. In summary, our results indicate that MECP2 is a marker of the differentiated state.

Absence of MECP2 is not compensated by altered expression of other MBD proteins in cultured cells and native tissues

Considering the specific binding of MECP2 to methyl-ated DNA, we questioned whether other proteins are able to replace MECP2 on 5-methylcytosine (5mC) in case of its absence. Though this has not been systematically investigated, the question has been addressed genetically
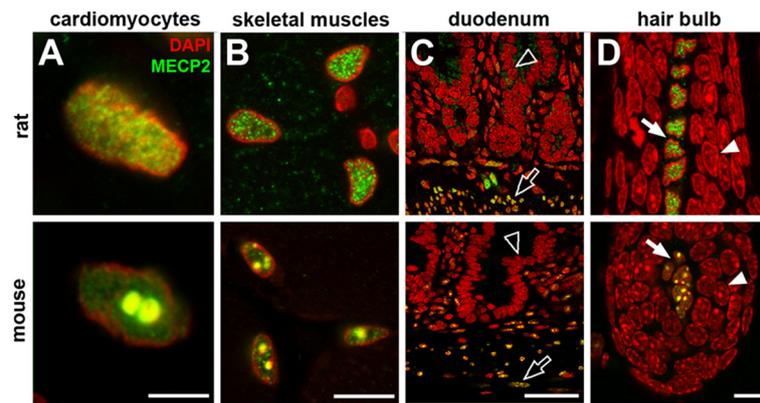
Figure 5 Comparison of MECP2 staining in selected mouse and rat tissues. Nuclei of striated muscle cells (**A**, cardiomyocytes; **B**, skeletal myotubes), smooth muscles (**C**, *empty arrows* in duodenum), and fibroblasts of dermal papilla (**D**, *solid arrows*) have strong MECP2 signal in both species. Similarly, gastrodermal epithelial cells (*empty arrowheads*) and matrix keratinocytes (*solid arrowheads*) lack MECP2 in both species. Single confocal sections. Scale bars: (A) 5 μm, (B, D) 10 μm, (C) 25 μm.

by Caballero and co-authors [64]. The authors showed that simultaneous deficiency of three methyl-CpG binding proteins MECP2, MBD2, and KAISO in mice is compatible with normal embryogenesis and provided evidence for redundancy of function between these proteins in postnatal mice. Since antibodies to other methyl-CpG binding proteins reliably working on cryosections are lacking, we quantitatively studied the expression level of all known 5mC-binding proteins in $Mecp2^{-/y}$ cultured cells and tissues by reverse transcription quantitative polymerase chain reaction (RT-qPCR). We focused on an expression analysis of the following methyl binding proteins: four MBD proteins, MBD1, MBD2, MBD3, and MBD6 (MBD4 and MBD5 were omitted due to the nearly undetectable expression level); UHRF1 and UHRF2; SETDB1; and three methyl-CpG binding zinc finger proteins, namely, ZBTB33, ZBTB38, and ZBTB4. First, we analyzed the expression of all the above genes in adult $Mecp2^{-/y}$, adult $Mecp2^{lox/y}$, and embryonic wild-type fibroblasts. The analyzed genes were transcribed at different levels in embryonic and adult fibroblasts. In particular, we noted a statistically significant decrease in the expression of *Mbd1* and *Mbd6*, *Uhrf1* and *Uhrf2*, *Zbtb33* and *Zbtb4*, and *Setdb1* in the embryonic fibroblasts compared to the adult cultured fibroblasts. However, we found no apparent difference in gene expression between the adult $Mecp2^{lox/y}$ and $Mecp2^{-/y}$ fibroblasts (Figure 8A). Similarly, comparison of gene expression in the skeletal muscle, heart, and small intestine did not reveal any differences between tissues from $Mecp2^{-/y}$ and $Mecp2^{wt}$ mice (Additional file 6). Unexpectedly, in the $Mecp2^{-/y}$ brain and liver, the expression of these proteins (e.g., MBD2) was even significantly decreased (Figure 8B,C). Thus, we demonstrated that absence of MECP2 is not compensated by any other known 5mC binding protein at least at the mRNA level.

Conclusions

Based on the above discussion, the following conclusions were made:

- All retinal neurons, except rods, express MECP2 at a high level and the onset of its expression coincides with neuron differentiation, in particular, with massive formation of neural synapses in the inner and outer plexiform layers.
- Low expression of MECP2 in rod photoreceptors was found in both the inverted rod nuclei of nocturnal mammals and the conventional rod nuclei of diurnal mammals. We relate this fact to an unusually high level of histone H1c in these cells in comparison to other retinal neurons [43].
- MECP2 is not detectable by immunostaining in the retinal microglial cells, nor in the microglia of the cortex, cerebellum, and spinal cord. In contrast to microglia, the astroglial cells in all neuronal tissues express MECP2 at a level comparable to that in neurons.
- The retina of *Mecp2*-null mice shows no apparent defects in the timing and morphology of the nuclear and plexiform layer formation. No noticeable difference in the distribution of certain neuron types, synapses, and neurotransmitters was found between *Mecp2*-null and wild-type retinas.
- The nuclear architecture of the neuroretinal cells and rod photoreceptors is generally preserved in *Mecp2*-null mice; in particular, there are no obvious changes in the distribution of pericentromeric heterochromatin and major epigenetic markers characteristic for eu- and heterochromatin.
- MECP2 is expressed in the majority of studied 64 non-neuronal cell types; cells which do not express MECP2 are epithelial cells of the intestine, cells of
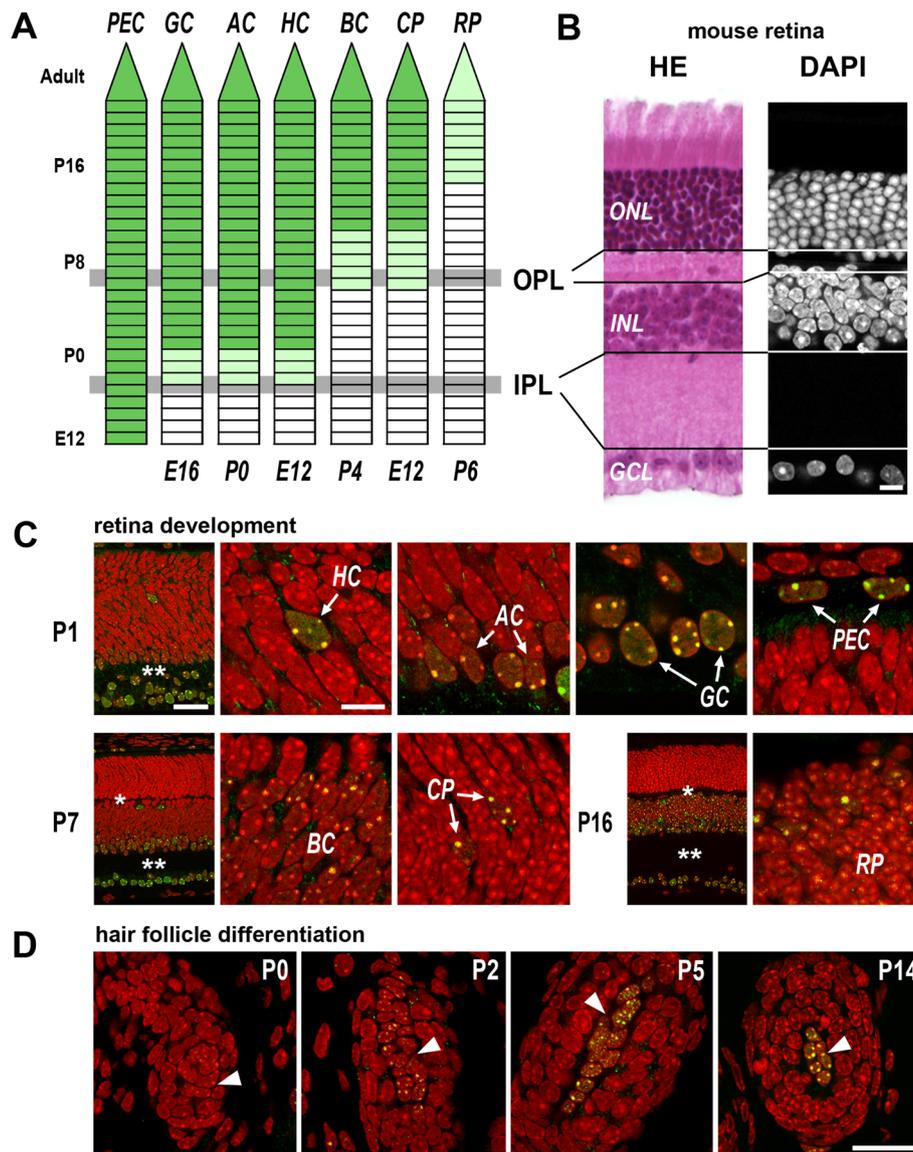
Figure 6 Expression of MECP2 during development and terminal cell differentiation. (A) The onset of MECP2 expression (*green*) in different cell types of mouse retina. Time lines are shown for pigment epithelial cells (PEC), ganglion cells (GC), amacrine cells (AC), horizontal cells (HC), bipolar cells (BC), cone photoreceptor (CP), and rod photoreceptor (RP). On the left, postnatal age points are shown; numbers below the time lines show the cell birthdays (the day of the last cell division; [60]). *Grey horizontal lines* mark age points when the outer and inner plexiform layers (OPL and IPL, respectively) become detectable (see also [57-59]). Light *green* marks a low MECP2 level. The onset of MECP2 expression in neurons coincides with massive formation of synapses and, consequently, IPL and OPL plexi. **(B)** Arrangement of the nuclear and plexiform layers in mouse retina revealed in a paraffin section after hemalaun-eosin staining and in a cryosection after nuclear counterstain with DAPI. The perikarya of GCs are located in the GCL; those of BCs, ACs, and HCs are in the INL; and those of the photoreceptors are in the ONL. **(C)** Examples of retinal cells (marked by *arrows*) with initiated MECP2 expression at three age stages. *Single* and *double asterisks* mark OPL and IPL, respectively; the abbreviations are the same as in (A). For comparison with adult mouse retina, see Figure 1A. **(D)** In the fibroblasts of the dermal papilla (*arrowheads*) of the hair follicle, MECP2 expression is initiated postnatally and becomes detectable at P2; later, the MECP2 expression in these cells remains stably high (see also Figure 4A,D). (C, D) Single confocal sections. Scale bars: (B) 10 μm; (C) overviews 50 μm, close-ups 10 μm; (D) 25 μm.

the erythropoietic lineage, hair matrix keratinocytes, and mature gonads; epidermis keratinocytes express MECP2 at a very low level.

- Similarly to neurons, the expression of MECP2 in non-neuronal cells is initiated at the late differentiation stages; in this respect, gonads show a reverse pattern

with no expression in differentiated oocytes and spermatozoids.

- An absence of MECP2 is not compensated by increased expression of other methyl binding proteins; in contrast, expression of some of them was downregulated.
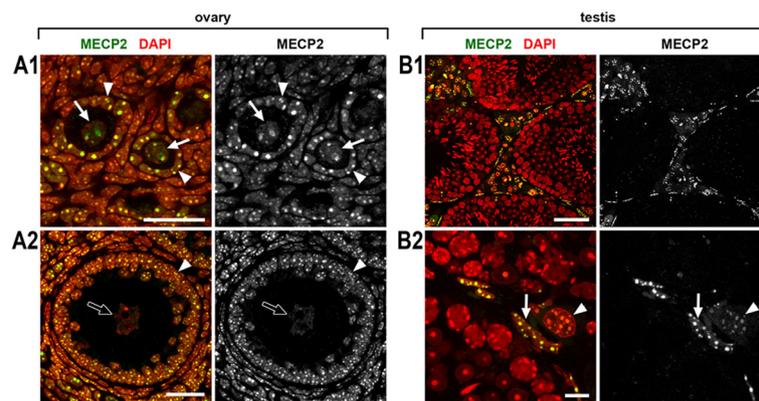
Figure 7 Expression of MECP2 in the ovary (A) and testis (B). Only young oocytes (**A1**, *arrows*) express MECP2; the more mature oocytes (**A2**) do not express MECP2 (**A2**, *empty arrow*). Neighboring follicular cells (*arrowheads*) strongly express MECP2. In testis, only Sertoli cells (**B2**, *arrowhead*) and fibroblasts (**B2**, *arrows*) express MECP2; spermatocytes at all stages of maturation and sperm cells are MECP2-negative. Single confocal sections. Scale bars: (A1, A2) 25 μm, (B1) 50 μm, (B2) 10 μm.

Methods

Animals and primary cell cultures

All procedures were approved by the Animal Ethic Committee of Munich University and Edinburgh University. CD1, C57Bl/6, and *Mecp2*-null mice were killed by cervical dislocation according to the standard protocol. *Mecp2*$^{-/y}$ mice (described in [9]; Jackson Laboratory stock number: 003890) were generated along with wild-type littermates by crossing *Mecp2*$^{+/-}$ females with wild-type male mice. The generation of mice ectopically expressing LBR in rod cells under the control of the *Nrl* promoter is described in [41]. Retinas of R7E mice [42] were studied at the age of 70 weeks. Retinas from mice with combined deletions of *Suv3-9* and *Suv4-20* were a kind gift from G. Schotta (University of Munich). Wild-type littermate controls for all genetically modified mice were studied in parallel. Tail fibroblast cell lines from *Mecp2*$^{-/y}$ and *Mecp2*$^{lox/y}$ mice are described in [9].

Tissues, fixation, and cryosections

The retinas of the ICR/CD1 mice were studied on each day between E12 and P28. The retinas of *Mecp2*$^{-/y}$ mice and their WT littermates were studied at the ages of P1, P7, P14, P30, and P53. Retina fixation, embedding in freezing medium, and preparation of cryosections were performed as described previously [38,39]. Briefly, the eyes were enucleated immediately after death; the retinas were dissected and fixed with 4% formaldehyde in phosphate-buffered saline (PBS) for various times (15 min, 30 min, 1 h, 3 h, and 24 h). After washing in PBS, the samples were infiltrated in 10%, 20%, and 30% sucrose in PBS before freezing in Jung freezing medium. Importantly, the retina samples at different ages, from WT and transgenic mice, and of various fixation times, were arranged in respective order in the same block to assure identification of all retina samples in a section [39]. Retinas from

monkey (*Macaca fascicularis*) and rat (*Rattus norvegicus*) were *post mortem* experimental materials from the MPI for Brain Research (Frankfurt, Germany). Other tissue samples from adult C57Bl/6 mice and rats were fixed with 4% formaldehyde in PBS for 24 h. For some tissues, the samples from different developmental stages – P0, P2, P5, P9, P14, and P28 – were used.

Immunostaining on cryosections

Immunostaining was performed according to the protocol described in detail by [38,39]. This protocol allows quick testing of a wide range of fixation and antigen retrieval times and detection of the range in which the results of staining are robust. Antigen retrieval was crucial for robust MECP2 staining and was performed by heating cryosections in 10 mM sodium citrate buffer at 80°C. MECP2 detection after 12–24 h of tissue fixation was most successful after 20–30 min of antigen retrieval. For MECP2 immunostaining, mostly rabbit polyclonal antibodies were used. Specificity of the antibody was checked using fibroblasts derived from *Mecp2*$^{-/y}$ and *Mecp2*$^{lox/y}$ mice (Additional file 1). In some cases, rat monoclonal antibodies were used as well [65]. The antibodies for cell type identification and for recognition of retinal structures are listed in Tables 1 and 3. Antibodies for the detection of histone modifications are listed in Table 2. Secondary antibodies were anti-mouse IgG conjugated to Alexa555 (A31570, Invitrogen, Renfrew, UK) or Alexa488 (A21202, Invitrogen), and anti-rabbit IgG conjugated to DyLight549 (711-505-152, Jackson ImmunoResearch, West Grove, PA, USA) or DyLight488 (711-485-152, Jackson ImmunoResearch). The nuclei were counterstained with DAPI added to the secondary antibody solution. After staining, the sections were mounted under a coverslip with Vectashield (Vector Laboratories, Inc., Burlingame, CA, USA).
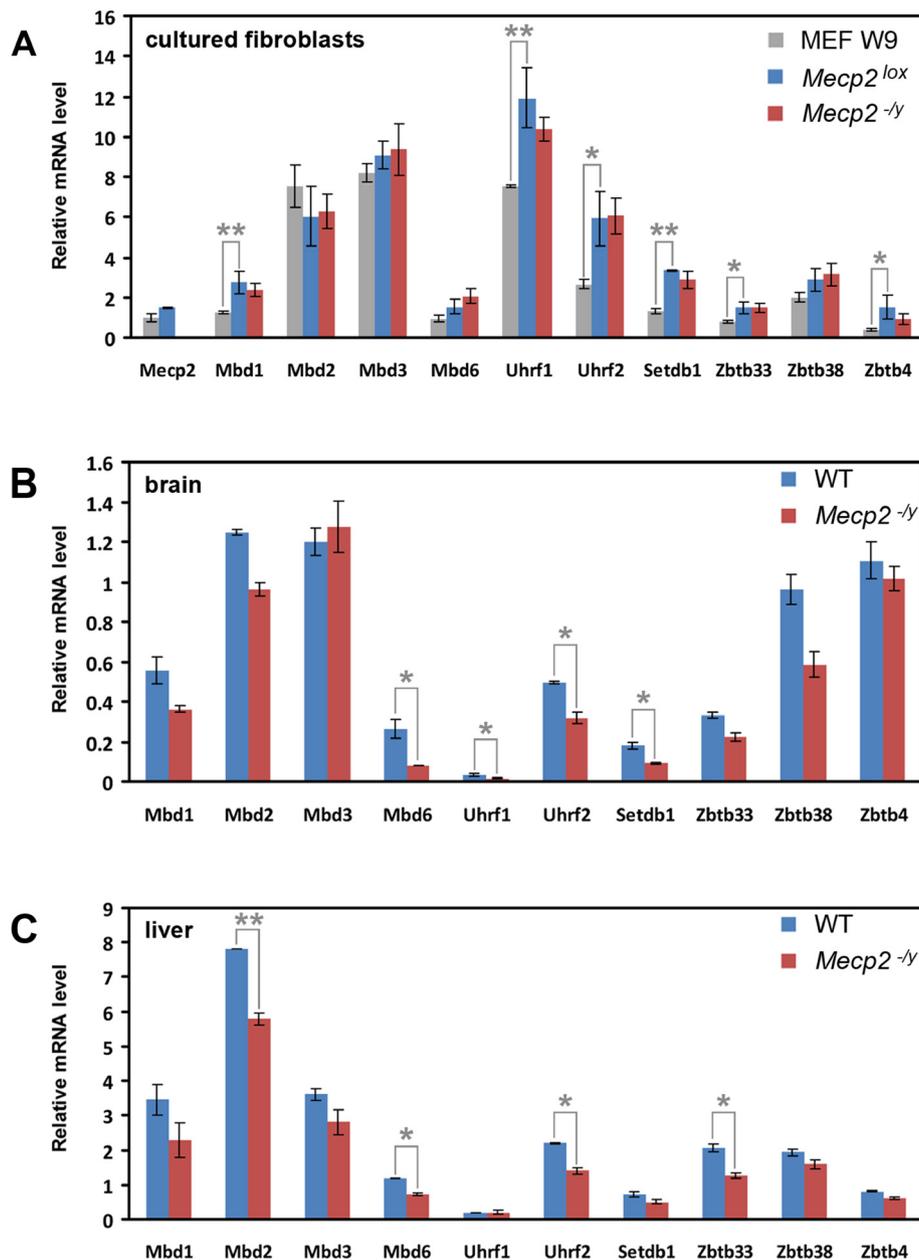
Figure 8 Analysis of expression of MBD proteins in cultured fibroblasts and tissues from *Mecp2$^{-/y}$* and wild-type mice. (A) Relative transcription level of MBD proteins in wild-type embryonic fibroblasts (MEF W9) and adult fibroblasts established from *Mecp2$^{-/y}$* and littermate *Mecp2$^{lox/y}$* mice. Values are normalized to the *Mecp2* transcript in the embryonic fibroblasts. Note that the mRNA levels in the embryonic and adult fibroblasts differ, whereas no difference in transcription was detected between *Mecp2$^{-/y}$* and *Mecp2$^{lox/y}$* genotypes. Relative transcription level of MBD proteins in the brain **(B)** and liver **(C)** from *Mecp2$^{-/y}$* and littermate *Mecp2^{wt}* mice. Values are normalized to the *Mecp2* transcript in the respective *Mecp2^{wt}* tissue. Note that there is no upregulation of MBD protein genes upon deletion of *Mecp2*. Results of real-time PCR analysis of two (for tissues) and three (for cells) biological replicates are given as mean ± S.E.M. Statistical difference between values was estimated by *t* test; statistically significant differences in transcription levels are marked by *asterisks* (*<0.05; **<0.01).

Light microscopy

Single optical sections or stacks of optical sections were collected using a Leica TCS SP5 confocal microscope (Milton Keynes, UK) equipped with Plan Apo 63×/1.4 NA oil immersion objective and lasers with excitation lines 405, 488, and 561 nm. Dedicated plug-ins in the ImageJ program were used to compensate for axial chromatic shift between fluorochromes in confocal stacks, to create RGB stacks/images, and to arrange optical sections into galleries [66,67].

Table 4 List of primers used for real-time PCR

Gene	Forward	Reverse
Mbd1*	GAGCACAGAGAATCGCCTTC	CACACCCCACAGTCCTCTTT
Mbd2*	CTGGCAAGATACCTGGGAAA	TTCCGGAGTCTCTGCTTGTT
Mbd3*	AGAAGAACCCTGGTGTGTGG	TGTACCAGCTCCTCCTGCTT
Mbd4*	ACAGGATGGCTCTGAAATGC	TCTACTTGTGTCCGTGGGATG
Mbd5 isoform 1**	GAGGCCATGAGCGAACTG	TCTTCCTCCTCTTGGGTTTG
Mbd6**	CCCGGGGATAGTCAGAAAGT	AGCTGCTCGCGTTGTAGG
Mecp2*	CAGGCAAAGCAGAAACATCA	GCAAGGTGGGGTCATCATAC
Zbtb33	ATCATTAGCTCCAGTCCAGACTCA	ATCTGCATCTTCTGTGTCAATGATC
Zbtb38*	CATCTTTTGGAGCCATACGATCT	TGACGGTTTCCTGTCTTTTGAC
Zbtb4	CCCTGCCGCTACTGTGAGA	CAGCAGAAGATGCACTGGTACCT
Setdb1	GGCCATTCCTCCCCTACTTC	GGCCAAAGGTGACCGATATG
Uhrf1	GGCAGCTGAAGCGGATGA	CCATGCACCGAAGATATTGTCA
Uhrf2UHRF2	CATGGTCGCAGCAATGATG	CACCGCTTCCAGTATACGTGAA
Gapdh	CATGGCCTTCCGTGTTCCTA	CTTCACCACCTTCTTGATGTCATC

Single asterisk denotes that the sequence was taken from [64]. *Double asterisks* signify that the sequence was taken from [69].

Chromocenter scoring

Chromocenters in the rod cells were scored at two age points, P30 and P53. For each age, three mice were used, two $Mecp2^{-/y}$ and one $Mecp2^{+/y}$ littermate. From each animal 25-μm-thick cryosections were prepared from the three retina areas: central, mid, and peripheral. To distinguish between individual nuclei in tightly packed rod perikarya, the nuclear envelope of rod cells was stained with anti-lamin B1 antibodies (sc-6217). Between 600 and 800 rod cell nuclei were scored in stacks collected from each retina area. Descriptive statistics was performed using SigmaStat software.

RNA isolation and RT-qPCR

The tissue samples of *Mecp2*-null mice were collected in 'RNAlater' (Qiagen, Venlo, Netherlands) and stored at −20°C. Isolation of RNA and reverse transcription were carried out as described previously [68]. Primers for RT-qPCR were either designed with the Primer Express software (Applied Biosystems Inc., Foster City, CA, USA) or used as previously published (Table 4). RT-qPCR was performed on the 7500 Fast Real-Time PCR System (Applied Biosystems) at standard reaction conditions using the *Power* SYBR Green PCR Master Mix (Applied Biosystems). Gene expression levels were normalized to *Gapdh* and calculated using the comparative CT method (ΔΔCT method). Relative quantification of gene expression was performed by the $2^{-\Delta\Delta CT}$ method based on the CT values of both target and reference genes. The results of the real-time PCR analysis of two (tissues) and three (cells) biological replicates are given as mean ± S.E.M. The statistical difference between the values was estimated by *t* test using SSPS.

Additional files

Additional file 1: Immunostaining and Western blot analysis with rabbit anti-MECP2 antibody. Specificity of the rabbit anti-MECP2 antibody and its application for Western blot analysis of MECP2 level in different mouse tissues.

Additional file 2: $Mecp2^{-/y}$ and $Mecp2^{wt}$ retinas at different developmental stages. $Mecp2^{-/y}$ and $Mecp2^{wt}$ littermate retinas are not different with respect to the time of layer formation, thickness of nuclear and plexiform layers, and other morphological features.

Additional file 3: Distribution of neurons, synapses, and neurotransmitters in $Mecp2^{wt}$ and $Mecp2^{-/y}$ retinas. Retinas of $Mecp2^{-/y}$ mice show no apparent defects in the distribution of neurons, synapses, and neurotransmitters in comparison to $Mecp2^{wt}$ littermates.

Additional file 4: Distribution of histone modifications in ganglion and INL cells of $Mecp2^{wt}$ and $Mecp2^{-/y}$ retinas. Similar distribution of histone modifications characteristic of euchromatin and heterochromatin in $Mecp2^{-/y}$ and $Mecp2^{wt}$ mice.

Additional file 5: MECP2 expression in retinal cells from Suv3-9/Suv4-20 double KO mice. Similar to WT mouse retina, rods of double KO mice express MECP2 at a very low level, whereas other retinal neurons strongly express MECP2.

Additional file 6: Gene expression analysis of MBD proteins in $Mecp2^{-/y}$ and wild-type mice. Relative transcription levels of MBD proteins were determined by RT-qPCR in gut, skeletal muscles and heart of $Mecp2^{-/y}$ and $Mecp2^{wt}$ mice.

Abbreviations

BDNF: Brain-derived neurotrophic factor; GCL: Ganglion cell layer; INL: Inner nuclear layer; MBD: Methyl binding domain; MECP2: Methyl-CpG binding protein 2; ONL: Outer nuclear layer; OPL: Outer plexiform layer; IPL: Plexiform layer; SCA7: Spinocerebellar ataxia type 7; WT: Wild-type.

Competing interests

The authors declare that they have no competing interests.

Authors' contributions

CS performed immunostainings, confocal microscopy, RT-qPCR experiments, and data analysis. YF performed immunostainings and confocal microscopy and contributed to manuscript writing. JG collected eye samples and tissues for RT-qPCR. LP supplied antibodies against neural tissues and contributed to manuscript writing. KLJ supplied anti-MECP2 antibodies and performed Western

blot analysis. HK supplied antibodies against histone modifications. MCC contributed to the study design and manuscript writing. AB contributed to manuscript writing. HL contributed to manuscript writing. BJ and IS designed and supervised the study; performed immunostainings, confocal microscopy, and data analysis; and wrote the paper. All authors read and approved the final manuscript.

Author details
[1]Department of Biology II, Center for Integrated Protein Science Munich (CIPSM), Ludwig Maximilians University Munich, Grosshadernerstrasse 2, 82152 Planegg-Martinsried, Germany. [2]Wellcome Trust Centre for Cell Biology, University of Edinburgh, EH9 3JR Edinburgh, UK. [3]Max Planck Institute for Brain Research, Max-von-Laue-Str. 4, Frankfurt am Main 60438, Germany. [4]Cell Biology and Epigenetics, Department of Biology, Technische Universität Darmstadt, Schnittspahnstr. 10, Darmstadt 64287, Germany. [5]Graduate School of Frontier Biosciences, Osaka University, 1-3 Yamadaoka, 565-0871 Suita, Osaka, Japan.

References
1. Lewis JD, Meehan RR, Henzel WJ, Maurer-Fogy I, Jeppesen P, Klein F, Bird A: **Purification, sequence, and cellular localization of a novel chromosomal protein that binds to methylated DNA.** *Cell* 1992, **69**:905–914.
2. Amir RE, Van den Veyver IB, Wan M, Tran CQ, Francke U, Zoghbi HY: **Rett syndrome is caused by mutations in X-linked MECP2, encoding methyl-CpG-binding protein 2.** *Nat Genet* 1999, **23**:185–188.
3. Chahrour M, Zoghbi HY: **The story of Rett syndrome: from clinic to neurobiology.** *Neuron* 2007, **56**:422–437.
4. Gonzales ML, LaSalle JM: **The role of MeCP2 in brain development and neurodevelopmental disorders.** *Curr Psychiatry Rep* 2010, **12**:127–134.
5. Moretti P, Zoghbi HY: **MeCP2 dysfunction in Rett syndrome and related disorders.** *Curr Opin Genet Dev* 2006, **16**:276–281.
6. Pinto D, Delaby E, Merico D, Barbosa M, Merikangas A, Klei L, Thiruvahindrapuram B, Xu X, Ziman R, Wang Z, Vorstman JA, Thompson A, Regan R, Pilorge M, Pellecchia G, Pagnamenta AT, Oliveira B, Marshall CR, Magalhaes TR, Lowe JK, Howe JL, Griswold AJ, Gilbert J, Duketis E, Dombroski BA, De Jonge MV, Cuccaro M, Crawford EL, Correia CT, Conroy J, *et al*: **Convergence of genes and cellular pathways dysregulated in autism spectrum disorders.** *Am J Hum Genet* 2014, **94**:677–694.
7. Bird A: **The methyl-CpG-binding protein MeCP2 and neurological disease.** *Biochem Soc Trans* 2008, **36**:575–583.
8. Chen RZ, Akbarian S, Tudor M, Jaenisch R: **Deficiency of methyl-CpG binding protein-2 in CNS neurons results in a Rett-like phenotype in mice.** *Nat Genet* 2001, **27**:327–331.
9. Guy J, Hendrich B, Holmes M, Martin JE, Bird A: **A mouse Mecp2-null mutation causes neurological symptoms that mimic Rett syndrome.** *Nat Genet* 2001, **27**:322–326.
10. Shahbazian MD, Zoghbi HY: **Rett syndrome and MeCP2: linking epigenetics and neuronal function.** *Am J Hum Genet* 2002, **71**:1259–1272.
11. Cobb S, Guy J, Bird A: **Reversibility of functional deficits in experimental models of Rett syndrome.** *Biochem Soc Trans* 2010, **38**:498–506.
12. Giacometti E, Luikenhuis S, Beard C, Jaenisch R: **Partial rescue of MeCP2 deficiency by postnatal activation of MeCP2.** *Proc Natl Acad Sci USA* 2007, **104**:1931–1936.
13. Guy J, Gan J, Selfridge J, Cobb S, Bird A: **Reversal of neurological defects in a mouse model of Rett syndrome.** *Science* 2007, **315**:1143–1147.
14. Luikenhuis S, Giacometti E, Beard CF, Jaenisch R: **Expression of MeCP2 in postmitotic neurons rescues Rett syndrome in mice.** *Proc Natl Acad Sci USA* 2004, **101**:6033–6038.
15. Chao HT, Zoghbi HY, Rosenmund C: **MeCP2 controls excitatory synaptic strength by regulating glutamatergic synapse number.** *Neuron* 2007, **56**:58–65.
16. Smrt RD, Eaves-Egenes J, Barkho BZ, Santistevan NJ, Zhao C, Aimone JB, Gage FH, Zhao X: **Mecp2 deficiency leads to delayed maturation and altered gene expression in hippocampal neurons.** *Neurobiol Dis* 2007, **27**:77–89.
17. Zhou Z, Hong EJ, Cohen S, Zhao WN, Ho HY, Schmidt L, Chen WG, Lin Y, Savner E, Griffith EC, Hu L, Steen JA, Weitz CJ, Greenberg ME: **Brain-specific phosphorylation of MeCP2 regulates activity-dependent Bdnf transcription, dendritic growth, and spine maturation.** *Neuron* 2006, **52**:255–269.
18. Dani VS, Chang Q, Maffei A, Turrigiano GG, Jaenisch R, Nelson SB: **Reduced cortical activity due to a shift in the balance between excitation and inhibition in a mouse model of Rett syndrome.** *Proc Natl Acad Sci U S A* 2005, **102**:12560–12565.
19. Wood L, Gray NW, Zhou Z, Greenberg ME, Shepherd GM: **Synaptic circuit abnormalities of motor-frontal layer 2/3 pyramidal neurons in an RNA interference model of methyl-CpG-binding protein 2 deficiency.** *J Neurosci* 2009, **29**:12440–12448.
20. Medrihan L, Tantalaki E, Aramuni G, Sargsyan V, Dudanova I, Missler M, Zhang W: **Early defects of GABAergic synapses in the brain stem of a MeCP2 mouse model of Rett syndrome.** *J Neurophysiol* 2008, **99**:112–121.
21. Ballas N, Lioy DT, Grunseich C, Mandel G: **Non-cell autonomous influence of MeCP2-deficient glia on neuronal dendritic morphology.** *Nat Neurosci* 2009, **12**:311–317.
22. Chen WG, Chang Q, Lin Y, Meissner A, West AE, Griffith EC, Jaenisch R, Greenberg ME: **Derepression of BDNF transcription involves calcium-dependent phosphorylation of MeCP2.** *Science* 2003, **302**:885–889.
23. Tao J, Hu K, Chang Q, Wu H, Sherman NE, Martinowich K, Klose RJ, Schanen C, Jaenisch R, Wang W, Sun YE: **Phosphorylation of MeCP2 at Serine 80 regulates its chromatin association and neurological function.** *Proc Natl Acad Sci USA* 2009, **106**:4882–4887.
24. Tudor M, Akbarian S, Chen RZ, Jaenisch R: **Transcriptional profiling of a mouse model for Rett syndrome reveals subtle transcriptional changes in the brain.** *Proc Natl Acad Sci USA* 2002, **99**:15536–15541.
25. Maezawa I, Swanberg S, Harvey D, LaSalle JM, Jin LW: **Rett syndrome astrocytes are abnormal and spread MeCP2 deficiency through gap junctions.** *J Neurosci* 2009, **29**:5051–5061.
26. Maezawa I, Jin LW: **Rett syndrome microglia damage dendrites and synapses by the elevated release of glutamate.** *J Neurosci* 2010, **30**:5346–5356.
27. Skene PJ, Illingworth RS, Webb S, Kerr AR, James KD, Turner DJ, Andrews R, Bird AP: **Neuronal MeCP2 is expressed at near histone-octamer levels and globally alters the chromatin state.** *Mol Cell* 2010, **37**:457–468.
28. Joffe B, Leonhardt H, Solovei I: **Differentiation and large scale spatial organization of the genome.** *Curr Opin Genet Dev* 2010, **20**:562–569.
29. Naumova N, Dekker J: **Integrating one-dimensional and three-dimensional maps of genomes.** *J Cell Sci* 2010, **123**:1979–1988.
30. Solovei I, Kreysing M, Lanctot C, Kosem S, Peichl L, Cremer T, Guck J, Joffe B: **Nuclear architecture of rod photoreceptor cells adapts to vision in mammalian evolution.** *Cell* 2009, **137**:356–368.
31. Brero A, Easwaran HP, Nowak D, Grunewald I, Cremer T, Leonhardt H, Cardoso MC: **Methyl CpG-binding proteins induce large-scale chromatin reorganization during terminal differentiation.** *J Cell Biol* 2005, **169**:733–743.
32. Gilbert N, Thomson I, Boyle S, Allan J, Ramsahoye B, Bickmore WA: **DNA methylation affects nuclear organization, histone modifications, and linker histone binding but not chromatin compaction.** *J Cell Biol* 2007, **177**:401–411.
33. Matsumura S, Persson LM, Wong L, Wilson AC: **The latency-associated nuclear antigen interacts with MeCP2 and nucleosomes through separate domains.** *J Virol* 2010, **84**:2318–2330.
34. Probst AV, Okamoto I, Casanova M, El Marjou F, Le Baccon P, Almouzni G: **A strand-specific burst in transcription of pericentric satellites is required for chromocenter formation and early mouse development.** *Dev Cell* 2010, **19**:625–638.
35. Singleton MK, Gonzales ML, Leung KN, Yasui DH, Schroeder DI, Dunaway K, LaSalle JM: **MeCP2 is required for global heterochromatic and nucleolar changes during activity-dependent neuronal maturation.** *Neurobiol Dis* 2011, **43**:190–200.
36. Bertulat B, De Bonis ML, Della Ragione F, Lehmkuhl A, Milden M, Storm C, Jost KL, Scala S, Hendrich B, D'Esposito M, Cardoso MC: **MeCP2 dependent heterochromatin reorganization during neural differentiation of a novel Mecp2-deficient embryonic stem cell reporter line.** *PLoS One* 2012, **7**:e47848.

37. Guy J, Cheval H, Selfridge J, Bird A: The role of MeCP2 in the brain. *Annu Rev Cell Dev Biol* 2011, **27**:631–652.

38. Eberhart A, Feodorova Y, Song C, Wanner G, Kiseleva E, Furukawa T, Kimura H, Schotta G, Leonhardt H, Joffe B, Solovei I: Epigenetics of eu- and heterochromatin in inverted and conventional nuclei from mouse retina. *Chromosome Res* 2013, **21**:535–554.

39. Eberhart A, Kimura H, Leonhardt H, Joffe B, Solovei I: Reliable detection of epigenetic histone marks and nuclear proteins in tissue cryosections. *Chromosome Res* 2012, **20**:849–858.

40. Popova EY, Grigoryev SA, Fan Y, Skoultchi AI, Zhang SS, Barnstable CJ: Developmentally regulated linker histone H1c promotes heterochromatin condensation and mediates structural integrity of rod photoreceptors in mouse retina. *J Biol Chem* 2013, **288**:17895–17907.

41. Solovei I, Wang AS, Thanisch K, Schmidt CS, Krebs S, Zwerger M, Cohen TV, Devys D, Foisner R, Peichl L, Herrmann H, Blum H, Engelkamp D, Stewart CL, Leonhardt H, Joffe B: LBR and lamin A/C sequentially tether peripheral heterochromatin and inversely regulate differentiation. *Cell* 2013, **152**:584–598.

42. Helmlinger D, Hardy S, Abou-Sleymane G, Eberlin A, Bowman AB, Gansmuller A, Picaud S, Zoghbi HY, Trottier Y, Tora L, Devys D: Glutamine-expanded ataxin-7 alters TFTC/STAGA recruitment and chromatin structure leading to photoreceptor dysfunction. *PLoS Biol* 2006, **4**:e67.

43. Siegert S, Cabuy E, Scherf BG, Kohler H, Panda S, Le YZ, Fehling HJ, Gaidatzis D, Stadler MB, Roska B: Transcriptional code and disease map for adult retinal cell types. *Nat Neurosci* 2012, **15**:487–495. S481-482.

44. Abou-Sleymane G, Chalmel F, Helmlinger D, Lardenois A, Thibault C, Weber C, Merienne K, Mandel JL, Poch O, Devys D, Trottier Y: Polyglutamine expansion causes neurodegeneration by altering the neuronal differentiation program. *Hum Mol Genet* 2006, **15**:691–703.

45. Kizilyaprak C, Spehner D, Devys D, Schultz P: The linker histone H1C contributes to the SCA7 nuclear phenotype. *Nucleus* 2011, **2**:444–454.

46. Derecki NC, Cronk JC, Lu Z, Xu E, Abbott SB, Guyenet PG, Kipnis J: Wild-type microglia arrest pathology in a mouse model of Rett syndrome. *Nature* 2012, **484**:105–109.

47. Durand S, Patrizi A, Quast KB, Hachigian L, Pavlyuk R, Saxena A, Carninci P, Hensch TK, Fagiolini M: NMDA receptor regulation prevents regression of visual cortical function in the absence of Mecp2. *Neuron* 2012, **76**:1078–1090.

48. Hahn M, Dambacher S, Dulev S, Kuznetsova AY, Eck S, Wörz S, Sadic D, Schulte M, Mallm JP, Maiser A, Debs P, von Melchner H, Leonhardt H, Schermelleh L, Rohr K, Rippe K, Storchova Z, Schotta G: Suv4-20 h2 mediates chromatin compaction and is important for cohesin recruitment to heterochromatin. *Genes Dev* 2013, **27**:859–872.

49. Shahbazian MD, Antalffy B, Armstrong DL, Zoghbi HY: Insight into Rett syndrome: MeCP2 levels display tissue- and cell-specific differences and correlate with neuronal maturation. *Hum Mol Genet* 2002, **11**:115–124.

50. Tochiki KK, Cunningham J, Hunt SP, Geranton SM: The expression of spinal methyl-CpG-binding protein 2: DNA methyltransferases and histone deacetylases is modulated in persistent pain states. *Mol Pain* 2012, **8**:14.

51. Darwanto A, Kitazawa R, Mori K, Kondo T, Kitazawa S: MeCP2 expression and promoter methylation of cyclin D1 gene are associated with cyclin D1 expression in developing rat epididymal duct. *Acta Histochem Cytochem* 2008, **41**:135–142.

52. Agarwal N, Becker A, Jost KL, Haase S, Thakur BK, Brero A, Hardt T, Kudo S, Leonhardt H, Cardoso MC: MeCP2 Rett mutations affect large scale chromatin organization. *Hum Mol Genet* 2011, **20**:4187–4195.

53. Baker SA, Chen L, Wilkins AD, Yu P, Lichtarge O, Zoghbi HY: An AT-hook domain in MeCP2 determines the clinical course of Rett syndrome and related disorders. *Cell* 2013, **152**:984–996.

54. Chahrour M, Jung SY, Shaw C, Zhou X, Wong ST, Qin J, Zoghbi HY: MeCP2, a key contributor to neurological disease, activates and represses transcription. *Science* 2008, **320**:1224–1229.

55. Nan X, Campoy FJ, Bird A: MeCP2 is a transcriptional repressor with abundant binding sites in genomic chromatin. *Cell* 1997, **88**:471–481.

56. Nan X, Ng HH, Johnson CA, Laherty CD, Turner BM, Eisenman RN, Bird A: Transcriptional repression by the methyl-CpG-binding protein MeCP2 involves a histone deacetylase complex. *Nature* 1998, **393**:386–389.

57. Fisher LJ: Development of synaptic arrays in the inner plexiform layer of neonatal mouse retina. *J Comp Neurol* 1979, **187**:359–372.

58. Johnson J, Tian N, Caywood MS, Reimer RJ, Edwards RH, Copenhagen DR: Vesicular neurotransmitter transporter expression in developing postnatal rodent retina: GABA and glycine precede glutamate. *J Neurosci* 2003, **23**:518–529.

59. Sherry DM, Wang MM, Bates J, Frishman LJ: Expression of vesicular glutamate transporter 1 in the mouse retina reveals temporal ordering in development of rod vs. cone and ON vs. OFF circuits. *J Comp Neurol* 2003, **465**:480–498.

60. Young RW: Cell differentiation in the retina of the mouse. *Anat Rec* 1985, **212**:199–205.

61. Huntriss J, Hinkins M, Oliver B, Harris SE, Beazley JC, Rutherford AJ, Gosden RG, Lanzendorf SE, Picton HM: Expression of mRNAs for DNA methyltransferases and methyl-CpG-binding proteins in the human female germ line, preimplantation embryos, and embryonic stem cells. *Mol Reprod Dev* 2004, **67**:323–336.

62. Kantor B, Makedonski K, Shemer R, Razin A: Expression and localization of components of the histone deacetylases multiprotein repressory complexes in the mouse preimplantation embryo. *Gene Expr Patterns* 2003, **3**:697–702.

63. Lin SL, Chang DC, Lin CH, Ying SY, Leu D, Wu DT: Regulation of somatic cell reprogramming through inducible mir-302 expression. *Nucleic Acids Res* 2011, **39**:1054–1065.

64. Caballero MI, Hansen J, Leaford D, Pollard S, Hendrich BD: The methyl-CpG binding proteins Mecp2, Mbd2 and Kaiso are dispensable for mouse embryogenesis, but play a redundant function in neural differentiation. *PLoS One* 2009, **4**:e4315.

65. Jost KL, Rottach A, Milden M, Bertulat B, Becker A, Wolf P, Sandoval J, Petazzi P, Huertas D, Esteller M, Kremmer E, Leonhardt H, Cardoso MC: Generation and characterization of rat and mouse monoclonal antibodies specific for MeCP2 and their use in X-inactivation studies. *PLoS One* 2011, **6**:e26499.

66. Ronneberger O, Baddeley D, Scheipl F, Verveer PJ, Burkhardt H, Cremer C, Fahrmeir L, Cremer T, Joffe B: Spatial quantitative analysis of fluorescently labeled nuclear structures: problems, methods, pitfalls. *Chromosome Res* 2008, **16**:523–562.

67. Walter J, Joffe B, Bolzer A, Albiez H, Benedetti PA, Muller S, Speicher MR, Cremer T, Cremer M, Solovei I: Towards many colors in FISH on 3D-preserved interphase nuclei. *Cytogenet Genome Res* 2006, **114**:367–378.

68. Szwagierczak A, Bultmann S, Schmidt CS, Spada F, Leonhardt H: Sensitive enzymatic quantification of 5-hydroxymethylcytosine in genomic DNA. *Nucleic Acids Res* 2010, **38**:e181.

69. Laget S, Joulie M, Le Masson F, Sasai N, Christians E, Pradhan S, Roberts RJ, Defossez PA: The human proteins MBD5 and MBD6 associate with heterochromatin but they do not bind methylated DNA. *PLoS One* 2010, **5**:e11982.

Specificity of rabbit-anti-MECP2 antibody (A) and its application for Western blot analysis of MECP2 level in different mouse tissues (B).

A. Immunostaining of cultured primary fibroblasts derived from *Mecp2$^{-/y}$* and *Mecp2$^{lox/y}$* mice. Chromocenters are stained with rabbit-anti-MECP2 antibody (green) in *Mecp2$^{lox/y}$* but not in *Mecp2$^{-/y}$* fibroblast nuclei which indicates to specificity of the antibody used. Chromocenters (arrows) comprise AT-rich major satellite repeat and consequently brightly stained with DAPI (red).
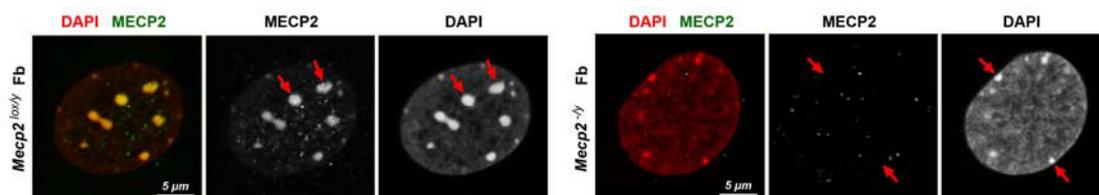
B. Western blot analysis of MECP2 level in different mouse tissues.
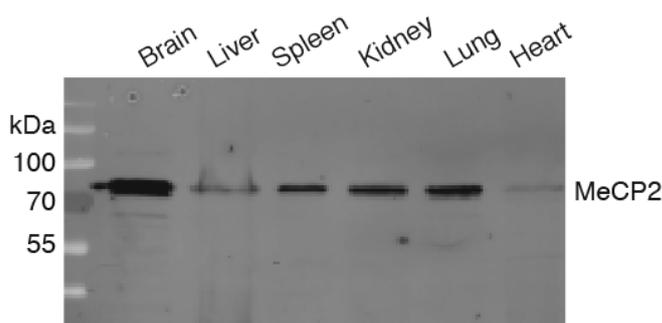
Nuclei were isolated as previously described (*Prusov, A.N. and Zatsepina, O.V. (2002) Isolation of the chromocenter fraction from mouse liver nuclei. Biochemistry (Mosc), 67, 423-431*). In short, mouse tissues were dissected, frozen with liquid nitrogen and pulverized using a mortar (3g tissue each), and homogenized in 15 ml buffer A (20 mM TEA, 30 mM KCl, 10 mM MgCl$_2$, 0.25 M sucrose) using a douncer. The homogenate was centrifuged for 10 min at 1000g using a Eppendorf Centrifuge 5810 R (rotor A 462), The resulting pellets were resuspended in buffer B (identical with A but containing 2.5 M sucrose) to a final concentration of 2.1 M sucrose, and centrifuged at 50.000g (SW28 rotor in a Beckmann ultracentrifuge L8-70 M") for 40 min with slow deceleration/acceleration. Resulting nuclei pellets were washed in 20 ml of buffer A and centrifuged at 1000 g for 10 min. All steps were carried out at 4°C. The obtained pellet contained mostly nuclei; the purity of the fraction was controlled by phase contrast microscopy (Zeiss Axioplan 200). Nuclei isolation yielded approx. 1x10^7 (brain, spleen, lung) and 1x10^8 nuclei (liver, kidney, heart) per sample. Proteins were extracted using RIPA buffer and subsequently boiled in Laemmli sample buffer. Proteins were separated on a 10% SDS-PAGE and western blot analysis was performed using affinity purified rabbit polyclonal anti-MeCP2 antibody (1:500) and secondary anti-rabbit antibody conjugated to Alexa 488 (*Jost KL, Rottach A, Milden M, Bertulat B, Becker A, et al. (2011) Generation and Characterization of Rat and Mouse Monoclonal Antibodies Specific forMeCP2 and Their Use in X-Inactivation Studies. PLoS ONE 6(11): e26499*).

Additional file 2.

Mecp2$^{-/y}$ and *Mecp2*^{wt} littermate retinas are not different with respect to the time of the layers formation, thickness of nuclear and plexiform layers, and other morphological features at postnatal ages P1, P7, P13, P30, and P53.

ONL, outer nuclear layer; INL, inner nuclear layer; GCL, ganglion cell layer; IPL, inner plexiform layer; OPL, outer plexiform layer. Single confocal sections. Scale bar: 50 µm
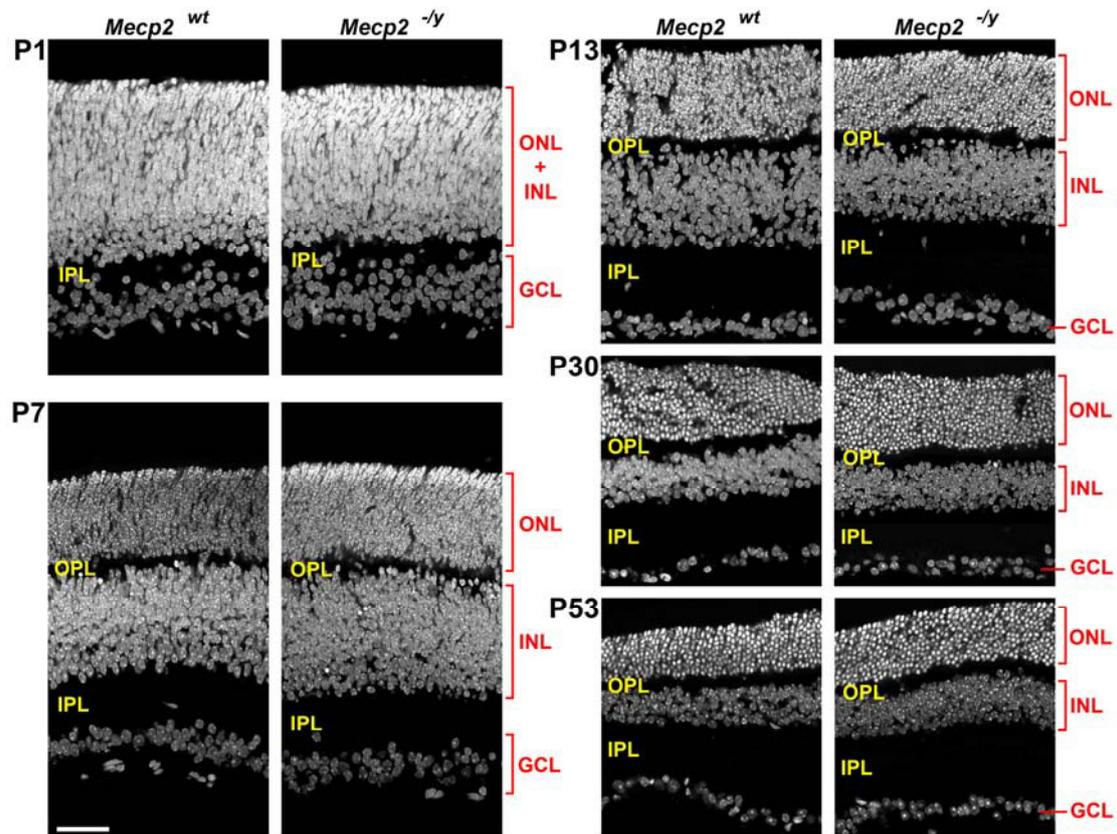
Additional file 3 (A, B).

Retinas of *Mecp2^{-/y}* mice show no apparent defects in the distribution of neurons, synapses, and neurotransmitters in comparison to *Mecp2^{wt}* littermates

Four other marker stainings are shown on Figure 3A. See Table 1 for structures selectively marked by immunostaining and for the source of the antibodies.

Additional file 3A:
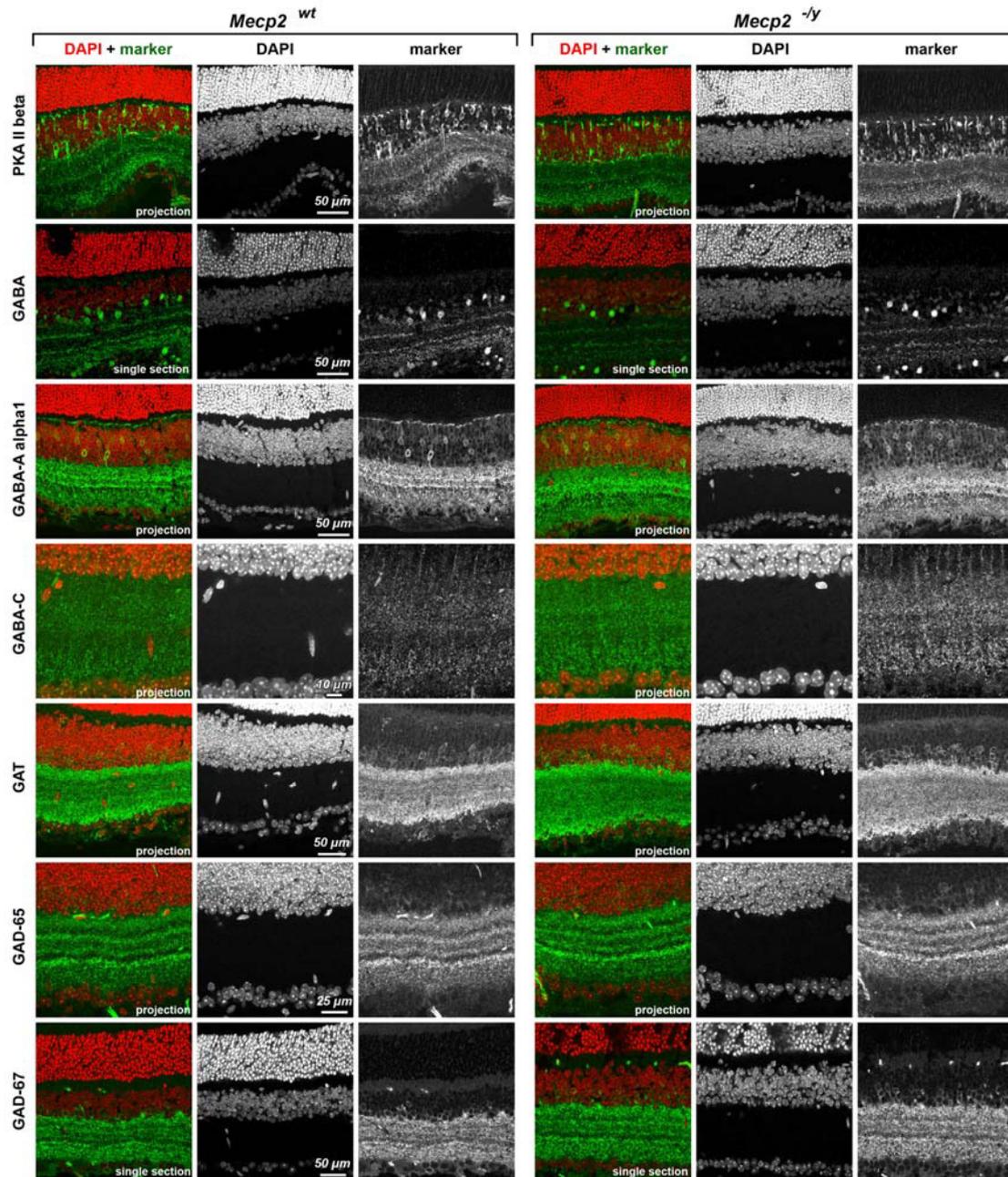
Additional file 3B:
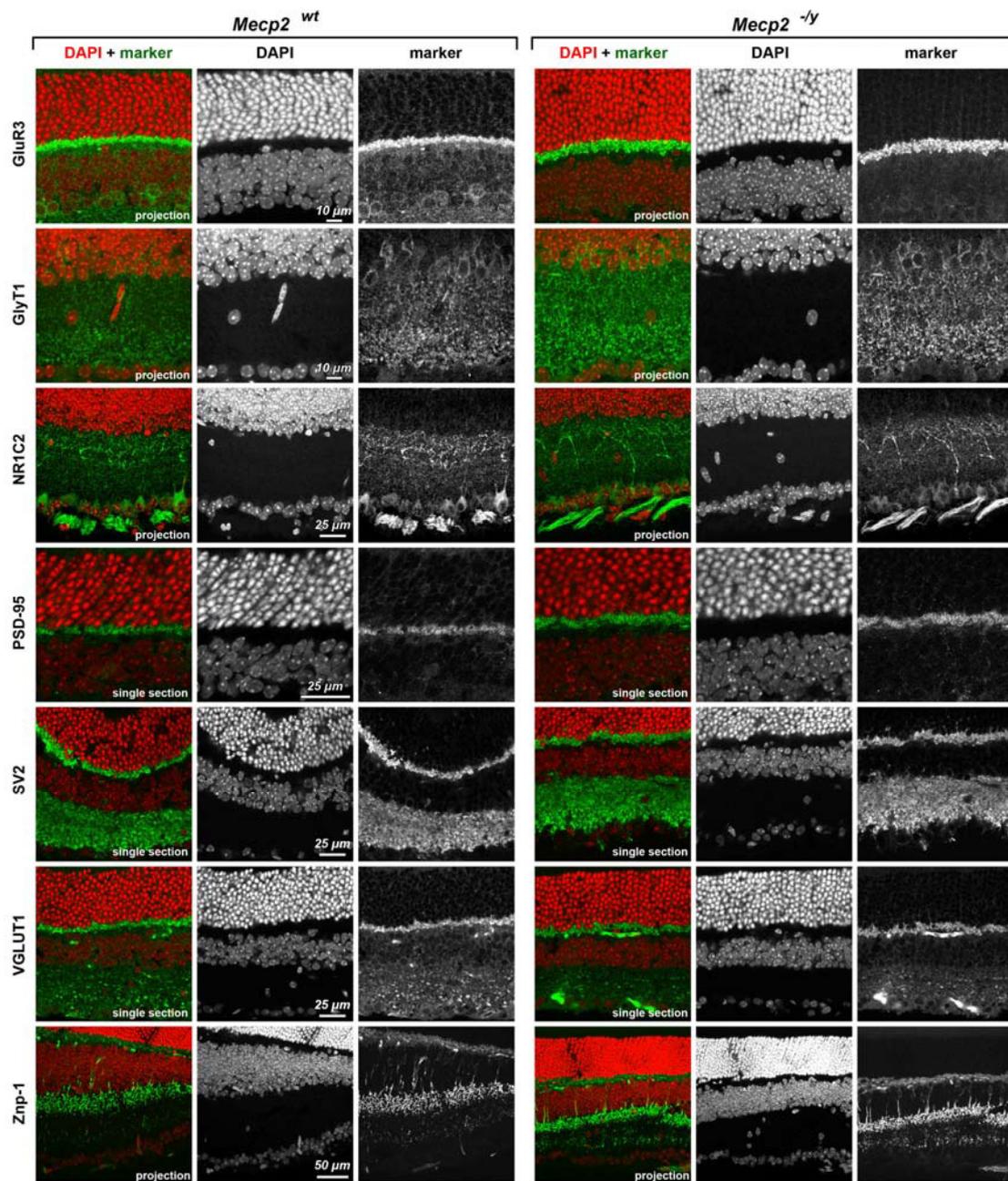
Similar distribution of histone modifications characteristic of euchromatin and heterochromatin in *Mecp2* [-/y] and *Mecp2* [wt]

Nuclei with conventional architecture, ganglion and INL cells, are shown. Histone modifications and DAPI nuclear counterstain are shown in green and red, respectively. Single confocal sections. Scale bars: 5 µm
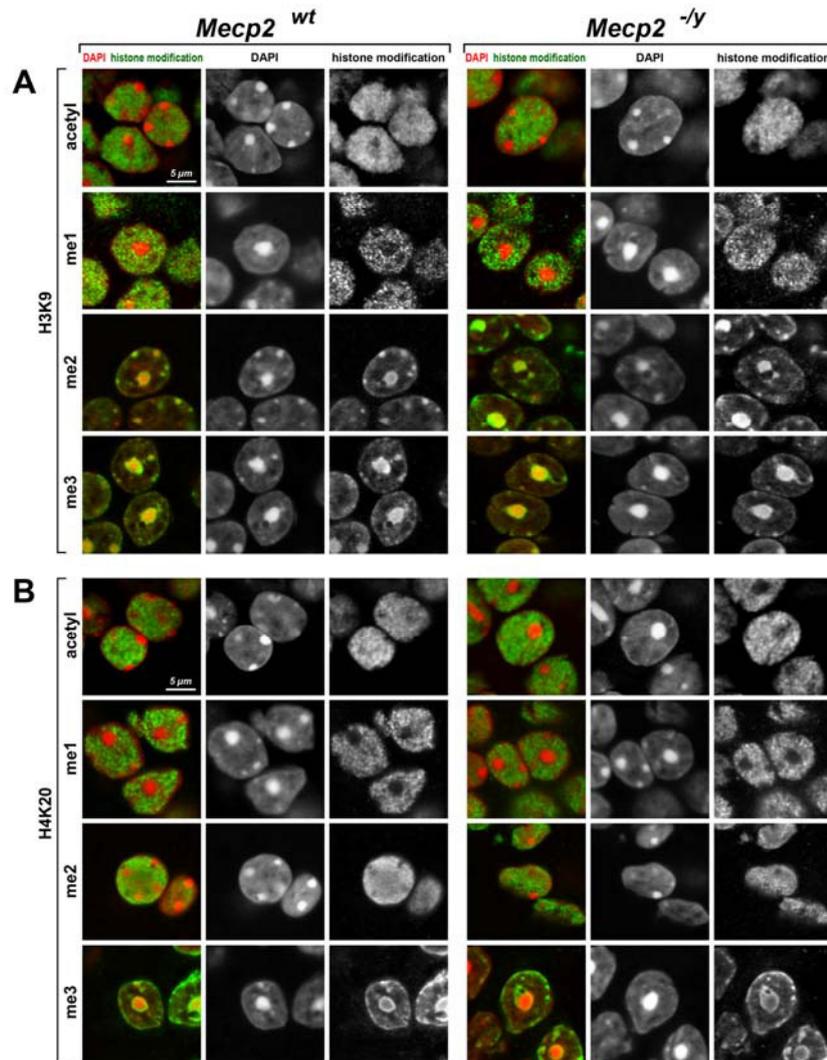
Additional file 5.

Expression of MECP2 in retinal cells from double KO mice with combined deletion of *Suv3-9* and *Suv4-20*

Similar to WT mouse retina, rods of double KO mice (arrowheads) express MeCP2 at a very low level, whereas cones (arrows) in ONL and other neurons from INL and GCL strongly express MeCP2. Note typical distribution of MeCP2 in nuclei (compare with WT retina cells on Figure 1A). Single confocal sections. Scale bars: upper panel, 25 µm; middle and lower panels, 5 µm
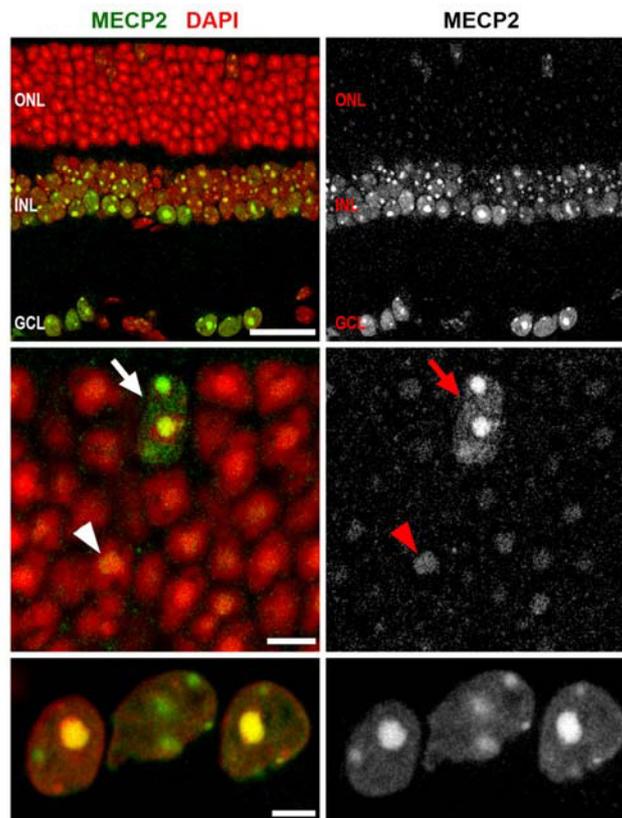
Additional file 6.

Analysis of expression of MBD proteins in three tissues from *Mecp2*^{-/y} and *Mecp2*^{wt} mice

Relative transcription level of MBD proteins in gut (A), skeletal muscles (B), and heart (C) from *Mecp2*^{-/y} and littermate *Mecp2*^{wt} mice. Values are normalized to transcript of *Mecp2* in *Mecp2*^{wt} of respective tissue. Note that there are no statistically significant changes in transcription of MBD protein genes upon deletion of *Mecp2*.
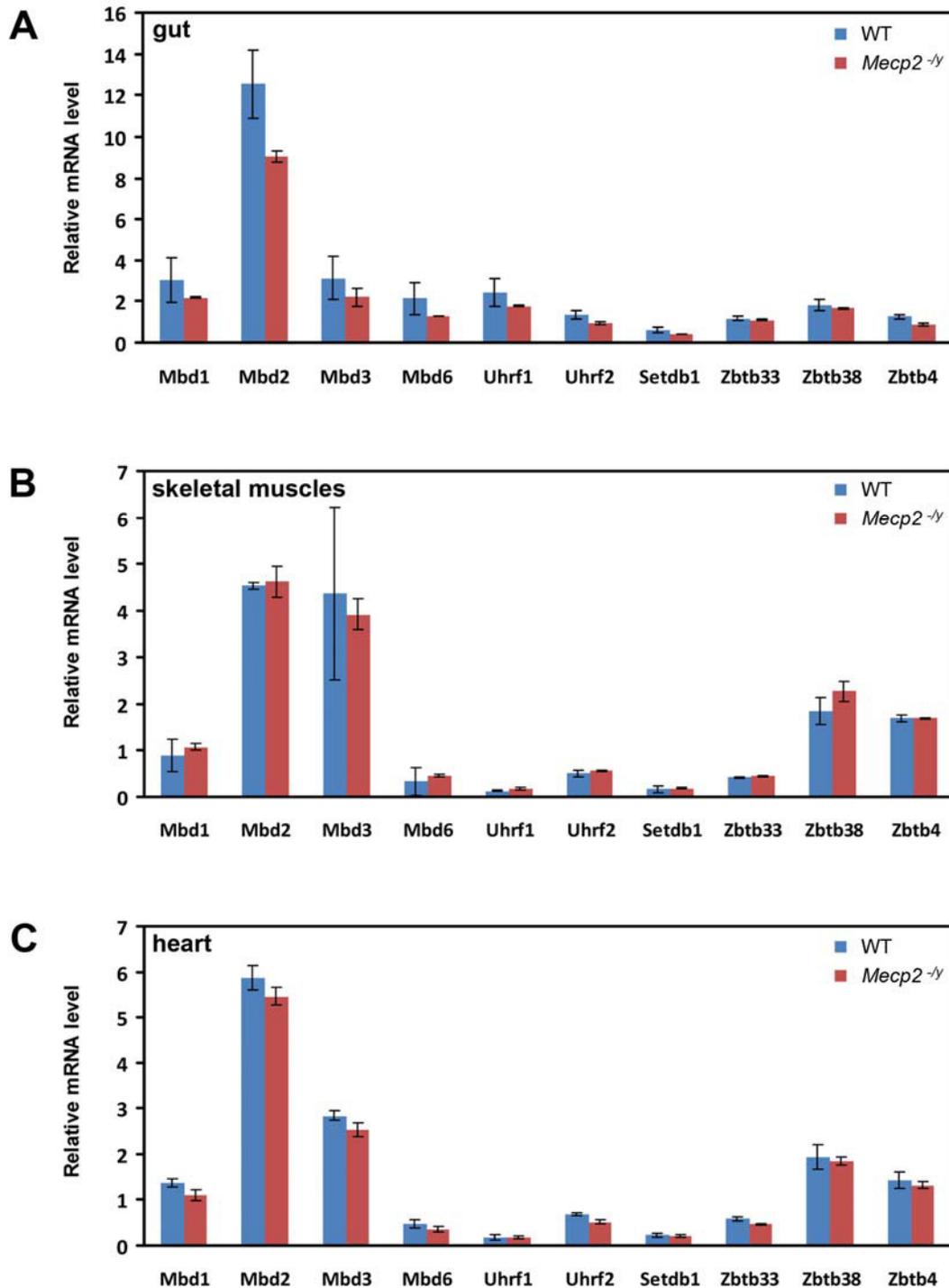
2.2 Lemd2 likely mediates lamin A/C-dependent peripheral heterochromatin tethering

Lemd2 likely mediates lamin A/C-dependent peripheral heterochromatin tethering

Katharina Thanisch*[1], Congdi Song*[1], Dieter Engelkamp[2], Einar Hallberg[3], Roland Foisner[4], Colin Stewart[5], Heinrich Leonhardt[1], Boris Joffe[1], Irina Solovei[1]

[1] Department of Biology II, Center for Integrated Protein Science Munich (CIPSM), Ludwig-Maximilians University Munich, Grosshadernerstrasse 2, 82152 Planegg-Martinsried, Germany

[2] Transgenic Service Facility, BTE, Franz-Penzoldt-Centre, Friedrich-Alexander-University of Erlangen-Nürnberg, Erwin-Rommel-Str.3, D-91058 Erlangen, Germany

[3] Department of Neurochemistry, Stockholm University, Se-106 91, Stockholm, Sweden

[4] Max F. Perutz Laboratories, Medical University of Vienna, Dr. Bohr-Gasse 9, A-1030, Vienna, Austria

[5] Institute of Medical Biology, 8A Biomedical Grove and Dept of Biological Sciences, NUS, 138648, Singapore

* Equally contributing authors

Abstract

In mammalian cells, peripheral heterochromatin is tethered to the nuclear envelope by two developmentally regulated mechanisms depending on the inner nuclear membrane (INM) protein lamin B receptor (LBR, B-tether) and the nuclear lamina component lamin A/C (LA/C, A-tether) (Solovei et al., 2013). While presence of at least one of the tethers suffices to maintain heterochromatin at the nuclear envelope, absence of both proteins results in peripheral heterochromatin release, its relocation to the nuclear interior and inversion of the nuclear architecture. Emerging evidence suggests that the major chromatin binding component of both tethers are integral inner nuclear membrane proteins, which interact with both lamins and chromatin. Accordingly, ectopic expression of LBR but not lamin C counteracts nuclear inversion in mouse rods. To identify the missing component of the A-tether, we performed immunostainings of wild type mouse tissues with antibodies against various INM proteins. We obtained cell-type specific signatures of their expression for about twenty cell types and revealed that the INM protein LEM2 is selectively missing in rod cells, as well as in other cell types lacking LA/C. Strikingly, in tissues and cultured cells derived from LA/C deficient mice, LEM2 is either missing or mislocalizes to the nuclear herniations, weakened nuclear envelope structures devoid of most NE components. Based on these results, we propose that LEM2 is the chromatin binding component mediating LA/C-dependent peripheral heterochromatin maintenance.

Keywords

Nuclear envelope, nuclear architecture, inner nuclear membrane, peripheral heterochromatin, LEM-D proteins, LEM2, emerin; MAN1, LAP2beta; LAP2alpha, LAP1B, Samp1, lamin A/C, LBR, lamin A/C knock out

Introduction

The spatial organization of chromatin within the nucleus is highly ordered and plays an important role in the regulation of the nuclear functions (Cremer and Cremer, 2010). Chromatin is spatially segregated in the nucleus according to gene-activity. Most nuclei exhibit a conventional architecture with transcriptionally active euchromatin (EC) localized within the nuclear interior and transcriptionally inactive heterochromatin adjacent to the periphery of the nucleoli and the nuclear envelope (NE) (Joffe et al., 2010). The NE, which is composed of two concentric lipid bilayers, underlined by a lamina scaffold and equipped with hundreds of nuclear envelope transmembrane proteins (NETs) including the inner nuclear membrane (INM) proteins (Schirmer et al., 2003; Korfali et al., 2012; Worman and Schirmer, 2015), emerged to regulate various biological key processes ranging from dynamic heterochromatin anchorage and silencing, over regulation of signaling to modulation of nuclear mechanics (Davidson and Lammerding, 2014).

Mutations in lamina and NETs are associated with a wide range of tissue-restricted human developmental diseases, the nuclear envelopathies, highlighting the functional relevance of NE integrity (Schreiber and Kennedy, 2013; Barton et al., 2015). NETs and lamins are widely expressed and appear to have at least partially overlapping interactomes (Barton et al., 2015) pointing towards a functional redundancy. Nevertheless, evidence is emerging that both lamina and NET composition varies between different tissues and cell types (Su et al., 2002; Schirmer et al., 2003; Korfali et al., 2010; Wilkie et al., 2011; Korfali et al., 2012), which suggests that the dynamic NE composition is linked to cell-type specific functions and corresponds to tissue-specificity of the described to-date envelopathies.

Spatial chromatin arrangements are not fixed but change during development and differentiation (Solovei et al., 2004; Brero et al., 2005; Solovei et al., 2009; Clowney et al., 2012). During the course of differentiation, many genes change their association with the nuclear periphery, depending on whether they are expressed or not (Guelen et al., 2008; Pickersgill et al., 2006; Towbin et al., 2010; Mattout et al., 2011; Peric-Hupkes et al., 2010). This can be mimicked by artificial tethering genes to the periphery (Finlan et al., 2008; Reddy et al., 2008; Dialynas et al., 2010), while targeted internal reposition and chromatin decondensation leads to gene activation (Chuang et al., 2006; Dundr et al., 2007; Therizols et al., 2014). The mechanisms anchoring heterochromatin to the periphery, however, remained largely elusive.

Recently, we uncovered two major mechanisms which independently anchor heterochromatin to the NE, the so called B-tether based on the integral INM protein Lamin B-receptor (LBR) and the A-tether characterized by presence of the nuclear lamina component Lamin A/C (LA/C) (Solovei et al., 2013). A- and B-tethers are differentially used, developmentally regulated, and oppositely affect gene expression and cellular differentiation. Usually, both or at least one of the two tethers are present. During development or cellular differentiation, LBR is expressed first and at the later developmental stages it is replaced or joined by LA/C expression. Depletion of LA/C is often compensated by prolonged LBR expression but not *vice versa*. Loss of both tethers results in release of the heterochromatin from the NE and its accumulation in the nuclear interior. In mouse cells, chromocenters, formed by densely packed subcentromeric blocks of major satellite repeat, detach from the NE and fuse in the nuclear interior. LINE-rich heterochromatin also detaches from the NE and accumulates around fused chromocenters, whereas SINE-rich EC becomes more

peripheral and partially underlies the NE. Thus, such nuclei have an inverted nuclear arrangement in comparison to all other conventional nuclei. Natural nuclear inversion has been described only in nuclei of rod photoreceptor cells from nocturnal mammals. Nuclei of nocturnal rods are lacking both A- and B-tethers and accumulate all heterochromatin in the nuclear center, where it forms a very dense optically active structure, functioning as a condensing microlense reducing light scattering in the retina (Sullivan et al., 1999; Solovei et al., 2009; 2013).

Notably, ectopic expression of LBR but not lamin C rescues the conventional nuclear architecture in mouse rod nuclei by maintenance of the peripheral heterochromatin. Thus LBR, which directly binds chromatin and is connected to B-type lamins (Makatsori et al., 2004; Olins et al., 2010; Hirano et al., 2012) appears to be sufficient for HETEROCHROMATIN tethering. In contrast, chromatin binding by LA/C is not sufficient to mediate its peripheral maintenance and therefore considered indirect and likely mediated by INM proteins, by LEM-D (LAP2 (lamina-associated polypeptide 2)/emerin/MAN1 domain) proteins in particular (Brachner and Foisner, 2011). LEM-D proteins bind both lamins and LINE-rich heterochromatin overlapping with lamina associated domains (LADs) (Gonzalez-Aguilera et al., 2014; Ikegami et al., 2010; Guelen et al., 2008). Moreover, apart from being causative for human nuclear envelopathies, recent evidence suggest a role of LEM-D proteins in maintenance of tissue homeostasis and cellular differentiation (Barton et al., 2015) making them likely candidates for peripheral heterochromatin tethering.

In this study, we attempted to identify the missing component of the A-tether by screening WT and Lmna-deficient mouse cells and tissues. Based on the comprehensive analysis of both cells and tissues, we demonstrate that LEM2 is synchronously expressed together with LA/C, is either absent or mislocalized in Lmna-deficient mouse cells and tissues, and selectively missing from rod cells at all developmental stages. Taken together, we reveal LEM2 as a likely candidate to mediate chromatin anchorage in LA/C dependent tethering, a hypothesis which are currently testing by transgenic coexpression of both LA/C and LEM2 in murine rods.

Materials and methods

Cell culture and immunostaining of cells. *Lmna* KO cells were cultured in Dulbecco's modified Eagle's medium supplemented with 20% fetal bovine serum (Biochrom) and1% penicillin/streptomycin. For immunostaining, cells cultured on coverslips were fixed with 4% paraformaldehyde for 10min, washed with PBST (PBS, 0.01% Tween20) and permeabilized with 0.5% Triton X-100. Both primary and secondary antibodies were diluted in blocking solution (PBST, 4% bovine serum albumin). Coverslips with cells were incubated with primary and secondary antibody solutions for 1h at room temperature, respectively, in dark humid chambers. Washings following primary and secondary antibody incubation were performed with PBST. For nuclear DNA counterstaining, DAPI was added to the secondary antibody solution (final concentration 2mg/ml). Coverslips were mounted in Vectashield antifade medium (Vector Laboratories) and sealed with colorless nail polish. The primary antibodies used in this study are listed in Table 1. Secondary antibodies were the same as used for cryosections (see below).

Animals, tissue fixation, and preparation of cryosections. Mice of inbred strain C57Bl6 were killed by cervical dislocation after anesthesia with isoflurane (Baxter) according to the

standard protocol approved by the Animal Ethic Committee of Ludwig Maximilian University of Munich (LMU). Tissues were dissected and fixed with 4% formaldehyde in PBS for approx. 20-24 h, washed thoroughly in PBS for a few hours, infiltrated with a series of sucrose in PBS with increasing concentration (10%, 20%, 30%), and transferred into molds (Peel-A-Way® Disposable Embedding Molds, Polysciences Inc., USA) filled with Jung freezing medium (Leica Microsystems). Frozen blocks were prepared by immersion of molds with tissues in freezing medium into ethanol bath chilled to -80°C. After freezing, blocks were transferred to dry ice and stored at -80°C. Cryosections with thickness of 14-20 µm were cut using Leica Cryostat (Leica Microsystems) and collected on SuperFrost microscopic slides (SuperFrost Ultra Plus, Roth, Germany). Sections were immediately frozen and stored at -80°C until use (for detailed protocol see (Solovei, 2010)).

Immunostaining of cryosections. The immunostaining procedure was described in detail elsewhere (Eberhart et al., 2012; Song et al., 2014). In brief, slides with cryosections were air-dried at room temperature for 30 min, re-hydrated in 10 mM sodium citrate buffer for 5 min. Antigen retrieval was performed by heating up to 80ºC in 10 mM sodium citrate buffer for 20-30 min. After brief rinsing in PBS, the slides were incubated with 0.5% Triton X-100 in PBS for 1 h. The primary antibodies used in this study are listed in Table 1. All antibodies were first tested on cultured mouse somatic cells, primary fibroblasts or C2C12 myoblast cells. Secondary antibodies were anti-mouse conjugated to Alexa 488 / 555 / 594 (Invitrogen, A21202 / A31570 / A21203), anti-rabbit conjugated to DyLight 488 / 549 / 594 (Jackson ImmunoResearch, 711-485-152 / 711-505-152 / 711-516-152), anti-guinea pig conjugated to DyLight 488 (ImmunoResearch, 706-486-148), anti-goat conjugated to DyLight 488 / Cy3 (ImmunoResearch, 705-486-147 / 705-166-147) or to Alexa 647 (Invitrogen, A21447). Both primary and secondary antibodies were diluted in blocking solution (PBS with 0.1 % Triton X100, 1% bovine serum albumin, and 0.1 % Saponin); slides with applied antibodies were incubated in dark humid chambers for 12-24 h. DAPI for the nuclear counterstaining was added to the secondary antibody to the final concentration of 2 µg/ml. Washings between and after antibody incubations were performed with 0.01% Triton X 100 in PBS at 37°C, 3 x 30 min. Stained sections were mounted under coverslips in Vectashield antifade medium (Vector) and sealed with colorless nail polish.

Microscopy. Single optical sections or image stacks were collected using a Leica TCS SP5 confocal microscope equipped with Plan Apo 63x/1.4 NA oil immersion objective and lasers for blue (405 nm), green (488 nm), orange (561 nm), red (594 nm), and far red (647 nm) fluorescence. Dedicated StackGroom plug-ins of ImageJ were used for axial chromatic shift correction and generation of TIFF RGB stacks, montages, and projections (Walter et al., 2006).

Generation and genotyping of emerin-2A-laminC-, LEM2-, and LEM2-2A-laminC-TER mice. The mouse coding sequences for *Lemd2* (Gene bank accession number NM_146075.2, base 21 to 1556) and *Emn* (Gene bank accession number NM_007927.3, base 266 to 1045) were amplified by polymerase chain reaction (PCR) using Phusion™ High-Fidelity DNA Polymerase (New England Biolabs) (Table 2) and cloned into the Nrl-LamC (Solovei et al., 2013) construct, comprising a 2.5-kb mouse *Nrl* promoter segment for rod-specific expression (Akimoto et al., 2006). *Nrl-Emn-2A-LamC* and *Nrl-Lemd2-2A-LamC* were generated by inserting *Emn* and *Lemd2*, respectively, into Nrl-LamC (Solovei et al., 2013) and in-frame linking by T2A (GSGEGRGSLLTCGDVEENPGP) (Szymczak et al., 2004; de Felipe et al., 2006) to generate a single ORF. To generate *Nrl-Lemd2*, *LamC* in *Nrl-LamC*

was replaced by *Lemd2*. Transgenes were excised from plasmid DNA using EcoRI-NotI for *Nrl-Emn-2A-LamC* and NdeI-NheI for *Nrl-Lemd2* and *Nrl-Lemd2-2A-LamC*. Preparation of DNA for microinjection and generation of transgenic mice were performed according to standard protocol (Nagy et al., 2003). Transgenic founder animals and their offspring were identified using standard PCR (MyTaq, Bioline). Genomic DNA was extracted from tail snips using QIAamp DNA Mini Kit (QIAGEN). Primers: for *Nrl-Lemd2* and *Nrl-Lemd2-2A-LamC are listed below.* Lemd2-For: 5' TGGACAAAGTGGTCTGCCTG 3'and Lemd2-Rev: 5' GGATTAGACTGTCCCGCACG 3' (Annealing temperature: 60°C, wild-type fragment: 0.3kb, transgene construct: 1kb); Emd-For: 5' CAGTGCCTACCAGAGCATCG 3'and LamC-Rev: 5' CGCTGTGACGGGGTCTCCAT 3' (Annealing temperature: 57°C, transgene construct: 0.5kb).

Results and Discussion

The set of INM proteins is highly cell-type specific

We recently uncovered that the temporal coordination of LBR and LA/C expression governs peripheral heterochromatin tethering and oppositely controls gene expression (Solovei et al., 2013). LBR is usually expressed first and either persists, is joined or replaced by LA/C. Loss of LBR triggers muscle specific gene expression, whereas depletion of peripheral LA/C causes downregulation. Moreover, transcriptomic and proteomic studies revealed that the NE composition is distinct for different tissues and cell types (Solovei et al., 2013; Su et al., 2002; Schirmer et al., 2003; Korfali et al., 2010; 2012; Wilkie et al., 2011). Considering the high variability of the NE composition, it is likely that other INM proteins might similarly to LBR and LA/C affect the epigenetic regulation of the nuclear architecture. However, a comprehensive characterization of NE composition for different cell types at different developmental stages within the native tissue context is still lacking. Therefore, we performed expression analysis for a set of twelve NE proteins using immunostainings in more than ten different mouse tissues (Table 3, Fig.1, SFig.1).

Indeed, the majority of studied cell types revealed a distinct signature of NE proteins. While all cell types constitutively express B-type lamins, expression of A-type lamins and other INM proteins, such as LBR, LAP2beta, MAN1, LEM2, emerin, LAP1B, and SAMP1, as well as nucleoplasmic LAP2alpha varied significantly between different cell types (Table 3, see also (Dechat et al., 2010; Solovei et al., 2013)). Only one cell type, smooth muscle cells, expressed the whole set of proteins studied. Many other cell types, such as endothelial cells or fibroblasts, expressed a subset of proteins (Table 3, SFig. 1G-I,). Emerin, which is considered ubiquitously expressed (Tunnah et al., 2005), was present in all studied cell types except for hepatocytes. Similarly, MAN1 was not found in crypt cells of the thin intestine (Table 3, SFig. 1A,J). Other proteins were more restricted in their tissue specific expression. In particular, spindle-associated membrane protein 1 (SAMP1) was selectively expressed in neuronal and muscle tissues. Nuclei of rod photoreceptors and other neurons in the retina and the cerebellum, as well as nuclei of smooth, skeletal and heart muscle cells exhibited a strong Samp1 staining, while nuclei of neighboring cells, such as glial, endothelial, or fibroblasts were negative for Samp1 (Table3, Fig.2). In retinal neurons, expression of Samp1 is especially pronounced in rod nuclei (Fig. 2B,C). To test whether expression of Samp1 is connected to rod inversion in nocturnal mammals, we tested retinas of nocturnal (dog, fox) and diurnal (macaque, vervet monkey) species, possessing inverted or conventional rod nuclei respectively. The NE of all rods, irrespective of their chromatin arrangement, was

strongly enriched in Samp1 (Fig. 2B,C). Moreover, we also noticed a striking increase in Samp1 expression during mouse retina differentiation (Fig. 2D). These results are in accordance with previous analysis of tissue-specific expression profiles, revealing that SAMP1, besides high expression in oocytes, is predominant in brain and skeletal muscles (Figueroa et al., 2010). Taken together this indicates that SAMP1 plays a role in early development and postmitotic cells, but not in rod inversion.

Notably, temporal expression depending on developmental and cellular differentiation state is common to many INM proteins, in particular LEM-D proteins. This is clearly demonstrated by their gradual staining in constantly renewing tissues, such as the intestine or the skin epithelium, where successive stages of differentiating cells are spatially segregated in the tissue. For instance, undifferentiated and highly proliferative cells, such as tissue stem cells found in the crypts of the thin intestine, or cells in the basal layer of the epidermis have high levels of the nucleoplasmic LEM-D protein LAP2alpha, which gradually diminishes with progressing differentiation (Fig.3, SFig.2), a pattern similar to LBR expression we described previously (Solovei et al., 2013). Instead, other NE-associated proteins reveal an opposite expression pattern. In differentiating cells, the levels of peripheral LA/C, MAN1, LEM2 and LAP1B constantly increase (Table 3, Fig. 1). Interestingly, the observed temporal expression patterns are in accordance with recent studies implicating LEM-D proteins in maintenance of tissue homeostasis as well as regulation of proliferation and differentiation, including gradual loss of LAP2alpha upon differentiation. In complex with nucleoplasmic lamins, LAP2alpha directly binds retinoblastoma protein (pRb), thereby affecting pRb/E2F signaling and regulating the proliferation of adult stem cells and progenitors of renewing tissues such as the intestine, skeletal muscle and hematopoietic cells (Naetar et al., 2008; Gotic et al., 2010). Downregulation of LAP2alpha might be implicated in loss of nucleoplasmic LA/C triggering the transition from proliferation to differentiation (Naetar et al., 2008; Gotic et al., 2010). LEM2 and MAN1, which constantly increase during differentiation, have been reported to be required for myogenesis *in vitro* (Huber et al., 2009). In mice, depletion of MAN1 is embryonic lethal and impairs both vasculogenesis and heart morphogenesis (Ishimura et al., 2006; Cohen et al., 2007; Ishimura et al., 2008). Mutations in MAN1 lead to bone and skin impairments in humans (Brachner and Foisner, 2014). While emerin mutations cause Emery Dreifuss muscular dystrophy (EDMD) in humans (Bione et al., 1994), emerin null mice practically normal except for defects in the muscles (Ozawa et al., 2006; Melcon et al., 2006; Frock et al., 2006; Barton et al., 2013). However, we do not observe a tissue or developmental-dependent expressoin of emerin, except for rods (see below, (Solovei et al., 2013)). In all other cell types, emerin appears to be ubiquitously expressed.

Besides differentiation-dependent changes, we noted an age-dependent effect on NE composition. For instance, LAP2ß is expressed in maturating myoblasts and cardiomyoblasts within the first two weeks of mouse development, but is absent in nuclei of differentiated skeletal muscles and cardiomyocytes in adult mice (Fig. 4, Table 3). Moreover, a similar dynamics of expression was observed for LAP1b, which is very weakly expressed in fully differentiated retinal neurons (Table 3).

LEMD2 is selectively missing in rod photoreceptors

We focused our interest on rod photoreceptor nuclei. In difference to all other cell types, rod photoreceptor nuclei are missing the developmental switch from LBR to LA/C expression. Upon downregulation of LBR during rod maturation, LA/C expression is not initiated resulting

in gradual nuclear inversion (Solovei et al., 2013). Transgenic expression of the INM protein LBR causes heterochromatin retention at the nuclear periphery in rods and thus counteracts nuclear inversion. In contrast, ectopic expression of Lamin C has no effect on nuclear inversion leading to the hypothesis, that at least one additional component is required to mediate LA/C-dependent tethering. Given that chromatin is considered to be primarily bound by INM proteins but not lamins (Zullo et al., 2012; Brachner and Foisner, 2011; Demmerle et al., 2012), we were prompted to assess the rod-specific set of NE proteins.

Based on immunostainings, we demonstrate that in rods, the NE proteins LAP2ß, MAN1 and SAMP1 are always present, whereas expression of emerin and LAP1b gradually diminishes during rod differentiation to very low levels weakly detected by antibodies (SFig. 1K, Table 3). Importantly, LEM2 is completely missing in rods and was not detected in this cell type at any stages of retina development (SFig.1K, Table 3). In addition to rods, we noticed that LEM2 is also absent in other cells devoid of LA/C, such as proliferating crypt cells and matrix keratinocytes. *Vice versa*, presence of LEM2 coincides with LA/C expression in all studied cell types except for neuroretina and hepatocytes (Table 3).

Being underrepresented in inverted mouse rod nuclei, all three proteins - LEM2, emerin, and LAP1b - could potentially mediate peripheral heterochromatin binding within the LA/C-dependent tether. However, the expression patterns of both LAP1b and emerin do not always correspond to LA/C. In particular, LAP1b is absent from cell types highly enriched in in A-type lamins, such as cerebellar neurons (SFig.1L, Table 3). Emerin, which is almost ubiquitously expressed, is also found in LA/C-negative cells, such as crypt cells and matrix keratinocytes of dermal papilla (Fig.1, SFig.1A, Table 3). Moreover, in our previous study of *Emd*-null mice, we revealed that emerin ablation neither caused inversion, nor triggered ecchronic LBR expression, arguing that emerin alone is dispensable for heterochromatin maintenance. At least in one case, in fibroblast of the dermal papilla, depletion of emerin was compensated by LAP2b expression pointing towards a potential role of these two proteins in heterochromatin tethering but probably not in rods (Solovei et al., 2013). Indeed, Lap2ß and emerin have been previously implicated in heterochromatin binding and repression at the nuclear periphery (Zullo et al., 2012; Demmerle et al., 2012). Both LEM-D proteins directly bind heterochromatin and repression is mediated by the recruitment and stimulation of HDAC3. In case of LAP2ß, sequences enriched for GAGA-repeats direct lamina association and are bound and silenced by Lap2ß in complex with the transcriptional repressor cKrox and HDAC3 (Zullo et al., 2012). Notably, the activity of the complex appears to be cell-type and developmental-stage dependent. Similarly, emerin recruits HDAC3 together with other components of the nuclear co-repressor complex (Demmerle et al., 2012). Accordingly, depletion of emerin interferes with heterochromatinization leading to a more open chromatin state (Mewborn et al., 2010; Meaburn et al., 2007; Ognibene et al., 1999; Demmerle et al., 2012), a phenotype similar HDAC3 null cells (Bhaskara et al., 2010). Moreover, the nuclear architecture in cells obtained from patients with X-linked EDMD, where *Emd* is mutated, has been shown to be severely compromised (Fidziańska et al., 1998; Meaburn et al., 2007). Taken together, we conclude that LEM2 but not emerin or LAP1b, is the most likely candidate as as the missing component of the LA/C-dependent tether.

LEMD2 is mislocalized or absent in LA-deficient tissues and cells

Based on our observation that LEM2 expression appears to be synchronized with LA/C and is selectively missing in rod cells, we were prompted to study cells and tissues derived from

LA/C deficient mice (Sullivan et al., 1999; Solovei et al., 2013). First, we assessed the distribution of various NE proteins in cultured cells derived from two different *Lmna* mutant mice, namely myoblasts originating from a global *Lmna*-KO (Solovei et al., 2013) and fibroblasts derived from mice with incomplete targeted disruption of the *Lmna* resulting in truncated gene missing 3.5 exons (Sullivan et al., 1999). Although in the incomplete KO, truncated LA/C still correctly localizes to the NE (Fig.5A, see also (Jahn et al., 2012)), cell types expressing only LA/C and no (or weak) LBR in WT tissues reveal the same elevated expression of LBR as observed for the global KO (Fig.5B). Irrespective of the genotype, cultured cells show a similar phenotype and are thus referred to as *Lmna* deficient cells.

Due to the impaired NE, *Lmna* deficient cells exhibit a range of defects specifically affecting the nuclear morphology. In particular, the cells frequently have abnormal nuclear membrane bulgings, called herniations, missing NE components such as lamins, LAP2b, and nuclear pore complexes (NPCs) (Sullivan et al., 1999). At the ultrastructural level, herniations correspond to areas with separated outer and inner nuclear membrane and show a thinning or lack of heterochromatin adjacent to the NE (Sullivan et al., 1999; Burke and Stewart, 2002; Fidziańska et al., 1998; Gupta et al., 2010). In *Lmna*-deficient cell cultures, we observe that only a fraction of cells possess herniations. Within herniations, heterochromatin is locally detached from the NE and chromocenters show pronounced clustering (Fig.5A, 6).

We have performed a comprehensive immunostaining analysis of *Lmna*-deficient cells with antibodies against the basic set of NE proteins, including lamins and LEM-D proteins, other inner and outer membrane proteins, and NPC (Fig.6). We confirm that herniations are devoid of lamins, LAP2b and NPCs (Sullivan et al., 1999). Moreover, seven additional proteins, LBR, MAN1, as well as members of the LINC complex including SUN1 and 2, nesprins 1 and 3, appear to be abolished from herniations (Fig.6). Distribution of emerin also follows this rule. In a proportion of nuclei, however, emerin was observed not only in the normal but also in the bulged part of the NE. In striking contrast to all other studied proteins, LEM2 is missing from *Lmna*-deficient cells and only a small proportion of the cells still express LEM2. In all cases, where LEM2 is expressed, it localizes selectively to herniations (Fig.6A).

Although mostly intact, nuclei of *Lmna* deficient cells appear to be mechanically instable and prone to rupture (Vigouroux et al., 2001; De Vos et al., 2011; Funkhouser et al., 2013). This was noticed especially in tissues where cells are under high tension, such as in muscles (Fidziańska et al., 1998; Gupta et al., 2010). Therefore we assessed the distribution of LEM2 on tissue cryosections of *Lmna* deficient mice: (i) global *Lmna*-KO at P13 and P16, and (ii) 1.5 month old mice with where LA/C is ablated by truncation. In total, we assessed 12 different tissues with antibodies against the LEM-D proteins emerin, MAN1, LAP2b, and LEM2. Overall, tissues of both mice showed similar changes in the nuclear morphology and the composition of the NE (SFig.3). While distribution of the first three LEMD proteins was not affected in *Lmna* deficient cells, LEM2 was either absent or barely detectable. Strikingly, in a subset of cells, such as skeletal and smooth muscles, as well as in some neurons and epithelial cells of epidermis and intestine, LEM2 was still expressed but prominently mislocalized (Fig.7). In skeletal muscle, nuclei still expressing LEM2 were distorted, resembling the nuclear herniations observed in cultured cells or having long extensions connecting the two separated parts of the distorted nuclei. Importantly, both herniations and extensions were marked by patchy accumulating of LEM2, generally absent from the apparently unaffected part of the NE (Fig.7; SFig.5). A very similar phenotype was observed in cardiomyocyte nuclei (Fig.7; SFig.5). In contrast to skeletal and heart muscles, nuclei of

smooth muscle cells were unaffected in shape but revealed selective polar accumulations of LEM2, which formed cap-like structures (Fig.7; SFig.5). Notably, bipolar enrichments, yet no accumulation, was also observed in the respective WT cells leaving the overall LEM2 distribution over the entire NE unaffected (Fig.7). Nuclear shape of epithelial cells in skin and intestine was not affected in *Lmna* deficient mice. However, a fraction of epithelial cells still expressing LEM2 showed a patchy NE accumulations of LEM2 (Fig.7; SFig.3). In tissue-specific KO mice, which have normal life span, K14-driven (2 month old) and villin-driven (3 month old), the skin and intestine epithelia showed the same patterns of LEM2 distribution as in 2 week old global KO mice, indicating that LEM2 absence or mislocalization is not age-dependent (SFig.6). Taken together, these results clearly demonstrate that the dynamics of LA/C and LEM2 are not only synchronized but that proper NE localization of LEM2 appears to be dependent on LA/C.

Apart from lack of Lamin B1, Nup153 and Lap2 (Sullivan et al., 1999) and partial mislocalization of emerin to the endoplasmatic reticulum (Burke and Stewart, 2002), which we confirm, we revealed that almost all components of the nuclear envelope, namely LBR, MAN1, as well as members of the LINC complex including SUN1 and 2, nesprins 1 and 3, appear to be abolished from herniations (Fig.6). Interestingly, only two inner nuclear membrane proteins appear to localize to the herniations in cultured cells, emerin and LEM2 (Fig.6A). Observations on LEM2 distribution in *Lmna*-deficient tissues confirm mislocalization of LEM2 to the herniations, and thus render this protein a likely candidate for the missing component of the LA/C-dependent tether. Moreover, as herniations are diminished in heterochromatin it is plausible that LEM2 alone is unable to anchor heterochromatin at the periphery. This is also conformed by the notion, that nuclear herniations, forming upon lamin B1 depletion, are enriched in gene-rich euchromatin (Shimi et al., 2008). Interestingly, mouse embryonic fibroblasts deficient in lamin B1 reveal strongly misshaped nuclei and a mislocalization of LAP2 to NE blebs (Vergnes et al., 2004).

To test our hypothesis that LEMD2 mediates heterochromatin binding, we are currently generating transgenic mice, ectopically expressing either LEM2 alone or LEM2 together with lamin C under the control of the rod-specific neural retina leucine zipper (Nrl) promoter (Akimoto et al., 2006). Restoration of the conventional nuclear architecture in transgenic rods will be a positive read-out of these experiments.

References

Akimoto, M., H. Cheng, D. Zhu, J.A. Brzezinski, R. Khanna, E. Filippova, E.C.T. Oh, Y. Jing, J.L. Linares, M. Brooks, S. Zareparsi, A.J. Mears, A. Hero, T. Glaser, and A. Swaroop. 2006. Targeting of GFP to newborn rods by Nrl promoter and temporal expression profiling of flow-sorted photoreceptors. *Proceedings of the National Academy of Sciences of the United States of America*. 103:3890–3895. doi:10.1073/pnas.0508214103.

Barton, L.J., A.A. Soshnev, and P.K. Geyer. 2015. Networking in the nucleus: a spotlight on LEM-domain proteins. *Curr. Opin. Cell Biol.* 34:1–8. doi:10.1016/j.ceb.2015.03.005.

Barton, L.J., B.S. Pinto, L.L. Wallrath, and P.K. Geyer. 2013. The Drosophila nuclear lamina protein otefin is required for germline stem cell survival. *Developmental Cell*. 25:645–654. doi:10.1016/j.devcel.2013.05.023.

Bhaskara, S., S.K. Knutson, G. Jiang, M.B. Chandrasekharan, A.J. Wilson, S. Zheng, A. Yenamandra, K. Locke, J.-L. Yuan, A.R. Bonine-Summers, C.E. Wells, J.F. Kaiser, M.K. Washington, Z. Zhao, F.F. Wagner, Z.-W. Sun, F. Xia, E.B. Holson, D. Khabele, and S.W. Hiebert. 2010. Hdac3 Is Essential for the Maintenance of Chromatin Structure and Genome Stability. *Cancer Cell*. 18:436–

447. doi:10.1016/j.ccr.2010.10.022.

Bione, S., E. Maestrini, S. Rivella, M. Mancini, S. Regis, G. Romeo, and D. Toniolo. 1994. Identification of a novel X-linked gene responsible for Emery-Dreifuss muscular dystrophy. *Nat. Genet.* 8:323–327. doi:10.1038/ng1294-323.

Brachner, A., and R. Foisner. 2011. Evolvement of LEM proteins as chromatin tethers at the nuclear periphery. *Biochem. Soc. Trans.* 39:1735–1741. doi:10.1083/jcb.200210026.

Brachner, A., and R. Foisner. 2014. Lamina-Associated Polypeptide (LAP)2alpha and Other LEM Proteins in Cancer Biology. *Adv Exp Med Biol.* 773:143–163. doi:10.1007/978-1-4899-8032-8_7.

Brero, A., H.P. Easwaran, D. Nowak, I. Grunewald, T. Cremer, H. Leonhardt, and M.C. Cardoso. 2005. Methyl CpG-binding proteins induce large-scale chromatin reorganization during terminal differentiation. *J. Cell Biol.* 169:733–743. doi:10.1083/jcb.200502062.

Burke, B., and C.L. Stewart. 2002. Life at the edge: the nuclear envelope and human disease. *Nat Rev Mol Cell Biol.* 3:575–585. doi:10.1038/nrm879.

Chuang, C.-H., A.E. Carpenter, B. Fuchsova, T. Johnson, P. de Lanerolle, and A.S. Belmont. 2006. Long-Range Directional Movement of an Interphase Chromosome Site. *Current Biology.* 16:825–831. doi:10.1016/j.cub.2006.03.059.

Clowney, E.J., M.A. LeGros, C.P. Mosley, F.G. Clowney, E.C. Markenskoff-Papadimitriou, M. Myllys, G. Barnea, C.A. Larabell, and S. Lomvardas. 2012. Nuclear Aggregation of Olfactory Receptor Genes Governs Their Monogenic Expression. *Cell.* 151:724–737. doi:10.1016/j.cell.2012.09.043.

Cohen, T.V., O. Kosti, and C.L. Stewart. 2007. The nuclear envelope protein MAN1 regulates TGFbeta signaling and vasculogenesis in the embryonic yolk sac. *Development.* 134:1385–1395. doi:10.1242/dev.02816.

Cremer, T., and M. Cremer. 2010. Chromosome Territories. *Cold Spring Harb Perspect Biol.* 2:a003889–a003889. doi:10.1101/cshperspect.a003889.

Davidson, P.M., and J. Lammerding. 2014. Broken nuclei--lamins, nuclear mechanics, and disease. *Trends Cell Biol.* 24:247–256. doi:10.1016/j.tcb.2013.11.004.

de Felipe, P., G.A. Luke, L.E. Hughes, D. Gani, C. Halpin, and M.D. Ryan. 2006. E unum pluribus: multiple proteins from a self-processing polyprotein. *Trends Biotechnol.* 24:68–75. doi:10.1016/j.tibtech.2005.12.006.

De Vos, W.H., F. Houben, M. Kamps, A. Malhas, F. Verheyen, J. Cox, E.M.M. Manders, V.L.R.M. Verstraeten, M.A.M. van Steensel, C.L.M. Marcelis, A. van den Wijngaard, D.J. Vaux, F.C.S. Ramaekers, and J.L.V. Broers. 2011. Repetitive disruptions of the nuclear envelope invoke temporary loss of cellular compartmentalization in laminopathies. *Human Molecular Genetics.* 20:4175–4186. doi:10.1093/hmg/ddr344.

Dechat, T., S.A. Adam, P. Taimen, T. Shimi, and R.D. Goldman. 2010. Nuclear Lamins. *Cold Spring Harb Perspect Biol.* 2:a000547–a000547. doi:10.1101/cshperspect.a000547.

Demmerle, J., A.J. Koch, and J.M. Holaska. 2012. The nuclear envelope protein emerin binds directly to histone deacetylase 3 (HDAC3) and activates HDAC3 activity. *J. Biol. Chem.* 287:22080–22088. doi:10.1074/jbc.M111.325308.

Dialynas, G., S. Speese, V. Budnik, P.K. Geyer, and L.L. Wallrath. 2010. The role of Drosophila Lamin C in muscle function and gene expression. *Development.* 137:3067–3077. doi:10.1242/dev.048231.

Dundr, M., J.K. Ospina, M.-H. Sung, S. John, M. Upender, T. Ried, G.L. Hager, and A.G. Matera. 2007. Actin-dependent intranuclear repositioning of an active gene locus in vivo. *J. Cell Biol.* 179:1095–1103. doi:10.1083/jcb.200710058.

Eberhart, A., H. Kimura, H. Leonhardt, B. Joffe, and I. Solovei. 2012. Reliable detection of epigenetic histone marks and nuclear proteins in tissue cryosections. *Chromosome Res.* 20:849–858. doi:10.1007/s10577-012-9318-8.

Fidziańska, A., D. Toniolo, and I. Hausmanowa-Petrusewicz. 1998. Ultrastructural abnormality of sarcolemmal nuclei in Emery-Dreifuss muscular dystrophy (EDMD). *Journal of the Neurological Sciences.* 159:88–93. doi:10.1016/S0022-510X(98)00130-0.

Figueroa, R., S. Gudise, V. Larsson, and E. Hallberg. 2010. A transmembrane inner nuclear membrane protein in the mitotic spindle. *Nucleus.* 1:249–253. doi:10.4161/nucl.1.3.11740.

Finlan, L.E., D. Sproul, I. Thomson, S. Boyle, E. Kerr, P. Perry, B. Ylstra, J.R. Chubb, and W.A.

Bickmore. 2008. Recruitment to the Nuclear Periphery Can Alter Expression of Genes in Human Cells. *PLoS Genet.* 4:e1000039. doi:10.1371/journal.pgen.1000039.

Frock, R.L., B.A. Kudlow, A.M. Evans, S.A. Jameson, S.D. Hauschka, and B.K. Kennedy. 2006. Lamin A/C and emerin are critical for skeletal muscle satellite cell differentiation. *Genes Dev.* 20:486–500. doi:10.1101/gad.1364906.

Funkhouser, C.M., R. Sknepnek, T. Shimi, A.E. Goldman, R.D. Goldman, and M. Olvera de la Cruz. 2013. Mechanical model of blebbing in nuclear lamin meshworks. *Proceedings of the National Academy of Sciences of the United States of America.* 110:3248–3253. doi:10.1073/pnas.1300215110.

Gonzalez-Aguilera, C., K. Ikegami, C. Ayuso, A. de Luis, M. Íñiguez, J. Cabello, J.D. Lieb, and P. Askjaer. 2014. Genome-wide analysis links emerin to neuromuscular junction activity in Caenorhabditis elegans
. *Genome Biol.* 15:R21. doi:10.1186/gb-2014-15-2-r21.

Gotic, I., W.M. Schmidt, K. Biadasiewicz, M. Leschnik, R. Spilka, J. Braun, C.L. Stewart, and R. Foisner. 2010. Loss of LAP2 alpha delays satellite cell differentiation and affects postnatal fiber-type determination. *Stem Cells.* 28:480–488. doi:10.1002/stem.292.

Guelen, L., L. Pagie, E. Brasset, W. Meuleman, M.B. Faza, W. Talhout, B.H. Eussen, A. de Klein, L. Wessels, W. de Laat, and B. van Steensel. 2008. Domain organization of human chromosomes revealed by mapping of nuclear lamina interactions. *Nature.* 453:948–951. doi:10.1038/nature06947.

Gupta, P., Z.T. Bilinska, N. Sylvius, E. Boudreau, J.P. Veinot, S. Labib, P.M. Bolongo, A. Hamza, T. Jackson, R. Ploski, M. Walski, J. Grzybowski, E. Walczak, G. Religa, A. Fidzianska, and F. Tesson. 2010. Genetic and ultrastructural studies in dilated cardiomyopathy patients: a large deletion in the lamin A/C gene is associated with cardiomyocyte nuclear envelope disruption. *Basic Res Cardiol.* 105:365–377. doi:10.1007/s00395-010-0085-4.

Hirano, Y., K. Hizume, H. Kimura, K. Takeyasu, T. Haraguchi, and Y. Hiraoka. 2012. Lamin B receptor recognizes specific modifications of histone H4 in heterochromatin formation. *J. Biol. Chem.* 287:42654–42663. doi:10.1074/jbc.M112.397950.

Huber, M.D., T. Guan, and L. Gerace. 2009. Overlapping functions of nuclear envelope proteins NET25 (Lem2) and emerin in regulation of extracellular signal-regulated kinase signaling in myoblast differentiation. *Mol Cell Biol.* 29:5718–5728. doi:10.1128/MCB.00270-09.

Ikegami, K., T.A. Egelhofer, S. Strome, and J.D. Lieb. 2010. Caenorhabditis elegans chromosome arms are anchored to the nuclear membrane via discontinuous association with LEM-2. *Genome Biol.* 11:R120. doi:10.1186/gb-2010-11-12-r120.

Ishimura, A., J.K. Ng, M. Taira, S.G. Young, and S.-I. Osada. 2006. Man1, an inner nuclear membrane protein, regulates vascular remodeling by modulating transforming growth factor beta signaling. *Development.* 133:3919–3928. doi:10.1242/dev.02538.

Ishimura, A., S. Chida, and S.-I. Osada. 2008. Man1, an inner nuclear membrane protein, regulates left-right axis formation by controlling nodal signaling in a node-independent manner. *Dev Dyn.* 237:3565–3576. doi:10.1002/dvdy.21663.

Jahn, D., S. Schramm, M. Schnolzer, C.J. Heilmann, C.G. de Koster, W. Schutz, R. Benavente, and M. Alsheimer. 2012. A truncated lamin A in the Lmna -/- mouse line: implications for the understanding of laminopathies. *Nucleus.* 3:463–474. doi:10.4161/nucl.21676.

Joffe, B., H. Leonhardt, and I. Solovei. 2010. Differentiation and large scale spatial organization of the genome. *Curr. Opin. Genet. Dev.* 20:562–569. doi:10.1016/j.gde.2010.05.009.

Korfali, N., G.S. Wilkie, S.K. Swanson, V. Srsen, D.G. Batrakou, E.A.L. Fairley, P. Malik, N. Zuleger, A. Goncharevich, J. de Las Heras, D.A. Kelly, A.R.W. Kerr, L. Florens, and E.C. Schirmer. 2010. The leukocyte nuclear envelope proteome varies with cell activation and contains novel transmembrane proteins that affect genome architecture. *Mol Cell Proteomics.* 9:2571–2585. doi:10.1074/mcp.M110.002915.

Korfali, N., G.S. Wilkie, S.K. Swanson, V. Srsen, J. de Las Heras, D.G. Batrakou, P. Malik, N. Zuleger, A.R.W. Kerr, L. Florens, and E.C. Schirmer. 2012. The nuclear envelope proteome differs notably between tissues. *Nucleus.* 3:552–564. doi:10.4161/nucl.22257.

Makatsori, D., N. Kourmouli, H. Polioudaki, L.D. Shultz, K. McLean, P.A. Theodoropoulos, P.B. Singh,

and S.D. Georgatos. 2004. The inner nuclear membrane protein lamin B receptor forms distinct microdomains and links epigenetically marked chromatin to the nuclear envelope. *J. Biol. Chem.* 279:25567–25573.

Mattout, A., A. Biran, and E. Meshorer. 2011. Global epigenetic changes during somatic cell reprogramming to iPS cells. *J Mol Cell Biol.* 3:341–350. doi:10.1093/jmcb/mjr028.

Meaburn, K.J., E. Cabuy, G. Bonne, N. Levy, G.E. Morris, G. Novelli, I.R. Kill, and J.M. Bridger. 2007. Primary laminopathy fibroblasts display altered genome organization and apoptosis. *Aging Cell.* 6:139–153. doi:10.1111/j.1474-9726.2007.00270.x.

Melcon, G., S. Kozlov, D.A. Cutler, T. Sullivan, L. Hernandez, P. Zhao, S. Mitchell, G. Nader, M. Bakay, J.N. Rottman, E.P. Hoffman, and C.L. Stewart. 2006. Loss of emerin at the nuclear envelope disrupts the Rb1/E2F and MyoD pathways during muscle regeneration. *Human Molecular Genetics.* 15:637–651. doi:10.1093/hmg/ddi479.

Mewborn, S.K., M.J. Puckelwartz, F. Abuisneineh, J.P. Fahrenbach, Y. Zhang, H. MacLeod, L. Dellefave, P. Pytel, S. Selig, C.M. Labno, K. Reddy, H. Singh, and E. McNally. 2010. Altered chromosomal positioning, compaction, and gene expression with a lamin A/C gene mutation. *PLoS ONE.* 5:e14342. doi:10.1371/journal.pone.0014342.

Naetar, N., B. Korbei, S. Kozlov, M.A. Kerenyi, D. Dorner, R. Kral, I. Gotic, P. Fuchs, T.V. Cohen, R. Bittner, C.L. Stewart, and R. Foisner. 2008. Loss of nucleoplasmic LAP2alpha-lamin A complexes causes erythroid and epidermal progenitor hyperproliferation. *Nat. Cell Biol.* 10:1341–1348. doi:10.1038/ncb1793.

Ognibene, A., P. Sabatelli, S. Petrini, S. Squarzoni, M. Riccio, S. Santi, M. Villanova, S. Palmeri, L. Merlini, and N.M. Maraldi. 1999. Nuclear changes in a case of X-linked Emery-Dreifuss muscular dystrophy. *Muscle Nerve.* 22:864–869. doi:10.1002/(SICI)1097-4598(199907)22:7<864::AID-MUS8>3.0.CO;2-G.

Olins, A.L., G. Rhodes, D.B.M. Welch, M. Zwerger, and D.E. Olins. 2010. Lamin B receptor: multi-tasking at the nuclear envelope. *Nucleus.* 1:53–70. doi:10.4161/nucl.1.1.10515.

Ozawa, R., Y.K. Hayashi, M. Ogawa, R. Kurokawa, H. Matsumoto, S. Noguchi, I. Nonaka, and I. Nishino. 2006. Emerin-lacking mice show minimal motor and cardiac dysfunctions with nuclear-associated vacuoles. *Am J Pathol.* 168:907–917. doi:10.2353/ajpath.2006.050564.

Peric-Hupkes, D., W. Meuleman, L. Pagie, S.W.M. Bruggeman, I. Solovei, W. Brugman, S. Gräf, P. Flicek, R.M. Kerkhoven, M. van Lohuizen, M. Reinders, L. Wessels, and B. van Steensel. 2010. Molecular Maps of the Reorganization of Genome-Nuclear Lamina Interactions during Differentiation. *Mol. Cell.* 38:603–613. doi:10.1016/j.molcel.2010.03.016.

Pickersgill, H., B. Kalverda, E. de Wit, W. Talhout, M. Fornerod, and B. van Steensel. 2006. Characterization of the Drosophila melanogaster genome at the nuclear lamina. *Nat. Genet.* 38:1005–1014. doi:10.1038/ng1852.

Reddy, K.L., J.M. Zullo, E. Bertolino, and H. Singh. 2008. Transcriptional repression mediated by repositioning of genes to the nuclear lamina. *Nature.* 452:243–247. doi:10.1038/nature06727.

Schirmer, E.C., L. Florens, T. Guan, J.R.3. Yates, and L. Gerace. 2003. Nuclear membrane proteins with potential disease links found by subtractive proteomics. *Science.* 301:1380–1382.

Schreiber, K.H., and B.K. Kennedy. 2013. When lamins go bad: nuclear structure and disease. *Cell.* 152:1365–1375. doi:10.1016/j.cell.2013.02.015.

Shimi, T., K. Pfleghaar, S.-I. Kojima, C.-G. Pack, I. Solovei, A.E. Goldman, S.A. Adam, D.K. Shumaker, M. Kinjo, T. Cremer, and R.D. Goldman. 2008. The A- and B-type nuclear lamin networks: microdomains involved in chromatin organization and transcription. *Genes Dev.* 22:3409–3421. doi:10.1101/gad.1735208.

Solovei, I. 2010. Fluorescence in situ hybridization (FISH) on tissue cryosections. *Methods Mol. Biol.* 659:71–82. doi:10.1007/978-1-60761-789-1_5.

Solovei, I., A.S. Wang, K. Thanisch, C.S. Schmidt, S. Krebs, M. Zwerger, T.V. Cohen, D. Devys, R. Foisner, L. Peichl, H. Herrmann, H. Blum, D. Engelkamp, C.L. Stewart, H. Leonhardt, and B. Joffe. 2013. LBR and lamin A/C sequentially tether peripheral heterochromatin and inversely regulate differentiation. *Cell.* 152:584–598. doi:10.1016/j.cell.2013.01.009.

Solovei, I., M. Kreysing, C. Lanctôt, S. Kösem, L. Peichl, T. Cremer, J. Guck, and B. Joffe. 2009. Nuclear architecture of rod photoreceptor cells adapts to vision in mammalian evolution. *Cell.*

137:356–368. doi:10.1016/j.cell.2009.01.052.

Solovei, I., N. Grandi, R. Knoth, B. Volk, and T. Cremer. 2004. Positional changes of pericentromeric heterochromatin and nucleoli in postmitotic Purkinje cells during murine cerebellum development. *Cytogenet Genome Res*. 105:302–310. doi:10.1159/000078202.

Song, C., Y. Feodorova, J. Guy, L. Peichl, K.L. Jost, H. Kimura, M.C. Cardoso, A. Bird, H. Leonhardt, B. Joffe, and I. Solovei. 2014. DNA methylation reader MECP2: cell type- and differentiation stage-specific protein distribution. *Epigenetics Chromatin*. 7:17.

Su, A.I., M.P. Cooke, K.A. Ching, Y. Hakak, J.R. Walker, T. Wiltshire, A.P. Orth, R.G. Vega, L.M. Sapinoso, A. Moqrich, A. Patapoutian, G.M. Hampton, P.G. Schultz, and J.B. Hogenesch. 2002. Large-scale analysis of the human and mouse transcriptomes. *Proceedings of the National Academy of Sciences*. 99:4465–4470. doi:10.1073/pnas.012025199.

Sullivan, T., D. Escalante-Alcalde, H. Bhatt, M. Anver, N. Bhat, K. Nagashima, C.L. Stewart, and B. Burke. 1999. Loss of A-type lamin expression compromises nuclear envelope integrity leading to muscular dystrophy. *J. Cell Biol.* 147:913–920.

Szymczak, A.L., C.J. Workman, Y. Wang, K.M. Vignali, S. Dilioglou, E.F. Vanin, and D.A.A. Vignali. 2004. Correction of multi-gene deficiency in vivo using a single "self-cleaving" 2A peptide–based retroviral vector. *Nat. Biotechnol.* 22:589–594. doi:10.1038/nbt957.

Therizols, P., R.S. Illingworth, C. Courilleau, S. Boyle, A.J. Wood, and W.A. Bickmore. 2014. Chromatin decondensation is sufficient to alter nuclear organization in embryonic stem cells. *Science*. 346:1238–1242. doi:10.1126/science.1259587.

Towbin, B.D., P. Meister, B.L. Pike, and S.M. Gasser. 2010. Repetitive transgenes in C. elegans accumulate heterochromatic marks and are sequestered at the nuclear envelope in a copy-number- and lamin-dependent manner. *Cold Spring Harbor symposia on quantitative biology*. 75:555–565. doi:10.1101/sqb.2010.75.041.

Tunnah, D., C.A. Sewry, D. Vaux, E.C. Schirmer, and G.E. Morris. 2005. The apparent absence of lamin B1 and emerin in many tissue nuclei is due to epitope masking. *J Mol Hist*. 36:337–344. doi:10.1007/s10735-005-9004-7.

Vergnes, L., M. Peterfy, M.O. Bergo, S.G. Young, and K. Reue. 2004. Lamin B1 is required for mouse development and nuclear integrity. *Proceedings of the National Academy of Sciences of the United States of America*. 101:10428–10433. doi:10.1073/pnas.0401424101.

Vigouroux, C., M. Auclair, E. Dubosclard, M. Pouchelet, J. Capeau, J.C. Courvalin, and B. Buendia. 2001. Nuclear envelope disorganization in fibroblasts from lipodystrophic patients with heterozygous R482Q/W mutations in the lamin A/C gene. *Journal of Cell Science*. 114:4459–4468.

Walter, J., B. Joffe, A. Bolzer, H. Albiez, P.A. Benedetti, S. Muller, M.R. Speicher, T. Cremer, M. Cremer, and I. Solovei. 2006. Towards many colors in FISH on 3D-preserved interphase nuclei. *Cytogenet Genome Res*. 114:367–378. doi:10.1159/000094227.

Wilkie, G.S., N. Korfali, S.K. Swanson, P. Malik, V. Srsen, D.G. Batrakou, J. de Las Heras, N. Zuleger, A.R.W. Kerr, L. Florens, and E.C. Schirmer. 2011. Several novel nuclear envelope transmembrane proteins identified in skeletal muscle have cytoskeletal associations. *Mol Cell Proteomics*. 10:M110.003129. doi:10.1074/mcp.M110.003129.

Worman, H.J., and E.C. Schirmer. 2015. Nuclear membrane diversity: underlying tissue-specific pathologies in disease? *Curr. Opin. Cell Biol.* 34:101–112. doi:10.1016/j.ceb.2015.06.003.

Zullo, J.M., I.A. Demarco, R. Pique-Regi, D.J. Gaffney, C.B. Epstein, C.J. Spooner, T.R. Luperchio, B.E. Bernstein, J.K. Pritchard, K.L. Reddy, and H. Singh. 2012. DNA sequence-dependent compartmentalization and silencing of chromatin at the nuclear lamina. *Cell*. 149:1474–1487. doi:10.1016/j.cell.2012.04.035.

Tables

Table 1. List of primary antibodies used in the study.

Proteins	Source (Cat No)	Host	Working dilutions	
			cells	sections
Lamin B1	Santa Crutz (SC-6217)	*goat*	1:100	1:50
Lamin A/C	Harald Herrmann, German Cancer Research	*mouse*	1:10	undiluted
LBR	Harald Herrmann, German Cancer Research	*guinea pig*	1:50	1:50
Emerin	Santa Crutz (SC-15378)	*rabbit*	1:100	1:50
Lem2	Atlas (HPA017340)	*rabbit*	1:100	1:50
Lap2α	Roland Roisner, Medical University of Vienna	*rabbit*	1:250	1:250
Lap2β	Roland Roisner, Medical University of Vienna	*mouse*	undiluted	undiluted
Man1	Santa Crutz (SC-50548)	*rabbit*	1:100	1:50
Lap1B	William Dauer, University of Michigan	*rabbit*	1:300	1:300
Samp1	Einar Hallberg, Stockholm University	*rabbit*	1:500	1:250

Table 2. Primers used for amplification of Lemd2 coding sequences. The mouse coding sequence (CDS) for Lemd2 (Gene bank accession number NM_146075.2, base 21 to 1556) was amplified by polymerase chain reaction (PCR) with Phusion™ High-Fidelity DNA Polymerase (New England Biolabs) in two separate PCR reactions (F1-R1 and F2-R2, respectively), which were joined in a third PCR reaction (F1-R2). Cardiac muscle DNA was used as a template. Due to the high GC content, the first 70bp of Lemd2 were synthesized (Eurofins, Ebersberg, Germany) and incorporated by ligation.

Protein	Forward primer (5' → 3')	Reverse primer (5' → 3')
LEM2	GGAACGTCTACCGCAACAAGC (F1)	GCCTGGCAGAACTCATCTGT (R1)
	TGCCGGTCGACTGTGAGAGA (F2)	AAAGGTCTGTGTCCTTGCCC (R2)

Table 3. Expression of studied proteins in adult mouse tissues. Blue fields indicate expression detected by immunostaining; white fields with "-" indicate absence of positive immunostaining; light-blue fields with "-/+" indicate very weak immunostaining.

tissues	cell types	lamins B1/B2	lamin A/C	LBR	LAP2b	MAN1	LEM2	Emerin	LAP1b	LAP2a	Samp1
retina	rods		-	-			-	-/+ 2	-/+ 2,6		
	neuroretinal cells			-			-		-/+ 2,6		
	endothelial cells										-
cerebellum	Purkinje cells			-					-	-	
	granular cells			-					-		-/+
peripheral nerves	Schwann cells			-							-
skeletal muscles	myotube nuclei			2	- 3	4					
heart mucles	cardiomyocytes			2	- 3						
various tissues	smooth muscle cells										
various tissues	fibroblasts			-							-
intestine: small	absorptive cells								-	7	-
	crypt cells		-			-	-		-		-
colon	crypt cells		1							8	-
liver	hepatocytes				2		-	-			-
	Kupffer cells		-				-				-
skin	basal keratinocytes										-
	suprabasal keratinocytes			-	2					9	-
hair	matrix keratinocytes		-			- 5	-		-		-
	dermal papilla cells			-	-					2	-

[1] there is a clear gradient in staining intensity: weak at the bottom and strong at the top of the crypt

[2] very weak signal in differentiated cells

[3] age-dependent variations: protein is detected only at P0-P14

[4] in addition to the nuclear envelope nucleoplasm is stained

[5] differentiating and fully differentiated hair keratinocytes express MAN1

[6] age-dependent variations: no expression at P0-P9, weak expression from P9 on, very weak from P28 on

[7] there is a clear gradient in staining intensity: weak at the top and strong at the base of the villi

[8] there is a clear gradient in staining intensity: weak at the top and strong at the bottom of the crypts

[9] suprabasal keratinocytes have weaker expression of LAP2alpha than basal keratinocytes

Figures

Figure 1. Expression of nuclear envelope protein subset in different cell types exemplified by immunostaining of the hair follicle. Dermal papilla fibroblasts and matrix keratinocytes demonstrate clearly different expression signatures. For each immunostained protein, upper panel shows positive (+) or negative (-) immunostaining and low panel shows DAPI counterstain of the nuclei. *Red line* depicts border of a dermal papillae (*dp*) and *green line* separats matrix keratinocytes (*mk*) from connective tissue sheath. All images are single confocal sections.
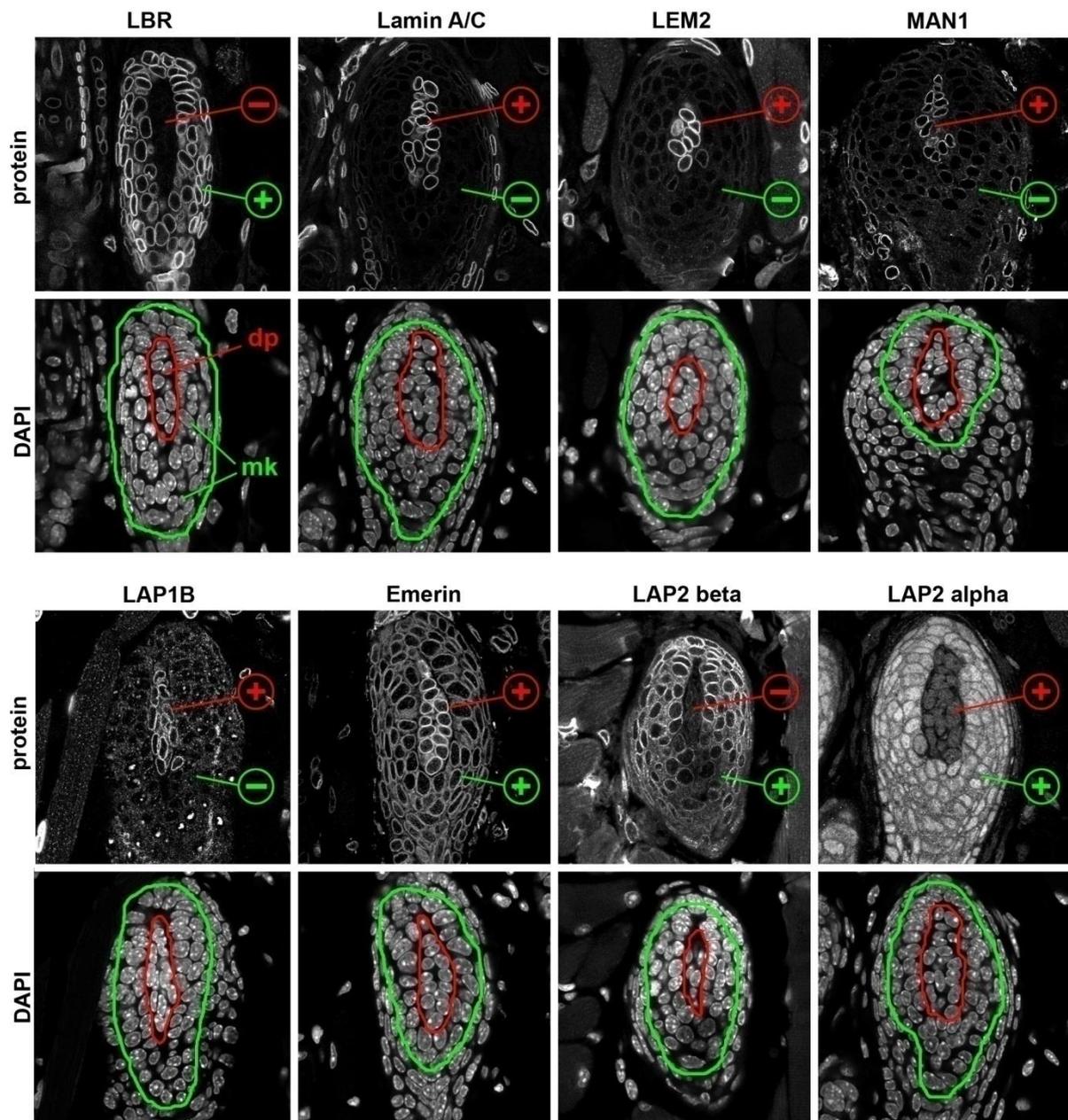
Figure 2. Selective expression of SAMP1 in muscle and neurons. A, staining of SAMP1 in three types of muscles (heart, skeletal and smooth) and in Purkinje neurons of the cerebellum. **B,C**, staining of SAMP1 in retinas of nocturnal (mouse, dog) and diurnal (vervet monkey) species. Note a particular strong staining of photoreceptors in the outer nuclear layer (*ONL*) and less prominent staining of cells in the inner nuclear layer (*INL*) and the ganglion cell layer (*GCL*). **D**, increasing expression of SAMP1 during mouse retina differentiation; retina neurons show much weaker expression of SAMP1 in two and three week (P15, P21) old pups in comparison to retina of adult (2.5 months) mouse. All images are single confocal sections.
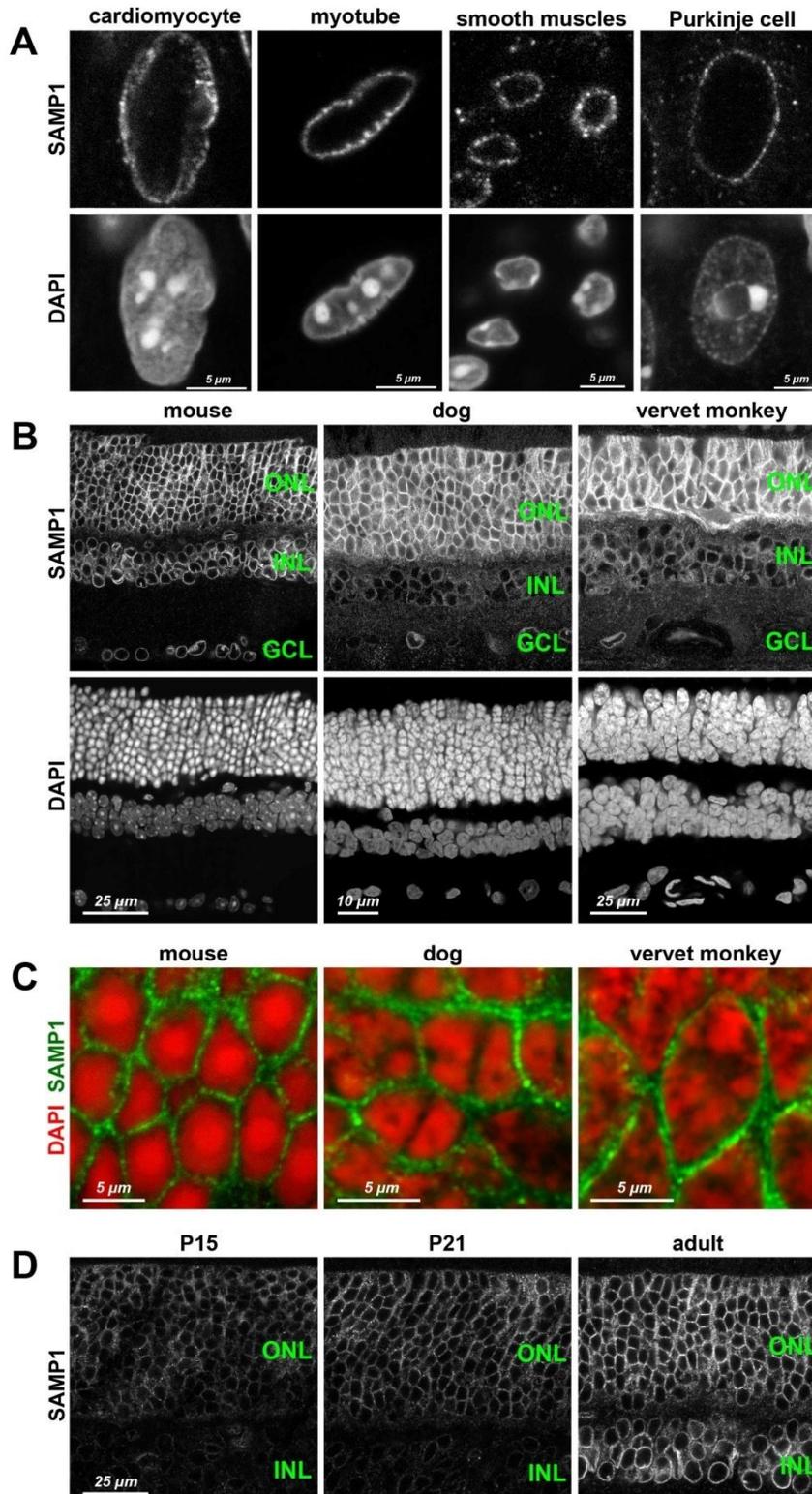
Figure 3. **Expression of LAP2alpha has a clear gradient in renewing epithelium of thin intestine with spatial separation of proliferating and differentiated cells. A**, dividing and differentiating cells in crypts and villi bases (*arrowhead*) are strongly positive after anti-LAP2alpha staining whereas differentiated absorptive and goblet cells on villi (*arrows*) show weak staining. **B**, a close up of a crypt showing intensely stained nucleoplasm of proliferating crypt cells in a clear difference to weak nuclear staining of differentiated Paneth cells (*empty arrowhead*); *asterisk* marks crypt lumen. All images are single confocal sections.
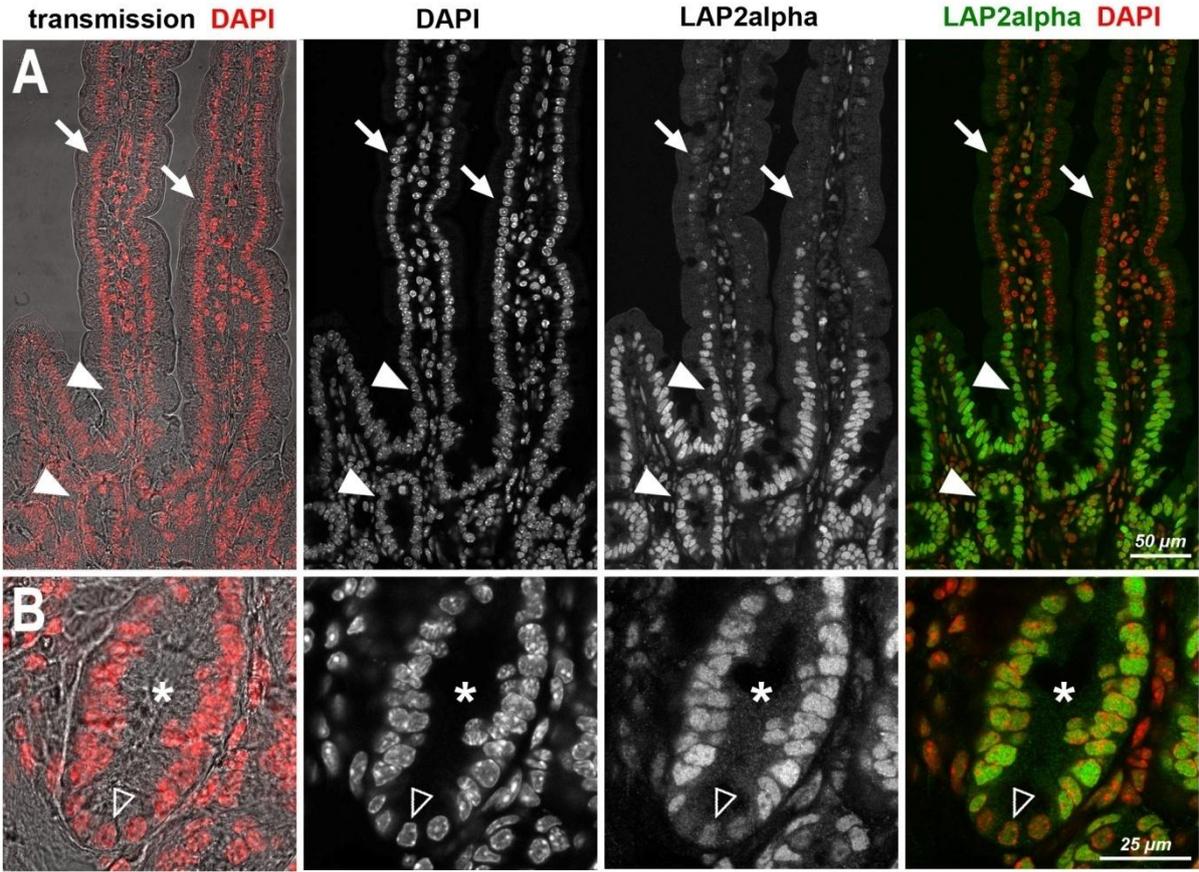
Figure 4. Age dependent expression of LAP2beta in myotube nuclei of skeletal muscles (A) and cardiomyocytes (B). LAP2beta is expressed in both muscle cell types at early postnatal development stages (e.g., P9) but not in adult mice. **A**, perpendicular sections through myotubes; *empty arrowheads* point at myotube nuclei. **B**, perpendicular sections through heart muscles; *solid arrowheads* point at cardiomyocyte nuclei. *Arrows* in both A and B point at fibroblast nuclei which are LAP2beta-positive at all developmental stages. All images are single confocal sections.
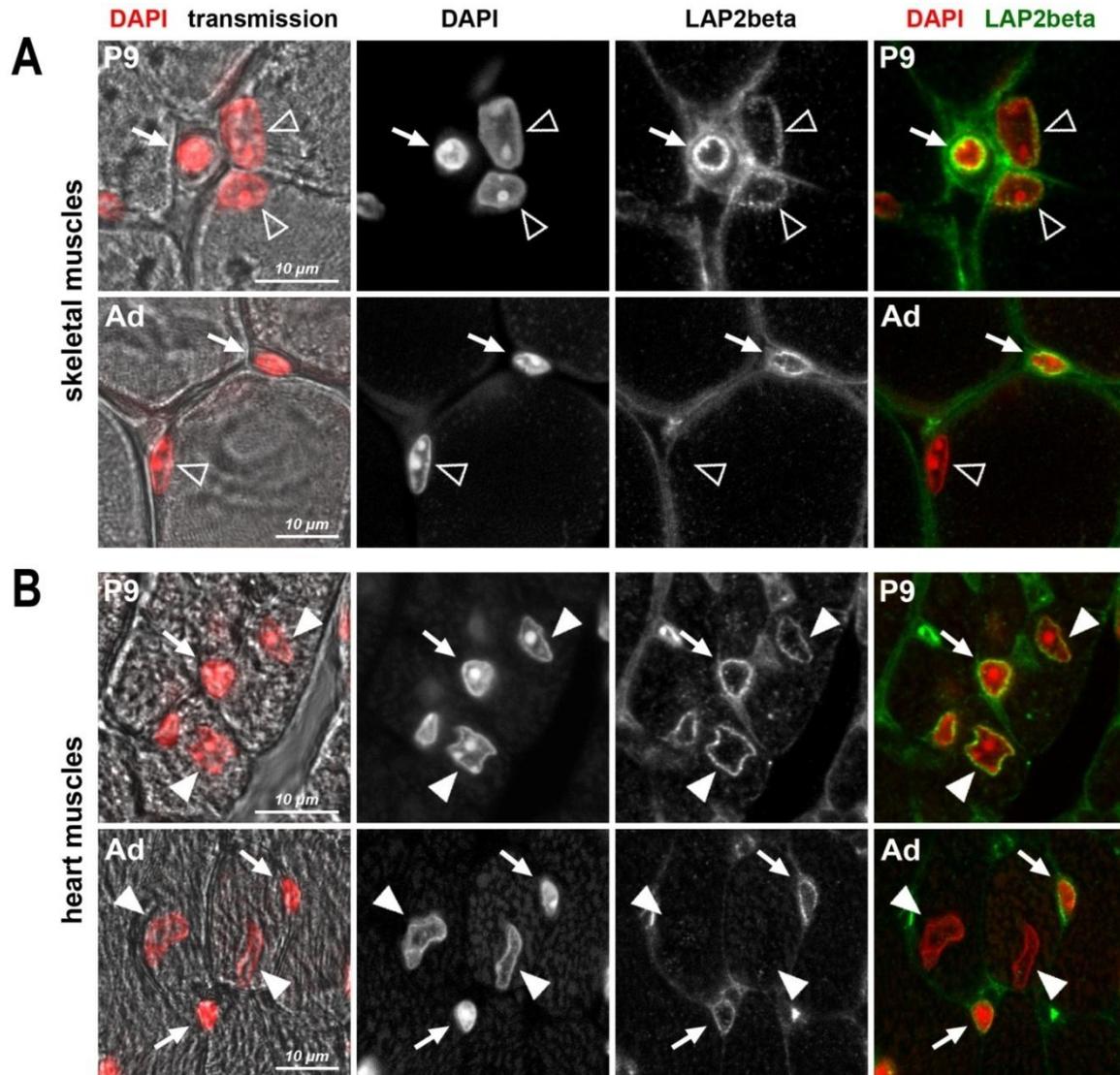
Figure 5. Compensatory expression of LBR in cells from LA/C-deficient mice with truncated *Lmna* gene. A, cultured primary fibroblast with typical NE herniation after immunostaining of lamins and LBR. Seemingly normal part of the NE, possessing A- and B-type lamins and LBR, is marked by *solid arrowhead*; *empty arrowhead* point at herniation, which is lacking lamins and LBR. Note chromocenter fusion (*red arrow*) in this nucleus and weak staining of the herniation with DAPI, indicating lost of the heterochromatin by this part of the nucleus. Single confocal sections or maximum intensity projections. **B**, multilayer epithelium of lip epidermis from WT (B1) and LA/C-deficient (B2) mice. **B1**, in WT skin, basal keratinocytes (*solid arrowheads*) express both LBR and LA/C; suprabasal keratinocytes (*arrows*) as well as dermal fibroblasts (*empty arrowhead*) express only LA/C. **B2**, in LA/C-deficient skin, all three cell types express LBR very strongly, in addition to a weak LA/C expression. Single confocal sections.
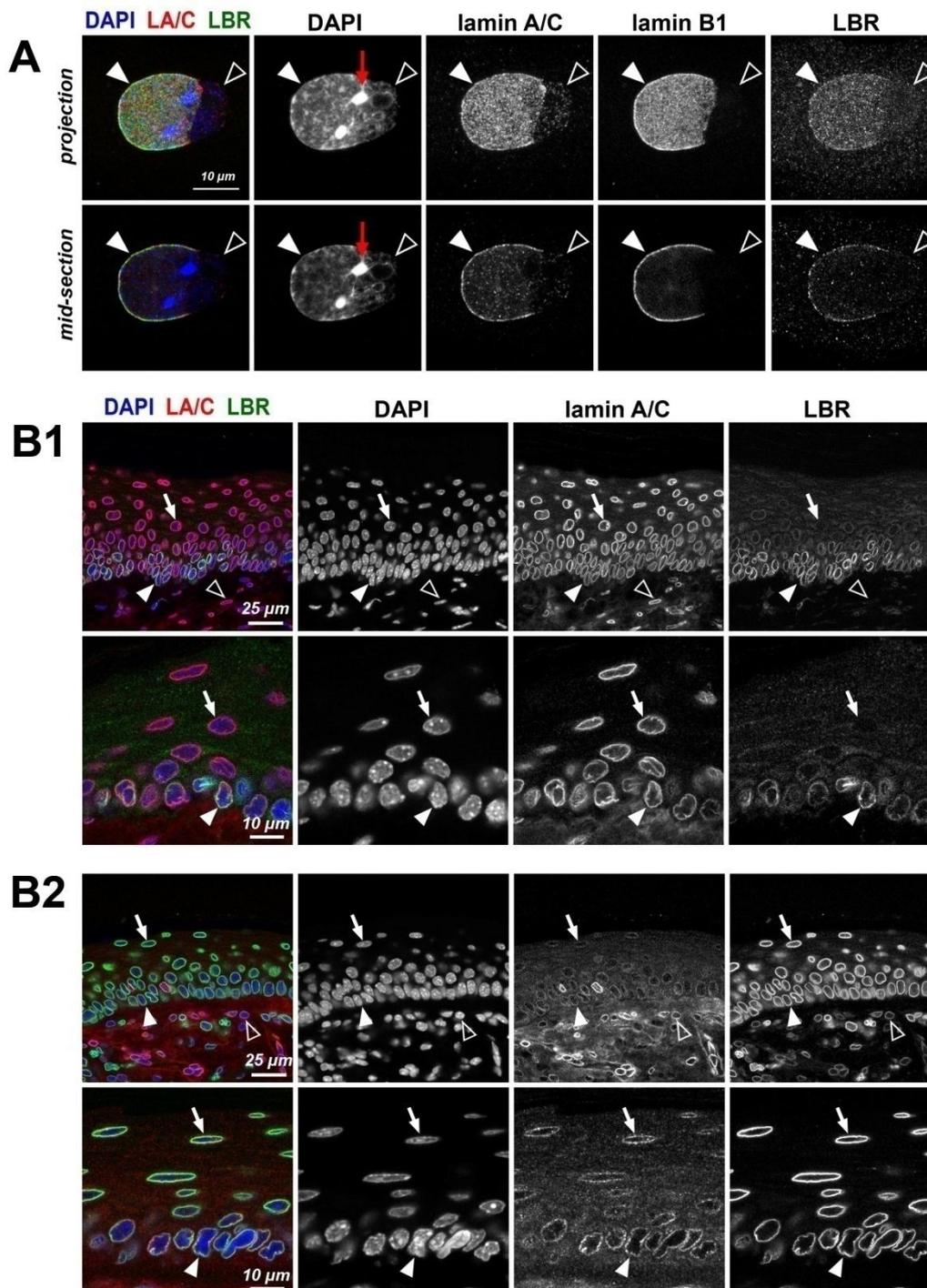
Figure 6. Immunostaining of lamin B and LEM-D (A) and other NE proteins (B) in cultured primary myoblasts derived from LA/C-KO mouse . Exemplified are nuclei possessing herniations (*empty arrowheads*). Most of NE proteins tested are expressed in LA/C-KO cells, correctly localize to the seemingly normal part of the nucleus (*solid arrowhead*) and are lacking in herniations. LEM2 is usually not expressed at the detectable by immunostaining level, however, when it is expressed, it is found in the herniations. Note chromocenter fusion (*red arrow*) and lack of heterochromatin in the herniation in the most of the cells. Maximum intensity projections (*left columns*) and single confocal sections (*right columns*) from the same cells are shown.

Figure 6A
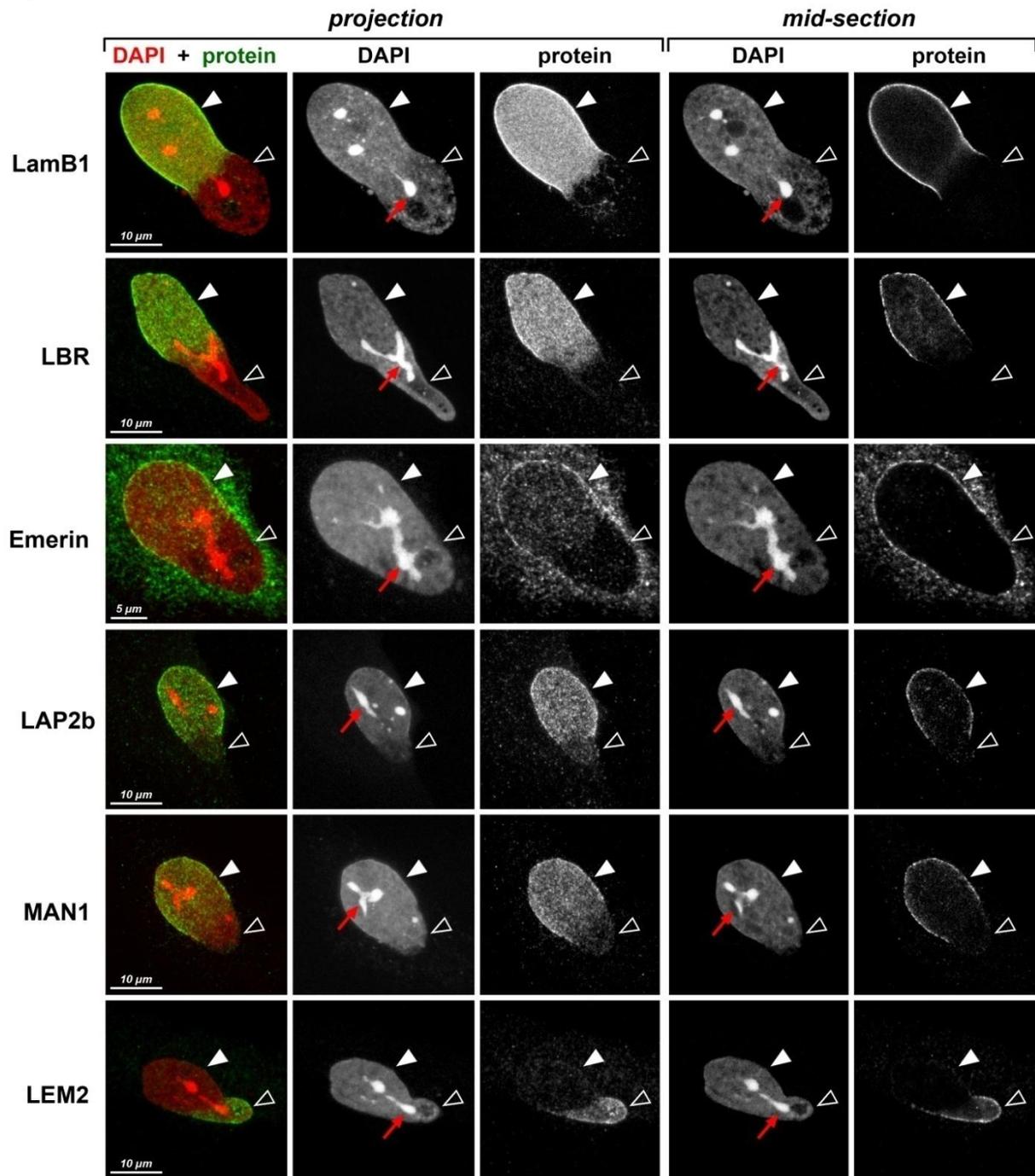
Figure 6B
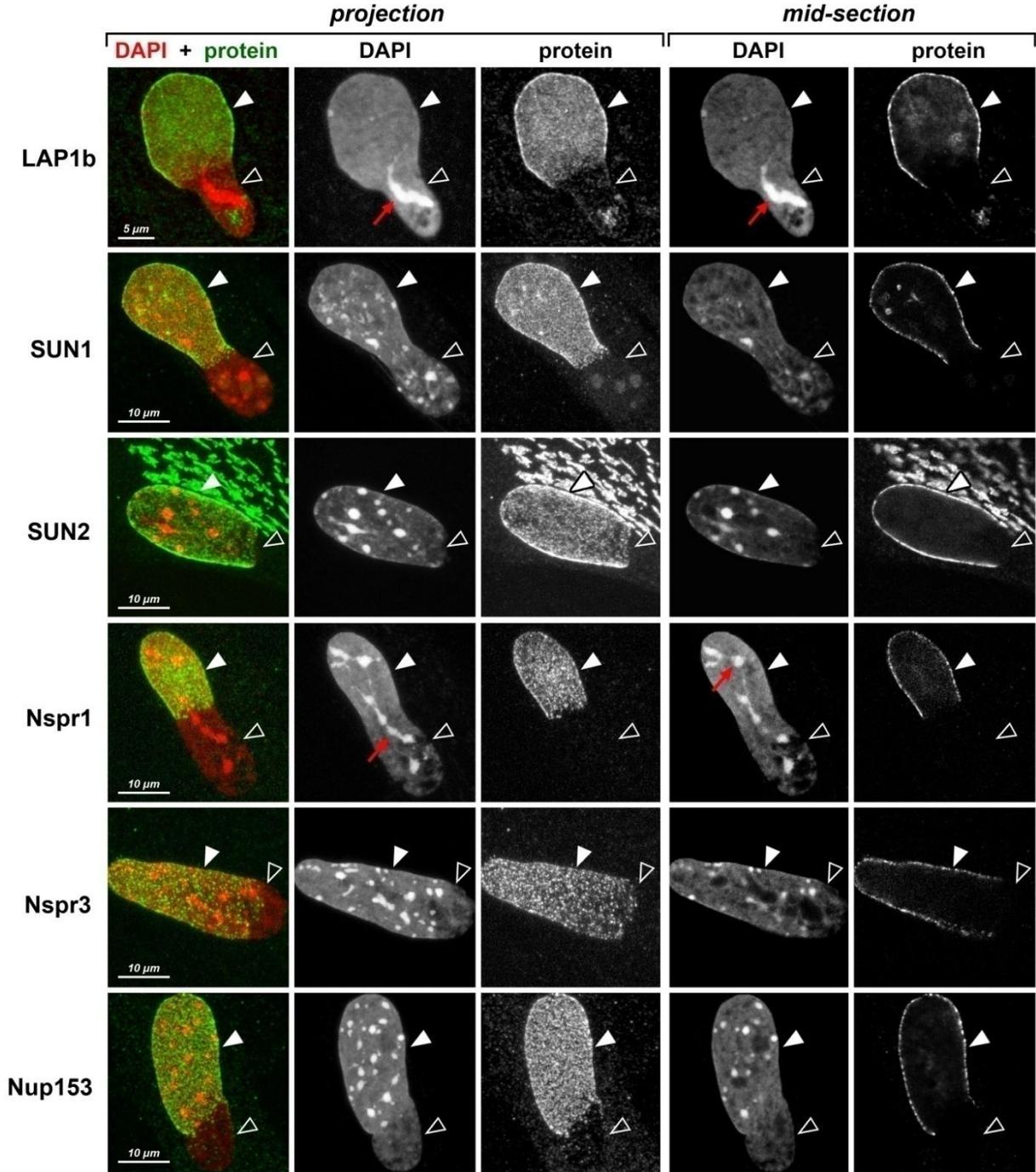
Figure 7. Mislocalization of LEM2 in the nuclei of native tissues from LA/C-KO mouse. Immunostaining of LEM2 in various cell types in tissues from WT (*left column*) and LA/C-KO (*right column*) mice. In WT cells, LEM2 is distributed over the entire NE. In KO cells, LEM2 is either absent or has pronouncedly aberrant localization (*arrows*). All images are maximum intensity projections of confocal stacks through 2-5 μm.
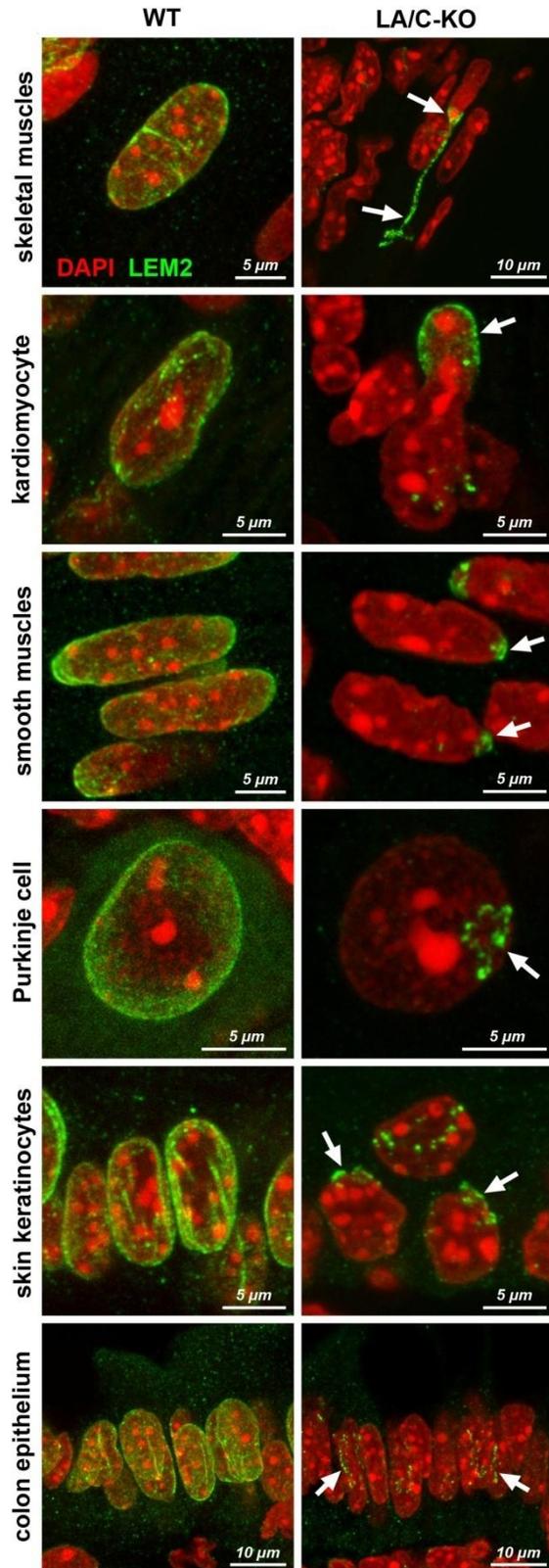
Supplementary figures

Supplementary Figure 1. Expression of emerin, LEM2, LAP2beta, MAN1, LAP2alpha, and LAP1B in different cell types: Immunostaining of mouse tissue cryosections.

A, duodenum epithelium
B, colon epithelium
C, skin
D, hair follicle
E, skeletal muscles
F, heart muscles
G, smooth muscles (colon)
H, fibroblasts (skin derma)
I, endothelial cells (retinal capillaries)
J, hepatocytes (liver)
K, neurons in retina
L, neurons in cerebellum
M, glial cells in peripheral nervous system

Positive or negative staining is indicated by green "+" or red "-" on the most right panels. All images are single confocal sections.

Supplementary Figure 1A. Duodenum

asterisks mark intestine lumen

asterisks mark crypts lumen
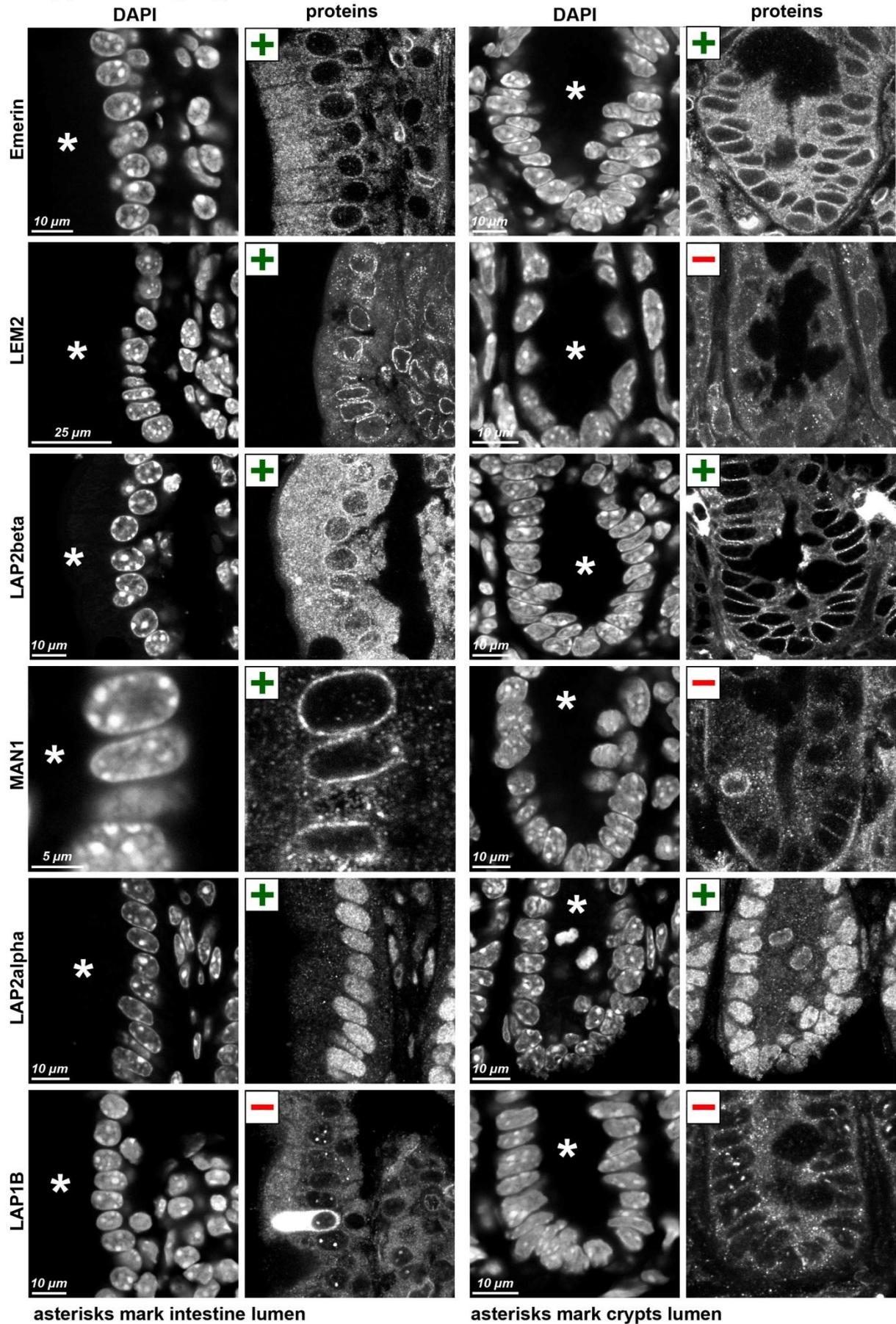
Supplementary Figure 1B. Colon
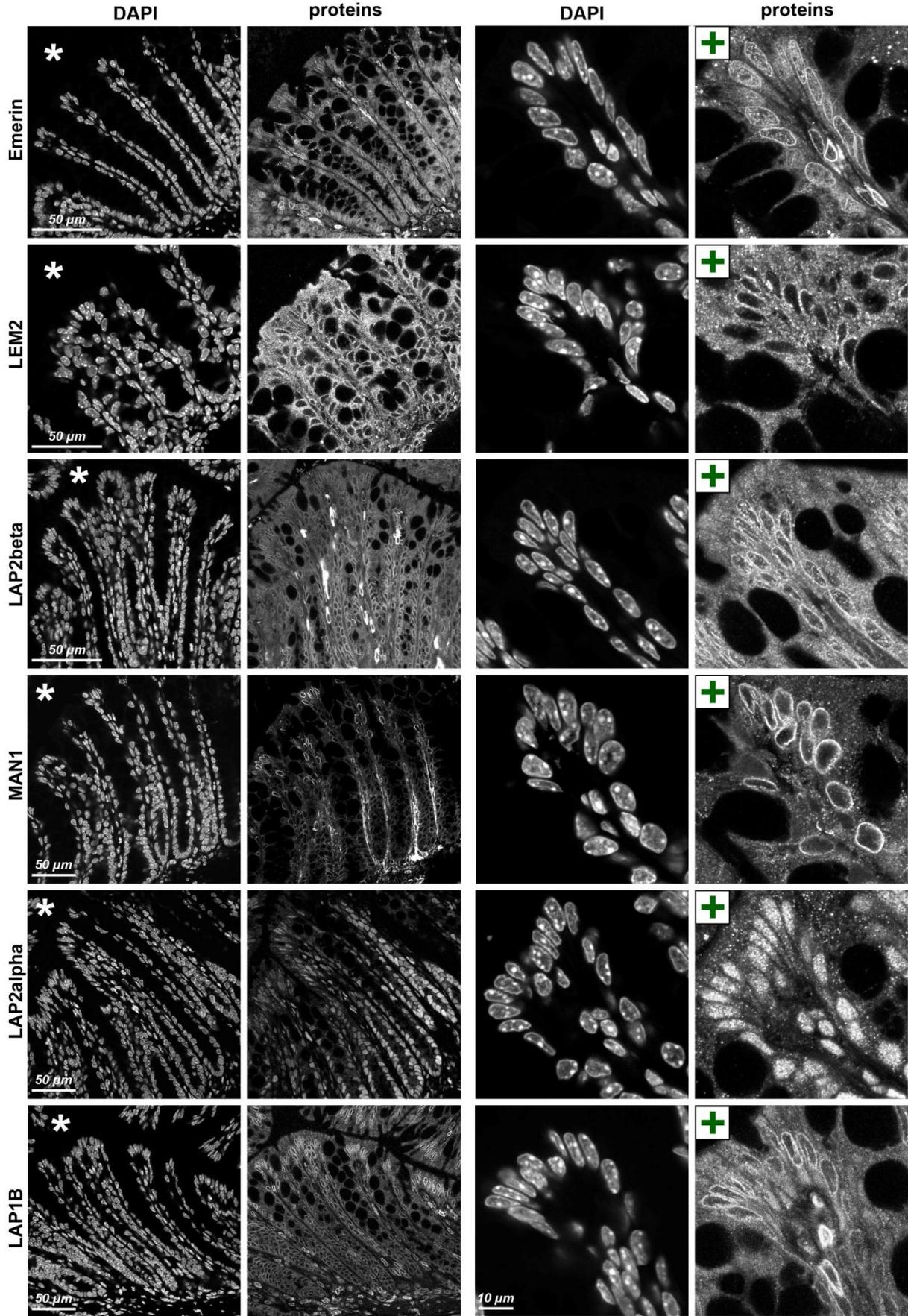

asterisks mark colon lumen

Supplementary Figure 1C. Skin
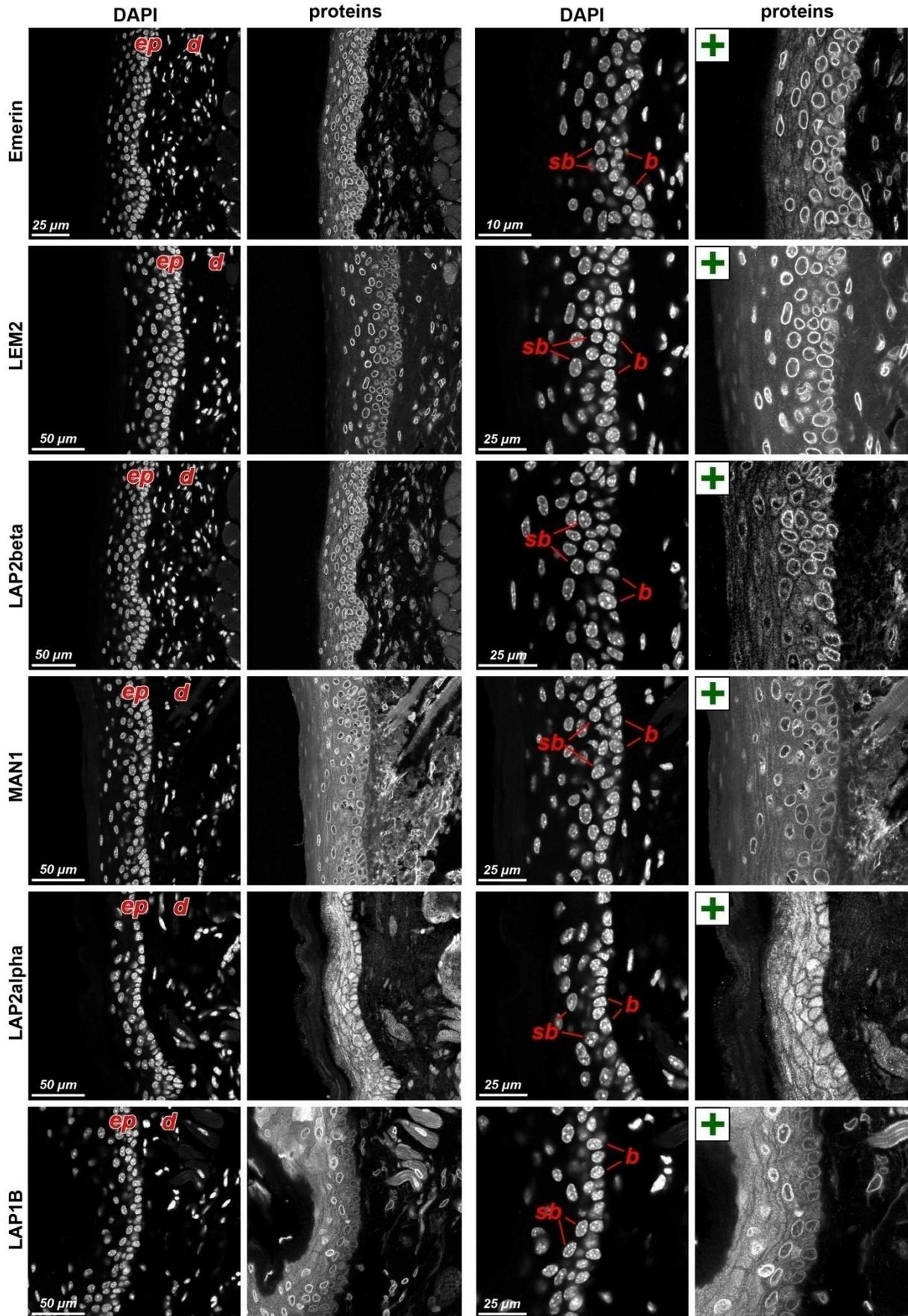

ep, epidermis; d, derma

b, basal; sb, suprabasal keratinocytes

## Supplementary Figure 1D. Hair follicle.
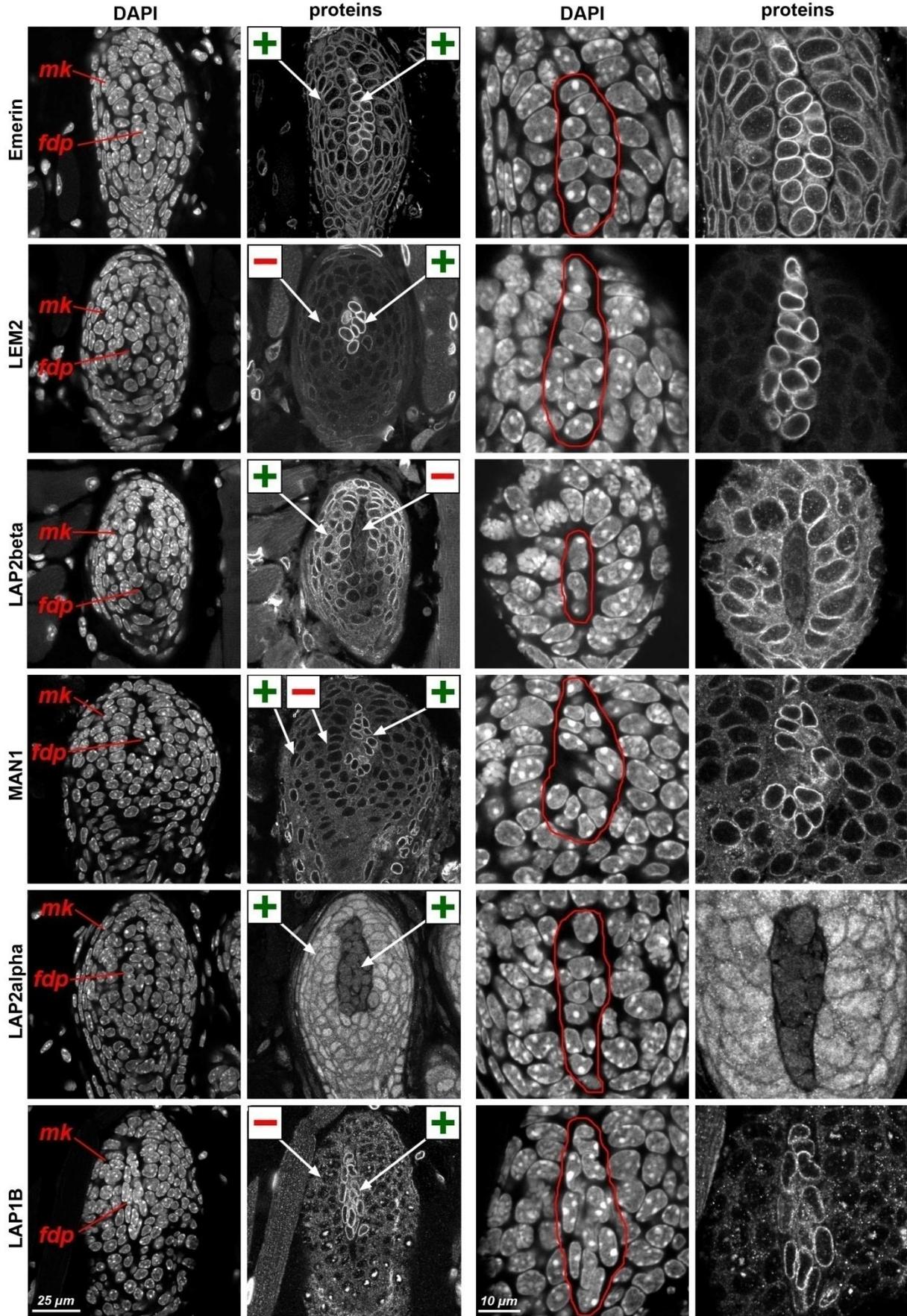
fdp, fibroblasts of dermal papilla;   *mk*, matrix keratinocytes;   red contor outlines dermal papilla

Supplementary Figure 1E. Skeletal muscles
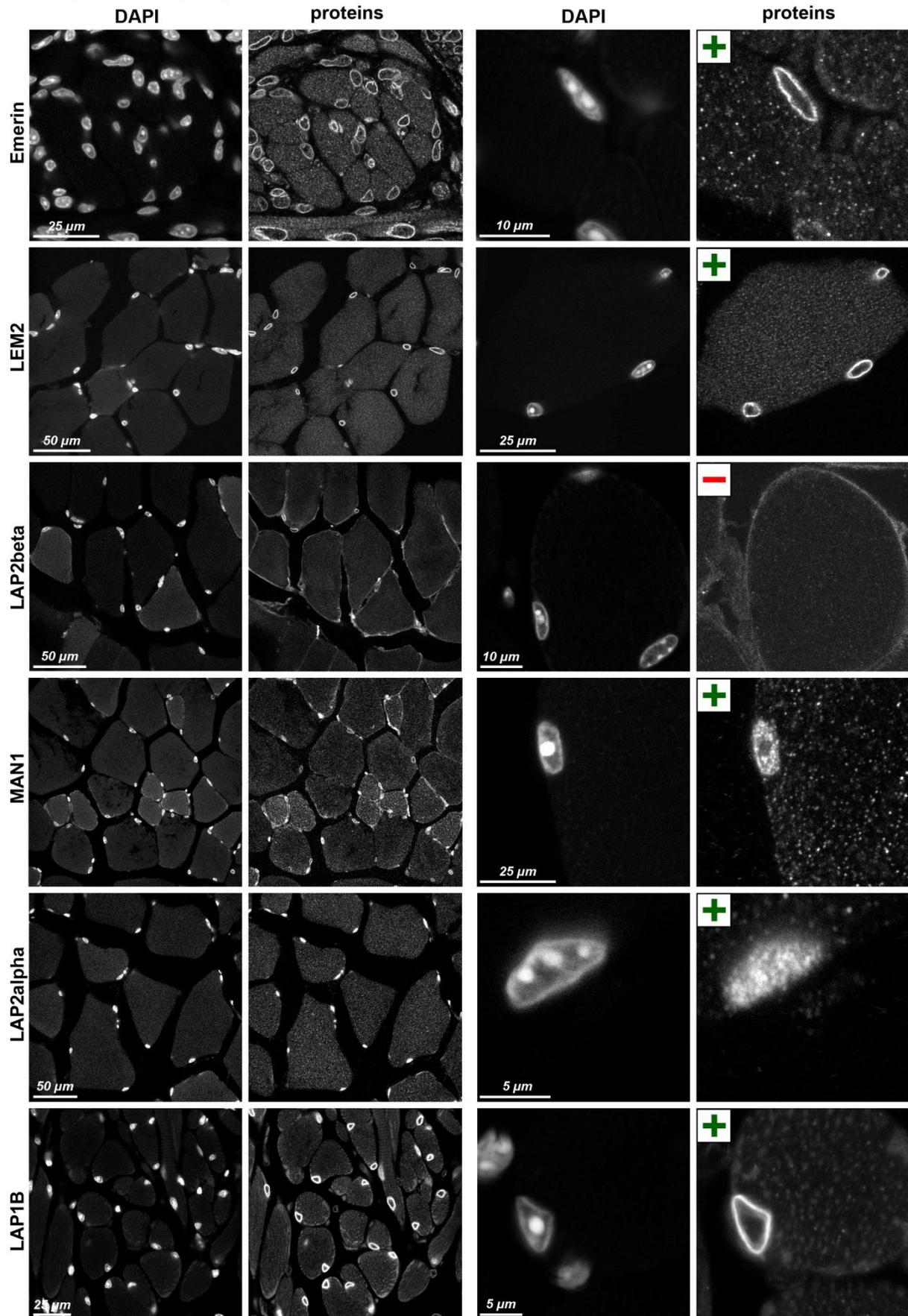
Supplementary Figure 1F. Heart muscles.
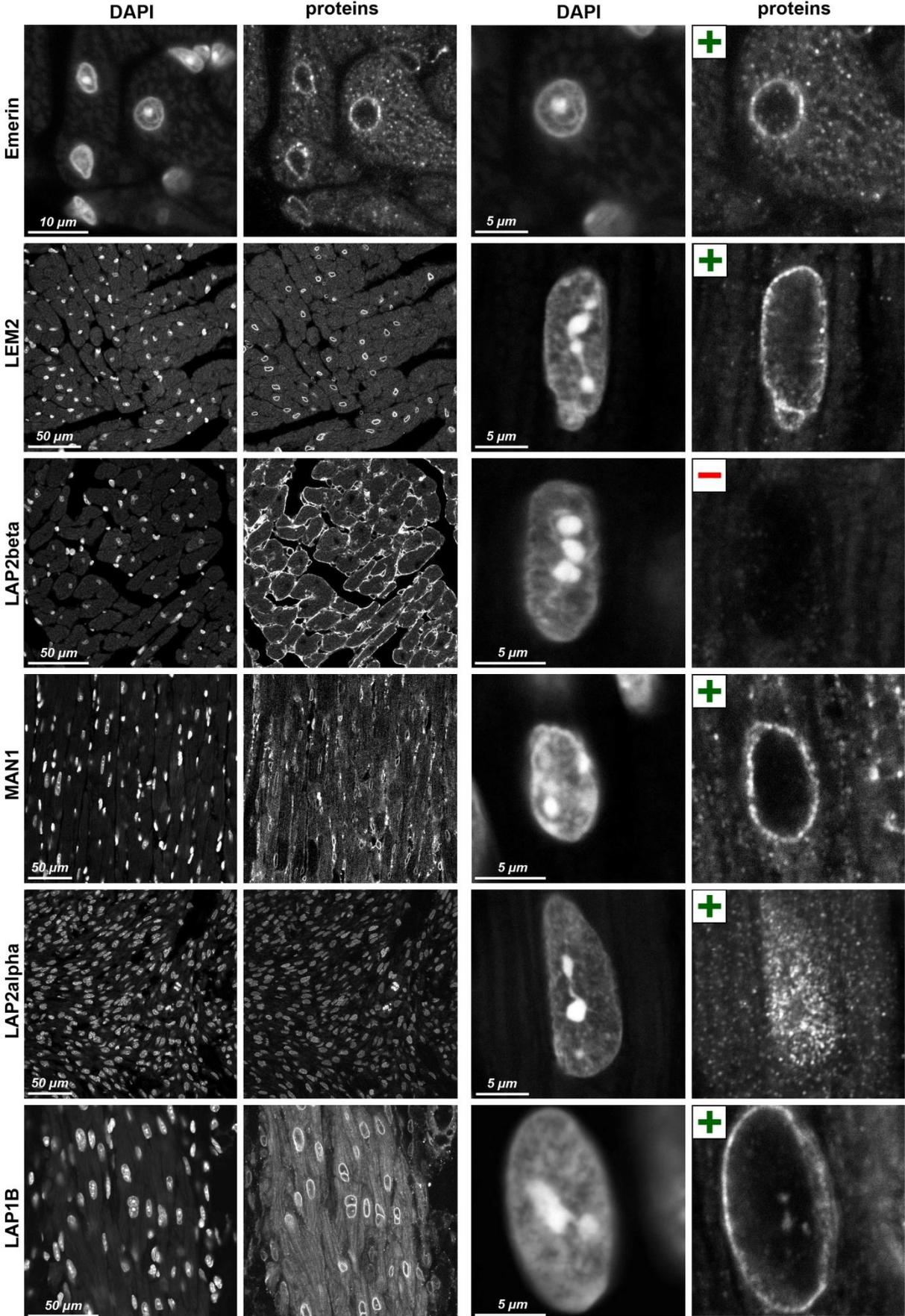
Supplementary Figure 1G. Smooth muscles (colon).
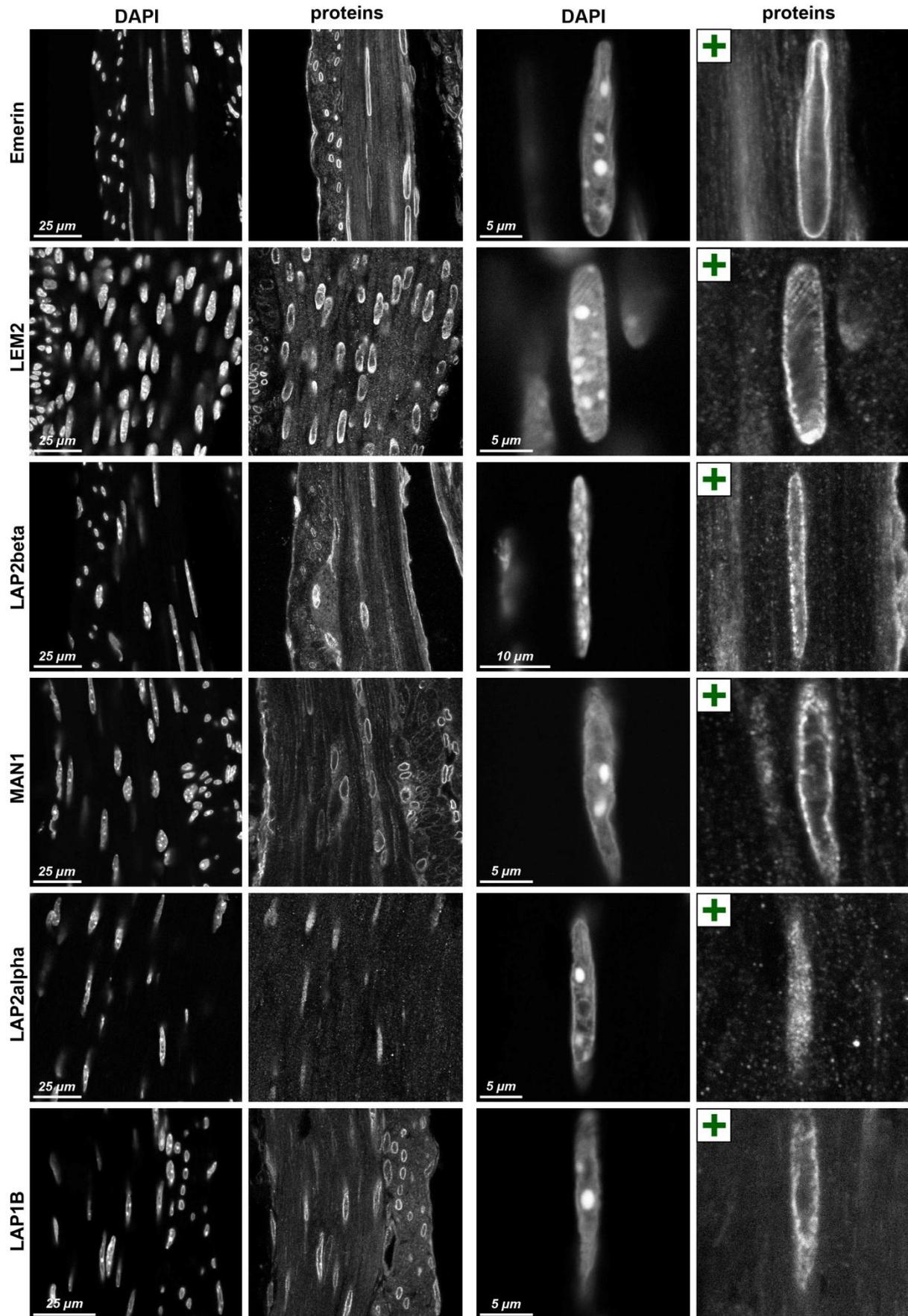
## Supplementary Figure 1H. Fibroblasts (derma).
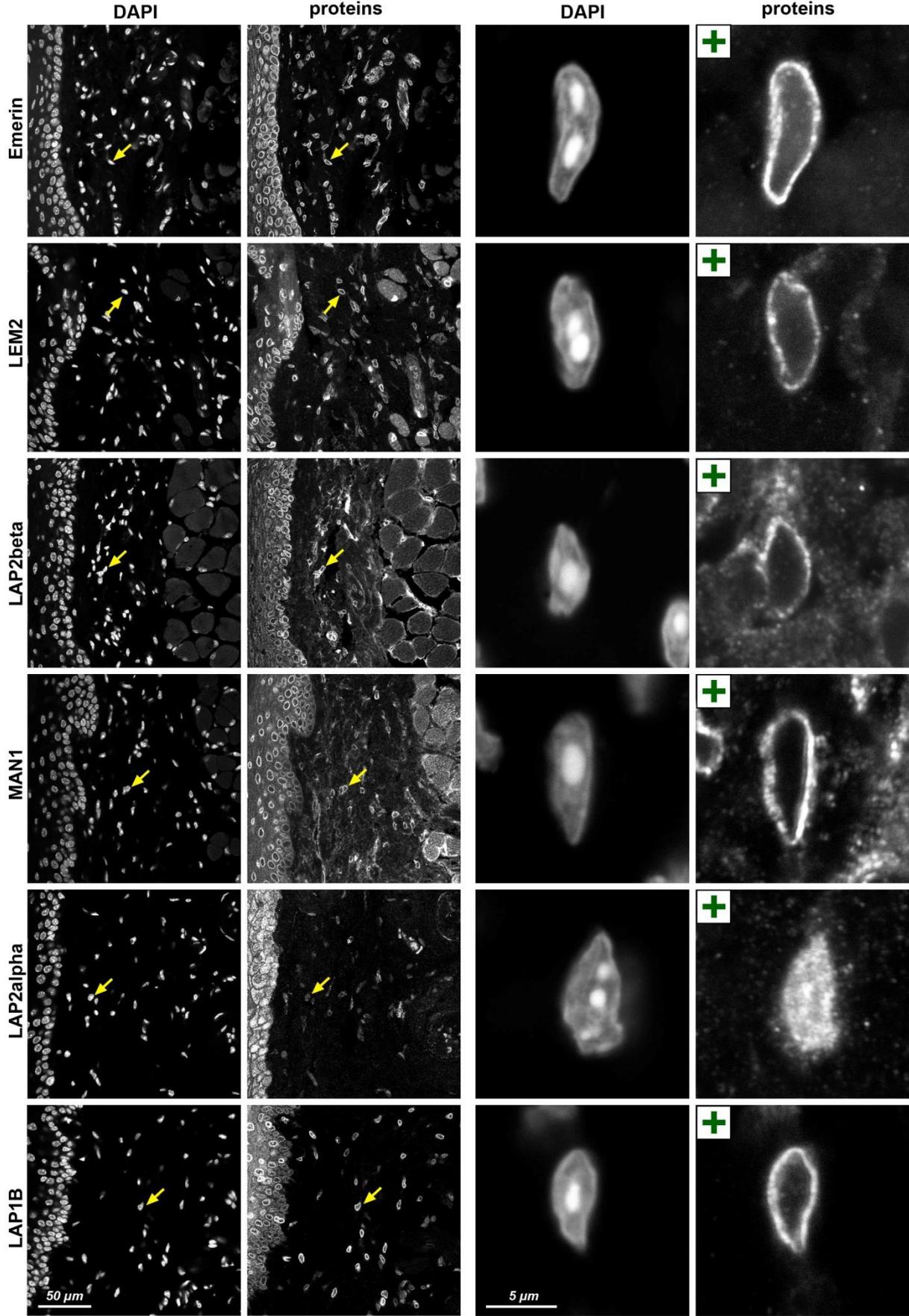
arrows point at fibroblast nuclei

## Supplementary Figure 1l. Endothelial cells (retinal capillaries)
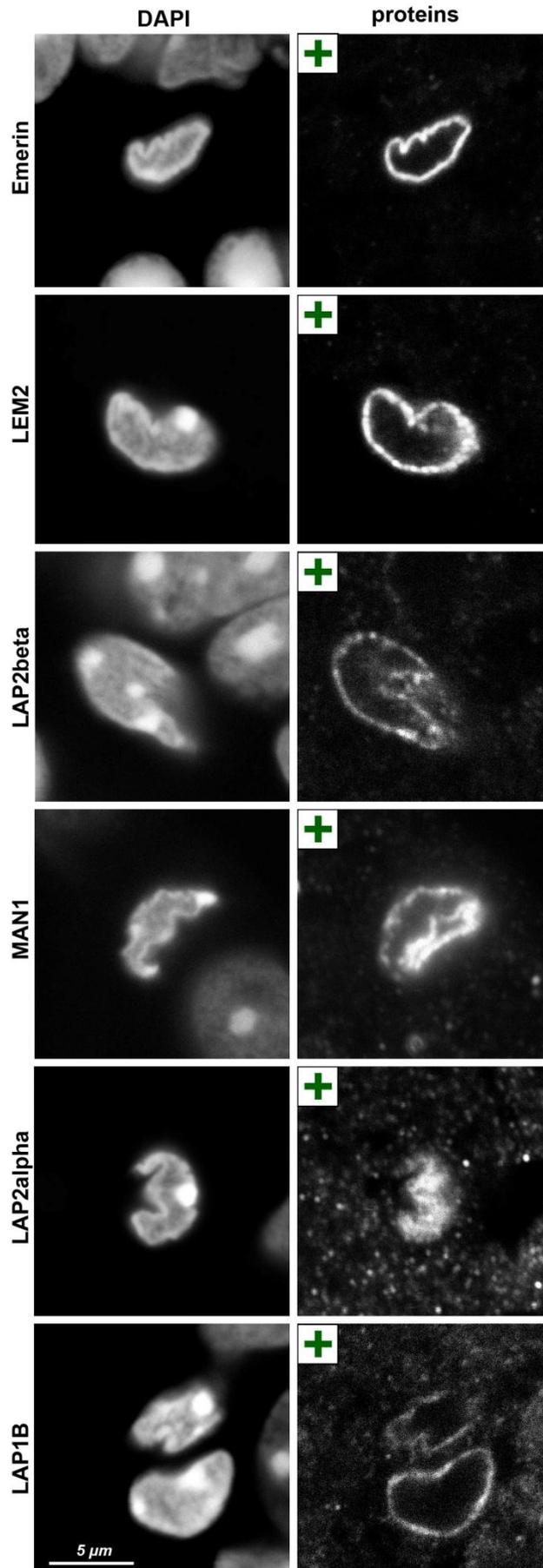
**Supplementary Figure 1J. Liver.**
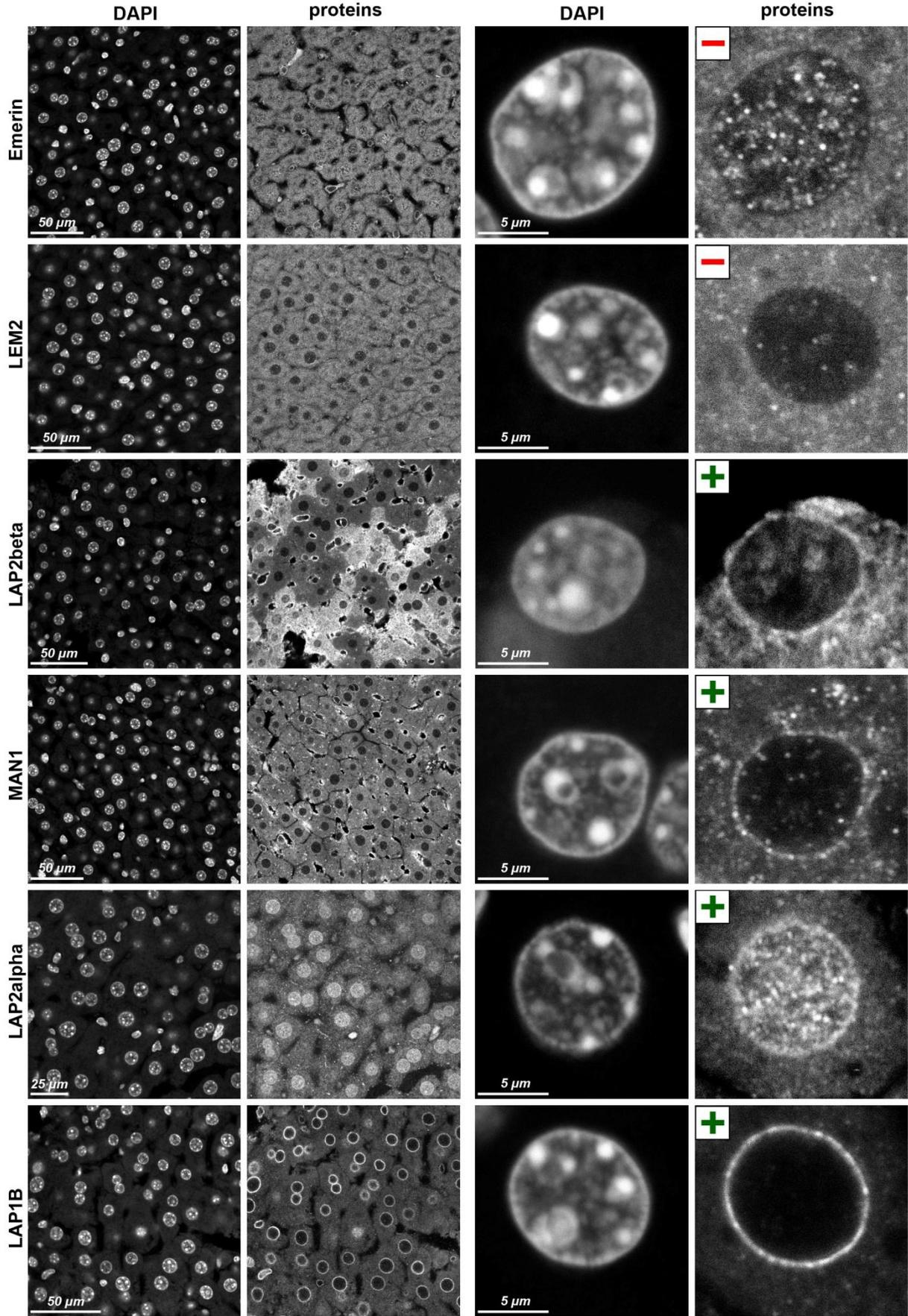
Supplementary Figure 1K. Retina.
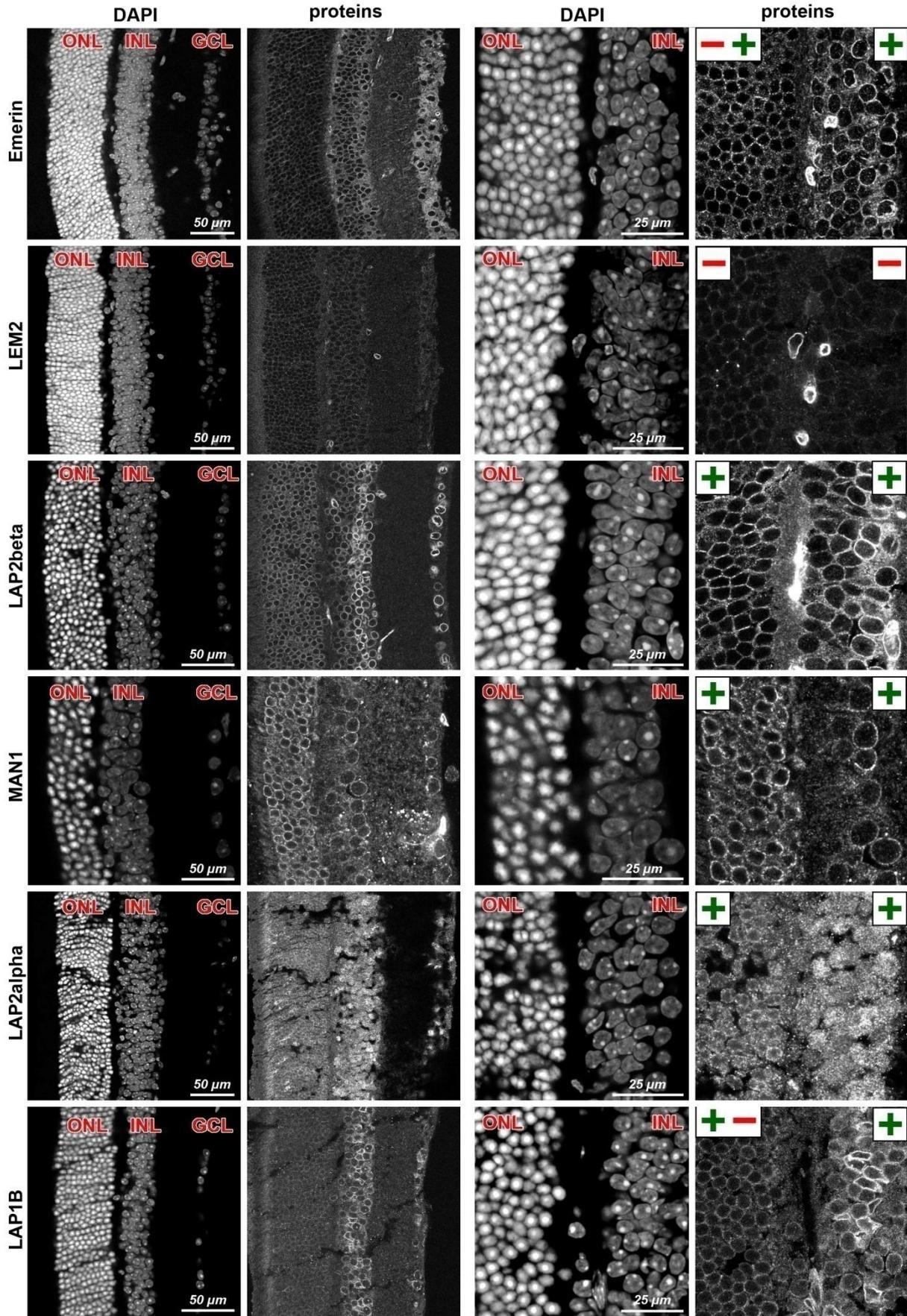
ONL, outer nuclear layer; INL, inner nuclear layer; GCL, ganglion cells layer

Supplementary Figure 1L. Cerebellum.

granular cells — Purkinje cells
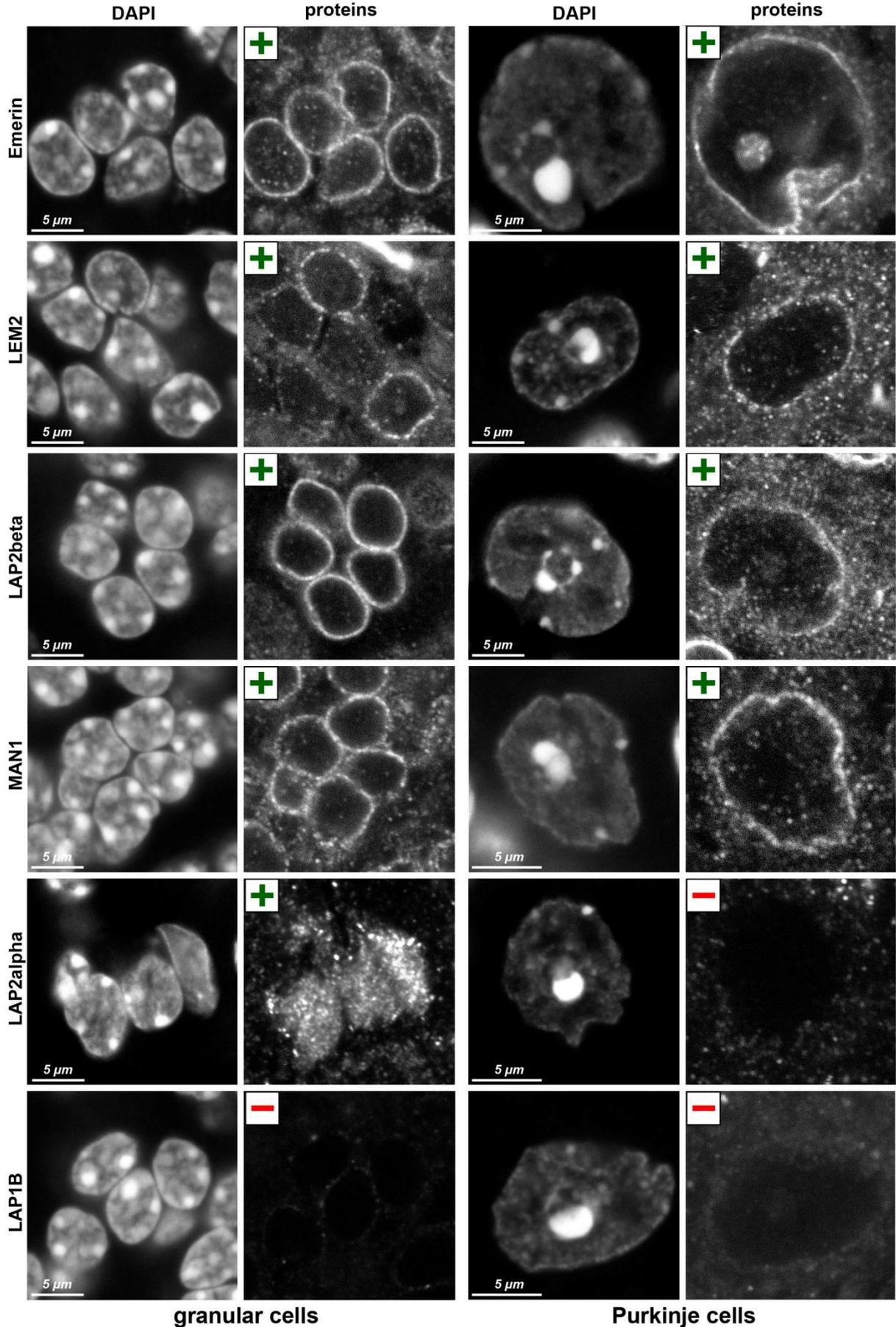
Supplementary Figure 1M. Glial cells of peripheral nerves.
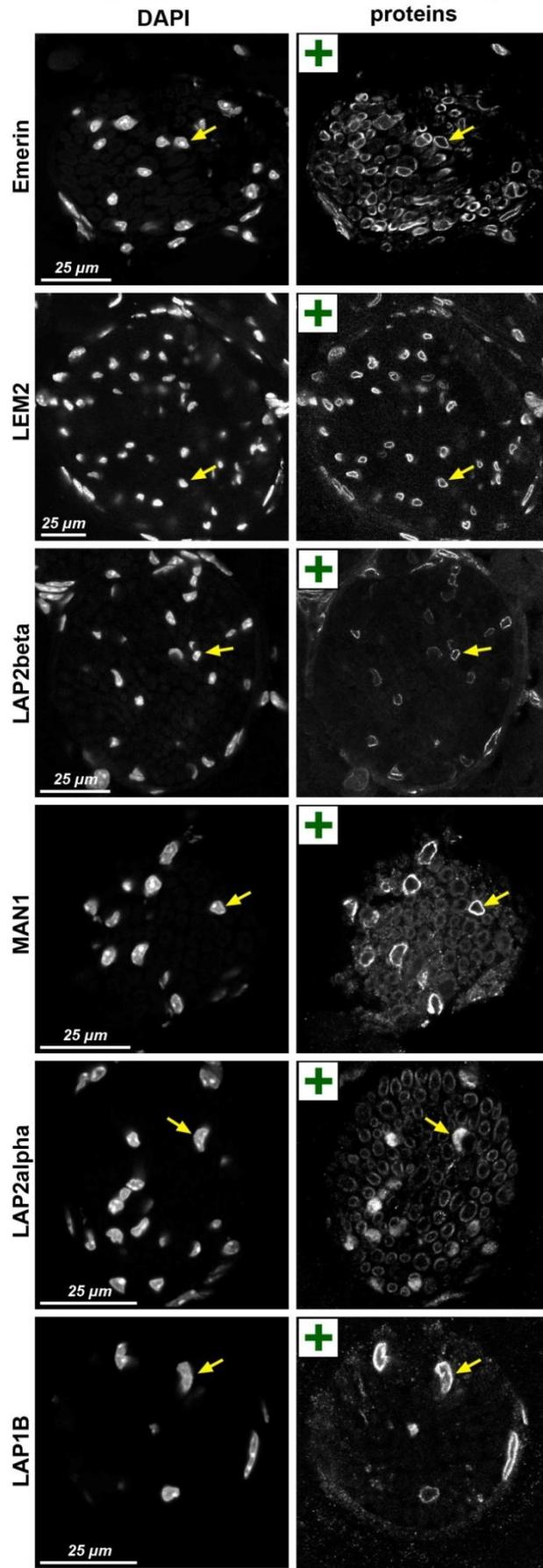
arrows point at nuclei of Schwann cells

Supplementary Figure 2. Expression of LAP2alpha has a clear gradient in renewing epithelia of colon (**A**) and skin epidermis (**B**). **A1**, colon epithelium cells have stronger LAP2alpha staining of their nuclei in the areas of cell proliferation, that is at the bottom and in the mid-part of the crypts; nuclei of differentiated goblet and absorptive cells in the upper crypt regions and colon surface have a weak staining. **A2**, a close up of the bottom parts of the crypts. **B1**, in the thin trunk skin, nuclei of proliferating basal keratinocytes (*b*) have more intense staining than nuclei of differentiated suprabasal keratinocytes (*sb*). **B2,3**, in thick skin of lower leg the gradient from bottom up is more clear due to multiple suprabasal layers of differentiated keratinocytes. *ks,* keratinized squames with degenerated nuclei*; d,* derma. All images are single confocal sections.
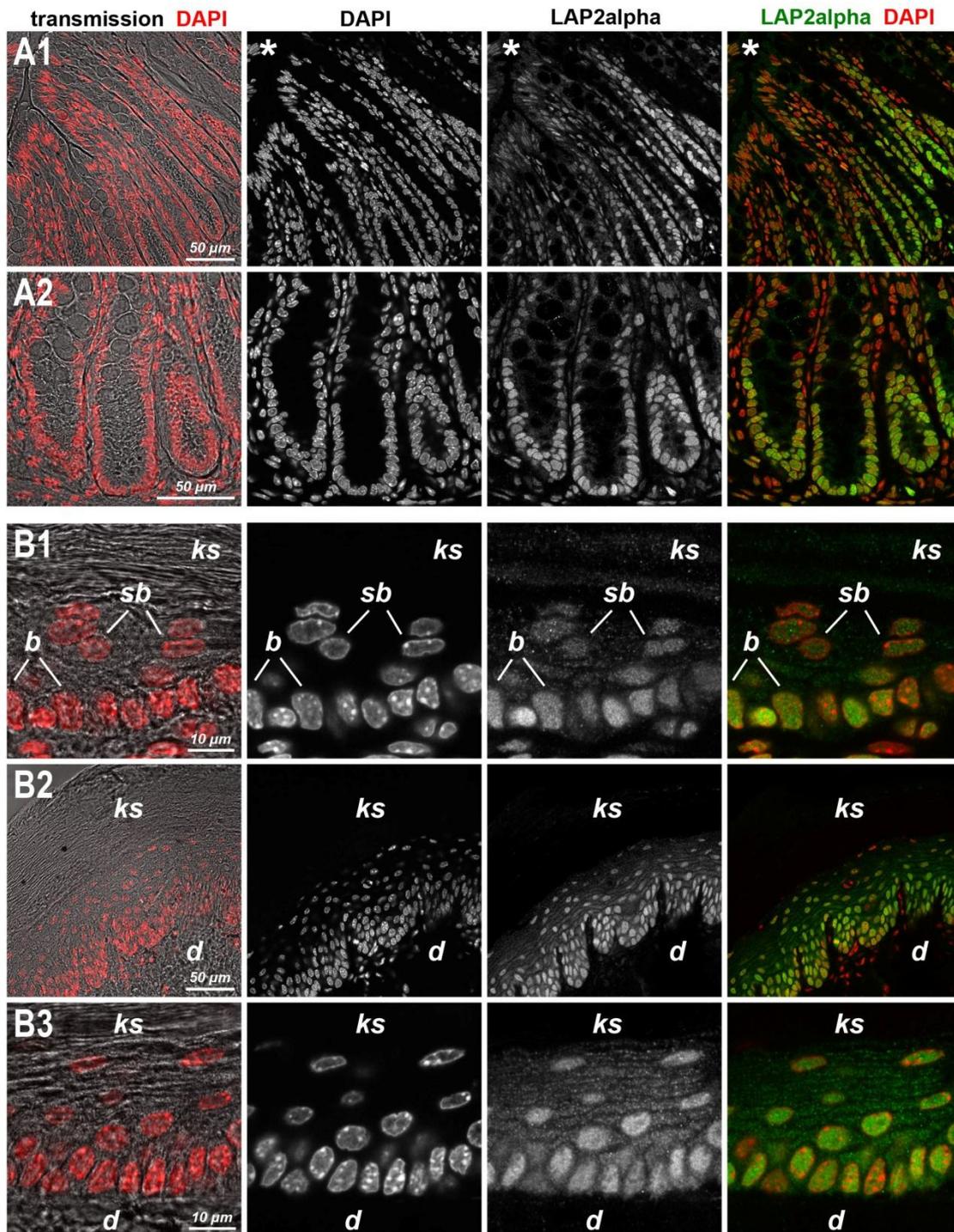
Supplementary Figure 3. Similar mislocalization of LEM2 in the nuclear envelope of keratinocytes in skin from A/C-KO mouse and mouse with truncated LA/C. Compare an even distribution of LEM2 over entire NE of suprabasal keratinocytes expressing high level of LA/C in WT mouse (*empty arrowheads*) *versus* patchy accumulations of LEM2 in LA/C-deficient cells of both mutated mice (*solid arrowheads*). All images are maximum intensity projections of confocal stacks through 2 µm.
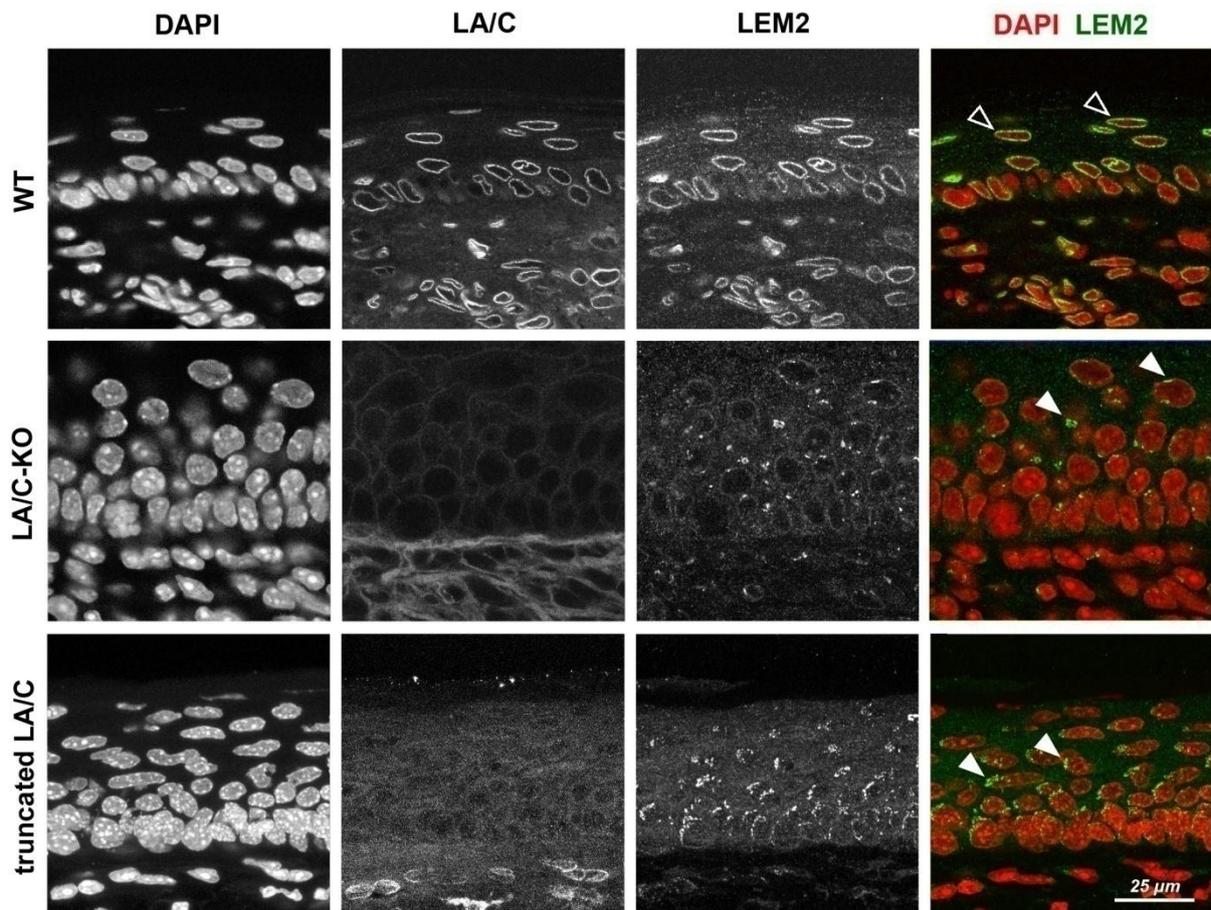
Supplementary Figure 4. Examples of LEM2 mislocalization in the nuclei of muscle tissues from LA/C-KO mouse. Immunostaining of LEM2 in limb skeletal muscles (*upper raw*), heart muscles (*middle raw*), and smooth muscles of colon (*bottom raw*) from WT and LA/C-KO mice. In WT cells, LEM2 is distributed over the entire NE. In KO cells of myotubes and cardiomyocytes, LEM2 is either absent or has pronouncedly aberrant localization to herniations or long NE extensions. In smooth muscles, LEM2 accumulates in patches at one or both poles of the elongated nuclei. All images are maximum intensity projections of confocal stacks through 2-5 µm.
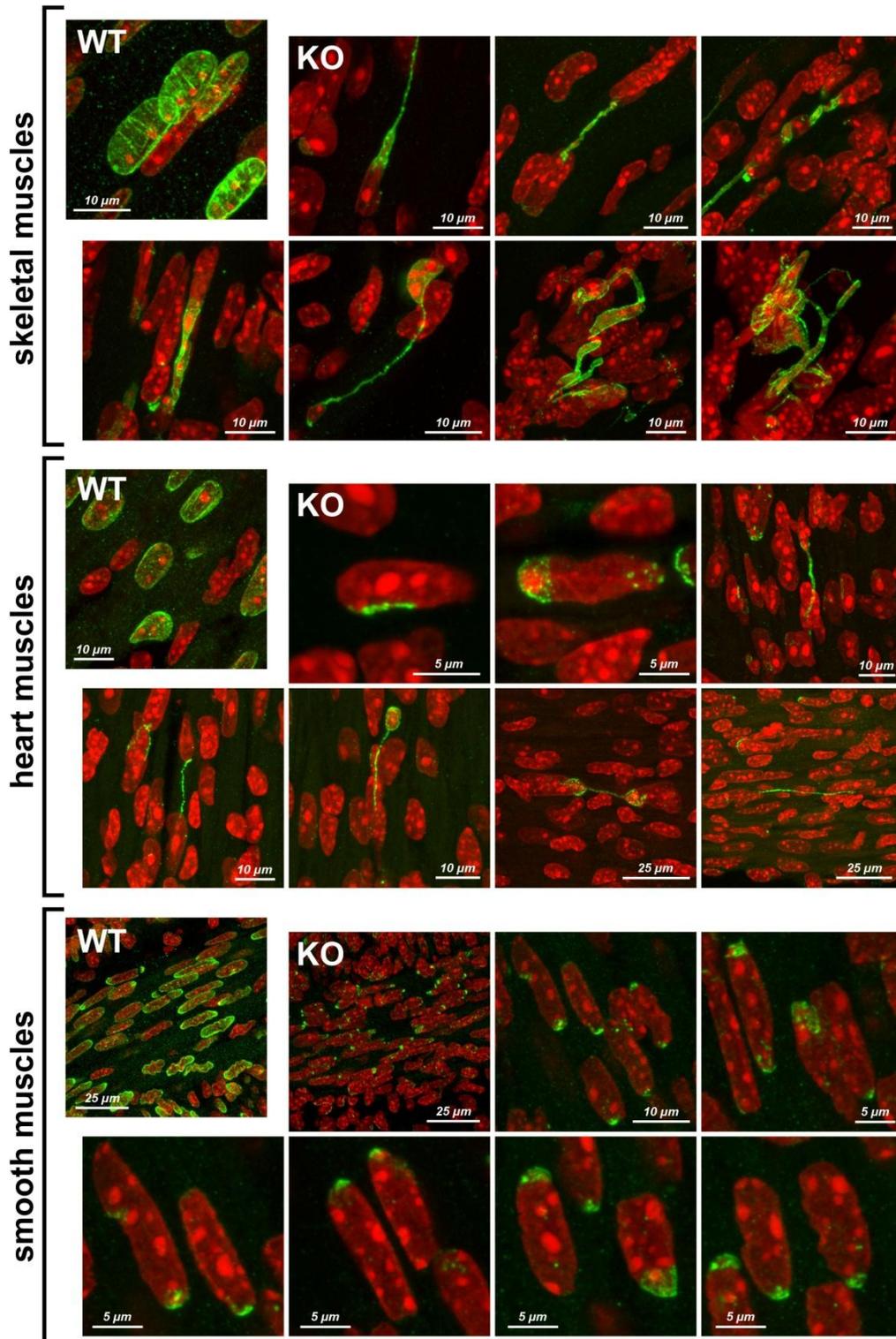
Supplementary Figure 5. LEM2 mislocalization in epithelial cells from mice with villin-driven (A;B) and keratin 14 (K14)-driven (C) LA/C-KO. Nuclei of epithelial cells depleted of LA/C do not express or have abnormal patchy NE accumulation of LEM2 (*empty arrowheads*), similarly to cells from global LA/C-KO (compare to Fig.7 and SFig.3,4). *Asterisks* mark crypt lumens in duodenum and colon. Red arrows point at LA/C-positive smooth muscles (in intestine) or fibroblasts (in skin derma). Note that in contrast to epithelial cells of villi (*solid arrowheads*), crypt cells in duodenum (*asterisk*) do not express LA/C and LEM2 in WT mice and therefore are lacking aberrant LEM2 patches. All images are maximum intensity projections of confocal stacks through 2 µm.
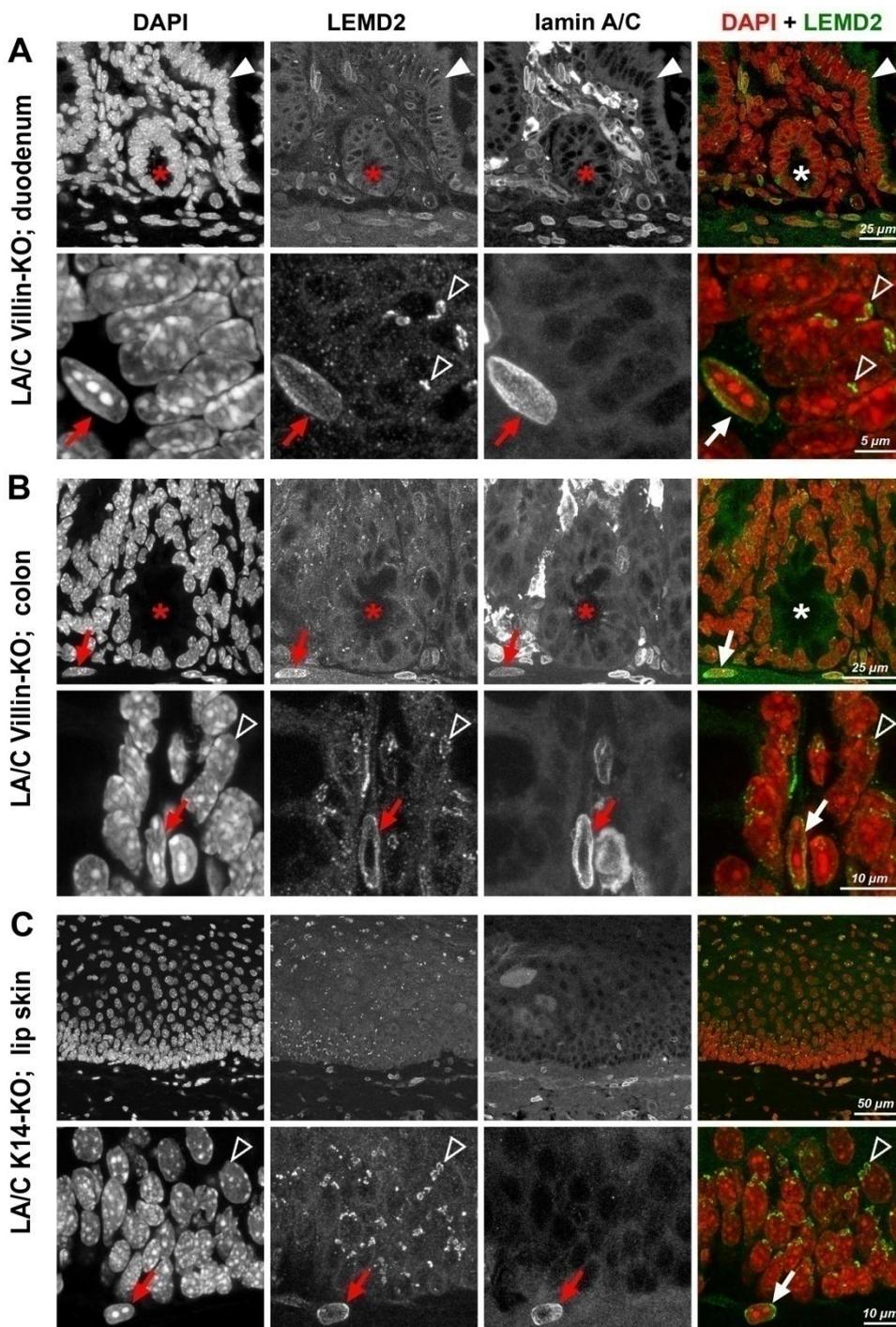
2.3 Epigenetics of eu- and heterochromatin in inverted and conventional nuclei from mouse retina

Epigenetics of eu- and heterochromatin in inverted and conventional nuclei from mouse retina

Anja Eberhart · Yana Feodorova · Congdi Song · Gerhard Wanner ·
Elena Kiseleva · Takahisa Furukawa · Hiroshi Kimura · Gunnar Schotta ·
Heinrich Leonhardt · Boris Joffe · Irina Solovei

Abstract To improve light propagation through the retina, the rod nuclei of nocturnal mammals are uniquely changed compared to the nuclei of other cells. In particular, the main classes of chromatin are segregated in them and form regular concentric shells in order; inverted in comparison to conventional nuclei. A broad study of the epigenetic landscape of the inverted and conventional mouse retinal nuclei indicated several differences between them and several features of general interest for the organization of the mammalian nuclei. In difference to nuclei with conventional architecture, the packing density of pericentromeric satellites and LINE-rich chromatin is similar in inverted rod nuclei; euchromatin has a lower packing density in both cases. A high global chromatin condensation in rod nuclei minimizes the structural difference between active and inactive X chromosome homologues. DNA methylation is observed primarily in the chromocenter, Dnmt1 is primarily associated with the euchromatic shell. Heterochromatin proteins HP1-alpha and HP1-beta localize in heterochromatic shells, whereas HP1-gamma is associated with euchromatin. For most of the 25 studied histone modifications, we observed

Responsible Editor: Dr. Beth Sullivan.

Anja Eberhart and Yana Feodorova contributed equally to this work.

A. Eberhart · Y. Feodorova · C. Song · H. Leonhardt ·
B. Joffe · I. Solovei (✉)
Department of Biology II, Center for Integrated Protein
Science Munich (CIPSM), Ludwig Maximilian University
Munich, Grosshadernerstrasse 2, Planegg-Martinsried,
82152 Munich, Germany
e-mail: Irina.Solovei@lrz.uni-muenchen.de

G. Wanner
Department of Biology I, Biocenter, Ludwig Maximilian
University Munich, Grosshadernerstrasse 2,
Planegg-Martinsried, 82152 Munich, Germany

E. Kiseleva
Institute of Cytology and Genetics, Siberian Branch of the
Russian Academy of Sciences, Novosibirsk 630090, Russia

T. Furukawa
Laboratory for Molecular and Developmental Biology,
Institute for Protein Research, Osaka University, 3-2
Yamadaoka, Suita, Osaka 565-0871, Japan

H. Kimura
Graduate School of Frontier Biosciences, Osaka University,
1-3 Yamadaoka, Suita, Osaka 565-0871, Japan

G. Schotta
Center for Integrated Protein Science Munich (CIPSM) at
the Adolf-Butenandt-Institute, Department of Molecular
Biology, Ludwig Maximilian University Munich,
80336 Munich, Germany

predominant colocalization with a certain main chromatin class. Both inversions in rod nuclei and maintenance of peripheral heterochromatin in conventional nuclei are not affected by a loss or depletion of the major silencing core histone modifications in respective knock-out mice, but for different reasons. Maintenance of peripheral heterochromatin appears to be ensured by redundancy both at the level of enzymes setting the epigenetic code (writers) and the code itself, whereas inversion in rods rely on the absence of the peripheral heterochromatin tethers (absence of code readers).

Keywords Spatial organization of the nucleus · Epigenetic code · Core histones · Histone modifications · Peripheral heterochromatin · LINE-rich chromatin · SINE-rich chromatin · X chromosome · Retina · Chromocenters · DNMT1 · HP1

Abbreviations

B1	Abundant mouse SINE repeat family
CKO	Conditional knockout
DAPI	4′,6-diamidino-2-phenylindole
DNMT1	DNA (cytosine-5)-methyltransferase 1
DOP-PCR	Degenerate oligonucleotide-primed PCR
ES cells	Embryonic stem cells
FISH	Fluorescence in situ hybridization
G9a	H3K9 methyltransferase
GCL	Ganglion cell layer
HP1	Heterochromatin binding protein 1
INL	Inner nuclear layer
KMTase	Histone-lysine N-methyltransferase
L1	Abundant mouse LINE repeat family
LBR	Lamin B receptor
LINE	Long interspersed nuclear elements
5mc	5-methylcytosine
5hmc	5-hydroxymethylcytosine
MSR	Major satellite repeat
RNA Pol-II CTDx	non-phosphorylated carboxy-terminal domain of RNA polymerase II
RNA Pol-II Ser2ph	Phosphorylated serine 2 of heptapeptide repeat on carboxy-terminal domain of RNA, polymerase II
RNA Pol-II Ser5ph	Phosphorylated serine 5 of heptapeptide repeat on carboxy-terminal domain of RNA, polymerase II
SEM	Scanning electron microscopy
SINE	Short interspersed nuclear elements
TEM	Transmission electron microscopy
Xa	X active chromosome
Xi	X inactive chromosome
Xist	X inactive specific transcript

Introduction

The vast majority of eukaryotic nuclei adopt the same "conventional" pattern of chromatin distribution: heterochromatin lines the nuclear envelope and the border of the nucleoli, whereas euchromatin is situated between the two heterochromatic domains (Fig. 1, middle). In mammals, this pattern is based on distinct nuclear locations of the main chromatin classes marked by enrichment in specific repeats (Korenberg and Rykowski 1988; Chen 1989). In brief, satellite repeats form pericentromeric C-bands in mitotic chromosomes; they cluster to foci adjoining the nuclear border or the border of the nucleoli in interphase and postmitotic nuclei. In humans, pericentromeric satellites are built of alphoid DNA. In mice, pericentromeric satellites are comprised of major satellite repeat (MSR) which is very abundant; mouse pericentromeric chromosome regions fuse to prominent spherical bodies, so-called chromocenters in interphase and differentiated cells. The rest of the nuclear periphery and the margins of the nucleoli are lined by heterochromatin forming G-bands of mitotic chromosomes; its hallmark is enrichment in long interspersed repeats (LINEs). Euchromatin corresponds to R-bands of mitotic chromosomes; it is situated in the nuclear interior, gene-rich, and enriched in short interspersed repeats (SINEs). The above mentioned main chromatin classes (Solovei et al. 2009) bear distinctly different epigenetic marks and the distribution of histone modifications largely corresponds to R/G-banding in mitotic chromosomes; most prominently, the distribution of active marks, such as H3K4me3, H3K9ac, and H3K27ac,
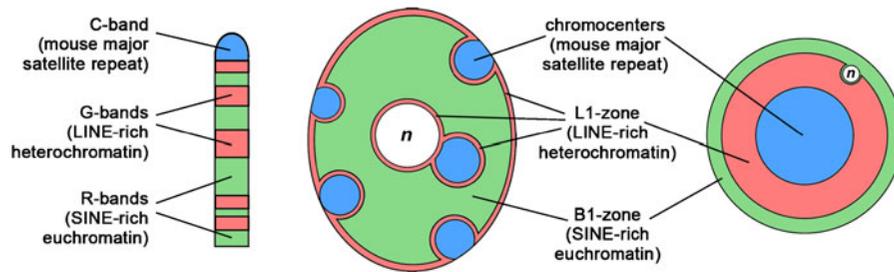
Fig. 1 Conventional and inverted nuclear architecture. Schematic of the positions of the main chromatin classes in mouse mitotic chromosome bands (*left*), conventional (*middle*), and inverted (*right*) nuclei. *n*, nucleolus

correlates with the density of genes and SINEs (Terrenoire et al. 2010).

The correspondence between chromosomal bands and chromatin type appears to have a key importance for the functional spatial organization on the nuclei. Early fluorescence in situ hybridization (FISH) studies demonstrated that euchromatin preferably localizes in the nuclear interior, whereas heterochromatin abuts the nuclear envelope and the border of nucleoli (Croft et al. 1999; Boyle et al. 2001; review: Joffe et al. 2010). Recent studies using chromosome conformation capture-based methods confirmed that this condition is faithfully observed in mammalian nuclei (Gibcus and Dekker 2013). In mammals (in human, in the first place, but also in mouse) there is a correlation between the size and gene-richness (respectively, GC-content and repeat composition) of chromosomes. The internal nuclear positioning of euchromatin in human nuclei correlates with preferable association of small chromosomes with the nucleolus (Carvalho et al. 2001), whereas larger, gene-poorer chromosomes more often bind to the nuclear envelope. Remarkably, this feature is possibly controlled by G-bands situated close to chromocenters, while the positions of chromosomes in the nucleus depend on, and can be experimentally changed by, modification of heterochromatin interactions with nuclear envelop proteins (Mehta et al. 2010).

The nuclei of rod photoreceptors from nocturnal mammals are a unique example of a nuclear architecture different from the conventional pattern described in the previous paragraph. These nuclei actually function as microlenses that help reduce photon loss in the retina, which is crucial for vision at very low light intensities (Solovei et al. 2009). The lensing properties are due to the dramatic reorganization of the nuclear architecture. Mouse rod nuclei are small, spherically symmetrical, and consist of three concentric shells (Fig. 1, right) corresponding to the main chromatin classes. The center

of the nucleus is occupied by the single chromocenter. It is encircled by a shell of LINE-rich chromatin, whereas SINE-rich euchromatin forms the outermost shell. Thus, relative positions of the three main chromatin classes are actually inverted compared to the conventional nuclei (Fig. 1). Remarkably, inverted nuclei of rod photoreceptors are fully functionally active and even have a very high overall transcriptional level (Siegert et al. 2012), which justifies using them as a model for studying the functional organization of the nucleus.

In mouse development, inversion occurs by slow remodeling of the conventional nuclear architecture during postnatal differentiation of rod cells. The two main components of the remodeling are (1) separation of heterochromatin from the nuclear envelope and its concentration around chromocenters accompanied by (2) chromocenter fusion (Solovei et al. 2009). We have recently shown that in mammalian cells, peripheral heterochromatin is maintained by two nuclear envelope-associated tethers (Solovei et al. 2013). One of them is formed by the inner nuclear membrane protein lamin B receptor (LBR) which is both necessary and sufficient for peripheral heterochromatin tethering. The other needs lamin A/C and a chromatin-binding mediator, probably, a protein complex including LEM-domain proteins. Rods of mice and other nocturnal mammals express neither LBR, nor lamin A/C which leads to inversion. Peripheral heterochromatin can be restored in mouse rod nuclei by transgenic expression of LBR (LBR-TER mice).

The findings described above raise the question what marks chromatin for binding by the tethers and recruitment to the nuclear periphery. LBR includes a Tudor domain which binds to chromatin with a range of silencing histone modifications in vitro (Hirano et al. 2012; Makatsori et al. 2004), suggesting that peripheral heterochromatin tethers read silencing histone modifications. Epigenetic factors play a pivotal role in heterochromatin

formation (Almouzni and Probst 2011; Black et al. 2012; Dambacher et al. 2010). They also contribute to the peripheral location of heterochromatin in the nuclei with conventional nuclear architecture (Kind et al. 2013; Towbin et al. 2012; Zullo et al. 2012). The distribution of several histone modification marks has recently been studied in the retina at the light microscopy (Helmlinger et al. 2006; Nasonkin et al. 2011; Popova et al. 2012, 2013; Rao et al. 2010) and electron microscopy levels (Kizilyaprak et al. 2010, 2011), but systematic testing of epigenetic marks has not been carried out. We undertook an extensive study of the epigenetic chromatin landscape in rods compared to retinal nuclei with conventional nuclear architecture and found several differences between them and several features of general interest for the organization of the mammalian nuclei.

Materials and methods

Animals, tissue fixation, and retina cryosections Wild type retinas from ICR/CD1 and C57Bl/6 mice were studied as wild type. Mice with combined deletions of Suv3-9 and Suv4-20 were bred from lines with single gene deletions described earlier (Peters et al. 2001; Schotta et al. 2008). Mice with *Dkk3*-driven G9a (*Ehmt2*) conditional knockout were bred as described earlier (Katoh et al. 2012).

Retinas were excised from mice killed by cervical dislocation according to the standard protocol. Eyes were enucleated immediately after death; retinas were dissected and fixed with 4 % formaldehyde in PBS for different time intervals (see below). Infiltration with sucrose, embedding in freezing medium and cryosection preparation were performed as described previously (Eberhart et al. 2012; Solovei 2010). Importantly, retina samples after various fixation times (15, 30 min, 1, 3 h, and in some cases—24 h) were arranged in the respective order in the same block to assure that each cryosection contains all five retinas.

Immunostaining of cryosections Immunostaining was performed according to the protocol described in detail earlier (Eberhart et al. 2012). This method allows quick testing of a wide range of fixation and antigen retrieval times and detection of the range in which the results of staining are robust. In brief, for every antibody, four pretreatments of cryosections were used: without antigen

retrieval and with antigen retrieval by heating in 10-mM sodium citrate buffer (up to 80 °C; She et al.1997, 2001) for 5, 10, or 20 min. In a few cases, a longer (30 min) heating was applied. Sections containing retina samples after four different fixation times were subjected to antigen retrieval and consequent immunostaining together. Thus, for each antibody we were able to compare 16 (in some cases 25) different variants of conditions and find the range of conditions under which staining results were robust to variation in fixation and antigen retrieval times (Fig. S1). Images of rod nuclei, inner nuclear layer (INL) cell nuclei (usually, bipolar cells) and, when needed, ganglion cells and cones were acquired.

The primary antibodies used in this study are listed in Table 1. Most of the antibodies against histone modifications were mouse monoclonal produced in the laboratory of H. Kimura (Chandra et al. 2012; Hayashi-Takanaka et al. 2011; Kimura et al. 2008). Secondary antibodies were anti-mouse conjugated to Alexa555 (Invitrogen A31570) or Alexa488 (Invitrogen A21202) and anti-rabbit conjugated to DyLight549 (Jackson Immuno-Research 711-505-152) or DyLight488 (Jackson ImmunoResearch 711-485-152). After staining, sections were mounted under a coverslip in Vectashield, (Vector).

FISH Paint probe for mouse X chromosome (MMU X) was a kind gift of J. Wienberg (University of Cambridge, UK). MMU X was amplified and labeled with biotin using DOP-PCR (Cremer et al. 2008). For Xist RNA detection, Xist exon 6 was amplified by PCR from mouse genomic DNA and labeled with digoxigenin by nick-translation. Retina fixation, preparation, cryosections pretreatment, and FISH were carried out as described elsewhere (Solovei 2010). All FISH experiments were performed on denatured sections, so that both DNA/DNA and DNA/RNA hybrids were detected. At these conditions, Xist probe hybridized to both Xist RNA decorating X inactive (Xi) chromosome and Xist genes; Xist-RNA signal is readily distinguishable from the dot-like signals of Xist genes.

Light microscopy Single optical sections or stacks of optical sections were collected using a Leica TCS SP5 confocal microscope equipped with Plan Apo ×63/1.4 NA oil immersion objective and lasers with excitation lines 405, 488, 561, 594, and 633 nm. Dedicated plug-ins in ImageJ program were used to compensate for axial chromatic shift between fluorochromes in confocal stacks, to

Table 1 List of used antibodies

Antibodies against 5-methylcytidine

Antigen	Antibody source
5mC	Eurogentec (MMS-900P-B)

List of antibodies against histone modifications

Residue	Modification	Antibody source
H3K9	acetyl	HK (CMA310)
	me1	HK (CMA316)
	me2	HK (CMA317)
	me2	Abcam (ab1220)
	me3	HK (CMA318)
H3K56	me3	S.Hake lab (Jack et al. 2013)
H4K20	acetyl	HK (CMA420)
	me1	HK (CMA421)
	me2	HK (CMA422)
	me3	HK (CMA423)
H3K27	acetyl	HK (CMA309)
	me1	HK (4C4)
	me2	Abcam (ab24684)
	me3	HK (CMA323)
	me3	Abcam (ab6002)
H3K4	acetyl	Active motif (#39382)
	me1	HK (CMA302)
	me2	HK (CMA303)
	me3	Abcam (ab8580)
H3K36	acetyl	Active motif (#39380)
	me1	HK (CMA331)
	me2	HK (CMA332)
	me3	HK (CMA333)
H4K5	acetyl	HK (CMA405)
H4K8	acetyl	HK (CMA408)
H4K12	acetyl	HK (CMA412)
H4K16	acetyl	HK (CMA416)

List of antibodies against nuclear proteins

Antigen		Antibody source
Pol-II	CTD	HK (CMA601)
	Ser 2 ph	HK (CMA602)
	Ser 5 ph	HK (CMA603)
HP1alpha		Euromedex (2HP-1H5-AS)
HP1beta		Euromedex (1MOD-1A9-AS)
HP1gamma		Euromedex (2MOD-1G6-AS)
DNMT1		Abnova (PAB15590)
B23		Sigma (B 0556)

create RGB stacks/images, and to arrange them into galleries (Ronneberger et al. 2008; Walter et al. 2006).

Transmission electron microscopy Whole eye-balls were fixed using the so-called phase-partition fixation (Kiseleva et al. 2001; Zalokar and Erk 1977) first for 5 min and then after puncturing with a needle for 12 h at 4 °C. Fixative was prepared by mixing and shaking of 10 ml 15 % glutaraldehyde in water with 7 ml n-heptane, which yielded a two-phase solution; the upper phase consisting of heptane saturated with glutaraldehyde was used for tissue fixation. After fixation, eye-balls were cut equatorially in two halves and the corneas with the vitreous were removed. The remaining eye-cups with retinas were then washed with 0.1-M cacodylate buffer and cut into smaller pieces (2×8 mm). Samples were postfixed with 1 % OsO_4 and 0.8 % potassium ferrocyanide in the same buffer for 1 h at room temperature. After washings in distilled water, samples were incubated in 1 % aqueous solution of uranyl acetate (Serva) for 1 h at 4 °C, dehydrated in ethanol series and acetone, and embedded in Agar 100 Resin (Agar Scientific Ltd.). Ultra-thin sections were stained with uranyl acetate and Reynolds lead citrate and were examined with a transmission electron microscope (JEM 100 SX, JEOL) at 60 kV.

Scanning electron microscopy Retinas were fixed with 2.5 % glutaraldehyde in buffer (50-mM cacaodylate, 2-mM MgCl2, and 100-mM NaCl pH 7.0) for 2 h, washed in buffer, postfixed with 1 % OsO_4 in buffer for 90 min, incubated in 30 % dimethylformamide in buffer, frozen in liquid nitrogen, fractured with razor blades, washed in buffer, and dehydrated in a graded series of acetone. The pieces were critical point dried from liquid CO_2, mounted with Tempfix onto aluminum stubs and ca. 5 nm sputter-coated with platinum. Specimens were examined with a Zeiss AURIGA CrossBeam Workstation. Micrographs were taken at an accelerating voltage of 1 kV with the chamber SE-detector.

Results and discussion

Freeze-fractured scanning EM shows little difference between the MSR- and LINE-rich heterochromatin shells of rod nuclei

Scanning electron microscopy (EM) of freeze-fractured retina samples revealed that the two central (heterochromatic) shells of rod nuclei are homogenously dense, whereas the narrow outer (euchromatic) shell has a much

lower density, due to which a fibrous structure becomes apparent (Fig. 2d,e). In rods, chromocenters proper (built of MSR) are indistinguishable from the LINE-rich material in freeze-fracture SEM images. Usually, they also remain

indistinguishable in conventional TEM images, but under appropriate conditions, the chromocenters can be distinguished as more electron-dense round profiles. We observed this difference both in adult rod nuclei
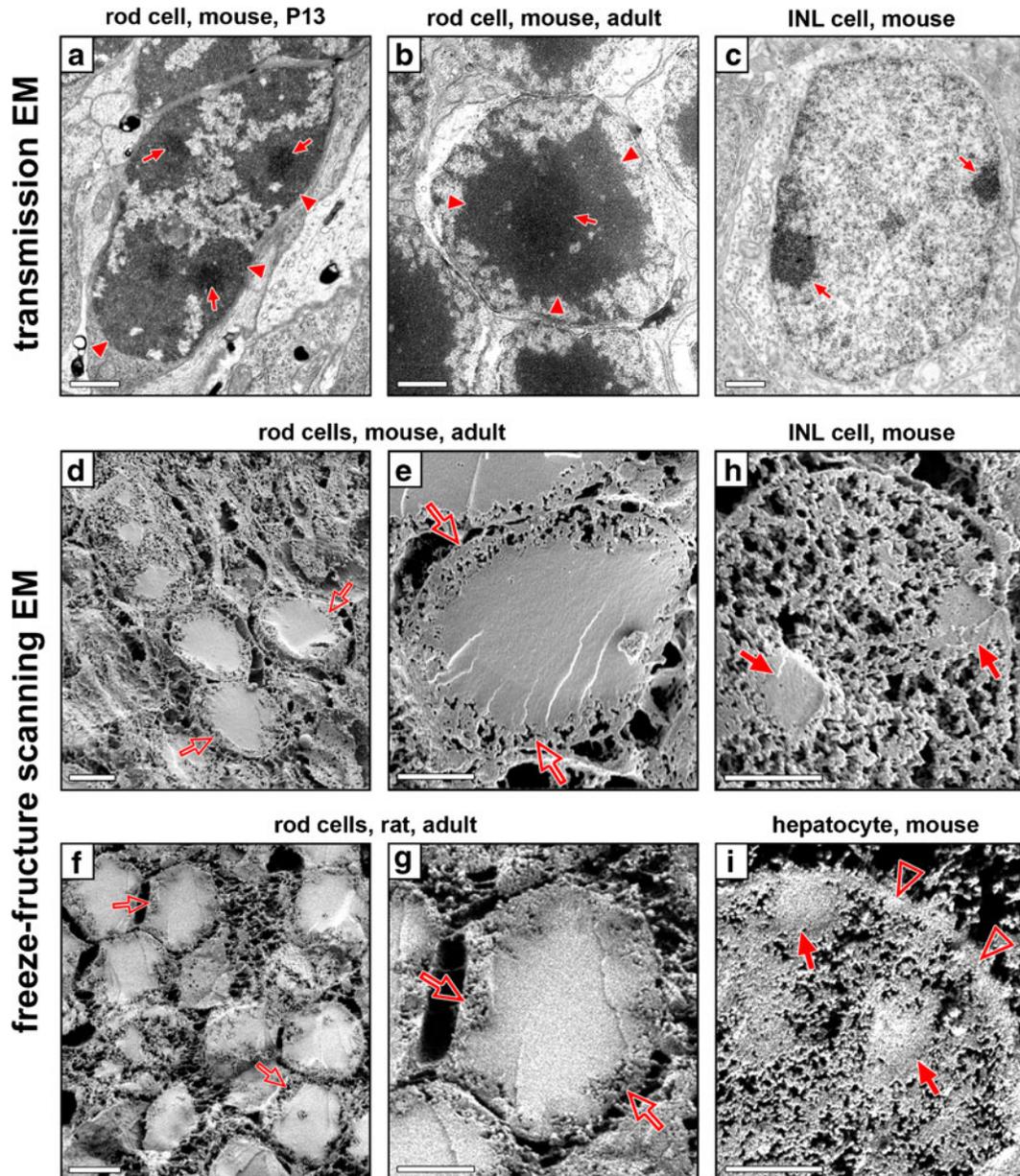
Fig. 2 Ultrastructure of nuclei in mouse and rat. a–c Transmission electron micrographs of ultrathin sections. a Rod cell from a P13 mouse. Note the large heterochromatic domains (arrowheads) with more electron dense chromocenters (arrows) in the middle. b Rod cell from adult mouse. Note the single heterochromatic domain (arrowheads) with more electron dense chromocenter (arrow) in the center of the nucleus. c Nucleus of mouse INL cell contains mostly decondensed chromatin and

possesses multiple small chromocenters (arrows). d–i Scanning electron micrographs of freeze-fractured retinas. d–g Rod photoreceptor nuclei from adult mouse (d, e) and rat (f, g). Note the dense chromatin filling of most of the nucleus and the peripheral zone of less condensed chromatin (empty arrows). h, i Mouse nuclei from INL (h) and liver (i) cells. Note chromocenters (arrows) and a thick layer of peripheral heterochromatin (empty arrowhead) Scale bars a-c, e, g–i 1 μm; d, f, 2 μm

(Fig. 2b) and in rod nuclei from P13 mice (Fig. 2a) which still have several chromocenters surrounded by clouds of LINE-rich heterochromatin. In the nuclei of other neurons, small much less electron-dense chromocenters can be readily seen (Fig. 2c). Most of the volume of nuclei with a conventional architecture is filled with chromatin of lower density than that of chromocenters. In TEM images of neurons, very little electron-dense material is observed close to the nuclear envelope (c.f. P13 and adult rods). Indeed, after freeze-fracturing, the layer of dense heterochromatin along the nuclear envelope is thin in most neurons (Fig. 2h) but much thicker and more prominent in other cell types, e.g., hepatocytes (Fig. 2i). In difference to mouse, the blocks of pericentric heterochromatin are small in rats and do not form chromocenters. Nevertheless, rat rod cells have an appearance very similar to that of mouse (Fig. 2f,g). Thus, in difference to nuclei with conventional architecture, packing of pericentromeric satellites and LINE-rich chromatin is similar in inverted rod nuclei irrespective of the presence (mouse) or absence (rat) of large blocks of pericentromeric satellite DNA.

Inactive X chromosome does not form Barr body in rod nuclei

The highly symmetric organization of rods, with three radially symmetrical shells (Fig. 1) raises the question about the state of the inactive X chromosome (Xi). X chromosome inactivation does take place in rods. It occurs at an early stage of retina formation and was initially used to selectively mark clones of retinal cells in which one or the other of the two X chromosomes was inactivated (Reese and Tan 1998; Zheng et al. 2009). In conventional nuclei, Xi usually forms the so-called Barr body that can be distinguished due to strong staining by DNA-specific dyes, e.g., DAPI. It is a cluster of condensed chromatin situated at the nuclear periphery or, less often, associated with the nucleolus. The difference typically observed between Xa and Xi after FISH with a whole chromosome paint probe can be exemplified by retinal ganglion cells (Fig. 3a). Xa is usually flat and spread along the nuclear envelope, whereas Xi is smaller, has a more spherical shape, and much less contact with the nuclear envelope. In rod nuclei, Xi and Xa have similar shape. FISH with X-paint probe reveals two similar chromosome territories extending in radial direction from the central chromocenter (Fig. 3b). In rods, as in all cell types with conventional architecture (Pinter et al. 2012), Xi is extensively decorated by H3K27me3 (Fig. 3c). At early stages of rod differentiation, XIST RNA can be readily demonstrated on Xi (Fig. 3d) but, despite numerous efforts, we failed to reveal XIST RNA in rod nuclei at P21 or elder. The absence of staining, however, might depend on increased chromatin density in rods that masks XIST RNA, rather than its real dislocation from Xi in adult rod nuclei. The unusual shape, position, and orientation of Xi in rods well conforms to the demand of symmetry set by the optical function of these nuclei. One can think that Xi is "seamlessly" integrated in the layer of L1-rich heterochromatin because it is highly condensed in rod nuclei.

DNA methylation and DNMT1 are differently distributed in retinal neurons

DNA methylation was observed using antibody to 5-methylcytosine in the pericentromeric heterochromatin and, at a lower level, in the L1-zone of rod cells (Fig. 4a). Recently it was shown that DNA methyltransferase (DNMT1)-dependent DNA methylation plays a crucial role in the expansion of the retinal progenitors and rod cell differentiation (Nasonkin et al. 2013; Rhee et al. 2012). We found that DNMT1 is present in the euchromatic zone of both rod and other retinal neurons (Fig. 4b). DNMTs are actually highly expressed in differentiated neurons (review: Kadriu et al. 2012). Recent results suggest that also demethylation of 5mC leading to its replacement by 5hmC has a critical cell-type-specific effect on gene expression in differentiating neurons (Mellén et al. 2012). In this connection, one can tentatively suggest that, even in differentiated neurons, the methylation status of a proportion of genes is dynamically supported by demethylation and remethylation. This notion corresponds well to euchromatic localization of DNMT1 found by us in retinal neurons, whereas DNA methylation itself is most prominent in the rod chromocenters, the least active part of rod nuclei.

In both photoreceptors and neuroretinal cells we also observed very bright signal in the nucleoli visualized with antibody against nucleophosmin (B23). This is in agreement with the previously demonstrated role of DNMT1 in silencing inactive ribosomal genes (Majumder et al. 2006). Remarkably, in rod cells, the signal from silenced rDNA is always situated at the side of the nucleolus looking to the L1-rich shell, which corresponds to the general gradient of

Fig. 3 Inactive X chromosome in retinal neurons. **a** FISH with X-chromosome paint and probe for Xist RNA in a ganglion cell of the retina. Note that Xa is spread along the nuclear border (*arrowhead*), while Xi (marked by Xist, *arrow*) is smaller and has a more spherical shape. In the shown cell, Xi is attached to a large central chromocenter associated with the nucleolus, but even more often, Xi abuts the nuclear envelope. **b** FISH with X-chromosome paint in a rod cell. Both X-chromosome territories, Xa and Xi, look similarly. **c** H3K27me3 mark in retinal neurons. In all three shown adult cell types (a ganglion cell, an INL cell and rod cells) X inactive is decorated by H3K27me3 (*arrows*). Note that while in neuroretina cells Barr body is visible after DAPI staining, in rod cells it is incorporated into strongly DAPI-positive L1-zone and cannot be discerned. **d** Xist visualized using FISH in a ganglion cell, an INL cell, a cone cell (*top row*) and in rods from retinas of different age (*bottom row*). With the protocol used, Xist genes are also visualized: they look as small dots clearly different from the extended Xist-RNA signals. In rods, Xist RNA is readily detectable until P13; lack of signal in elder mice might depend either on Xist RNA absence (note the two *Xist* genes in the same nucleus), or on masking of Xist RNA due to increased chromatin density. **a**, **c**, **d**, single confocal sections; **b**, maximum intensity projections of 5–8 confocal sections with axial distance 200 nm. *Scale bars* **a**, **c**, **d**, 2 μm; **b** 5 μm
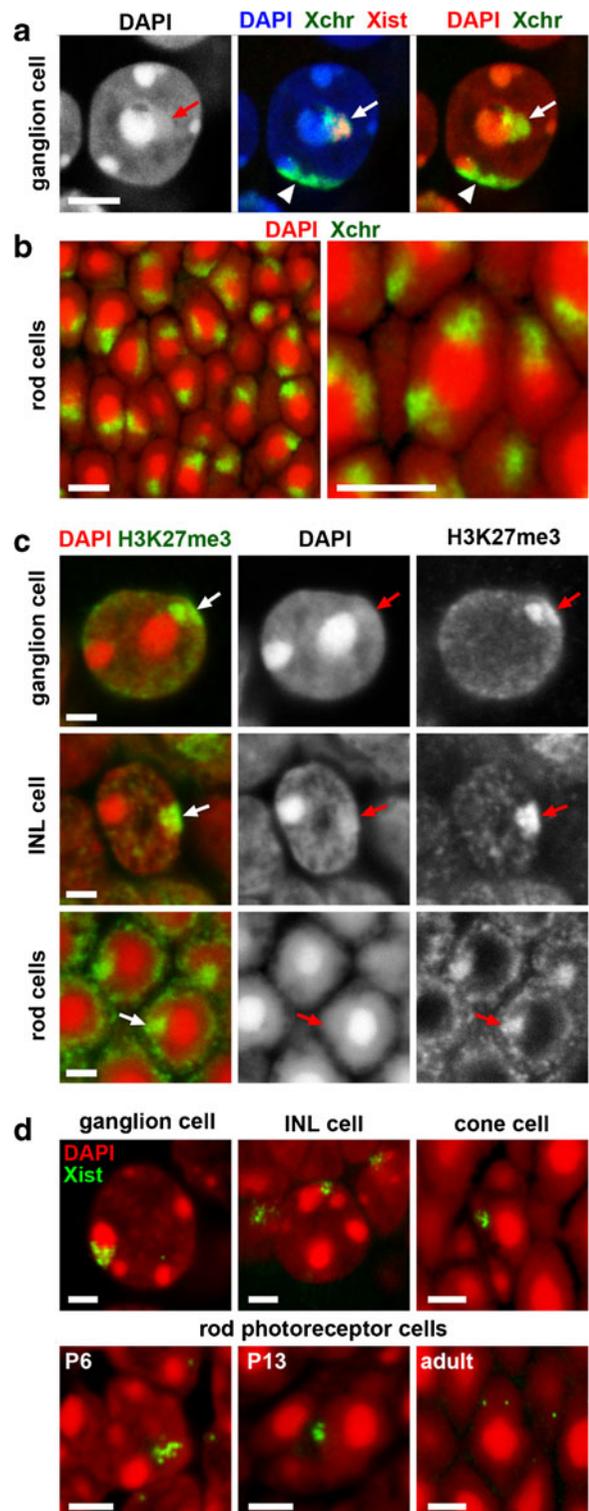
transcriptional activity and chromatin density in rod nuclei (Fig. 4b,c).

Core histone modifications mostly mark the same chromatin classes in conventional and inverted nuclei

Reliability of the results of an immunocytochemical study on tissue sections depends on two factors. Firstly, as with all immunocytochemical studies, it is the sensitivity and specificity of the antibodies used. For this study, we used antibodies generated and extensively tested earlier (Egelhofer et al. 2011; Kimura et al. 2008). Secondly, immunostaining on sections after formaldehyde fixation usually demands antigen retrieval (antigen de-masking after fixation), and the observations should be robust to variation in fixation time and antigen retrieval duration. To this end, we used the approach (Eberhart et al. 2012) which allows quick testing a wide range of fixation and retrieval times and defining an interval in which staining produces robust results (see a brief explanation in Fig. S1).

The results of mapping 25 histone modifications are illustrated in Fig. 5 and summarized in Fig. 6. Due to the clear spatial separation of the main chromatin classes in inverted nuclei, our data highlight prevailing (though not exclusive) association of histone modifications with certain chromatin classes (see also Kizilyaprak et al. 2010

for TEM study of histone modification distribution, including several not covered in our study). Histone
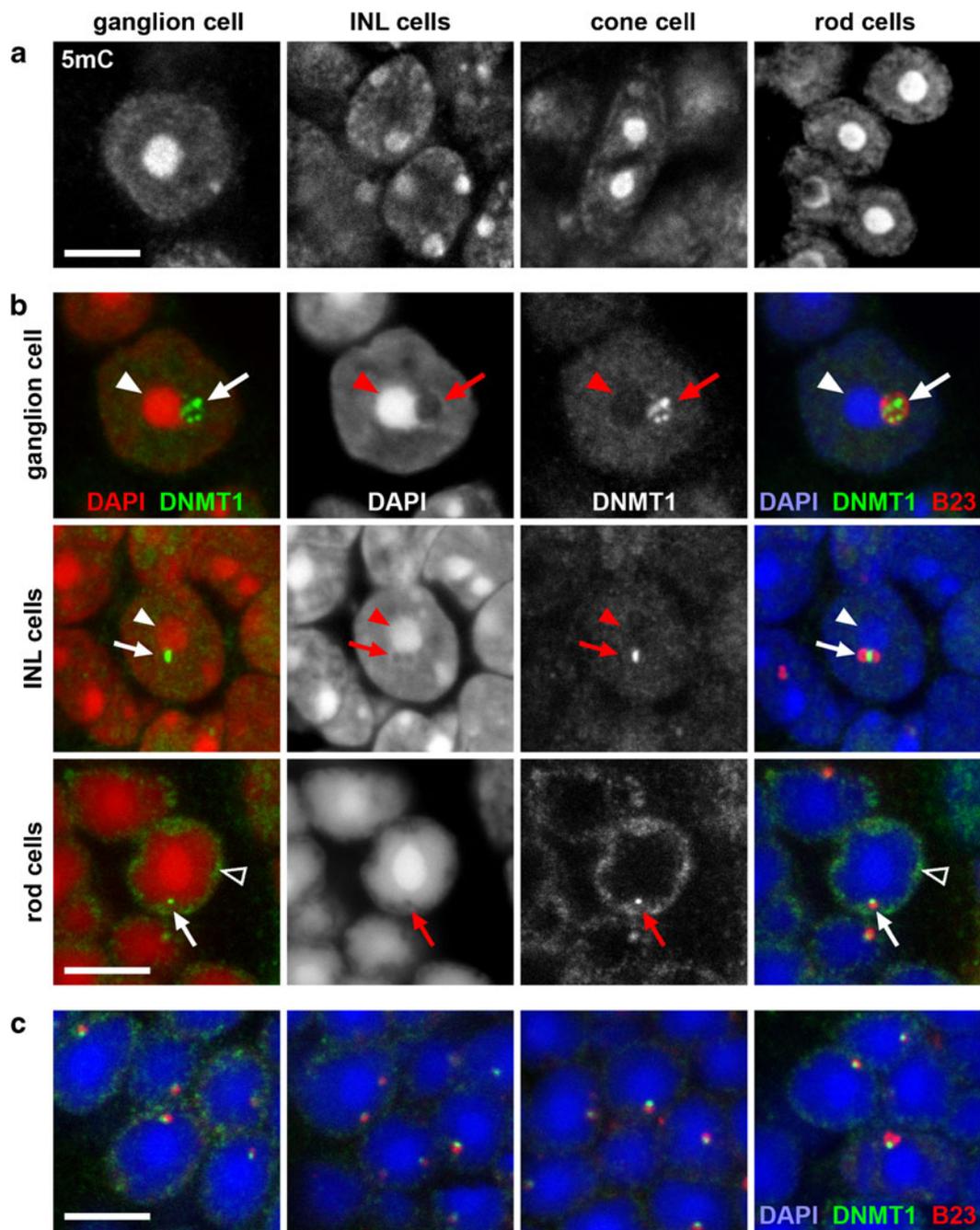
Fig. 4 5-methylcytosine (5mC) and DNMT1. **a** 5mC in ganglion, INL, cone and rod cells. Note the bright signal in the chromocenters and much lower florescence in L1 zone of rod nuclei. DNA staining is not shown because tissue digestion using HCl and DNase, both needed for 5mC immunodetection, prevented normal staining with DAPI. **b** DNMT1 in ganglion, INL, and rod cells. Note diffuse weak signal throughout the nucleoplasm of the ganglion and INL cells. A spot of bright signal (corresponding to inactive rDNA) is situated in the nucleolus marked by anti-pB23 staining (*arrows*); chromocenters adjacent to nucleoli are marked by *solid arrowheads*. In rods, the signal is relatively bright and restricted to B1 shell (*empty arrowhead*) the rod nucleolus also bears a bright spot-like signal. **c** DNMT1 focus always occupies the inner (L1) side of the nucleolus marked by B23. Single confocal sections. *Scale bars*: 5 μm

modifications marking transcriptionally active chromatin or chromatin poised for transcription are associated with euchromatin and their abundance is below the detection level in heterochromatic shells (Fig. 5a). In particular, histone acetylation with a single exception among the studied modifications (for H3K4ac, see below) is associated with the euchromatic shell. Conforming to this distribution of active histone modification marks, all forms of RNA Pol-II have been observed exclusively in the euchromatic shell (Fig. S2): we have not found any differences between the distributions of RNA Pol II in general (anti-CTD, generated against non-phosphorylated peptide), the pausing form (anti-phosphorylated serine 5) and the elongating form (anti-phosphorylated serine 2). H3K27 monomethylation is also abundant in the euchromatic shell, whereas H3K27me2 and me3 show an unusual distribution pattern being common in both euchromatin and LINE-rich heterochromatin (but not in chromocenters, c.f. Kizilyaprak et al. 2010). The same distribution was observed for acetylated H3K4. The latter distribution pattern conforms to involvement of H3K4ac in heterochromatin formation (Xhemalce and Kouzarides 2010). In the case of H3K27 methylation, this pattern is actually rather surprising because these marks are primarily involved in gene silencing via Polycomb pathway and X-chromosome inactivation; they are separated from H3K9 and H4K20 methylation marks and, at least in Xi, are actually depleted in LINE-rich regions (Pauler et al. 2009; Pinter et al. 2012). In bipolar neurons, exemplifying nuclei with a conventional architecture, we found increased abundance of H3K27me2 at the nuclear periphery and around nucleoli, whereas H3K27me3 was rather associated with euchromatin (Fig. 5b).

All histone modifications abundant in pericentromeric heterochromatin are also abundant in LINE-rich chromatin. In contrast, the LINE-rich shell shows some modifications not found in chromocenters. Silencing histone modifications play a pivotal role in heterochromatin formation and several studies indicate the special importance of H3K9 and H4K20 methylation (Dambacher et al. 2010). In particular, H3K9me3 and H4K20me3 are hallmarks of pericentromeric heterochromatin and H3K9-me2,3 play an essential role in heterochromatin formation and positioning in *Caenorhabditis elegans* (Towbin et al. 2012). H3K9me2 has been ascribed a crucial role in transition from pluripotent state (Tachibana et al. 2002, 2008). Written primarily by histone methyl transferase G9a, this epigenetic mark is already very

abundant in ES cells (Lienert et al. 2011) and affects numerous genes, including e.g., the pivotal pluripotency determinants *Oct3/4* and *Nanog* (Yamamizu et al. 2012). H3K9 dimethylation by G9a has also been ascribed a cardinal role in peripheral targeting of lamina-associated DNA (which forms a proportion of AT- and LINE-rich DNA) to the nuclear periphery (Kind et al. 2013).

Given the importance of heterochromatin for the spatial organization of the nucleus, in addition to retina, we studied the distribution of silencing histone modifications in several other cell types. We focused attention on the distribution of H4K20me3, H3K9me3, and H3K9me2. To visualize the latter histone modification we used two antisera (Table S1). One was generated in H. Kimura laboratory (CMA317), the other one, was available from Abcam (Ab1220) and was used in the majority of the earlier studies. Both published (Egelhofer et al. 2011; Hayashi-Takanaka et al. 2011) and our data showed that there is no difference in specificity between the two antibodies; CMA317 antibody produced a brighter signal on sections but the results obtained with the two antibodies were essentially identical (Fig. S3). All three histone modifications mentioned above were abundant in peripheral heterochromatin of other studied cell types. The other typical locations were chromocenters, the layer of LINE-rich chromatin at the periphery of chromocenters, and the periphery of the nucleolus; some positive foci in the nucleoplasm were also regularly observed. A similar distribution of Suv3-9 h1 was observed in rat cells in vivo using Suv3-9 h1-GFP (Bancaud et al. 2009). We found only one noteworthy difference in the distribution of H4K20me3, H3K9me3, and H3K9me2 between the studied cell types. H3K9me2 is undetectable in rod chromocenters, even though it is abundant in chromocenters of other neurons, including cones. More so, H3K9me2 was absent from chromocenters of all studied non-neuronal cell types: skin keratinocytes, colon epithelium, pancreas acinar cells, smooth muscle cells (Fig. 7). The distribution of H3K56me3 followed that of H3K9me3 in tissues, as it did in cultured cells (Jack et al. 2013).

Remarkably, in the rat, which lacks large blocks of pericentromeric satellite repeats and hence chromocenters, the distribution of histone marks in rod nuclei is very similar to that in mouse. We exemplify this by a staining of H4K20 modifications in rat rods (Fig. S4). This similarity conforms to the similar packing density along the radius of rod nuclei observed at the EM level (Fig. 2). Of course, the absence of chromocenters in species without
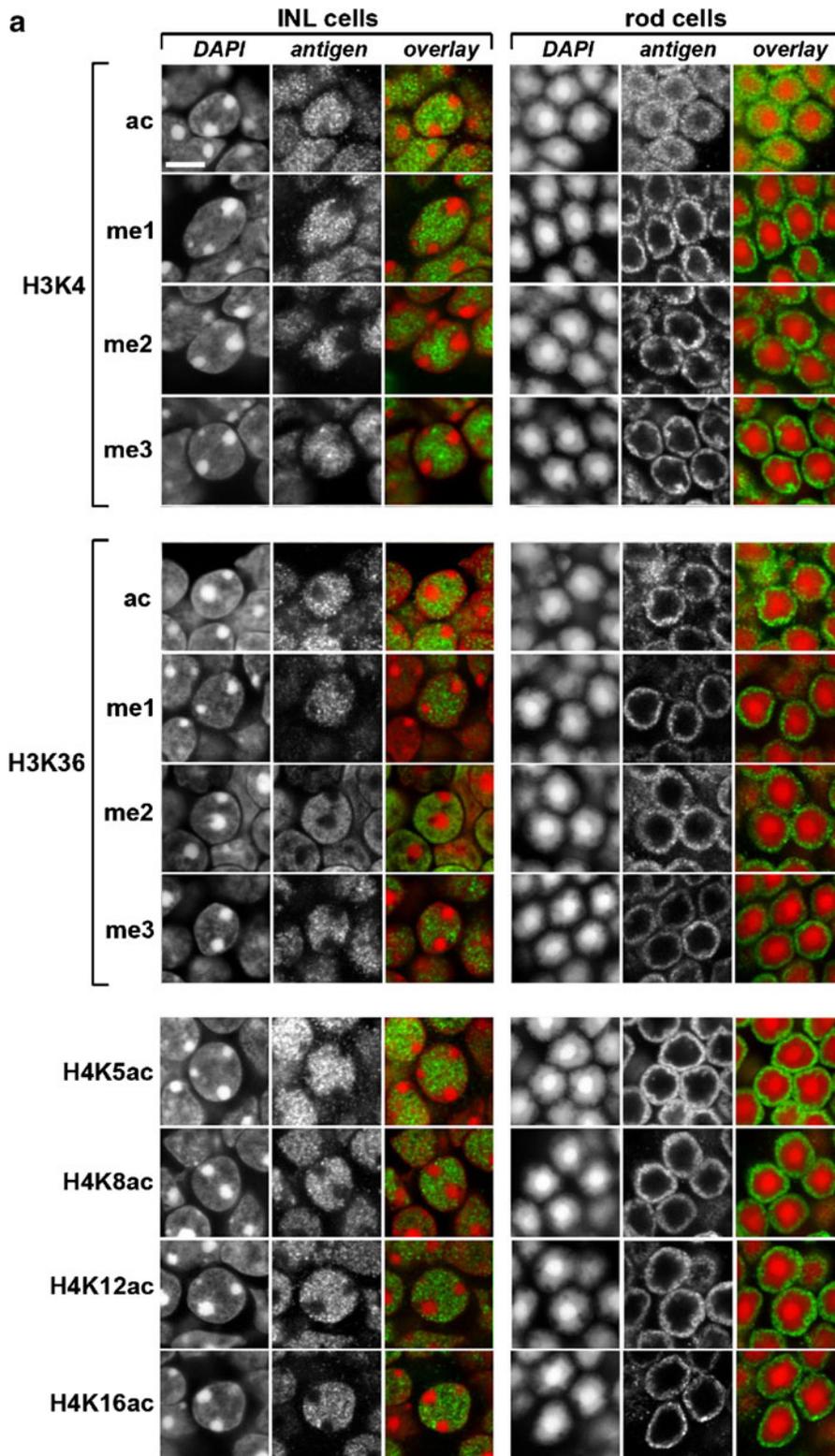
Fig. 5 Histone modifications staining in retinal cells with conventional (*INL*) and inverted (*rods*) nuclear architecture. Single confocal sections. *Scale bars* 5 μm
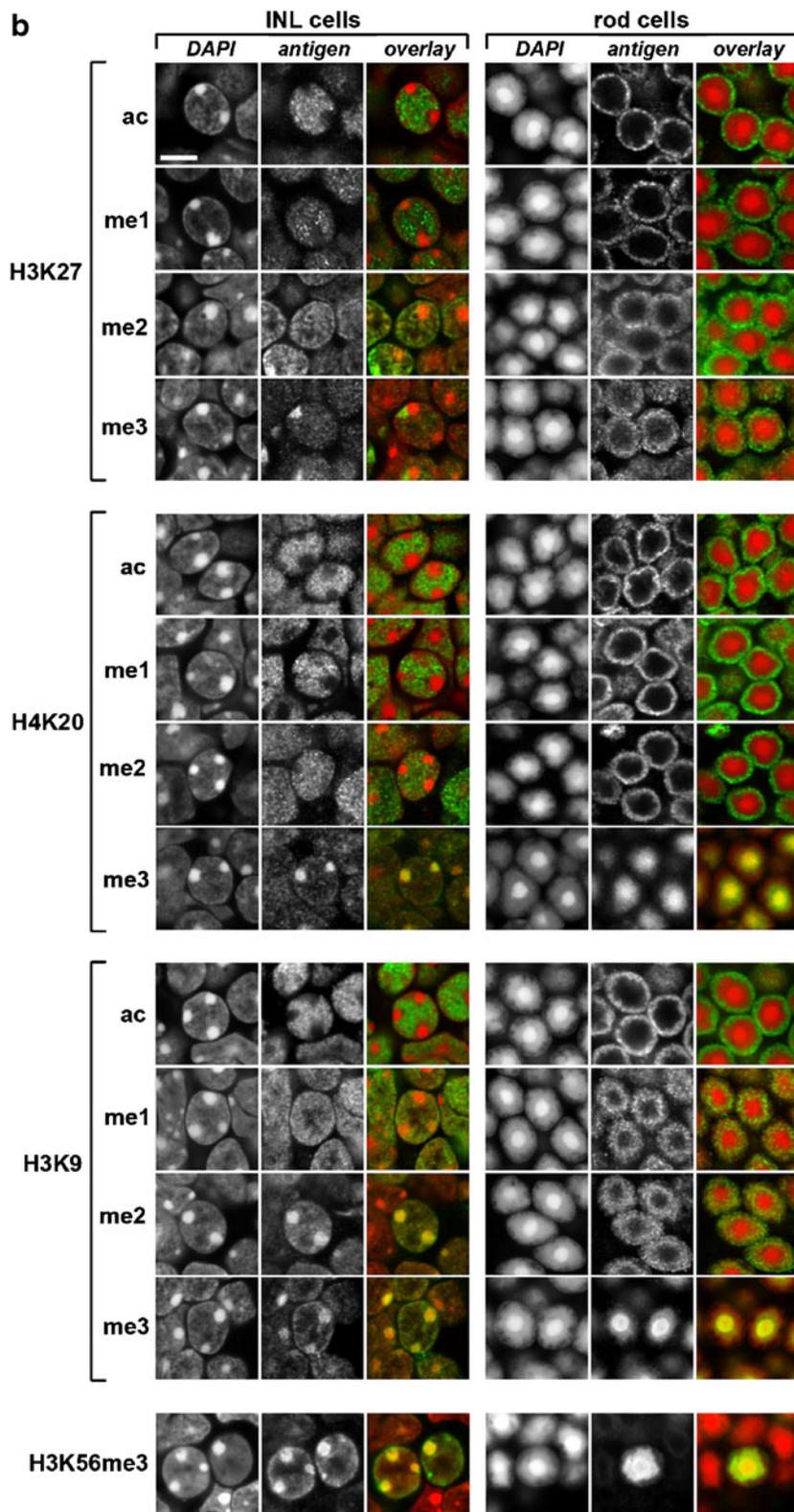
Fig. 5 (continued)

core histones				
residue	modification	CC	L1	B1
H3K9	acetyl	-	-	+
	me1	-	+	-
	me2	+/-	+	-
	me3	+	+	-
H3K56	me3	+	+	-
H4K20	acetyl	-	-	+
	me1	-	-	+
	me2	-	-	+
	me3	+	+	-
H3K27	acetyl	-	-	+
	me1	-	-	+
	me2	-	+	+
	me3	-	+[1]	+
H3K4	acetyl	-	+	+
	me1	-	-	+
	me2	-	-	+
	me3	-	-	+
H3K36	acetyl	-	-	+
	me1	-	-	+
	me2	-	-	+
	me3	-	-	+
H4K5	acetyl	-	-	+
H4K8	acetyl	-	-	+
H4K12	acetyl	-	-	+
H4K16	acetyl	-	-	+

DNA methylation and selected proteins				
5mC		+	+	-
DNMT1		-	-	+[2]
HP1 alpha		+	+	-
HP1 beta		+	+	-
HP1 gamma		-	-	+
RNA Pol-II	nph CTD	-	-	+
	Ser2 ph	-	-	+
	Ser5 ph	-	-	+

Fig. 6 The distribution of histone modifications and selected nuclear proteins in rods and cells with the conventional architecture: a summary. H3K9me2 was detected in chromocenters of neurons with conventional nuclei but not in the chromocenter of rod cells. [1] H3K27me3 also intensely stains inactive X chromosome. [2] DNMT1 also produces bright focal staining in nucleoli where it marks silent ribosomal genes. CC, chromocenters; L1, LINE-rich chromatin; B1, SINE-rich chromatin. For nuclear distribution of these three chromatin classes see Fig. 1

large pericentromeric satellites, like rat or human, makes a notable difference from mouse in cells with a conventional nuclear architecture.

HP1-alpha and HP1-beta are associated with heterochromatin, HP1-gamma predominantly resides in the euchromatin

Data on heterochromatin protein 1 (HP1), a protein hallmark of silent chromatin, conform to the observations on
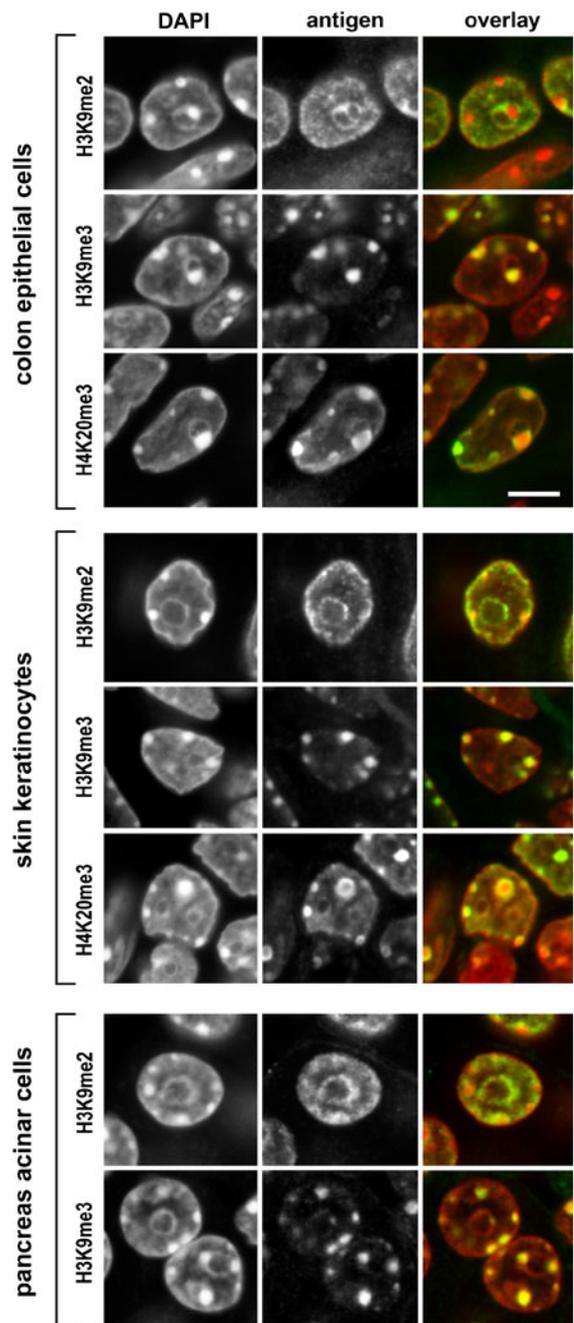
Fig. 7 Distribution of histone modification marks characteristic of heterochromatin in nuclei of some non-retinal mouse cells: colon epithelial cells, skin keratinocytes and pancreatic acinar cells. H3K9me2 is associated with LINE-rich heterochromatin chromatin lining nuclear periphery and surrounding nucleoli and chromocenters. This histone modification is lacking in chromocenters of non-neuronal cells. H3K9me3 is found predominantly in the chromocenters formed by satellite DNA (major satellite repeat). H4K20me3 is a marker of both chromocenter heterochromatin and heterochromatin at the nuclear, nucleoli and chromocenter periphery. Single confocal sections. *Scale bars* 5 μm

silencing histone marks. HP1-alpha and HP1-beta silence repeat-rich heterochromatin (Cheutin et al. 2003; Schotta et al. 2004); the former binds to LINEs but not to SINEs (Vogel et al. 2006) which wholly conforms to the distribution observed by us. We detected HP1-alpha and HP1-beta in chromocenters of both inverted and conventional nuclei (Figs. 6 and 8). The level of HP1-alpha decreases in mature rod nuclei (Popova et al. 2013), which corresponds to the notion that HP1-beta is specifically important for chromocenter formation (Probst et al. 2010), whereas HP1-alpha appears to play a special role at the initial stages of HP1 recruitment to satellite heterochromatin (Maison et al. 2011). In contrast to HP1-alpha and HP1-beta, HP1-gamma colocalizes with euchromatin (Figs. 6 and 8). Interestingly, its level in photoreceptor cells is 2–3 times upregulated in rods compared to neuroretinal cells (Siegert et al. 2012). There is a growing body of evidence that HP1-gamma is associated with transcription in gene-rich chromatin regions and is involved in regulation of alternative splicing (Saint-Andre et al. 2011; Vakoc et al. 2005). Similarly to H3K27me3, HP1-gamma is dispensable for chromocenter formation (Abe et al. 2011).

H3K9me2,3 and H4K20me3 are dispensable for nuclear inversion in rods, in conventional nuclei their role is more complicated

As differentiating rod nuclei loose peripheral heterochromatin, we used appropriate knockout mice to test whether the hallmarks of peripheral heterochromatin, H3K9me2,3 and H4K20me3 are necessary for nuclear inversion in rods. We studied retinas from mice lacking H4K20me3 due to deletion of Suv4-20h2 and mice lacking both H4K20me3 and H3K9me3 due to deletion of Suv4-20 and Suv3-9h1,2 KMTases. In mice of both genotypes, rod nuclei underwent inversion and were not different from the rod nuclei in the wild-type littermate controls (Fig. 9a). Remarkably, peripheral heterochromatin layer and peripheral chromocenters were also retained by other retinal cells, showing that these histone marks were dispensable for maintenance of the conventional nuclear architecture as well (Fig. 9b). Although we have found no influence of Suv3-9 and Suv4-20 loss on the spatial organization of the nucleus, their deletion affects chromatin organization in some other aspects. In particular, the number of chromocenters in Suv4-20h double knockout mouse fibroblasts strongly increases (Hahn et al. 2013). This effect, however, does not take place in the native tissue cells (retinal neurons) studied by us. It remains unknown
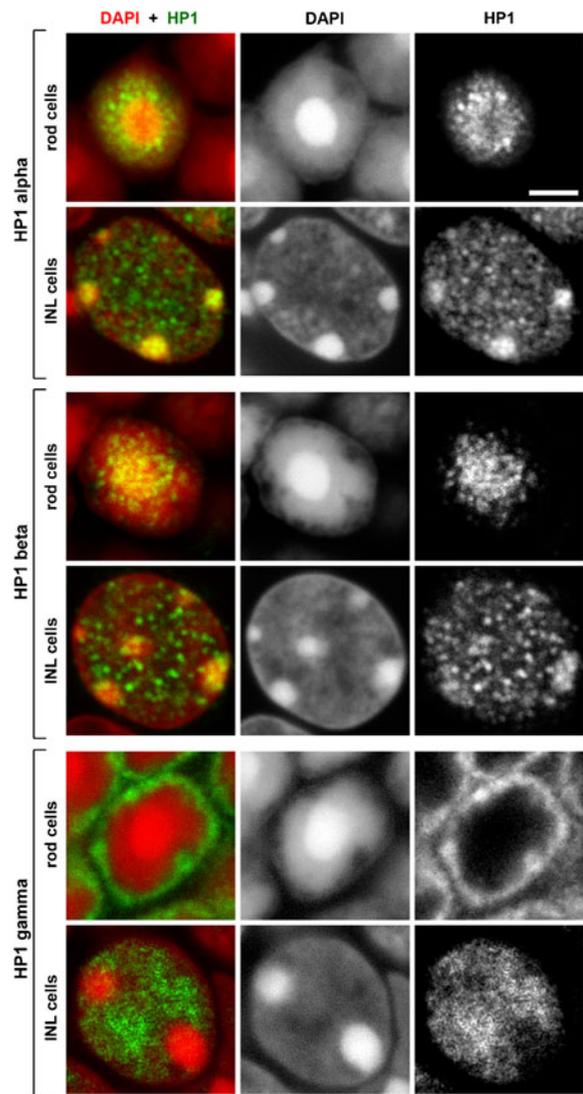
Fig. 8 Nuclear distribution of the three variants of heterochromatin protein 1 (HP1-alpha, HP1-beta, and HP1-gamma) in retinal cells with conventional (INL) and inverted (rod) nuclear organization. HP1-alpha and HP1-beta are associated with heterochromatin of chromocenters and, to lesser degree, L1-zone. HP1-gamma clearly marks euchromatin in the outer shall in rods and nuclear interior in INL cells Single confocal sections. Scale bar 2 μm

whether the effect of Suv4-20h on chromocenter fusion is specific for cultured fibroblasts or the absence of Suv4-20h is compensated in native tissues by some mechanism not available in cultured fibroblasts.

The main enzyme depositing H3K9me2 mark is G9a; its deletion is lethal in utero about E12. We studied retinas of mice with conditional G9a knockout (CKO) driven by Dkk3 expressed in the retina. Mice were studied at postnatal day 14 when LINE-rich chromatin starts to release from

Organization of retinal nuclei from mice with deleted ▶ H3K9me3 and H4K20me3 and with depleted H3K9me2 in the retina. **a** Rod nuclei from retina of wild type (*left column*), Suv 4-20h2 single knockout (*middle column*) and Suv 4-20h2, Suv 3-9h1,2 triple knockout (*right column*) mice have the same architecture. In particular, absence of corresponding histone modifications does not interfere with formation of single central chromocenter surrounded by L1-rich heterochromatin. **b** Nuclear architecture of neuroretinal cells (GCL and INL) is also not affected by deletion of H3K9 and H4K20 trimethylation. DAPI staining. **c** Deletion of G9a strongly reduces the abundance of H3K9me2 in L1-rich chromatin but does not prevent its clustering around chromocenters in developing rods. Note that nuclei of P14 rods in both wild type and Dkk3 G9a CKO in particular, possess only a few chromocenters and L1-rich chromatin is clustered around them. Tri-methylation of H3K9 in chromocenters and L1-chromatin is not affected in G9a CKO mice (*middle* and *bottom rows*), H3K9me3 is abundant in chromocenters and L1-rich chromatin close to them, which conforms to the possible role of Suv3-9 in H3K2me2 deposition: note the similarity in H3K9me2 and H3K9me3 distribution in ganglion cells. Single confocal sections. *Scale bar* 5 μm
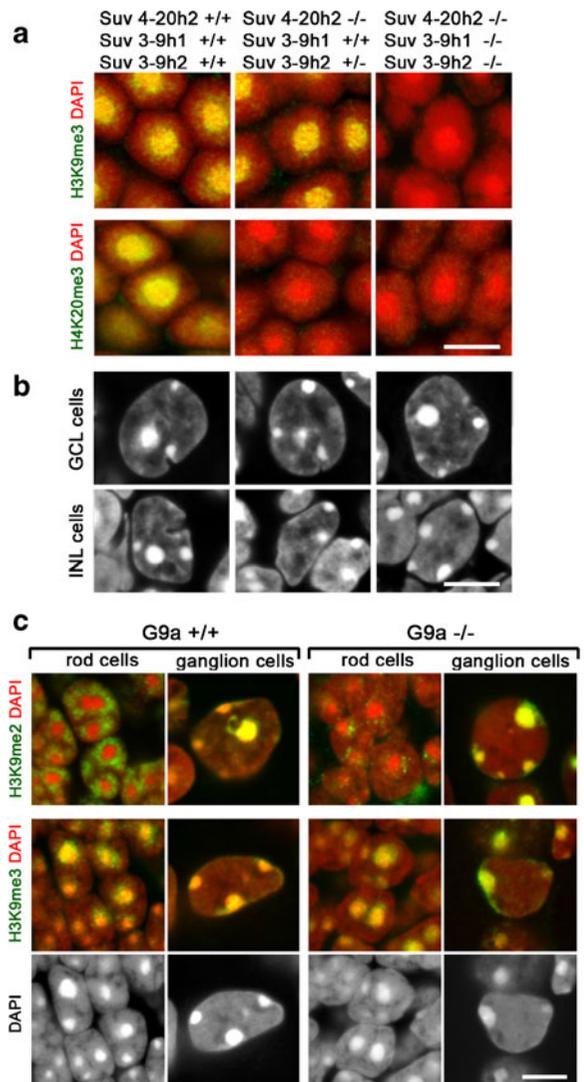

the nuclear envelope and to cluster around chromocenters, the number of which is already reduced (Solovei et al. 2009). In wild type rods, in which H3K9me2 is absent in chromocenters, LINE-rich chromatin was brightly stained (Fig. 9c). In CKO rods, the phenotype is very strong, only residual sparse dot-like H3K9me2 signals were observed in LINE-rich chromatin. The progress of inversion was not different between CKO and wild type rods (Fig. 9c, bottom row), showing that H3K9me2 is dispensable for inversion. In difference to rods, the chromocenters of neuroretinal cells were clearly H3K9m2-positive in the CKO retina, and small areas of LINE-rich heterochromatin close to chromocenters and nuclear envelope were also positive. Chromocenters actually retain H3K9me2 also in ES cells with global G9a knockout, which was tentatively explained by methylation by Suv3-9 KMTases to about 1/8 of the wild type level (Shinkai and Tachibana 2011; Tachibana et al. 2002). It is noteworthy that the reduction in H3K9me2 level in *Dkk3*-driven conditional knockout is sufficient for major changes in the organization of the retina (Katoh et al. 2012). Thus, the nuclei of the neuroretinal cells in CKO do not show apparent differences from wild type when H3K9me2 is strongly depleted. However, due to residual H3K9 dimethylation, it remains unknown if H3K9me2 is dispensable for the maintenance of the conventional nuclear architecture in mouse neurons.

The studied silencing histone modifications appear to be dispensable for maintenance of peripheral heterochromatin in nuclei with conventional nuclear architecture. These data confirm for tissues the results obtained earlier using cultured cells (Peters et al. 2001; Schotta et al. 2004). Even though mice with deleted Suv3-9 and/or Suv4-20 have distinctly low viability and loss of G9a is lethal, their absence/depletion had no apparent effect on the global organization of the studied nuclei. Although the same epigenetic modifications can be generated by a number of different enzymes (Black et al. 2012), loss of Suv3-9 and Suv4-20 indeed decreases the abundance of the respective modifications below the detection level (Peters et al. 2001; Schotta et al. 2004; our data) or significantly reduces it (Tachibana et al. 2002). The fact, that the absence of the important silencing epigenetic marks does not affect nuclear architecture has rather to be explained by the high degree of redundancy in epigenetic code itself,

Fig. 10 Distribution of histone modification marks in chromosome bands and in eu- and heterochromatin of conventional and inverted nuclei. Histone modifications in LINE-rich heterochromatin (*red*) are the same in the layers under the nuclear envelope, around chromocenters and around nucleoli. H3K9me2 is marked in *red* to emphasize its absence in the chromocenters of inverted rod nuclei
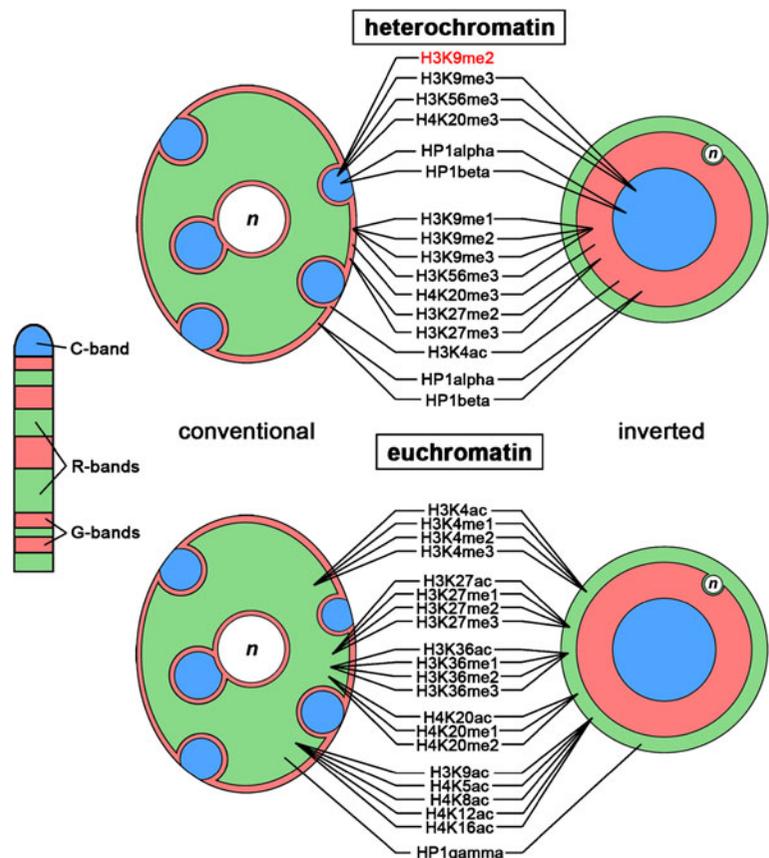
meaning that different modifications can provide the same functional signal. By now nearly 70 different histone modifications are known (Tan et al. 2011), but they form only 3–4 groups with correlated occupancy and, supposedly, functions (Wang et al. 2008; Zhu et al. 2013). A characteristic example is H3K56me3. This epigenetic mark phenocopies H3K9me3, with the exception that it is not masked by phosphorylation of the neighboring serine (H3S10ph) in mitotic chromosomes (Jack et al. 2013). Also, in rod nuclei and neuroretinal cells with conventional nuclear architecture, H3K56me3 has the same global distribution, as H3K9me3. In *C. elegans*, integrated arrays of gene promoters acquire silencing epigenetic marks and are sequestrated to the nuclear periphery (Gonzalez-Sandoval et al. 2013; Meister et al. 2010; Towbin et al. 2010). Although peripheral targeting is affected by deletion of H3K9 thrimethylase *set-25*, mono- and dimethylase *met-2* should also be deleted for the complete release of peripheral heterochromatin, showing that in *C. elegans* absence of H3K9me3 is compensated by H3K9me1,2 marks. Remarkably, a crucial role of H3K9 monomethylases for chromatin formation has

recently been shown also for cultured human cells (Pinheiro et al. 2012). Furthermore, in cultured human cells dimethylase G9a affected peripheral position of at least a proportion of LINE-rich heterochromatin, lamina-associated domains (Kind et al. 2013). Our results show for the first time that the major silencing epigenetic marks (H3K9me3 and H4K20me3, in the first place) are dispensable for maintenance of peripheral heterochromatin not only in cultured cells, but also in tissues in vivo. Taken together, our results well conform to the notion that this redundancy depends both on redundant depositing of epigenetic marks by different enzymes (H3K9me2) and redundancy of epigenetic code itself (H3K9me3, H4K20me3).

Our results also show that nuclear inversion in rods does not need H3K9me3 and H4K20me3, separately or together, and takes place despite strong depletion of H3K9me2. It is noteworthy that nuclear inversion results from absence of two peripheral heterochromatin tethers, LBR- and lamin A/C-dependent, which are in fact readers of epigenetic code (Solovei et al. 2013). LBR directly includes a Tudor domain, a known reader of silencing

histone modifications (Hirano et al. 2012; Makatsori et al. 2004). Lamin A/C, although it binds chromatin directly, is a scaffold protein in the first place, and forms complexes with numerous proteins, reading epigenetic code or modifying it (reviewed in Solovei et al. 2013). In particular, progeric mutations of lamin A/C and inhibition of farnesyltransferase (involved in lamin A/C maturation) appear to directly affect chromosome and heterochromatin positioning in the nucleus (Mehta et al. 2010). In summary, epigenetic marking typical for peripheral heterochromatin does not prevent inversion in absence of the both peripheral heterochromatin tethers, that is nuclear envelope-bounded readers of epigenetic code. These facts suggest that inversion in rod photoreceptor nuclei simply relies on complete loss of tethers in differentiating rod nuclei which takes place in mouse by the age of about 2 weeks.

Conclusions

A broad study of the epigenetic landscape of the inverted mouse rod nuclei and nuclei with conventional nuclear architecture indicated several differences between them and several features of general interest for the organization of the mammalian nuclei:

- Packing density of pericentromeric satellites and LINE-rich chromatin is more similar in inverted rod nuclei, than in the nuclei with a conventional architecture; euchromatin has a lower packing density in both cases.
- A high global chromatin condensation in rod nuclei minimizes the structural difference between Xi and Xa.
- DNA methylation is observed primarily in the chromocenter, DNMT1 is primarily associated with the euchromatic shell.
- Heterochromatin proteins HP1-alpha and HP1-beta localize in heterochromatic shells, whereas HP1-gamma is associated with euchromatin.
- For most of the 25 studied histone modifications, we observed predominant colocalization with a certain main chromatin class (Fig. 10).
- Both inversion in rod nuclei and maintenance of peripheral heterochromatin in conventional nuclei are not affected by a loss or depletion of the major silencing core histone modifications, but for different reasons. Maintenance of peripheral heterochromatin

appears to be ensured by redundancy both at the level of enzymes setting the code (writers) and the code itself, whereas inversion in rods relies on absence of the peripheral heterochromatin tethers (absence of code readers).

References

Abe K, Naruse C, Kato T, Nishiuchi T, Saitou M, Asano M (2011) Loss of heterochromatin protein 1 gamma reduces the number of primordial germ cells via impaired cell cycle progression in mice. Biol Reprod 85:1013–1024

Almouzni G, Probst AV (2011) Heterochromatin maintenance and establishment: lessons from the mouse pericentromere. Nucleus 2:332–338

Bancaud A, Huet S, Daigle N, Mozziconacci J, Beaudouin J, Ellenberg J (2009) Molecular crowding affects diffusion and binding of nuclear proteins in heterochromatin and reveals the fractal organization of chromatin. Embo J 28:3785–3798

Black JC, Van Rechem C, Whetstine JR (2012) Histone lysine methylation dynamics: establishment, regulation, and biological impact. Mol Cell 48:491–507

Boyle S, Gilchrist S, Bridger JM, Mahy NL, Ellis JA, Bickmore WA (2001) The spatial organization of human chromosomes within the nuclei of normal and emerin-mutant cells. Hum Mol Genet 10:211–219

Carvalho C, Pereira HM, Ferreira J, Pina C, Mendonça D, Rosa AC, Carmo-Fonseca M (2001) Chromosomal G-dark bands determine the spatial organization of centromeric heterochromatin in the nucleus. Mol Biol Cell 12:3563–3572

Chandra T, Kirschner K, Thuret JY, Pope BD, Ryba T, Newman S, Ahmed K et al (2012) Independence of repressive histone marks and chromatin compaction during senescent heterochromatic layer formation. Mol Cell 47:203–214

Chen TL, Manuelidis L (1989) SINEs and LINEs cluster in distinct DNA fragments of Giemsa band size. Chromosoma 98:309–316

Cheutin T, McNairn AJ, Jenuwein T, Gilbert DM, Singh PB, Misteli T (2003) Maintenance of stable heterochromatin domains by dynamic HP1 binding. Science 299:721–725

Cremer M, Grasser F, Lanctot C, Muller S, Neusser M, Zinner R, Solovei I, Cremer T (2008) Multicolor 3D fluorescence in situ hybridization for imaging interphase chromosomes. Methods Mol Biol 463:205–239

Croft JA, Bridger JM, Boyle S, Perry P, Teague P, Bickmore WA (1999) Differences in the localization and morphology of chromosomes in the human nucleus. J Cell Biol 145:1119–1131

Dambacher S, Hahn M, Schotta G (2010) Epigenetic regulation of development by histone lysine methylation. J Hered (Edinb) 105:24–37

Eberhart A, Kimura H, Leonhardt H, Joffe B, Solovei I (2012) Reliable detection of epigenetic histone marks and nuclear proteins in tissue cryosections. Chromosome Res 20(7):849–858

Egelhofer TA, Minoda A, Klugman S, Lee K, Kolasinska-Zwierz P, Alekseyenko AA, Cheung MS et al (2011) An assessment of histone-modification antibody quality. Nat Struct Mol Biol 18:91–93

Gibcus JH, Dekker J (2013) The hierarchy of the 3D genome. Mol Cell 49:773–782

Gonzalez-Sandoval A, Towbin BD, Gasser SM (2013) The formation and sequestration of heterochromatin during development. Febs J 280(14):3212–3219

Hahn M, Dambacher S, Dulev S, Kuznetsova AY, Eck S, Worz S, Sadic D, Schulte M, Mallm JP, Maiser A, Debs P, von Melchner H, Leonhardt H, Schermelleh L, Rohr K, Rippe K, Storchova Z, Schotta G (2013) Suv4-20h2 mediates chromatin compaction and is important for cohesin recruitment to heterochromatin. Genes Dev 27:859–872

Hayashi-Takanaka Y, Yamagata K, Wakayama T, Stasevich TJ, Kainuma T, Tsurimoto T, Tachibana M, Shinkai Y, Kurumizaka H, Nozaki N, Kimura H (2011) Tracking epigenetic histone modifications in single cells using Fab-based live endogenous modification labeling. Nucleic Acids Res 39:6475–6488

Helmlinger D, Hardy S, Abou-Sleymane G, Eberlin A, Bowman AB, Gansmuller A, Picaud S, Zoghbi HY, Trottier Y, Tora L, Devys D (2006) Glutamine-expanded ataxin-7 alters TFTC/STAGA recruitment and chromatin structure leading to photoreceptor dysfunction. PLoS Biol 4:e67

Hirano Y, Hizume K, Kimura H, Takeyasu K, Haraguchi T, Hiraoka Y (2012) Lamin B receptor recognizes specific modifications of histone H4 in heterochromatin formation. J Biol Chem 287:42654–42663

Jack AP, Bussemer S, Hahn M, Punzeler S, Snyder M, Wells M, Csankovszki G, Solovei I, Schotta G, Hake SB (2013) H3K56me3 is a novel, conserved heterochromatic mark that largely but not completely overlaps with H3K9me3 in both regulation and localization. PLoS One 8:e51765

Joffe B, Leonhardt H, Solovei I (2010) Differentiation and large scale spatial organization of the genome. Curr Opin Genet Dev 20:562–569

Kadriu B, Guidotti A, Chen Y, Grayson DR (2012) DNA methyltransferases1 (DNMT1) and 3a (DNMT3a) colocalize with GAD67-positive neurons in the GAD67-GFP mouse brain. J Comp Neurol 520:1951–1964

Katoh K, Yamazaki R, Onishi A, Sanuki R, Furukawa T (2012) G9a histone methyltransferase activity in retinal progenitors is essential for proper differentiation and survival of mouse retinal cells. J Neurosci 32:17658–17670

Kimura H, Hayashi-Takanaka Y, Goto Y, Takizawa N, Nozaki N (2008) The organization of histone H3 modifications as revealed by a panel of specific monoclonal antibodies. Cell Struct Funct 33:61–73

Kind J, Pagie L, Ortabozkoyun H, Boyle S, de Vries SS, Janssen H, Amendola M, Nolen LD, Bickmore WA, van Steensel B (2013) Single-cell dynamics of genome-nuclear lamina interactions. Cell 153:178–192

Kiseleva E, Rutherford S, Cotter LM, Allen TD, Goldberg MW (2001) Steps of nuclear pore complex disassembly and reassembly during mitosis in early Drosophila embryos. J Cell Sci 114:3607–3618

Kizilyaprak C, Spehner D, Devys D, Schultz P (2010) In vivo chromatin organization of mouse rod photoreceptors correlates with histone modifications. PLoS One 5:e11039

Kizilyaprak C, Spehner D, Devys D, Schultz P (2011) The linker histone H1C contributes to the SCA7 nuclear phenotype. Nucleus 2:444–454

Korenberg JR, Rykowski MC (1988) Human genome organization: Alu, lines, and the molecular structure of metaphase chromosome bands. Cell 53:391–400

Lienert F, Mohn F, Tiwari VK, Baubec T, Roloff TC, Gaidatzis D, Stadler MB, Schubeler D (2011) Genomic prevalence of heterochromatic H3K9me2 and transcription do not discriminate pluripotent from terminally differentiated cells. PLoS Genet 7:e1002090

Maison C, Bailly D, Roche D, Montes de Oca R, Probst AV, Vassias I, Dingli F, Lombard B, Loew D, Quivy JP, Almouzni G (2011) SUMOylation promotes de novo targeting of HP1alpha to pericentric heterochromatin. Nat Genet 43:220–227

Majumder S, Ghoshal K, Datta J, Smith DS, Bai S, Jacob ST (2006) Role of DNA methyltransferases in regulation of human ribosomal RNA gene transcription. J Biol Chem 281:22062–22072

Makatsori D, Kourmouli N, Polioudaki H, Shultz LD, McLean K, Theodoropoulos PA, Singh PB, Georgatos SD (2004) The inner nuclear membrane protein lamin B receptor forms distinct microdomains and links epigenetically marked chromatin to the nuclear envelope. J Biol Chem 279:25567–25573

Mehta IS, Bridger JM, Kill IR (2010) Progeria, the nucleolus and farnesyltransferase inhibitors. Biochem Soc Trans 38:287–291

Meister P, Towbin BD, Pike BL, Ponti A, Gasser SM (2010) The spatial dynamics of tissue-specific promoters during C. elegans development. Genes Dev 24:766–782

Mellén M, Ayata P, Dewell S, Kriaucionis S, Heintz N (2012) MeCP2 binds to 5hmC enriched within active genes and accessible chromatin in the nervous system. Cell 151:1417–1430

Nasonkin IO, Lazo K, Hambright D, Brooks M, Fariss R, Swaroop A (2011) Distinct nuclear localization patterns of DNA methyltransferases in developing and mature mammalian retina. J Comp Neurol 519:1914–1930

Nasonkin IO, Merbs SL, Lazo K, Oliver VF, Brooks M, Patel K, Enke RA, Nellissery J, Jamrich M, Le YZ, Bharti K, Fariss RN, Rachel RA, Zack DJ, Rodriguez-Boulan EJ, Swaroop A (2013) Conditional knockdown of DNA methyltransferase 1 reveals a key role of retinal pigment epithelium integrity in photoreceptor outer segment morphogenesis. Development 140:1330–1341

Pauler FM, Sloane MA, Huang R, Regha K, Koerner MV, Tamir I, Sommer A, Aszodi A, Jenuwein T, Barlow DP (2009) H3K27me3 forms BLOCs over silent genes and intergenic regions and specifies a histone banding pattern on a mouse autosomal chromosome. Genome Res 19:221–233

Peters AH, O'Carroll D, Scherthan H, Mechtler K, Sauer S, Schofer C, Weipoltshammer K, Pagani M, Lachner M, Kohlmaier A, Opravil S, Doyle M, Sibilia M, Jenuwein T (2001) Loss of the Suv39h histone methyltransferases impairs mammalian heterochromatin and genome stability. Cell 107:323–337

Pinheiro I, Margueron R, Shukeir N, Eisold M, Fritzsch C, Richter FM, Mittler G, Genoud C, Goyama S, Kurokawa M, Son J, Reinberg D, Lachner M, Jenuwein T (2012) Prdm3 and Prdm16 are H3K9me1 methyltransferases required for mammalian heterochromatin integrity. Cell 150:948–960

Pinter SF, Sadreyev RI, Yildirim E, Jeon Y, Ohsumi TK, Borowsky M, Lee JT (2012) Spreading of X chromosome inactivation via a hierarchy of defined Polycomb stations. Genome Res 22:1864–1876

Popova EY, Grigoryev SA, Fan Y, Skoultchi AI, Zhang SS, Barnstable CJ (2013) Developmentally regulated linker histone h1c promotes heterochromatin condensation and mediates structural integrity of rod photoreceptors in mouse retina. J Biol Chem 288(24):17895–17907

Popova EY, Xu X, DeWan AT, Salzberg AC, Berg A, Hoh J, Zhang SS, Barnstable CJ (2012) Stage and gene specific signatures defined by histones H3K4me2 and H3K27me3 accompany mammalian retina maturation in vivo. PLoS One 7:e46867

Probst AV, Okamoto I, Casanova M, El Marjou F, Le Baccon P, Almouzni G (2010) A strand-specific burst in transcription of pericentric satellites is required for chromocenter formation and early mouse development. Dev Cell 19:625–638

Rao RC, Tchedre KT, Malik MT, Coleman N, Fang Y, Marquez VE, Chen DF (2010) Dynamic patterns of histone lysine methylation in the developing retina. Invest Ophthalmol Vis Sci 51:6784–6792

Reese BE, Tan SS (1998) Clonal boundary analysis in the developing retina using X-inactivation transgenic mosaic mice. Semin Cell Dev Biol 9:285–292

Rhee KD, Yu J, Zhao CY, Fan G, Yang XJ (2012) Dnmt1-dependent DNA methylation is essential for photoreceptor terminal differentiation and retinal neuron survival. Cell Death Dis 3:e427

Ronneberger O, Baddeley D, Scheipl F, Verveer PJ, Burkhardt H, Cremer C, Fahrmeir L, Cremer T, Joffe B (2008) Spatial quantitative analysis of fluorescently labeled nuclear structures: problems, methods, pitfalls. Chromosome Res 16:523–562

Saint-Andre V, Batsche E, Rachez C, Muchardt C (2011) Histone H3 lysine 9 trimethylation and HP1gamma favor inclusion of alternative exons. Nat Struct Mol Biol 18:337–344

Schotta G, Lachner M, Sarma K, Ebert A, Sengupta R, Reuter G, Reinberg D, Jenuwein T (2004) A silencing pathway to induce H3-K9 and H4-K20 trimethylation at constitutive heterochromatin. Genes Dev 18:1251–1262

Schotta G, Sengupta R, Kubicek S, Malin S, Kauer M, Callen E, Celeste A, Pagani M, Opravil S, De La Rosa-Velazquez IA, Espejo A, Bedford MT, Nussenzweig A, Busslinger M, Jenuwein T (2008) A chromatin-wide transition to H4K20 monomethylation impairs genome integrity and programmed DNA rearrangements in the mouse. Genes Dev 22:2048–2061

She SR, Cote RJ, Taylor CR (1997) Antigen retrieval immuno-histochemistry: past, present, and future. J Histochem Cytochem 45:327–343

She SR, Cote RJ, Taylor CR (2001) Antigen retrieval techniques: current perspectives. J Histochem Cytochem 49:931–937

Shinkai Y, Tachibana M (2011) H3K9 methyltransferase G9a and the related molecule GLP. Genes Dev 25:781–788

Siegert S, Cabuy E, Scherf BG, Kohler H, Panda S, Le YZ, Fehling HJ, Gaidatzis D, Stadler MB, Roska B (2012) Transcriptional code and disease map for adult retinal cell types. Nat Neurosci 15(487–495):S481–S482

Solovei I (2010) Fluorescence in situ hybridization (FISH) on tissue cryosections. Methods Mol Biol 659:71–82

Solovei I, Kreysing M, Lanctot C, Kosem S, Peichl L, Cremer T, Guck J, Joffe B (2009) Nuclear architecture of rod photoreceptor cells adapts to vision in mammalian evolution. Cell 137:356–368

Solovei I, Wang AS, Thanisch K, Schmidt CS, Krebs S, Zwerger M, Cohen TV, Devys D, Foisner R, Peichl L, Herrmann H, Blum H, Engelkamp D, Stewart CL, Leonhardt H, Joffe B (2013) LBR and Lamin A/C sequentially tether peripheral heterochromatin and inversely regulate differentiation. Cell 152:584–598

Tachibana M, Matsumura Y, Fukuda M, Kimura H, Shinkai Y (2008) G9a/GLP complexes independently mediate H3K9 and DNA methylation to silence transcription. Embo J 27:2681–2690

Tachibana M, Sugimoto K, Nozaki M, Ueda J, Ohta T, Ohki M, Fukuda M, Takeda N, Niida H, Kato H, Shinkai Y (2002) G9a histone methyltransferase plays a dominant role in euchromatic histone H3 lysine 9 methylation and is essential for early embryogenesis. Genes Dev 16:1779–1791

Tan M, Luo H, Lee S, Jin F, Yang JS, Montellier E, Buchou T, Cheng Z, Rousseaux S, Rajagopal N, Lu Z, Ye Z, Zhu Q, Wysocka J, Ye Y, Khochbin S, Ren B, Zhao Y (2011) Identification of 67 histone marks and histone lysine crotonylation as a new type of histone modification. Cell 146:1016–1028

Terrenoire E, McRonald F, Halsall JA, Page P, Illingworth RS, Taylor AM, Davison V, O'Neill LP, Turner BM (2010) Immunostaining of modified histones defines high-level features of the human metaphase epigenome. Genome Biol 11:R110

Towbin BD, Gonzalez-Aguilera C, Sack R, Gaidatzis D, Kalck V, Meister P, Askjaer P, Gasser SM (2012) Step-wise methylation of histone H3K9 positions heterochromatin at the nuclear periphery. Cell 150:934–947

Towbin BD, Meister P, Pike BL, Gasser SM (2010) Repetitive transgenes in C. elegans accumulate heterochromatic marks and are sequestered at the nuclear envelope in a copy-number- and lamin-dependent manner. Cold Spring Harb Symp Quant Biol 75:555–565

Vakoc CR, Mandat SA, Olenchock BA, Blobel GA (2005) Histone H3 lysine 9 methylation and HP1gamma are associated with transcription elongation through mammalian chromatin. Mol Cell 19:381–391

Vogel MJ, Guelen L, de Wit E, Peric-Hupkes D, Lodén M, Talhout W, Feenstra M, Abbas B, Classen AK, van Steensel B (2006) Human heterochromatin proteins form large domains containing KRAB-ZNF genes. Genome Res 16:1493–1504

Walter J, Joffe B, Bolzer A, Albiez H, Benedetti PA, Muller S, Speicher MR, Cremer T, Cremer M, Solovei I (2006) Towards many colors in FISH on 3D-preserved interphase nuclei. Cytogenet Genome Res 114:367–378

Wang Z, Zang C, Rosenfeld JA, Schones DE, Barski A, Cuddapah S, Cui K, Roh TY, Peng W, Zhang MQ, Zhao K (2008) Combinatorial patterns of histone acetylations and methylations in the human genome. Nat Genet 40:897–903

Xhemalce B, Kouzarides T (2010) A chromodomain switch mediated by histone H3 Lys 4 acetylation regulates heterochromatin assembly. Genes Dev 24:647–652

Yamamizu K, Fujihara M, Tachibana M, Katayama S, Takahashi A, Hara E, Imai H, Shinkai Y, Yamashita JK (2012) Protein kinase A determines timing of early differentiation through epigenetic regulation with G9a. Cell Stem Cell 10:759–770

Zalokar M, Erk I (1977) Phase-partition fixation and staining of *Drosophila* eggs. Stain Technol 52:89–95

Zheng MH, Shi M, Pei Z, Gao F, Han H, Ding YQ (2009) The transcription factor RBP-J is essential for retinal cell differentiation and lamination. Mol Brain 2:38

Zhu J, Adli M, Zou JY, Verstappen G, Coyne M, Zhang X, Durham T, Miri M, Deshpande V, De Jager PL, Bennett DA, Houmard JA, Muoio DM, Onder TT, Camahort R, Cowan CA, Meissner A, Epstein CB, Shoresh N, Bernstein BE (2013) Genome-wide chromatin state transitions associated with developmental and environmental cues. Cell 152:642–654

Zullo JM, Demarco IA, Pique-Regi R, Gaffney DJ, Epstein CB, Spooner CJ, Luperchio TR, Bernstein BE, Pritchard JK, Reddy KL, Singh H (2012) DNA sequence-dependent compartmentalization and silencing of chromatin at the nuclear lamina. Cell 149:1474–1487

Figure S1. Explanation of the method to obtain robust immunostaining

a Iimmunostaining of H3K4me2 in rod nuclei after different fixation and antigen retrieval times. Single optical sections are shown as gray scale images.

b Depending on fixation and antigen retrieval times (shown in panel *a*) staining varies from very strong ("+++" on green background) to absence of a signal ("-" at white background). Note similarity in the general character of staining and a satisfactorily wide range of conditions assuring optimal staining.

c False-colored overlay of H3K4me2 immunostaining and DAPI for rod nuclei using one of the optimal conditions, as used to illustrate the distribution of immunostaining in the main text.

Scale bars: 2 µm in *a*; 5 µm in *c*
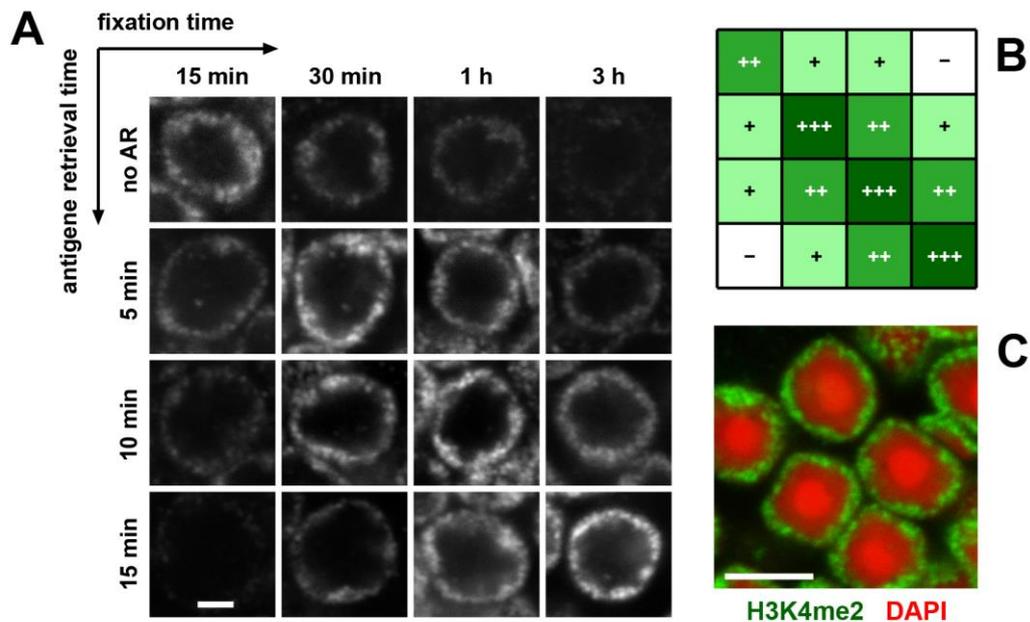
Figure S2. The distribution of RNA-polymerase II (Pol-II) in conventional nuclei of retinal neurons (INL) and inverted nuclei of rod cells

Note that all forms of Pol-II – inactive (top raw), elongating (mid raw), and pausing (bottom raw) – are found at the peripheral euchromatic nuclear shell of rods (B1-rich shell).

Single confocal sections. Scale bars: 5 μm
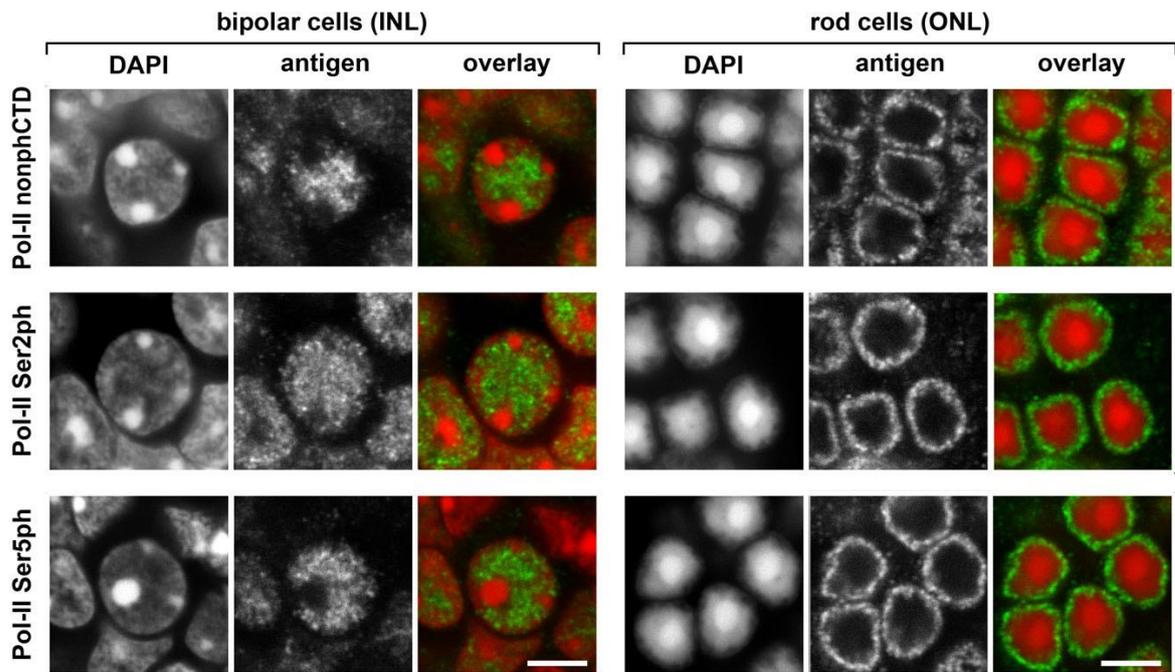
Figure S3. Comparison of the staining patterns of two antibodies against H3K9me2 in retinal cells with conventional (INL) and inverted (rods) nuclear architecture

The two antibodies produce practically identical staining patterns. *Abcam*, commercially available monoclonal antibody from Abcam (ab1220); *HK*, monoclonal antibody produced in the laboratory of H.Kimura (clone 6D11)

Single confocal sections. Scale bar: 5 µm
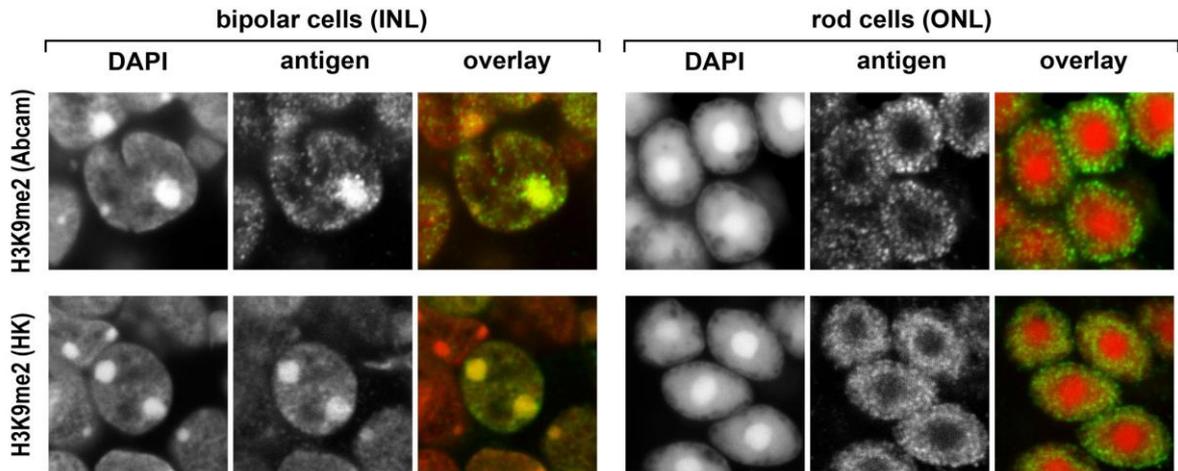
Figure S4. Several histone marks visualized in rod nuclei from adult rat retina.

The distribution of all marks is the same as in mouse rod nuclei (c.f. Figure 5b).

Single confocal sections. Scale bar: 5 µm
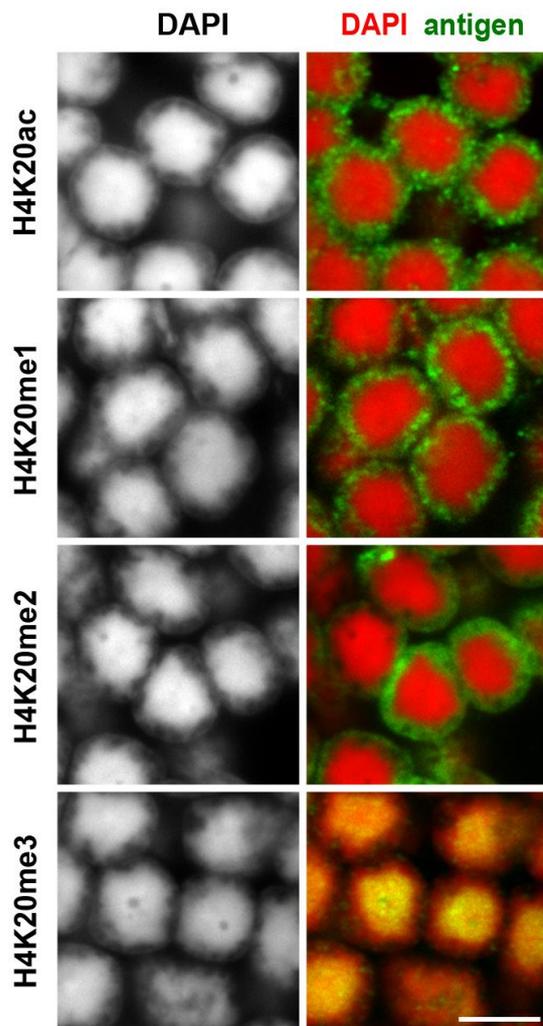
3 Discussion

3.1 Roles of epigenetic factors in nuclear inversion

Murine rod photoreceptors are terminally differentiated cells possessing a unique inverted nuclear architecture. The nucleus of rod cells contains highly condensed constitutive heterochromatin at the nuclear centre, which is surrounded by a layer of facultative heterochromatin and a layer of euchromatin (Solovei et al., 2009). Epigenetic properties of chromatin defining its peripheral or internal positioning remained unknown. Particularly, we were interested to know which histone modifications mark heterochromatin to be released from the nuclear periphery and/or accumulated in the nuclear interior. To answer this question, I and coauthors carried out extensive analysis of several epigenetic factors which might be involved in the nuclear inversion. We mapped the distribution of a major reader of DNA methylation, MECP2 and main histone marks, including methylation and acetylation in rod cells with inverted nuclear architecture and other retinal neuron cell types with conventional nuclear architecture (Eberhart et al., 2013; Song et al., 2014). No obvious differences were found in the distribution of epigenetic marks in the same chromatin classes between nuclei with conventional and inverted nuclear architecture. In both case of nuclear architecture, histone modifications marking transcriptional active/silencing chromatin are associated with euchromatin/heterochromatin, their abundance is below the detection level in the opposite chromatin class (Figure 9). Exclusive distribution of all forms of RNA Pol-II in the euchromatin shell conforms to the euchromatin distribution of active histone modification marks (Eberhart et al., 2013).
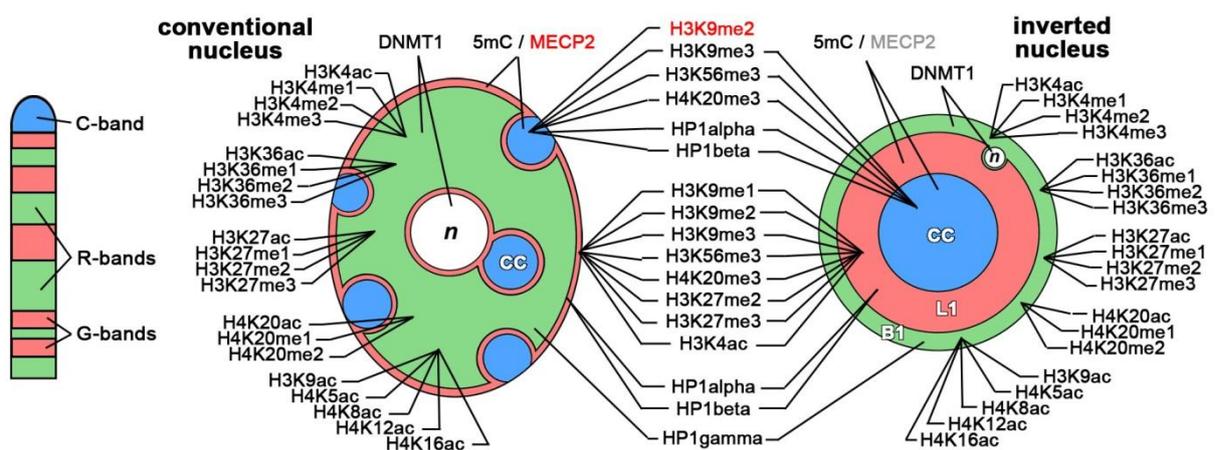

Figure 9. Distribution of major histone modification marks and selected nuclear proteins in chromosome bands and in eu- and heterochromatin of rods and cells with the conventional nuclear architecture. Core histone modifications mostly mark the same chromatin classes in conventional and inverted nuclei. H3K9me2 is marked in red to emphasize its absence in the chromocenters of inverted rod nuclei. MECP2 is marked in red in conventional and in light grey in inverted nuclei to emphasize its pronounced presence in the chromocenters of the former and absence in the chromocenters of the latter.

Zooming in to different histone modification types, histone acetylation is associated with euchromatin shell, the only exception among the studied modifications is H3K4ac. H3K4ac is distributed in both euchromatin and LINE-rich heterochromatin. The unusual distribution conforms to the involvement of H3K4ac in heterochromatin assembly (Xhemalce and Kouzarides, 2010). Histone methylation distribution differs depending on which histones are modified as well as the methylation type: mono-, di- or trimethylation. For both H3K4 and H3K36, the signals of all three types of methylation were observed exclusively in the euchromatin shell (Song et al., 2014).

The finding that H3K27me3 is associated with euchromatin shell in nuclei of bipolar and rod cells is actually rather surprising, since this mark is generally considered as repressive histone marks and to be primarily involved in gene silencing and X-chromosome inactivation (Pauler et al., 2009; Pinter et al., 2012). Moreover, H3K27me3 was found to be enriched at the borders of developmentally regulated variable LADs (Guelen et al., 2008; Harr et al., 2015), its enrichment is necessary and directly involved in the repositioning and targeting ectopic integrated sequences to the nuclear lamina.

The pivotal roles that silencing histone modifications play in heterochromatin formation led us to investigate the effect of H3K9me3, H4K20me3 deficiency in chromosome organization. Loss of single H4K20me3 and combination loss with H3K9me3 affects neither the inversion of rod nuclei nor the retaining of peripheral heterochromatin layer as well as peripheral chromocenters in other retinal cells with conventional nuclear architecture. Taken together, our results indicate that the redundancy of histone modifications depends both on the enzymes depositing of epigenetic marks and redundancy of epigenetic code itself (Eberhart et al., 2013).

H3K27me3 and H3K9me3 are hallmarks of facultative and constitutive heterochromatin, respectively. The two chromatin types generally mutually exclusive from each other and do not coexist at the same loci. The absence of H3K9me3 allows BEND3 to recruit H3K27me3, and thus results in a redundant pathway to generate repressive chromatin (Saksouk et al., 2014). Taken these into consideration, it would be interesting in the future to investigate the involvement of H3K27me3 in the inversion of nuclear architecture during the process to maturation in mouse rod photoreceptors.

Supporting evidence of the involvement of H3K9me2 in chromosome organization comes from the finding that H3K9me2 has been reported to be enriched in the LADs (Guelen et al., 2008; Towbin et al., 2012; Wen et al., 2009) and it is required for targeting an ectopic site to the nuclear lamina (Harr et al., 2015). In *C. elegans*, elimination of two histone methyltransferase MET-2 (mediates H3K9 mono- and dimethylation) and SET-25 (mediates H3K9me3) abrogates the perinuclear attachment of native chromosomal arms rich in methylated H3K9, implying the role of histone methylation in perinuclear heterochromatic

distribution (Towbin et al., 2012). This effect, however, doesn't take place in the native tissue cells (retinal neurons) studied by us. Interestingly, H3K9me2 was detected in the chromocenter of retinal neurons with conventional nuclei but not in the chromocenter of rod cells. Bright H3K9me2 signals were only observed in LINE-rich chromatin in wild type rods. Conditional knockout (CKO) of H3K9me2 driven by Dkk3 expressed in the retina results in only residual sparse dot-like H3K9me2 signals in LINE-rich chromatin. With the absence of H3K9me2 in the chromocenter and only sparse spot-like distribution in LINE-rich chromatin, the progress of inversion was not affected in CKO when compared to wild type rods. The unaffected nucleus organization in CKO rods shows that H3K9me2 is dispensable for inversion. The overall morphology of conventional nuclei was also not affected (Eberhart et al., 2013). It is of special note that our studies were performed by microscopic, which might risk missing the detection of small scale chromosome reorgananization. Consistent with our study, in another two studies the authors were unable to detect loss of association with the nuclear lamina when H3K9me2 was down-regulated by treating cells with 5 μM BIX-01924. Their assays were designed to detect the association with lamina within 0.5 μm, and therefore, a subtle loss of association might be missed (Bian et al., 2013; Harr et al., 2015).

During retina maturation, the mouse rod nucleus undergoes extensive reorganization (Solovei et al., 2009) which is accompanied by extensive and specific methylation (Merbs et al., 2012). Epigenetic control of retinal development in general is poorly understood. It is known that DNMT1 plays an important role in mammalian retinal development. Although in hypomethylated Dnmt1-mutant mice, the commitment of Dnmt1-deficient progenitor towards the photoreceptor fate is not affected, the retinal progenitor cells continue to proliferate. The photoreceptor progenitors do not differentiate and massively die together with other retinal neurons (Rhee et al., 2012). Surprisingly, complete deletion of MECP2 does not cause apparent defects in the morphology and development of the retina. The nuclear architecture of retinal neurons is also unaffected: the degree of chromocenter fusion and the distribution of major histone modifications do not differ between Mecp2−/y and Mecp2 WT mice.

We found that mammalian rods have low expression of MECP2, although it is a protein especially abundant in neurons (Gabel et al., 2015; Kinde et al., 2015). Particularly, a prominent difference was observed between rods and other retinal and non-retinal cells with conventional nuclear organization. We relate this phenomenon with an unusually high level of histone H1c demonstrated recently in mouse rod cells (Siegert et al., 2012). It is known that both proteins compete for DNA binding, and in brain neurons MECP2 replaces almost half of H1 (Skene et al., 2010). Therefore, we speculate that high level of H1c might be crucial for extremely dense heterochromatin packaging in the rod nuclear center. This idea is supported by partial heterochromatin decompaction in rods from triple-KO mice deficient for H1 linker histone variants (Popova et al., 2013) and by increasing MECP2 expression in rods

of SCA7 mice (Song et al., 2014), which lose heterochromatin compaction and reduce histone H1 expression (Kizilyaprak et al., 2011). Importantly and in agreement with accumulated knowledge about neuron differentiation (Young, 1985), the onset of MECP2 expression during normal retina development coincides with massive synapse formation. Surprisingly, I did not find the compensatory expression of any other methyl-CpG binding proteins in cultured cells and several tissues upon MECP2 deletion (Song et al., 2014).

In addition, the distribution of MECP2 in 60 cell types of 16 mouse neuronal as well as non-neuronal tissues shows that MECP2 is almost universally expressed in all studied cell types with few exceptions, e.g., microglia. Absence of MECP2 in microglia cells is especially intriguing in view of recent data on the involvement of microglia cells in the Rett phenotype and questions the role of these cells in neuropathologic consequences of MECP2 deficiency (Derecki et al., 2013; Derecki et al., 2012). Our results are supported by the recent study shown that genetic reconstitution of Mecp2 in microglia does not rescue Mecp2-null mice (Wang et al., 2015). MECP2 is also lacking in the renewed cells, e.g., intestine epithelial cells, erythropoietic cells and hair matrix keratinocytes. Combining with the observation that MECP2 expression initiates at late differentiation stage and increases during tissue development and terminal cell differentiation, we conclude that MECP2 serves as a marker of the differentiated state. Our study reveals the significance of MECP2 function in cell differentiation and sets the basis for future investigations in this direction (Song et al., 2014).

3.2 Roles of LBR- and Lamin A/C-dependent tethers in nuclear inversion

Immunostaining of wild type mouse tissues shows that presence of at least one of the heterochromatin tethers, Lamin A/C-dependent tether (A-tether) or LBR-dependent tether (B-tether), is sufficient for maintenance of the conventional nuclear organization. Absence of both tethers results in loss of peripheral heterochromatin, thereby causing inversion of the nuclear architecture. Inversion is observed in nuclei of rod photoreceptors of wild type mice and other nocturnal mammals. All studied so far nocturnal mammals express neither LBR nor Lamin A/C in their rod cells. Ectopic expression of LBR in mouse rods was shown to be sufficient to counteract inversion in these cells and restore a conventional nuclear organization with heterochromatin abutting the nuclear envelope (Solovei et al., 2013).

LBR interacts selectively with heterochromatin via its Tudor domain (Hirano et al., 2012; Makatsori et al., 2004; Olins et al., 2010a; Olins et al., 2010b). LBR also preferentially binds to B-type lamins (Worman et al., 1988). Thus B-type lamins, INM and LBR build a heterochromatin tether to maintain the peripheral heterochromatin. It is still on debate whether the B-type lamins are indispensable in the chromatin binding, since cells from mice lacking both Lmnb1 and Lmnb2 have the conventional nuclear architecture in the absence of Lamin A/C (Kim et al., 2011; Yang et al., 2011).

The mechanism of how LBR mediates heterochromatin formation and repression remains elusive. One proposed model is that LBR binds to histone H4 with dimethylated lysine 20. After binding to chromatin, LBR tethers those chromatin regions together to form a stable LBR-chromatin complex, so-called primitive heterochromatin. The primitive heterochromatin serves as a structural framework to recruit transcriptional repressors, including HP1, MECP2 (Guarda et al., 2009) and Lamin B (Worman et al., 1988) to form mature heterochromatin. The transcription repressors may corporately reduce transcription (Hirano et al., 2012). Further work has to be done to confirm the hypothesis.

Expression of LBR and Lamin A/C was shown to be temporarily coordinated to maintain peripheral heterochromatin. On early developmental stages embryonic cells express only LBR, later the LBR expression is replaced by Lamin A/C expression in many different tissues. In the developing retina, Lamin A/C appears and replaces LBR ca. 10-14 days after the last division of the retinal neuronal progenitor cells. The only exception is rod photoreceptors where LBR expression ceases at P14 without an onset of the Lamin A/C expression. Several other cell types, such as muscle and endothelial cells, express both proteins constantly.

Spatial changes related to cellular differentiation can result in spatial changes in LBR/Lamin A/C expression. This could be observed in tissues where differentiation is spatially ordered, e.g., in epithelium of small intestine with cells proliferating in the crypts and differentiating while moving along the villi. Crypt cells do not express Lamin A/C but LBR, while differentiating and differentiated absorptive and goblet cells co-express both proteins. Similar expression pattern was observed in the mouse multilayer skin: basal keratinocytes express both proteins, whereas differentiating cells move away from the basal membrane and gradually stop LBR expression but increase Lamin A/C expression. The precede expression of LBR and its constant expression in the renewed cell types imply that LBR is correlated with the undifferentiation status (Solovei et al., 2013).

The important roles of A-type lamins in proper chromatin organization are supported by data on diverse laminopathies (reviewed in (Luo et al., 2014). In particular, progeric mutation forms of Lamin A/C and inhibition of farnesyltransferase (involved in the first step of posttranslational modifications of preLamin A) appear to directly affect heterochromatin positioning in the nucleus (Mehta et al., 2010). Moreover, in C. elegans loss of heterochromatin and occurrence of developmental defects were found when lamin was mutated (Liu et al., 2000). A-type lamins serve as the scaffold proteins at the first place and mainly interact with chromatin indirectly through bridging proteins. This is consistent with the results that expression of Lamin C in mouse rod cells is not sufficient to tether heterochromatin to the periphery of the nucleus (Solovei et al., 2013). This view is also

supported by recent observations that in cells deficient in B- and/or A-type lamins, lamina associated domains are fully preserved (Amendola and van Steensel, 2015).

Lamin C together with bridging proteins is already sufficient to maintain peripheral heterochromatin, correspondingly, mice which express only Lamin C and no Lamin A are viable and the nuclei organization are similar with WT mice (Fong et al., 2006). Moreover, recent studies showed that contrary to the common opinion about functional redundancy between Lamin A and C, Lamin C may be specifically involved in instructing peripheral positioning of chromatin (Harr et al., 2015). These findings rule out the inability of Lamin C to mediate the heterochromatin positioning in rod cells in transgenic mice. Another equally important subject is the difference in binding properties between Lamin A, Lamin C and transmembrane proteins (Al-Saaidi and Bross, 2015). For example, Sakaki and co-authors found that the interaction of emerin is stronger with Lamin A than with Lamin C (Sakaki et al., 2001), and the localization of SUN2 has been demonstrated to be restored by the rescued expression of Lamin A but not Lamin C (Liang et al., 2011). Further work has to be done to confirm the binding affinities of Lamin C to the studied INM proteins, especially the identified candidate mediators for A-type tethers.

Intriguingly, although the laminopathies are caused by the missense mutation and/or deletions throughout the LMNA gene, it is the mislocalization of Lamin A/C interaction proteins that are progeric. Golgi accumulation of Sun1 is pathogenic in Lmna null and progeroid mice, in Sun1-/-Lmna-/- mice the tissue pathologies are ameliorated (Chen et al., 2012). DYT1 dystonia is due to the perinuclear space accumulation of pathogenic torsinA variant, which is typically located to the lumen of the endoplasmic reticulum (Gonzalez-Alegre and Paulson, 2004; Goodchild and Dauer, 2004). LAP1 serves as the nuclear envelope torsinA interaction protein (Goodchild and Dauer, 2005). In the laminapathies the cardiac and skeletal muscle are commonly affected. Taken these into consideration, one would deduce it is the interruption of interaction between Lamin A/C and the partners in the skeletal or cardiac muscle, which might lead to the mislocalization of the interaction partner, that causes the pathologies. Moreover, one proposed model to explain the laminopathies is that the mutated LMNA disrupts the lamina integrity, leading to mechanical weakening of the nucleus and making it more vulnerable to mechanical stress (Burke et al., 2001; Burke and Stewart, 2002, 2006; Chi et al., 2009; Worman and Courvalin, 2004). Therefore, the aforementioned interaction partners might be also involved in the mechanical response.

3.3 INM proteins as candidates for missing mediators of heterochromatin binding in A-tether

Lamin A/C interact with chromatin perhaps via a complex with INM proteins, LEM-D proteins in particular. First of all, all identified LEM-D proteins bind either A- or B-type lamins, or both,

directly (Brachner et al., 2005; Clements et al., 2000; Lee et al., 2001; Mansharamani and Wilson, 2005; Sakaki et al., 2001). Second, published data suggest that LEM-D proteins are implicated in heterochromatin anchoring to the nuclear envelope, which suggests their involvement in the A-type tethers. Indeed, in C. elegans, a complex of Lamin and any of the two LEM domain proteins is formed to target the heterochromatic chromosome arms to the nuclear lamina (Ikegami et al., 2010; Mattout et al., 2011).

LEM-D proteins tether peripheral chromatin through different mechanisms. The shared LEM domain binds to chromatin interacting protein BAF (Margalit et al., 2007). Moreover, some LEM-D proteins have additional domains that directly bind DNA, or chromatin proteins. For example, LAP2 contains a second LEM-like domain that binds directly to DNA (Cai et al., 2001; Laguri et al., 2001); MAN1 and probably LEM2 bind DNA directly via the C-terminal winged helix MAN1/Scr1p/C-terminal domain (Caputo et al., 2006). LAP2β also binds chromatin protein HA95 (Martins et al., 2003).

LEM-D proteins might function redundantly in chromatin organization, since loss of function of any single LEM gene studied so far does not grossly disrupt chromatin organization. Moreover, the tissue-selective disease phenotypes caused by mutations of the ubiquitously expressed genes encoding LEM-D proteins support the LEM-D protein function redundancy in the unaffected tissues (Table 3). The functional redundancy might be partially explained by the ability of LEMD proteins to bind to the same interaction partners. For example, LAP2ß, emerin and MAN1 bind the transcriptional repressor GCL (Holaska et al., 2003; Mansharamani et al., 2001; Nili et al., 2001). The other shared partners include Btf, to which both emerin (Haraguchi et al., 2004) and MAN1 bind (Wagner and Krohne, 2007).

Despite the functional redundancy, none of the studied INM proteins are present in all cell types not expressing LBR, and therefore, no individual protein could be universal cofactor of the A-type tethers. The previously published results show that the INM proteins involved in NE-chromatin interactions are ubiquitously expressed proteins (Mattout-Drubezki and Gruenbaum, 2003) mediating interaction with heterochromatin (Brown et al., 2008; Capelson et al., 2010; Kalverda and Fornerod, 2010; Makatsori et al., 2004; Pickersgill et al., 2006).

Table 3. Knock out phenotypes in mice and associated human diseases caused by mutations in genes encoding studied integral proteins of the INM and LAP2α.

Protein	Knock-out phenotype (mice)	Key references	Associated human disease	Key references
LBR	severe skeletal abnormality, utero/perinatal lethality, absence of hair, and scaly skin	(Hoffmann et al., 2002)	Pelger-Hue¨t anomaly (heterozygous) Greenberg skeletal dysplasia (homozygous)	(Hoffmann et al., 2002; Waterham et al., 2003)
LEM2	die by E11.5, most tissues are reduced in size, overactivation of multiple MAP kinases and AKT	(Tapia et al., 2015)	Not known	
MAN1	die by E11.5, with a defect in vasculogenesis associated with overactive TGF-β	(Cohen et al., 2007; Ishimura et al., 2006)	sclerosing bone dysplasias osteopoikilosis, non-sporadic melorheostosis, and Buschke- Ollendorf syndrome	(Hellemans et al., 2004)
emerin	phenotypically normal, except for subtle muscle abnormalities	(Melcon et al., 2006; Ozawa et al., 2006)	X-linked recessive Emery–Dreifuss muscular dystrophy (EDMD)	(Bione et al., 1994)
LAP2β	Not known		Not known	
LAP1B	die perinatally, typically by E18 or P0	(Shin et al., 2013)	Muscular dystrophy	(Goodchild and Dauer, 2005)
SAMP1	Not known		Not known	
LAP2α	viable and morphologically normal, while epidermal, erythroid progenitor hyperproliferate in regenerative tissues	(Naetar et al., 2008)	dilated cardiomyopathy (DCM)	(Taylor et al., 2005)

The thorough immunostaining-based screening of WT mouse tissues with antibodies against a large set of INM proteins allowed me to obtain the cell-type specific signature of the INM proteins expression for more than 20 cell types. In contrast to the published data, our results show that the expression patterns of LEM-D proteins, LAP1B and SAMP1 are cell-type specific. The most prominent example is SAMP1 which is exclusively expressed in neurons and muscle cells (our unpublished data). Consistent with our results, in certain cell types, different INM proteins, or the combinations of these INM proteins, are involved in the localization of chromosome to and from the nuclear periphery (Zuleger et al., 2008). Correspondingly, the localization of certain chromosomes exhibits tissue-specific pattern. Patterns of chromosome positioning in the nucleus differ in different cell types, such as LAP2β was implicated in gene silencing and heterochromatin localization at the nuclear periphery in mammals (Zullo et al., 2012) . It forms a protein complex with HDAC3 and cKrox which can recognize extended GAGA motif of lamina-associated sequences (LAS). LAS serve as the primary basis by which chromatin is targeted to the nuclear lamina. HDAC3 promotes heterochromatinization via the deacetylase activitities, LAP2β binds the whole complex to the NE (Zullo et al., 2012). Notably, the complex activity is cell-type- and developmental-stage-specific.

Apart from LAP2β, other INM proteins also mediate heterochromatin tethering to the nuclear periphery, cell-type- and developmental-stage-specifically (Worman and Schirmer, 2015; Zuleger et al., 2013). Emerin also binds and recruits HDAC3 to the nuclear envelope and contribute to deacetylation of targeted genes (Demmerle et al., 2012; Zullo et al., 2012). Recent studies show that LADs organization originated by Lamin B1 expression is in conjunction with LAP2β and HDAC (Zullo et al., 2012), LBR is involved in tethering heterochromatin to the nuclear periphery (Solovei et al., 2013). Therefore, we propose that instead of initiating chromatin tethering, lamins might reinforce a chromosome arrangement initially established by a tissue-specific INM proteins.

Data received in my study strongly indicate that chromatin-binding components of the A-tether are indeed tissue- and cell type-specific. In mouse rod nuclei MAN1, LAP2β, SAMP1 are expressed at all developmental stages (unpublished data), which rules out the possibility of these proteins as cofactors in A-type tethers. Intriguingly, I found that rod cells lack one of the LEM-D proteins, LEM2. Moreover, absence of LEM2 in other cell types coincides with lack of Lamin A/C, and vice versa, presence of LEM2 coincides with expression of Lamin A/C in all cells studied. Screening of Lmna-KO mouse tissues confirmed the above observation: in cell types which express both Lamin A/C and LEM2 in WT mice, LEM2 is either absent from the nuclear envelope, or prominently mislocalized upon Lmna deficiency. Additionally, absence or mislocalization of LEM2 was also found in nuclei of myoblasts derived from muscles of Lmna-KO mice. These data strongly suggest LEM2 as a promising candidate to

mediate heterochromatin binding in the Lamin A/C-dependent tether. The Lamin A/C dependent LEM2 localization is supported by the diffusion-retention trafficking model on the journey from the ER to the INM (Katta et al., 2014; Ungricht and Kutay, 2015). The newly synthesized LEM2 trafficks through the continuous ER system and accumulates in the INM relying on removal of molecules from a diffusive pool by binding to nuclear interaction partners, most probably Lamin A/C.

To test our hypothesis, both components of the A-tether, Lamin A/C and LEM2, have to be transgenically expressed in rod photoreceptors. Re-establishing of conventional nuclear architecture in transgenic mice would confirm our hypothesis. Therefore, I have cloned the two LEM-D proteins, LEM2 and emerin, together with Lamin C under the rod cell specific Nrl promoter (Akimoto et al., 2006). Though emerin is not mislocalized in Lmna-KO cells, it is weakly expressed in rods (Solovei et al., 2013) and has been implemented in strong chromatin binding (Berk et al., 2013b). The transgenic mice expressing both Lamin C and LEM-D proteins, LEM2+LaminC and emerin+LaminC, in rod photoreceptors are currently under preparation.

4 Annex

4.1 References

Aagaard, L., Laible, G., Selenko, P., Schmid, M., Dorn, R., Schotta, G., Kuhfittig, S., Wolf, A., Lebersorger, A., Singh, P.B., et al. (1999). Functional mammalian homologues of the Drosophila PEV-modifier Su(var)3-9 encode centromere-associated proteins which complex with the heterochromatin component M31. The EMBO journal 18, 1923-1938.

Akimoto, M., Cheng, H., Zhu, D., Brzezinski, J.A., Khanna, R., Filippova, E., Oh, E.C., Jing, Y., Linares, J.L., Brooks, M., et al. (2006). Targeting of GFP to newborn rods by Nrl promoter and temporal expression profiling of flow-sorted photoreceptors. Proceedings of the National Academy of Sciences of the United States of America 103, 3890-3895.

Al-Saaidi, R., and Bross, P. (2015). Do lamin A and lamin C have unique roles? Chromosoma 124, 1-12.

Almouzni, G., and Probst, A.V. (2011). Heterochromatin maintenance and establishment: lessons from the mouse pericentromere. Nucleus 2, 332-338.

Amendola, M., and van Steensel, B. (2015). Nuclear lamins are not required for lamina-associated domain organization in mouse embryonic stem cells. EMBO reports 16, 610-617.

Apel, E.D., Lewis, R.M., Grady, R.M., and Sanes, J.R. (2000). Syne-1, a dystrophin- and Klarsicht-related protein associated with synaptic nuclei at the neuromuscular junction. The Journal of biological chemistry 275, 31986-31995.

Asencio, C., Davidson, I.F., Santarella-Mellwig, R., Ly-Hartig, T.B., Mall, M., Wallenfang, M.R., Mattaj, I.W., and Gorjanacz, M. (2012). Coordination of kinase and phosphatase activities by Lem4 enables nuclear envelope reassembly during mitosis. Cell 150, 122-135.

Bacolla, A., Pradhan, S., Larson, J.E., Roberts, R.J., and Wells, R.D. (2001). Recombinant human DNA (cytosine-5) methyltransferase. III. Allosteric control, reaction order, and influence of plasmid topology and triplet repeat length on methylation of the fragile X CGG.CCG sequence. The Journal of biological chemistry 276, 18605-18613.

Bacolla, A., Pradhan, S., Roberts, R.J., and Wells, R.D. (1999). Recombinant human DNA (cytosine-5) methyltransferase. II. Steady-state kinetics reveal allosteric activation by methylated dna. The Journal of biological chemistry 274, 33011-33019.

Bank, E.M., and Gruenbaum, Y. (2011). The nuclear lamina and heterochromatin: a complex relationship. Biochemical Society transactions 39, 1705-1709.

Bao, X., Girton, J., Johansen, J., and Johansen, K.M. (2007). The lamin Dm0 allele Ari3 acts as an enhancer of position effect variegation of the wm4 allele in Drosophila. Genetica 129, 339-342.

Bau, D., and Marti-Renom, M.A. (2011). Structure determination of genomic domains by satisfaction of spatial restraints. Chromosome research : an international journal on the molecular, supramolecular and evolutionary aspects of chromosome biology 19, 25-35.

Beck, L.A., Hosick, T.J., and Sinensky, M. (1990). Isoprenylation is required for the processing of the lamin A precursor. The Journal of cell biology 110, 1489-1499.

Becker, P.B., Ruppert, S., and Schutz, G. (1987). Genomic footprinting reveals cell type-specific DNA binding of ubiquitous factors. Cell 51, 435-443.

Belmont, A.S., Zhai, Y., and Thilenius, A. (1993). Lamin B distribution and association with peripheral chromatin revealed by optical sectioning and electron microscopy tomography. The Journal of cell biology 123, 1671-1685.

Berger, R., Theodor, L., Shoham, J., Gokkel, E., Brok-Simoni, F., Avraham, K.B., Copeland, N.G., Jenkins, N.A., Rechavi, G., and Simon, A.J. (1996). The characterization and localization of the mouse thymopoietin/lamina-associated polypeptide 2 gene and its alternatively spliced products. Genome research 6, 361-370.

Berger, S.L. (2007). The complex language of chromatin regulation during transcription. Nature 447, 407-412.

Berk, J.M., Maitra, S., Dawdy, A.W., Shabanowitz, J., Hunt, D.F., and Wilson, K.L. (2013a). O-Linked beta-N-acetylglucosamine (O-GlcNAc) regulates emerin binding to barrier to autointegration factor (BAF) in a chromatin- and lamin B-enriched "niche". The Journal of biological chemistry 288, 30192-30209.

Berk, J.M., Tifft, K.E., and Wilson, K.L. (2013b). The nuclear envelope LEM-domain protein emerin. Nucleus 4, 298-314.

Bernstein, B.E., Meissner, A., and Lander, E.S. (2007). The mammalian epigenome. Cell 128, 669-681.

Bestor, T., Laudano, A., Mattaliano, R., and Ingram, V. (1988). Cloning and sequencing of a cDNA encoding DNA methyltransferase of mouse cells. The carboxyl-terminal domain of the mammalian enzymes is related to bacterial restriction methyltransferases. Journal of molecular biology 203, 971-983.

Bian, Q., Khanna, N., Alvikas, J., and Belmont, A.S. (2013). beta-Globin cis-elements determine differential nuclear targeting through epigenetic modifications. The Journal of cell biology 203, 767-783.

Bickmore, W.A. (2013). The spatial organization of the human genome. Annual review of genomics and human genetics 14, 67-84.

Bickmore, W.A., and van Steensel, B. (2013). Genome architecture: domain organization of interphase chromosomes. Cell 152, 1270-1284.

Bione, S., Maestrini, E., Rivella, S., Mancini, M., Regis, S., Romeo, G., and Toniolo, D. (1994). Identification of a novel X-linked gene responsible for Emery-Dreifuss muscular dystrophy. Nature genetics 8, 323-327.

Bird, A. (2002). DNA methylation patterns and epigenetic memory. Genes & development 16, 6-21.

Bird, A.P., and Wolffe, A.P. (1999). Methylation-induced repression--belts, braces, and chromatin. Cell 99, 451-454.

Bohn, M., and Heermann, D.W. (2010). Diffusion-driven looping provides a consistent framework for chromatin organization. PloS one 5, e12218.

Bolzer, A., Kreth, G., Solovei, I., Koehler, D., Saracoglu, K., Fauth, C., Muller, S., Eils, R., Cremer, C., Speicher, M.R., et al. (2005). Three-dimensional maps of all chromosomes in human male fibroblast nuclei and prometaphase rosettes. PLoS biology 3, e157.

Bone, C.R., Tapley, E.C., Gorjanacz, M., and Starr, D.A. (2014). The Caenorhabditis elegans SUN protein UNC-84 interacts with lamin to transfer forces from the cytoplasm to the nucleoskeleton during nuclear migration. Molecular biology of the cell 25, 2853-2865.

Borrego-Pinto, J., Jegou, T., Osorio, D.S., Aurade, F., Gorjanacz, M., Koch, B., Mattaj, I.W., and Gomes, E.R. (2012). Samp1 is a component of TAN lines and is required for nuclear movement. Journal of cell science 125, 1099-1105.

Bourgeois, B., Gilquin, B., Tellier-Lebegue, C., Ostlund, C., Wu, W., Perez, J., El Hage, P., Lallemand, F., Worman, H.J., and Zinn-Justin, S. (2013). Inhibition of TGF-beta signaling at the nuclear envelope: characterization of interactions between MAN1, Smad2 and Smad3, and PPM1A. Science signaling 6, ra49.

Boyle, S., Gilchrist, S., Bridger, J.M., Mahy, N.L., Ellis, J.A., and Bickmore, W.A. (2001). The spatial organization of human chromosomes within the nuclei of normal and emerin-mutant cells. Human molecular genetics 10, 211-219.

Brachner, A., Braun, J., Ghodgaonkar, M., Castor, D., Zlopasa, L., Ehrlich, V., Jiricny, J., Gotzmann, J., Knasmuller, S., and Foisner, R. (2012). The endonuclease Ankle1 requires its LEM and GIY-YIG motifs for DNA cleavage in vivo. Journal of cell science 125, 1048-1057.

Brachner, A., and Foisner, R. (2011). Evolvement of LEM proteins as chromatin tethers at the nuclear periphery. Biochemical Society transactions 39, 1735-1741.

Brachner, A., Reipert, S., Foisner, R., and Gotzmann, J. (2005). LEM2 is a novel MAN1-related inner nuclear membrane protein associated with A-type lamins. Journal of cell science 118, 5797-5810.

Brero, A., Easwaran, H.P., Nowak, D., Grunewald, I., Cremer, T., Leonhardt, H., and Cardoso, M.C. (2005). Methyl CpG-binding proteins induce large-scale chromatin reorganization during terminal differentiation. The Journal of cell biology 169, 733-743.

Brown, C.R., Kennedy, C.J., Delmar, V.A., Forbes, D.J., and Silver, P.A. (2008). Global histone acetylation induces functional genomic reorganization at mammalian nuclear pore complexes. Genes & development 22, 627-639.

Buch, C., Lindberg, R., Figueroa, R., Gudise, S., Onischenko, E., and Hallberg, E. (2009). An integral protein of the inner nuclear membrane localizes to the mitotic spindle in mammalian cells. Journal of cell science 122, 2100-2107.

Burke, B., Mounkes, L.C., and Stewart, C.L. (2001). The nuclear envelope in muscular dystrophy and cardiovascular diseases. Traffic 2, 675-683.

Burke, B., and Stewart, C.L. (2002). Life at the edge: the nuclear envelope and human disease. Nature reviews Molecular cell biology 3, 575-585.

Burke, B., and Stewart, C.L. (2006). The laminopathies: the functional architecture of the nucleus and its contribution to disease. Annual review of genomics and human genetics 7, 369-405.

Cai, M., Huang, Y., Ghirlando, R., Wilson, K.L., Craigie, R., and Clore, G.M. (2001). Solution structure of the constant region of nuclear envelope protein LAP2 reveals two LEM-domain structures: one binds BAF and the other binds DNA. The EMBO journal 20, 4399-4407.

Cai, M., Huang, Y., Suh, J.Y., Louis, J.M., Ghirlando, R., Craigie, R., and Clore, G.M. (2007). Solution NMR structure of the barrier-to-autointegration factor-Emerin complex. The Journal of biological chemistry 282, 14525-14535.

Cao, R., Wang, L., Wang, H., Xia, L., Erdjument-Bromage, H., Tempst, P., Jones, R.S., and Zhang, Y. (2002). Role of histone H3 lysine 27 methylation in Polycomb-group silencing. Science 298, 1039-1043.

Capelson, M., Liang, Y., Schulte, R., Mair, W., Wagner, U., and Hetzer, M.W. (2010). Chromatin-bound nuclear pore components regulate gene expression in higher eukaryotes. Cell 140, 372-383.

Caputo, S., Couprie, J., Duband-Goulet, I., Konde, E., Lin, F., Braud, S., Gondry, M., Gilquin, B., Worman, H.J., and Zinn-Justin, S. (2006). The carboxyl-terminal nucleoplasmic region of MAN1 exhibits a DNA binding winged helix domain. The Journal of biological chemistry 281, 18208-18215.

Carlton, P.M. (2008). Three-dimensional structured illumination microscopy and its application to chromosome structure. Chromosome research : an international journal on the molecular, supramolecular and evolutionary aspects of chromosome biology 16, 351-365.

Chen, C.Y., Chi, Y.H., Mutalif, R.A., Starost, M.F., Myers, T.G., Anderson, S.A., Stewart, C.L., and Jeang, K.T. (2012). Accumulation of the inner nuclear envelope protein Sun1 is pathogenic in progeric and dystrophic laminopathies. Cell 149, 565-577.

Chen, I.H., Huber, M., Guan, T., Bubeck, A., and Gerace, L. (2006). Nuclear envelope transmembrane proteins (NETs) that are up-regulated during myogenesis. BMC cell biology 7, 38.

Chi, Y.H., Chen, Z.J., and Jeang, K.T. (2009). The nuclear envelopathies and human diseases. Journal of biomedical science 16, 96.

Chubb, J.R., Boyle, S., Perry, P., and Bickmore, W.A. (2002). Chromatin motion is constrained by association with nuclear compartments in human cells. Current biology : CB 12, 439-445.

Clements, L., Manilal, S., Love, D.R., and Morris, G.E. (2000). Direct interaction between emerin and lamin A. Biochemical and biophysical research communications 267, 709-714.

Cohen, T.V., Kosti, O., and Stewart, C.L. (2007). The nuclear envelope protein MAN1 regulates TGFbeta signaling and vasculogenesis in the embryonic yolk sac. Development 134, 1385-1395.

Collas, P., Lund, E.G., and Oldenburg, A.R. (2014). Closing the (nuclear) envelope on the genome: how nuclear lamins interact with promoters and modulate gene expression. BioEssays : news and reviews in molecular, cellular and developmental biology 36, 75-83.

Cook, P.R. (2010). A model for all genomes: the role of transcription factories. Journal of molecular biology 395, 1-10.

Cremer, M., Kupper, K., Wagler, B., Wizelman, L., von Hase, J., Weiland, Y., Kreja, L., Diebold, J., Speicher, M.R., and Cremer, T. (2003). Inheritance of gene density-related higher order chromatin arrangements in normal and tumor cell nuclei. The Journal of cell biology 162, 809-820.

Cremer, T., and Cremer, C. (2001). Chromosome territories, nuclear architecture and gene regulation in mammalian cells. Nature reviews Genetics 2, 292-301.

Cremer, T., Cremer, C., Baumann, H., Luedtke, E.K., Sperling, K., Teuber, V., and Zorn, C. (1982). Rabl's model of the interphase chromosome arrangement tested in Chinese hamster cells by premature chromosome condensation and laser-UV-microbeam experiments. Human genetics 60, 46-56.

Cremer, T., and Cremer, M. (2010). Chromosome territories. Cold Spring Harbor perspectives in biology 2, a003889.

Crisp, M., Liu, Q., Roux, K., Rattner, J.B., Shanahan, C., Burke, B., Stahl, P.D., and Hodzic, D. (2006). Coupling of the nucleus and cytoplasm: role of the LINC complex. The Journal of cell biology 172, 41-53.

Croft, J.A., Bridger, J.M., Boyle, S., Perry, P., Teague, P., and Bickmore, W.A. (1999). Differences in the localization and morphology of chromosomes in the human nucleus. The Journal of cell biology 145, 1119-1131.

Daujat, S., Weiss, T., Mohn, F., Lange, U.C., Ziegler-Birling, C., Zeissler, U., Lappe, M., Schubeler, D., Torres-Padilla, M.E., and Schneider, R. (2009). H3K64 trimethylation marks heterochromatin and is dynamically remodeled during developmental reprogramming. Nature structural & molecular biology 16, 777-781.

Dechat, T., Adam, S.A., Taimen, P., Shimi, T., and Goldman, R.D. (2010). Nuclear lamins. Cold Spring Harbor perspectives in biology 2, a000547.

Dechat, T., Gajewski, A., Korbei, B., Gerlich, D., Daigle, N., Haraguchi, T., Furukawa, K., Ellenberg, J., and Foisner, R. (2004). LAP2alpha and BAF transiently localize to telomeres and specific regions on chromatin during nuclear assembly. Journal of cell science 117, 6117-6128.

Dechat, T., Gotzmann, J., Stockinger, A., Harris, C.A., Talle, M.A., Siekierka, J.J., and Foisner, R. (1998). Detergent-salt resistance of LAP2alpha in interphase nuclei and phosphorylation-dependent association with chromosomes early in nuclear assembly implies functions in nuclear structure dynamics. The EMBO journal 17, 4887-4902.

Dechat, T., Korbei, B., Vaughan, O.A., Vlcek, S., Hutchison, C.J., and Foisner, R. (2000a). Lamina-associated polypeptide 2alpha binds intranuclear A-type lamins. Journal of cell science 113 Pt 19, 3473-3484.

Dechat, T., Vlcek, S., and Foisner, R. (2000b). Review: lamina-associated polypeptide 2 isoforms and related proteins in cell cycle-dependent nuclear structure dynamics. Journal of structural biology 129, 335-345.

Dekker, J. (2014). Two ways to fold the genome during the cell cycle: insights obtained with chromosome conformation capture. Epigenetics & chromatin 7, 25.

Dekker, J., Marti-Renom, M.A., and Mirny, L.A. (2013). Exploring the three-dimensional organization of genomes: interpreting chromatin interaction data. Nature reviews Genetics 14, 390-403.

Dekker, J., Rippe, K., Dekker, M., and Kleckner, N. (2002). Capturing chromosome conformation. Science 295, 1306-1311.

Demmerle, J., Koch, A.J., and Holaska, J.M. (2012). The nuclear envelope protein emerin binds directly to histone deacetylase 3 (HDAC3) and activates HDAC3 activity. The Journal of biological chemistry 287, 22080-22088.

Deng, W., and Blobel, G.A. (2014). Manipulating nuclear architecture. Current opinion in genetics & development 25, 1-7.

Derecki, N.C., Cronk, J.C., and Kipnis, J. (2013). The role of microglia in brain maintenance: implications for Rett syndrome. Trends in immunology 34, 144-150.

Derecki, N.C., Cronk, J.C., Lu, Z., Xu, E., Abbott, S.B., Guyenet, P.G., and Kipnis, J. (2012). Wild-type microglia arrest pathology in a mouse model of Rett syndrome. Nature 484, 105-109.

Dillon, N., and Festenstein, R. (2002). Unravelling heterochromatin: competition between positive and negative factors regulates accessibility. Trends in genetics : TIG 18, 252-258.

Dittmer, T.A., and Misteli, T. (2011). The lamin protein family. Genome biology 12, 222.

Dixon, J.R., Jung, I., Selvaraj, S., Shen, Y., Antosiewicz-Bourget, J.E., Lee, A.Y., Ye, Z., Kim, A., Rajagopal, N., Xie, W., et al. (2015). Chromatin architecture reorganization during stem cell differentiation. Nature 518, 331-336.

Dixon, J.R., Selvaraj, S., Yue, F., Kim, A., Li, Y., Shen, Y., Hu, M., Liu, J.S., and Ren, B. (2012). Topological domains in mammalian genomes identified by analysis of chromatin interactions. Nature 485, 376-380.

Dorner, D., Vlcek, S., Foeger, N., Gajewski, A., Makolm, C., Gotzmann, J., Hutchison, C.J., and Foisner, R. (2006). Lamina-associated polypeptide 2alpha regulates cell cycle progression and differentiation via the retinoblastoma-E2F pathway. The Journal of cell biology 173, 83-93.

Duband-Goulet, I., and Courvalin, J.C. (2000). Inner nuclear membrane protein LBR preferentially interacts with DNA secondary structures and nucleosomal linker. Biochemistry 39, 6483-6488.

Eberhart, A., Feodorova, Y., Song, C., Wanner, G., Kiseleva, E., Furukawa, T., Kimura, H., Schotta, G., Leonhardt, H., Joffe, B., et al. (2013). Epigenetics of eu- and heterochromatin in inverted and conventional nuclei from mouse retina. Chromosome research : an international journal on the molecular, supramolecular and evolutionary aspects of chromosome biology 21, 535-554.

Eberhart, A., Kimura, H., Leonhardt, H., Joffe, B., and Solovei, I. (2012). Reliable detection of epigenetic histone marks and nuclear proteins in tissue cryosections. Chromosome research : an international journal on the molecular, supramolecular and evolutionary aspects of chromosome biology 20, 849-858.

Figueroa, R., Gudise, S., Larsson, V., and Hallberg, E. (2010). A transmembrane inner nuclear membrane protein in the mitotic spindle. Nucleus 1, 249-253.

Filion, G.J., Zhenilo, S., Salozhin, S., Yamada, D., Prokhortchouk, E., and Defossez, P.A. (2006). A family of human zinc finger proteins that bind methylated DNA and repress transcription. Molecular and cellular biology 26, 169-181.

Finlan, L.E., Sproul, D., Thomson, I., Boyle, S., Kerr, E., Perry, P., Ylstra, B., Chubb, J.R., and Bickmore, W.A. (2008). Recruitment to the nuclear periphery can alter expression of genes in human cells. PLoS genetics 4, e1000039.

Fisher, D.Z., Chaudhary, N., and Blobel, G. (1986). cDNA sequencing of nuclear lamins A and C reveals primary and secondary structural homology to intermediate filament proteins. Proceedings of the National Academy of Sciences of the United States of America 83, 6450-6454.

Foisner, R., and Gerace, L. (1993). Integral membrane proteins of the nuclear envelope interact with lamins and chromosomes, and binding is modulated by mitotic phosphorylation. Cell 73, 1267-1279.

Fong, L.G., Ng, J.K., Lammerding, J., Vickers, T.A., Meta, M., Cote, N., Gavino, B., Qiao, X., Chang, S.Y., Young, S.R., et al. (2006). Prelamin A and lamin A appear to be dispensable in the nuclear lamina. The Journal of clinical investigation 116, 743-752.

Fudenberg, G., and Mirny, L.A. (2012). Higher-order chromatin structure: bridging physics and biology. Current opinion in genetics & development 22, 115-124.

Furukawa, K. (1999). LAP2 binding protein 1 (L2BP1/BAF) is a candidate mediator of LAP2-chromatin interaction. Journal of cell science 112 (Pt 15), 2485-2492.

Furukawa, K., and Hotta, Y. (1993). cDNA cloning of a germ cell specific lamin B3 from mouse spermatocytes and analysis of its function by ectopic expression in somatic cells. The EMBO journal 12, 97-106.

Furukawa, K., Pante, N., Aebi, U., and Gerace, L. (1995). Cloning of a cDNA for lamina-associated polypeptide 2 (LAP2) and identification of regions that specify targeting to the nuclear envelope. The EMBO journal 14, 1626-1636.

Gabel, H.W., Kinde, B., Stroud, H., Gilbert, C.S., Harmin, D.A., Kastan, N.R., Hemberg, M., Ebert, D.H., and Greenberg, M.E. (2015). Disruption of DNA-methylation-dependent long gene repression in Rett syndrome. Nature 522, 89-93.

Gajewski, A., and Krohne, G. (1999). Subcellular distribution of the Xenopus p58/lamin B receptor in oocytes and eggs. Journal of cell science 112 (Pt 15), 2583-2596.

Gerace, L., and Blobel, G. (1980). The nuclear envelope lamina is reversibly depolymerized during mitosis. Cell 19, 277-287.

Gianakopoulos, P.J., Mehta, V., Voronova, A., Cao, Y., Yao, Z., Coutu, J., Wang, X., Waddington, M.S., Tapscott, S.J., and Skerjanc, I.S. (2011). MyoD directly up-regulates premyogenic mesoderm factors during induction of skeletal myogenesis in stem cells. The Journal of biological chemistry 286, 2517-2525.

Gibcus, J.H., and Dekker, J. (2013). The hierarchy of the 3D genome. Molecular cell 49, 773-782.

Gilbert, N., Gilchrist, S., and Bickmore, W.A. (2005). Chromatin organization in the mammalian nucleus. International review of cytology 242, 283-336.

Gonzalez-Alegre, P., and Paulson, H.L. (2004). Aberrant cellular behavior of mutant torsinA implicates nuclear envelope dysfunction in DYT1 dystonia. The Journal of neuroscience : the official journal of the Society for Neuroscience 24, 2593-2601.

Goodchild, R.E., and Dauer, W.T. (2004). Mislocalization to the nuclear envelope: an effect of the dystonia-causing torsinA mutation. Proceedings of the National Academy of Sciences of the United States of America 101, 847-852.

Goodchild, R.E., and Dauer, W.T. (2005). The AAA+ protein torsinA interacts with a conserved domain present in LAP1 and a novel ER protein. The Journal of cell biology 168, 855-862.

Gotic, I., and Foisner, R. (2010). Multiple novel functions of lamina associated polypeptide 2alpha in striated muscle. Nucleus 1, 397-401.

Gotic, I., Schmidt, W.M., Biadasiewicz, K., Leschnik, M., Spilka, R., Braun, J., Stewart, C.L., and Foisner, R. (2010). Loss of LAP2 alpha delays satellite cell differentiation and affects postnatal fiber-type determination. Stem cells 28, 480-488.

Guarda, A., Bolognese, F., Bonapace, I.M., and Badaracco, G. (2009). Interaction between the inner nuclear membrane lamin B receptor and the heterochromatic methyl binding protein, MeCP2. Experimental cell research 315, 1895-1903.

Gudise, S., Figueroa, R.A., Lindberg, R., Larsson, V., and Hallberg, E. (2011). Samp1 is functionally associated with the LINC complex and A-type lamina networks. Journal of cell science 124, 2077-2085.

Guelen, L., Pagie, L., Brasset, E., Meuleman, W., Faza, M.B., Talhout, W., Eussen, B.H., de Klein, A., Wessels, L., de Laat, W., et al. (2008). Domain organization of human chromosomes revealed by mapping of nuclear lamina interactions. Nature 453, 948-951.

Guenatri, M., Bailly, D., Maison, C., and Almouzni, G. (2004). Mouse centric and pericentric satellite repeats form distinct functional heterochromatin. The Journal of cell biology 166, 493-505.

Hakim, O., and Misteli, T. (2012). SnapShot: Chromosome confirmation capture. Cell 148, 1068 e1061-1062.

Haque, F., Lloyd, D.J., Smallwood, D.T., Dent, C.L., Shanahan, C.M., Fry, A.M., Trembath, R.C., and Shackleton, S. (2006). SUN1 interacts with nuclear lamin A and cytoplasmic nesprins to provide a physical connection between the nuclear lamina and the cytoskeleton. Molecular and cellular biology 26, 3738-3751.

Haraguchi, T., Holaska, J.M., Yamane, M., Koujin, T., Hashiguchi, N., Mori, C., Wilson, K.L., and Hiraoka, Y. (2004). Emerin binding to Btf, a death-promoting transcriptional repressor, is disrupted by a missense mutation that causes Emery-Dreifuss muscular dystrophy. European journal of biochemistry / FEBS 271, 1035-1045.

Harewood, L., Schutz, F., Boyle, S., Perry, P., Delorenzi, M., Bickmore, W.A., and Reymond, A. (2010). The effect of translocation-induced nuclear reorganization on gene expression. Genome research 20, 554-564.

Harr, J.C., Luperchio, T.R., Wong, X., Cohen, E., Wheelan, S.J., and Reddy, K.L. (2015). Directed targeting of chromatin to the nuclear lamina is mediated by chromatin state and A-type lamins. The Journal of cell biology 208, 33-52.

Harris, C.A., Andryuk, P.J., Cline, S., Chan, H.K., Natarajan, A., Siekierka, J.J., and Goldstein, G. (1994). Three distinct human thymopoietins are derived from alternatively spliced mRNAs. Proceedings of the National Academy of Sciences of the United States of America 91, 6283-6287.

Hasan, S., Guttinger, S., Muhlhausser, P., Anderegg, F., Burgler, S., and Kutay, U. (2006). Nuclear envelope localization of human UNC84A does not require nuclear lamins. FEBS letters 580, 1263-1268.

Hatakeyama, M., and Weinberg, R.A. (1995). The role of RB in cell cycle control. Progress in cell cycle research 1, 9-19.

Hellemans, J., Preobrazhenska, O., Willaert, A., Debeer, P., Verdonk, P.C., Costa, T., Janssens, K., Menten, B., Van Roy, N., Vermeulen, S.J., et al. (2004). Loss-of-function mutations in LEMD3 result in osteopoikilosis, Buschke-Ollendorff syndrome and melorheostosis. Nature genetics 36, 1213-1218.

Hellman, A., and Chess, A. (2007). Gene body-specific methylation on the active X chromosome. Science 315, 1141-1143.

Hendrich, B., and Bird, A. (1998). Identification and characterization of a family of mammalian methyl-CpG binding proteins. Molecular and cellular biology 18, 6538-6547.

Hennekes, H., and Nigg, E.A. (1994). The role of isoprenylation in membrane attachment of nuclear lamins. A single point mutation prevents proteolytic cleavage of the lamin A precursor and confers membrane binding properties. Journal of cell science 107 (Pt 4), 1019-1029.

Herrmann, H., Bar, H., Kreplak, L., Strelkov, S.V., and Aebi, U. (2007). Intermediate filaments: from cell architecture to nanomechanics. Nature reviews Molecular cell biology 8, 562-573.

Hirano, Y., Hizume, K., Kimura, H., Takeyasu, K., Haraguchi, T., and Hiraoka, Y. (2012). Lamin B receptor recognizes specific modifications of histone H4 in heterochromatin formation. The Journal of biological chemistry 287, 42654-42663.

Hoffmann, K., Dreger, C.K., Olins, A.L., Olins, D.E., Shultz, L.D., Lucke, B., Karl, H., Kaps, R., Muller, D., Vaya, A., et al. (2002). Mutations in the gene encoding the lamin B receptor produce an altered nuclear morphology in granulocytes (Pelger-Huet anomaly). Nature genetics 31, 410-414.

Holaska, J.M., Lee, K.K., Kowalski, A.K., and Wilson, K.L. (2003). Transcriptional repressor germ cell-less (GCL) and barrier to autointegration factor (BAF) compete for binding to emerin in vitro. The Journal of biological chemistry 278, 6969-6975.

Holmer, L., and Worman, H.J. (2001). Inner nuclear membrane proteins: functions and targeting. Cellular and molecular life sciences : CMLS 58, 1741-1747.

Huber, M.D., Guan, T., and Gerace, L. (2009). Overlapping functions of nuclear envelope proteins NET25 (Lem2) and emerin in regulation of extracellular signal-regulated kinase signaling in myoblast differentiation. Molecular and cellular biology 29, 5718-5728.

Ikegami, K., Egelhofer, T.A., Strome, S., and Lieb, J.D. (2010). Caenorhabditis elegans chromosome arms are anchored to the nuclear membrane via discontinuous association with LEM-2. Genome biology 11, R120.

Illingworth, R.S., and Bird, A.P. (2009). CpG islands--'a rough guide'. FEBS letters 583, 1713-1720.

Ishijima, Y., Toda, T., Matsushita, H., Yoshida, M., and Kimura, N. (1996). Expression of thymopoietin beta/lamina-associated polypeptide 2 (TP beta/LAP2) and its family proteins

as revealed by specific antibody induced against recombinant human thymopoietin. Biochemical and biophysical research communications 226, 431-438.

Ishimura, A., Ng, J.K., Taira, M., Young, S.G., and Osada, S. (2006). Man1, an inner nuclear membrane protein, regulates vascular remodeling by modulating transforming growth factor beta signaling. Development 133, 3919-3928.

Ito, S., D'Alessio, A.C., Taranova, O.V., Hong, K., Sowers, L.C., and Zhang, Y. (2010). Role of Tet proteins in 5mC to 5hmC conversion, ES-cell self-renewal and inner cell mass specification. Nature 466, 1129-1133.

Jia, D., Jurkowska, R.Z., Zhang, X., Jeltsch, A., and Cheng, X. (2007). Structure of Dnmt3a bound to Dnmt3L suggests a model for de novo DNA methylation. Nature 449, 248-251.

Joffe, B., Leonhardt, H., and Solovei, I. (2010). Differentiation and large scale spatial organization of the genome. Current opinion in genetics & development 20, 562-569.

Joseph, A., Mitchell, A.R., and Miller, O.J. (1989). The organization of the mouse satellite DNA at centromeres. Experimental cell research 183, 494-500.

Kalverda, B., and Fornerod, M. (2010). Characterization of genome-nucleoporin interactions in Drosophila links chromatin insulators to the nuclear pore complex. Cell cycle 9, 4812-4817.

Katta, S.S., Smoyer, C.J., and Jaspersen, S.L. (2014). Destination: inner nuclear membrane. Trends in cell biology 24, 221-229.

Ketema, M., Wilhelmsen, K., Kuikman, I., Janssen, H., Hodzic, D., and Sonnenberg, A. (2007). Requirements for the localization of nesprin-3 at the nuclear envelope and its interaction with plectin. Journal of cell science 120, 3384-3394.

Kilic, F., Johnson, D.A., and Sinensky, M. (1999). Subcellular localization and partial purification of prelamin A endoprotease: an enzyme which catalyzes the conversion of farnesylated prelamin A to mature lamin A. FEBS letters 450, 61-65.

Kim, C.E., Perez, A., Perkins, G., Ellisman, M.H., and Dauer, W.T. (2010). A molecular mechanism underlying the neural-specific defect in torsinA mutant mice. Proceedings of the National Academy of Sciences of the United States of America 107, 9861-9866.

Kim, S.H., McQueen, P.G., Lichtman, M.K., Shevach, E.M., Parada, L.A., and Misteli, T. (2004). Spatial genome organization during T-cell differentiation. Cytogenetic and genome research 105, 292-301.

Kim, Y., Sharov, A.A., McDole, K., Cheng, M., Hao, H., Fan, C.M., Gaiano, N., Ko, M.S., and Zheng, Y. (2011). Mouse B-type lamins are required for proper organogenesis but not by embryonic stem cells. Science 334, 1706-1710.

Kind, J., Pagie, L., Ortabozkoyun, H., Boyle, S., de Vries, S.S., Janssen, H., Amendola, M., Nolen, L.D., Bickmore, W.A., and van Steensel, B. (2013). Single-cell dynamics of genome-nuclear lamina interactions. Cell 153, 178-192.

Kind, J., and van Steensel, B. (2014). Stochastic genome-nuclear lamina interactions: modulating roles of Lamin A and BAF. Nucleus 5, 124-130.

Kinde, B., Gabel, H.W., Gilbert, C.S., Griffith, E.C., and Greenberg, M.E. (2015). Reading the unique DNA methylation landscape of the brain: Non-CpG methylation,

hydroxymethylation, and MeCP2. Proceedings of the National Academy of Sciences of the United States of America 112, 6800-6806.

King, M.C., Drivas, T.G., and Blobel, G. (2008). A network of nuclear envelope membrane proteins linking centromeres to microtubules. Cell 134, 427-438.

Kizilyaprak, C., Spehner, D., Devys, D., and Schultz, P. (2011). The linker histone H1C contributes to the SCA7 nuclear phenotype. Nucleus 2, 444-454.

Koehler, D., Zakhartchenko, V., Ketterl, N., Wolf, E., Cremer, T., and Brero, A. (2010). FISH on 3D preserved bovine and murine preimplantation embryos. Methods in molecular biology 659, 437-445.

Kohwi, M., Lupton, J.R., Lai, S.L., Miller, M.R., and Doe, C.Q. (2013). Developmentally regulated subnuclear genome reorganization restricts neural progenitor competence in Drosophila. Cell 152, 97-108.

Kondo, Y., Kondoh, J., Hayashi, D., Ban, T., Takagi, M., Kamei, Y., Tsuji, L., Kim, J., and Yoneda, Y. (2002). Molecular cloning of one isotype of human lamina-associated polypeptide 1s and a topological analysis using its deletion mutants. Biochemical and biophysical research communications 294, 770-778.

Kosak, S.T., Skok, J.A., Medina, K.L., Riblet, R., Le Beau, M.M., Fisher, A.G., and Singh, H. (2002). Subnuclear compartmentalization of immunoglobulin loci during lymphocyte development. Science 296, 158-162.

Kouzarides, T. (2007). Chromatin modifications and their function. Cell 128, 693-705.

Kreth, G., Finsterle, J., von Hase, J., Cremer, M., and Cremer, C. (2004). Radial arrangement of chromosome territories in human cell nuclei: a computer model approach based on gene density indicates a probabilistic global positioning code. Biophysical journal 86, 2803-2812.

Kriaucionis, S., and Heintz, N. (2009). The nuclear DNA base 5-hydroxymethylcytosine is present in Purkinje neurons and the brain. Science 324, 929-930.

Kumaran, R.I., Thakar, R., and Spector, D.L. (2008). Chromatin dynamics and gene positioning. Cell 132, 929-934.

Kuroda, M., Tanabe, H., Yoshida, K., Oikawa, K., Saito, A., Kiyuna, T., Mizusawa, H., and Mukai, K. (2004). Alteration of chromosome positioning during adipocyte differentiation. Journal of cell science 117, 5897-5903.

Kutateladze, T.G. (2011). SnapShot: Histone readers. Cell 146, 842-842 e841.

Laguri, C., Gilquin, B., Wolff, N., Romi-Lebrun, R., Courchay, K., Callebaut, I., Worman, H.J., and Zinn-Justin, S. (2001). Structural characterization of the LEM motif common to three human inner nuclear membrane proteins. Structure 9, 503-511.

Lee, K.K., Haraguchi, T., Lee, R.S., Koujin, T., Hiraoka, Y., and Wilson, K.L. (2001). Distinct functional domains in emerin bind lamin A and DNA-bridging protein BAF. Journal of cell science 114, 4567-4573.

Lee, K.K., and Wilson, K.L. (2004). All in the family: evidence for four new LEM-domain proteins Lem2 (NET-25), Lem3, Lem4 and Lem5 in the human genome. Symposia of the Society for Experimental Biology, 329-339.

Lehner, C.F., Stick, R., Eppenberger, H.M., and Nigg, E.A. (1987). Differential expression of nuclear lamin proteins during chicken development. The Journal of cell biology 105, 577-587.

Lehnertz, B., Ueda, Y., Derijck, A.A., Braunschweig, U., Perez-Burgos, L., Kubicek, S., Chen, T., Li, E., Jenuwein, T., and Peters, A.H. (2003). Suv39h-mediated histone H3 lysine 9 methylation directs DNA methylation to major satellite repeats at pericentric heterochromatin. Current biology : CB 13, 1192-1200.

Lei, K., Zhang, X., Ding, X., Guo, X., Chen, M., Zhu, B., Xu, T., Zhuang, Y., Xu, R., and Han, M. (2009). SUN1 and SUN2 play critical but partially redundant roles in anchoring nuclei in skeletal muscle cells in mice. Proceedings of the National Academy of Sciences of the United States of America 106, 10207-10212.

Leonhardt, H., and Cardoso, M.C. (2000). DNA methylation, nuclear structure, gene expression and cancer. Journal of cellular biochemistry Supplement Suppl 35, 78-83.

Lewis, J.D., Meehan, R.R., Henzel, W.J., Maurer-Fogy, I., Jeppesen, P., Klein, F., and Bird, A. (1992). Purification, sequence, and cellular localization of a novel chromosomal protein that binds to methylated DNA. Cell 69, 905-914.

Li, E. (2002). Chromatin modification and epigenetic reprogramming in mammalian development. Nature reviews Genetics 3, 662-673.

Liang, Y., Chiu, P.H., Yip, K.Y., and Chan, S.Y. (2011). Subcellular localization of SUN2 is regulated by lamin A and Rab5. PloS one 6, e20507.

Lieberman-Aiden, E., van Berkum, N.L., Williams, L., Imakaev, M., Ragoczy, T., Telling, A., Amit, I., Lajoie, B.R., Sabo, P.J., Dorschner, M.O., et al. (2009). Comprehensive mapping of long-range interactions reveals folding principles of the human genome. Science 326, 289-293.

Lin, F., Blake, D.L., Callebaut, I., Skerjanc, I.S., Holmer, L., McBurney, M.W., Paulin-Levasseur, M., and Worman, H.J. (2000). MAN1, an inner nuclear membrane protein that shares the LEM domain with lamina-associated polypeptide 2 and emerin. The Journal of biological chemistry 275, 4840-4847.

Lin, F., Morrison, J.M., Wu, W., and Worman, H.J. (2005). MAN1, an integral protein of the inner nuclear membrane, binds Smad2 and Smad3 and antagonizes transforming growth factor-beta signaling. Human molecular genetics 14, 437-445.

Liu, J., Lee, K.K., Segura-Totten, M., Neufeld, E., Wilson, K.L., and Gruenbaum, Y. (2003). MAN1 and emerin have overlapping function(s) essential for chromosome segregation and cell division in Caenorhabditis elegans. Proceedings of the National Academy of Sciences of the United States of America 100, 4598-4603.

Liu, J., Rolef Ben-Shahar, T., Riemer, D., Treinin, M., Spann, P., Weber, K., Fire, A., and Gruenbaum, Y. (2000). Essential roles for Caenorhabditis elegans lamin gene in nuclear organization, cell cycle progression, and spatial organization of nuclear pore complexes. Molecular biology of the cell 11, 3937-3947.

Luo, Y.B., Mastaglia, F.L., and Wilton, S.D. (2014). Normal and aberrant splicing of LMNA. Journal of medical genetics 51, 215-223.

Ma, Y., Cai, S., Lv, Q., Jiang, Q., Zhang, Q., Sodmergen, Zhai, Z., and Zhang, C. (2007). Lamin B receptor plays a role in stimulating nuclear envelope production and targeting

membrane vesicles to chromatin during nuclear envelope assembly through direct interaction with importin beta. Journal of cell science 120, 520-530.

Maison, C., and Almouzni, G. (2004). HP1 and the dynamics of heterochromatin maintenance. Nature reviews Molecular cell biology 5, 296-304.

Maiti, A., and Drohat, A.C. (2011). Thymine DNA glycosylase can rapidly excise 5-formylcytosine and 5-carboxylcytosine: potential implications for active demethylation of CpG sites. The Journal of biological chemistry 286, 35334-35338.

Makatsori, D., Kourmouli, N., Polioudaki, H., Shultz, L.D., McLean, K., Theodoropoulos, P.A., Singh, P.B., and Georgatos, S.D. (2004). The inner nuclear membrane protein lamin B receptor forms distinct microdomains and links epigenetically marked chromatin to the nuclear envelope. The Journal of biological chemistry 279, 25567-25573.

Mancini, M.A., Shan, B., Nickerson, J.A., Penman, S., and Lee, W.H. (1994). The retinoblastoma gene product is a cell cycle-dependent, nuclear matrix-associated protein. Proceedings of the National Academy of Sciences of the United States of America 91, 418-422.

Mansharamani, M., Hewetson, A., and Chilton, B.S. (2001). Cloning and characterization of an atypical Type IV P-type ATPase that binds to the RING motif of RUSH transcription factors. The Journal of biological chemistry 276, 3641-3649.

Mansharamani, M., and Wilson, K.L. (2005). Direct binding of nuclear membrane protein MAN1 to emerin in vitro and two modes of binding to barrier-to-autointegration factor. The Journal of biological chemistry 280, 13863-13870.

Manuelidis, L. (1985). Individual interphase chromosome domains revealed by in situ hybridization. Human genetics 71, 288-293.

Maraldi, N.M., Lattanzi, G., Cenni, V., Bavelloni, A., Marmiroli, S., and Manzoli, F.A. (2010). Laminopathies and A-type lamin-associated signalling pathways. Advances in enzyme regulation 50, 248-261.

Margalit, A., Brachner, A., Gotzmann, J., Foisner, R., and Gruenbaum, Y. (2007). Barrier-to-autointegration factor--a BAFfling little protein. Trends in cell biology 17, 202-208.

Margalit, A., Liu, J., Fridkin, A., Wilson, K.L., and Gruenbaum, Y. (2005a). A lamin-dependent pathway that regulates nuclear organization, cell cycle progression and germ cell development. Novartis Foundation symposium 264, 231-240; discussion 240-235.

Margalit, A., Segura-Totten, M., Gruenbaum, Y., and Wilson, K.L. (2005b). Barrier-to-autointegration factor is required to segregate and enclose chromosomes within the nuclear envelope and assemble the nuclear lamina. Proceedings of the National Academy of Sciences of the United States of America 102, 3290-3295.

Markaki, Y., Gunkel, M., Schermelleh, L., Beichmanis, S., Neumann, J., Heidemann, M., Leonhardt, H., Eick, D., Cremer, C., and Cremer, T. (2010). Functional nuclear organization of transcription and DNA replication: a topographical marriage between chromatin domains and the interchromatin compartment. Cold Spring Harbor symposia on quantitative biology 75, 475-492.

Markiewicz, E., Dechat, T., Foisner, R., Quinlan, R.A., and Hutchison, C.J. (2002). Lamin A/C binding protein LAP2alpha is required for nuclear anchorage of retinoblastoma protein. Molecular biology of the cell 13, 4401-4413.

Markiewicz, E., Ledran, M., and Hutchison, C.J. (2005). Remodelling of the nuclear lamina and nucleoskeleton is required for skeletal muscle differentiation in vitro. Journal of cell science 118, 409-420.

Markiewicz, E., Tilgner, K., Barker, N., van de Wetering, M., Clevers, H., Dorobek, M., Hausmanowa-Petrusewicz, I., Ramaekers, F.C., Broers, J.L., Blankesteijn, W.M., et al. (2006). The inner nuclear membrane protein emerin regulates beta-catenin activity by restricting its accumulation in the nucleus. The EMBO journal 25, 3275-3285.

Martins, S., Eikvar, S., Furukawa, K., and Collas, P. (2003). HA95 and LAP2 beta mediate a novel chromatin-nuclear envelope interaction implicated in initiation of DNA replication. The Journal of cell biology 160, 177-188.

Martins, S.B., Eide, T., Steen, R.L., Jahnsen, T., Skalhegg, B.S., and Collas, P. (2000). HA95 is a protein of the chromatin and nuclear matrix regulating nuclear envelope dynamics. Journal of cell science 113 Pt 21, 3703-3713.

Mattout-Drubezki, A., and Gruenbaum, Y. (2003). Dynamic interactions of nuclear lamina proteins with chromatin and transcriptional machinery. Cellular and molecular life sciences : CMLS 60, 2053-2063.

Mattout, A., Pike, B.L., Towbin, B.D., Bank, E.M., Gonzalez-Sandoval, A., Stadler, M.B., Meister, P., Gruenbaum, Y., and Gasser, S.M. (2011). An EDMD mutation in C. elegans lamin blocks muscle-specific gene relocation and compromises muscle integrity. Current biology : CB 21, 1603-1614.

McCord, R.P., Nazario-Toole, A., Zhang, H., Chines, P.S., Zhan, Y., Erdos, M.R., Collins, F.S., Dekker, J., and Cao, K. (2013). Correlated alterations in genome organization, histone methylation, and DNA-lamin A/C interactions in Hutchinson-Gilford progeria syndrome. Genome research 23, 260-269.

Mehta, I.S., Bridger, J.M., and Kill, I.R. (2010). Progeria, the nucleolus and farnesyltransferase inhibitors. Biochemical Society transactions 38, 287-291.

Melcon, G., Kozlov, S., Cutler, D.A., Sullivan, T., Hernandez, L., Zhao, P., Mitchell, S., Nader, G., Bakay, M., Rottman, J.N., et al. (2006). Loss of emerin at the nuclear envelope disrupts the Rb1/E2F and MyoD pathways during muscle regeneration. Human molecular genetics 15, 637-651.

Mellad, J.A., Warren, D.T., and Shanahan, C.M. (2011). Nesprins LINC the nucleus and cytoskeleton. Current opinion in cell biology 23, 47-54.

Merbs, S.L., Khan, M.A., Hackler, L., Jr., Oliver, V.F., Wan, J., Qian, J., and Zack, D.J. (2012). Cell-specific DNA methylation patterns of retina-specific genes. PloS one 7, e32602.

Meuleman, W., Peric-Hupkes, D., Kind, J., Beaudry, J.B., Pagie, L., Kellis, M., Reinders, M., Wessels, L., and van Steensel, B. (2013). Constitutive nuclear lamina-genome interactions are highly conserved and associated with A/T-rich sequence. Genome research 23, 270-280.

Milon, B.C., Cheng, H., Tselebrovsky, M.V., Lavrov, S.A., Nenasheva, V.V., Mikhaleva, E.A., Shevelyov, Y.Y., and Nurminsky, D.I. (2012). Role of histone deacetylases in gene regulation at nuclear lamina. PloS one 7, e49692.

Misteli, T. (2007). Beyond the sequence: cellular organization of genome function. Cell 128, 787-800.

Muchir, A., Pavlidis, P., Bonne, G., Hayashi, Y.K., and Worman, H.J. (2007). Activation of MAPK in hearts of EMD null mice: similarities between mouse models of X-linked and autosomal dominant Emery Dreifuss muscular dystrophy. Human molecular genetics 16, 1884-1895.

Muller, U., Bauer, C., Siegl, M., Rottach, A., and Leonhardt, H. (2014). TET-mediated oxidation of methylcytosine causes TDG or NEIL glycosylase dependent gene reactivation. Nucleic acids research 42, 8592-8604.

Naetar, N., and Foisner, R. (2009). Lamin complexes in the nuclear interior control progenitor cell proliferation and tissue homeostasis. Cell cycle 8, 1488-1493.

Naetar, N., Korbei, B., Kozlov, S., Kerenyi, M.A., Dorner, D., Kral, R., Gotic, I., Fuchs, P., Cohen, T.V., Bittner, R., et al. (2008). Loss of nucleoplasmic LAP2alpha-lamin A complexes causes erythroid and epidermal progenitor hyperproliferation. Nature cell biology 10, 1341-1348.

Nigg, E.A., Kitten, G.T., and Vorburger, K. (1992). Targeting lamin proteins to the nuclear envelope: the role of CaaX box modifications. Biochemical Society transactions 20, 500-504.

Nili, E., Cojocaru, G.S., Kalma, Y., Ginsberg, D., Copeland, N.G., Gilbert, D.J., Jenkins, N.A., Berger, R., Shaklai, S., Amariglio, N., et al. (2001). Nuclear membrane protein LAP2beta mediates transcriptional repression alone and together with its binding partner GCL (germ-cell-less). Journal of cell science 114, 3297-3307.

Nora, E.P., Dekker, J., and Heard, E. (2013). Segmental folding of chromosomes: a basis for structural and regulatory chromosomal neighborhoods? BioEssays : news and reviews in molecular, cellular and developmental biology 35, 818-828.

Nora, E.P., Lajoie, B.R., Schulz, E.G., Giorgetti, L., Okamoto, I., Servant, N., Piolot, T., van Berkum, N.L., Meisig, J., Sedat, J., et al. (2012). Spatial partitioning of the regulatory landscape of the X-inactivation centre. Nature 485, 381-385.

Okano, M., Bell, D.W., Haber, D.A., and Li, E. (1999). DNA methyltransferases Dnmt3a and Dnmt3b are essential for de novo methylation and mammalian development. Cell 99, 247-257.

Okano, M., Xie, S., and Li, E. (1998). Dnmt2 is not required for de novo and maintenance methylation of viral DNA in embryonic stem cells. Nucleic acids research 26, 2536-2540.

Olins, A.L., Ernst, A., Zwerger, M., Herrmann, H., and Olins, D.E. (2010a). An in vitro model for Pelger-Huet anomaly: stable knockdown of lamin B receptor in HL-60 cells. Nucleus 1, 506-512.

Olins, A.L., Rhodes, G., Welch, D.B., Zwerger, M., and Olins, D.E. (2010b). Lamin B receptor: multi-tasking at the nuclear envelope. Nucleus 1, 53-70.

Ozaki, T., Saijo, M., Murakami, K., Enomoto, H., Taya, Y., and Sakiyama, S. (1994). Complex formation between lamin A and the retinoblastoma gene product: identification of the domain on lamin A required for its interaction. Oncogene 9, 2649-2653.

Ozawa, R., Hayashi, Y.K., Ogawa, M., Kurokawa, R., Matsumoto, H., Noguchi, S., Nonaka, I., and Nishino, I. (2006). Emerin-lacking mice show minimal motor and cardiac dysfunctions with nuclear-associated vacuoles. The American journal of pathology 168, 907-917.

Pan, D., Estevez-Salmeron, L.D., Stroschein, S.L., Zhu, X., He, J., Zhou, S., and Luo, K. (2005). The integral inner nuclear membrane protein MAN1 physically interacts with the R-Smad proteins to repress signaling by the transforming growth factor-{beta} superfamily of cytokines. The Journal of biological chemistry 280, 15992-16001.

Pauler, F.M., Sloane, M.A., Huang, R., Regha, K., Koerner, M.V., Tamir, I., Sommer, A., Aszodi, A., Jenuwein, T., and Barlow, D.P. (2009). H3K27me3 forms BLOCs over silent genes and intergenic regions and specifies a histone banding pattern on a mouse autosomal chromosome. Genome research 19, 221-233.

Peric-Hupkes, D., Meuleman, W., Pagie, L., Bruggeman, S.W., Solovei, I., Brugman, W., Graf, S., Flicek, P., Kerkhoven, R.M., van Lohuizen, M., et al. (2010). Molecular maps of the reorganization of genome-nuclear lamina interactions during differentiation. Molecular cell 38, 603-613.

Peric-Hupkes, D., and van Steensel, B. (2010). Role of the nuclear lamina in genome organization and gene expression. Cold Spring Harbor symposia on quantitative biology 75, 517-524.

Peters, A.H., Mermoud, J.E., O'Carroll, D., Pagani, M., Schweizer, D., Brockdorff, N., and Jenuwein, T. (2002). Histone H3 lysine 9 methylation is an epigenetic imprint of facultative heterochromatin. Nature genetics 30, 77-80.

Peterson, C.L., and Laniel, M.A. (2004). Histones and histone modifications. Current biology : CB 14, R546-551.

Pickersgill, H., Kalverda, B., de Wit, E., Talhout, W., Fornerod, M., and van Steensel, B. (2006). Characterization of the Drosophila melanogaster genome at the nuclear lamina. Nature genetics 38, 1005-1014.

Pinter, S.F., Sadreyev, R.I., Yildirim, E., Jeon, Y., Ohsumi, T.K., Borowsky, M., and Lee, J.T. (2012). Spreading of X chromosome inactivation via a hierarchy of defined Polycomb stations. Genome research 22, 1864-1876.

Polioudaki, H., Kourmouli, N., Drosou, V., Bakou, A., Theodoropoulos, P.A., Singh, P.B., Giannakouros, T., and Georgatos, S.D. (2001). Histones H3/H4 form a tight complex with the inner nuclear membrane protein LBR and heterochromatin protein 1. EMBO reports 2, 920-925.

Popova, E.Y., Grigoryev, S.A., Fan, Y., Skoultchi, A.I., Zhang, S.S., and Barnstable, C.J. (2013). Developmentally regulated linker histone H1c promotes heterochromatin condensation and mediates structural integrity of rod photoreceptors in mouse retina. The Journal of biological chemistry 288, 17895-17907.

Pradhan, S., Bacolla, A., Wells, R.D., and Roberts, R.J. (1999). Recombinant human DNA (cytosine-5) methyltransferase. I. Expression, purification, and comparison of de novo and maintenance methylation. The Journal of biological chemistry 274, 33002-33010.

Prokhortchouk, A., Hendrich, B., Jorgensen, H., Ruzov, A., Wilm, M., Georgiev, G., Bird, A., and Prokhortchouk, E. (2001). The p120 catenin partner Kaiso is a DNA methylation-dependent transcriptional repressor. Genes & development 15, 1613-1618.

Raith, M., Cremer, T., Cremer, C., and Speit, G. (1984). Sister chromatid exchange (SCE) induced by laser-UV-microirradiation: correlation between the distribution of photolesions and the distribution of SCEs. Basic life sciences 29 Pt A, 181-197.

Rao, S.S., Huntley, M.H., Durand, N.C., Stamenova, E.K., Bochkov, I.D., Robinson, J.T., Sanborn, A.L., Machol, I., Omer, A.D., Lander, E.S., et al. (2014). A 3D map of the human genome at kilobase resolution reveals principles of chromatin looping. Cell 159, 1665-1680.

Rauch, T.A., Wu, X., Zhong, X., Riggs, A.D., and Pfeifer, G.P. (2009). A human B cell methylome at 100-base pair resolution. Proceedings of the National Academy of Sciences of the United States of America 106, 671-678.

Reddy, K.L., Zullo, J.M., Bertolino, E., and Singh, H. (2008). Transcriptional repression mediated by repositioning of genes to the nuclear lamina. Nature 452, 243-247.

Rhee, K.D., Yu, J., Zhao, C.Y., Fan, G., and Yang, X.J. (2012). Dnmt1-dependent DNA methylation is essential for photoreceptor terminal differentiation and retinal neuron survival. Cell death & disease 3, e427.

Rober, R.A., Weber, K., and Osborn, M. (1989). Differential timing of nuclear lamin A/C expression in the various organs of the mouse embryo and the young animal: a developmental study. Development 105, 365-378.

Roux, K.J., Crisp, M.L., Liu, Q., Kim, D., Kozlov, S., Stewart, C.L., and Burke, B. (2009). Nesprin 4 is an outer nuclear membrane protein that can induce kinesin-mediated cell polarization. Proceedings of the National Academy of Sciences of the United States of America 106, 2194-2199.

Saito, Y., Kanai, Y., Sakamoto, M., Saito, H., Ishii, H., and Hirohashi, S. (2002). Overexpression of a splice variant of DNA methyltransferase 3b, DNMT3b4, associated with DNA hypomethylation on pericentromeric satellite regions during human hepatocarcinogenesis. Proceedings of the National Academy of Sciences of the United States of America 99, 10060-10065.

Sakaki, M., Koike, H., Takahashi, N., Sasagawa, N., Tomioka, S., Arahata, K., and Ishiura, S. (2001). Interaction between emerin and nuclear lamins. Journal of biochemistry 129, 321-327.

Saksouk, N., Barth, T.K., Ziegler-Birling, C., Olova, N., Nowak, A., Rey, E., Mateos-Langerak, J., Urbach, S., Reik, W., Torres-Padilla, M.E., et al. (2014). Redundant mechanisms to form silent chromatin at pericentromeric regions rely on BEND3 and DNA methylation. Molecular cell 56, 580-594.

Santos, M., Rebelo, S., Van Kleeff, P.J., Kim, C.E., Dauer, W.T., Fardilha, M., da Cruz, E.S.O.A., and da Cruz, E.S.E.F. (2013). The nuclear envelope protein, LAP1B, is a novel protein phosphatase 1 substrate. PloS one 8, e76788.

Schardin, M., Cremer, T., Hager, H.D., and Lang, M. (1985). Specific staining of human chromosomes in Chinese hamster x man hybrid cell lines demonstrates interphase chromosome territories. Human genetics 71, 281-287.

Schermelleh, L., Carlton, P.M., Haase, S., Shao, L., Winoto, L., Kner, P., Burke, B., Cardoso, M.C., Agard, D.A., Gustafsson, M.G., et al. (2008). Subdiffraction multicolor imaging of the nuclear periphery with 3D structured illumination microscopy. Science 320, 1332-1336.

Schirmer, E.C., and Foisner, R. (2007). Proteins that associate with lamins: many faces, many functions. Experimental cell research 313, 2167-2179.

Schirmer, E.C., and Gerace, L. (2005). The nuclear membrane proteome: extending the envelope. Trends in biochemical sciences 30, 551-558.

Schneider, R., and Grosschedl, R. (2007). Dynamics and interplay of nuclear architecture, genome organization, and gene expression. Genes & development 21, 3027-3043.

Schotta, G., Lachner, M., Sarma, K., Ebert, A., Sengupta, R., Reuter, G., Reinberg, D., and Jenuwein, T. (2004). A silencing pathway to induce H3-K9 and H4-K20 trimethylation at constitutive heterochromatin. Genes & development 18, 1251-1262.

Senior, A., and Gerace, L. (1988). Integral membrane proteins specific to the inner nuclear membrane and associated with the nuclear lamina. The Journal of cell biology 107, 2029-2036.

Sexton, T., Yaffe, E., Kenigsberg, E., Bantignies, F., Leblanc, B., Hoichman, M., Parrinello, H., Tanay, A., and Cavalli, G. (2012). Three-dimensional folding and functional organization principles of the Drosophila genome. Cell 148, 458-472.

Shevelyov, Y.Y., Lavrov, S.A., Mikhaylova, L.M., Nurminsky, I.D., Kulathinal, R.J., Egorova, K.S., Rozovsky, Y.M., and Nurminsky, D.I. (2009). The B-type lamin is required for somatic repression of testis-specific gene clusters. Proceedings of the National Academy of Sciences of the United States of America 106, 3282-3287.

Shimi, T., Butin-Israeli, V., Adam, S.A., Hamanaka, R.B., Goldman, A.E., Lucas, C.A., Shumaker, D.K., Kosak, S.T., Chandel, N.S., and Goldman, R.D. (2011). The role of nuclear lamin B1 in cell proliferation and senescence. Genes & development 25, 2579-2593.

Shimi, T., Koujin, T., Segura-Totten, M., Wilson, K.L., Haraguchi, T., and Hiraoka, Y. (2004). Dynamic interaction between BAF and emerin revealed by FRAP, FLIP, and FRET analyses in living HeLa cells. Journal of structural biology 147, 31-41.

Shin, J.Y., Mendez-Lopez, I., Wang, Y., Hays, A.P., Tanji, K., Lefkowitch, J.H., Schulze, P.C., Worman, H.J., and Dauer, W.T. (2013). Lamina-associated polypeptide-1 interacts with the muscular dystrophy protein emerin and is essential for skeletal muscle maintenance. Developmental cell 26, 591-603.

Shumaker, D.K., Lee, K.K., Tanhehco, Y.C., Craigie, R., and Wilson, K.L. (2001). LAP2 binds to BAF.DNA complexes: requirement for the LEM domain and modulation by variable regions. The EMBO journal 20, 1754-1764.

Siegert, S., Cabuy, E., Scherf, B.G., Kohler, H., Panda, S., Le, Y.Z., Fehling, H.J., Gaidatzis, D., Stadler, M.B., and Roska, B. (2012). Transcriptional code and disease map for adult retinal cell types. Nature neuroscience 15, 487-495, S481-482.

Skene, P.J., Illingworth, R.S., Webb, S., Kerr, A.R., James, K.D., Turner, D.J., Andrews, R., and Bird, A.P. (2010). Neuronal MeCP2 is expressed at near histone-octamer levels and globally alters the chromatin state. Molecular cell 37, 457-468.

Smith, S., and Blobel, G. (1993). The first membrane spanning region of the lamin B receptor is sufficient for sorting to the inner nuclear membrane. The Journal of cell biology 120, 631-637.

Solovei, I., Kreysing, M., Lanctot, C., Kosem, S., Peichl, L., Cremer, T., Guck, J., and Joffe, B. (2009). Nuclear architecture of rod photoreceptor cells adapts to vision in mammalian evolution. Cell 137, 356-368.

Solovei, I., Wang, A.S., Thanisch, K., Schmidt, C.S., Krebs, S., Zwerger, M., Cohen, T.V., Devys, D., Foisner, R., Peichl, L., et al. (2013). LBR and lamin A/C sequentially tether peripheral heterochromatin and inversely regulate differentiation. Cell 152, 584-598.

Song, C., Feodorova, Y., Guy, J., Peichl, L., Jost, K.L., Kimura, H., Cardoso, M.C., Bird, A., Leonhardt, H., Joffe, B., et al. (2014). DNA methylation reader MECP2: cell type- and differentiation stage-specific protein distribution. Epigenetics & chromatin 7, 17.

Sosa, B.A., Rothballer, A., Kutay, U., and Schwartz, T.U. (2012). LINC complexes form by binding of three KASH peptides to domain interfaces of trimeric SUN proteins. Cell 149, 1035-1047.

Starr, D.A. (2009). A nuclear-envelope bridge positions nuclei and moves chromosomes. Journal of cell science 122, 577-586.

Starr, D.A., and Fridolfsson, H.N. (2010). Interactions between nuclei and the cytoskeleton are mediated by SUN-KASH nuclear-envelope bridges. Annual review of cell and developmental biology 26, 421-444.

Stick, R., Angres, B., Lehner, C.F., and Nigg, E.A. (1988). The fates of chicken nuclear lamin proteins during mitosis: evidence for a reversible redistribution of lamin B2 between inner nuclear membrane and elements of the endoplasmic reticulum. The Journal of cell biology 107, 397-406.

Stick, R., and Hausen, P. (1985). Changes in the nuclear lamina composition during early development of Xenopus laevis. Cell 41, 191-200.

Su, R.C., Brown, K.E., Saaber, S., Fisher, A.G., Merkenschlager, M., and Smale, S.T. (2004). Dynamic assembly of silent chromatin during thymocyte maturation. Nature genetics 36, 502-506.

Tahiliani, M., Koh, K.P., Shen, Y., Pastor, W.A., Bandukwala, H., Brudno, Y., Agarwal, S., Iyer, L.M., Liu, D.R., Aravind, L., et al. (2009). Conversion of 5-methylcytosine to 5-hydroxymethylcytosine in mammalian DNA by MLL partner TET1. Science 324, 930-935.

Takizawa, T., Gudla, P.R., Guo, L., Lockett, S., and Misteli, T. (2008). Allele-specific nuclear positioning of the monoallelically expressed astrocyte marker GFAP. Genes & development 22, 489-498.

Tapia, O., Fong, L.G., Huber, M.D., Young, S.G., and Gerace, L. (2015). Nuclear envelope protein Lem2 is required for mouse development and regulates MAP and AKT kinases. PloS one 10, e0116196.

Taylor, M.R., Slavov, D., Gajewski, A., Vlcek, S., Ku, L., Fain, P.R., Carniel, E., Di Lenarda, A., Sinagra, G., Boucek, M.M., et al. (2005). Thymopoietin (lamina-associated polypeptide 2) gene mutation associated with dilated cardiomyopathy. Human mutation 26, 566-574.

Towbin, B.D., Gonzalez-Aguilera, C., Sack, R., Gaidatzis, D., Kalck, V., Meister, P., Askjaer, P., and Gasser, S.M. (2012). Step-wise methylation of histone H3K9 positions heterochromatin at the nuclear periphery. Cell 150, 934-947.

Towbin, B.D., Meister, P., Pike, B.L., and Gasser, S.M. (2010). Repetitive transgenes in C. elegans accumulate heterochromatic marks and are sequestered at the nuclear envelope in a copy-number- and lamin-dependent manner. Cold Spring Harbor symposia on quantitative biology 75, 555-565.

Tunnah, D., Sewry, C.A., Vaux, D., Schirmer, E.C., and Morris, G.E. (2005). The apparent absence of lamin B1 and emerin in many tissue nuclei is due to epitope masking. Journal of molecular histology 36, 337-344.

Ungricht, R., and Kutay, U. (2015). Establishment of NE asymmetry-targeting of membrane proteins to the inner nuclear membrane. Current opinion in cell biology.

Unoki, M., Nishidate, T., and Nakamura, Y. (2004). ICBP90, an E2F-1 target, recruits HDAC1 and binds to methyl-CpG through its SRA domain. Oncogene 23, 7601-7610.

van Driel, R., Fransz, P.F., and Verschure, P.J. (2003). The eukaryotic genome: a system regulated at different hierarchical levels. Journal of cell science 116, 4067-4075.

van Steensel, B., and Dekker, J. (2010). Genomics tools for unraveling chromosome architecture. Nature biotechnology 28, 1089-1095.

Wagner, N., and Krohne, G. (2007). LEM-Domain proteins: new insights into lamin-interacting proteins. International review of cytology 261, 1-46.

Wagner, N., Weber, D., Seitz, S., and Krohne, G. (2004). The lamin B receptor of Drosophila melanogaster. Journal of cell science 117, 2015-2028.

Wagner, N., Weyhersmuller, A., Blauth, A., Schuhmann, T., Heckmann, M., Krohne, G., and Samakovlis, C. (2010). The Drosophila LEM-domain protein MAN1 antagonizes BMP signaling at the neuromuscular junction and the wing crossveins. Developmental biology 339, 1-13.

Wan, M., Lee, S.S., Zhang, X., Houwink-Manville, I., Song, H.R., Amir, R.E., Budden, S., Naidu, S., Pereira, J.L., Lo, I.F., et al. (1999). Rett syndrome and beyond: recurrent spontaneous and familial MECP2 mutations at CpG hotspots. American journal of human genetics 65, 1520-1529.

Wang, J., Wegener, J.E., Huang, T.W., Sripathy, S., De Jesus-Cortes, H., Xu, P., Tran, S., Knobbe, W., Leko, V., Britt, J., et al. (2015). Wild-type microglia do not reverse pathology in mouse models of Rett syndrome. Nature 521, E1-4.

Waterham, H.R., Koster, J., Mooyer, P., Noort Gv, G., Kelley, R.I., Wilcox, W.R., Wanders, R.J., Hennekam, R.C., and Oosterwijk, J.C. (2003). Autosomal recessive HEM/Greenberg skeletal dysplasia is caused by 3 beta-hydroxysterol delta 14-reductase deficiency due to mutations in the lamin B receptor gene. American journal of human genetics 72, 1013-1017.

Weber, K., Plessmann, U., and Traub, P. (1989). Maturation of nuclear lamin A involves a specific carboxy-terminal trimming, which removes the polyisoprenylation site from the precursor; implications for the structure of the nuclear lamina. FEBS letters 257, 411-414.

Wen, B., Wu, H., Shinkai, Y., Irizarry, R.A., and Feinberg, A.P. (2009). Large histone H3 lysine 9 dimethylated chromatin blocks distinguish differentiated from embryonic stem cells. Nature genetics 41, 246-250.

Williams, R.R., Azuara, V., Perry, P., Sauer, S., Dvorkina, M., Jorgensen, H., Roix, J., McQueen, P., Misteli, T., Merkenschlager, M., et al. (2006). Neural induction promotes large-scale chromatin reorganisation of the Mash1 locus. Journal of cell science 119, 132-140.

Wilson, K.L., and Foisner, R. (2010). Lamin-binding Proteins. Cold Spring Harbor perspectives in biology 2, a000554.

Worman, H.J., and Courvalin, J.C. (2004). How do mutations in lamins A and C cause disease? The Journal of clinical investigation 113, 349-351.

Worman, H.J., Evans, C.D., and Blobel, G. (1990). The lamin B receptor of the nuclear envelope inner membrane: a polytopic protein with eight potential transmembrane domains. The Journal of cell biology 111, 1535-1542.

Worman, H.J., and Schirmer, E.C. (2015). Nuclear membrane diversity: underlying tissue-specific pathologies in disease? Current opinion in cell biology 34, 101-112.

Worman, H.J., Yuan, J., Blobel, G., and Georgatos, S.D. (1988). A lamin B receptor in the nuclear envelope. Proceedings of the National Academy of Sciences of the United States of America 85, 8531-8534.

Xhemalce, B., and Kouzarides, T. (2010). A chromodomain switch mediated by histone H3 Lys 4 acetylation regulates heterochromatin assembly. Genes & development 24, 647-652.

Yang, S.H., Jung, H.J., Coffinier, C., Fong, L.G., and Young, S.G. (2011). Are B-type lamins essential in all mammalian cells? Nucleus 2, 562-569.

Young, R.W. (1985). Cell differentiation in the retina of the mouse. The Anatomical record 212, 199-205.

Zhang, Q., Ragnauth, C., Greener, M.J., Shanahan, C.M., and Roberts, R.G. (2002). The nesprins are giant actin-binding proteins, orthologous to Drosophila melanogaster muscle protein MSP-300. Genomics 80, 473-481.

Zhang, Q., Skepper, J.N., Yang, F., Davies, J.D., Hegyi, L., Roberts, R.G., Weissberg, P.L., Ellis, J.A., and Shanahan, C.M. (2001). Nesprins: a novel family of spectrin-repeat-containing proteins that localize to the nuclear membrane in multiple tissues. Journal of cell science 114, 4485-4498.

Zhang, X., Lei, K., Yuan, X., Wu, X., Zhuang, Y., Xu, T., Xu, R., and Han, M. (2009). SUN1/2 and Syne/Nesprin-1/2 complexes connect centrosome to the nucleus during neurogenesis and neuronal migration in mice. Neuron 64, 173-187.

Zuleger, N., Kelly, D.A., and Schirmer, E.C. (2013). Considering discrete protein pools when measuring the dynamics of nuclear membrane proteins. Methods in molecular biology 1042, 275-298.

Zuleger, N., Korfali, N., and Schirmer, E.C. (2008). Inner nuclear membrane protein transport is mediated by multiple mechanisms. Biochemical Society transactions 36, 1373-1377.

Zullo, J.M., Demarco, I.A., Pique-Regi, R., Gaffney, D.J., Epstein, C.B., Spooner, C.J., Luperchio, T.R., Bernstein, B.E., Pritchard, J.K., Reddy, K.L., et al. (2012). DNA sequence-dependent compartmentalization and silencing of chromatin at the nuclear lamina. Cell 149, 1474-1487.

4.2 Abbreviations

3C	chromatin conformation capture
3D	three-dimensional
4C	circularized chromosome conformation capture or 3C-on-chip
5C	carbon copy chromosome conformation capture
5caC	5-carboxycytocine
5fC	5-formylcytocine
5hmC	5-hydroxymethylcytosine
5mC	5-methylcytosine
A	adenine
aa	amino acid
Ankle	ankyrin and LEM-D-containing protein
ATP	adenosine triphosphate
B1	abundant mouse SINE repeat family
B23	nucleophosmin
BAC	bacterial artificial chromosome
BAF	Barrier-to-autointegration factor
BAF	Barrier-to-autointegration factor
BDNF	brain-derived neurotrophic factor
bp	base pairs
C	cytosine
CC	chromocenter
CD	chromatin domain
cHC	constitutive heterochromatin
CKO	conditional knockout
cLADs	constitutive LADs
CT	chromosome territory
CTCF	CCCTC-binding factor
CTD	C-terminal domain
C-terminal	carboxy-terminal
D	day of embryonic development
Dam	DNA adenine methyltransferase
DamID	DNA adenine methyltransferase identification
DAPI	4',6-diamindino-2-phenylindole
DNA	Deoxyribonucleic acid
DNMT	DNA methyltranferase
DNMT1	DNA methyltransferase 1
DNMT3a	DNA methyltransferase 3a
DNMT3b	DNA methyltransferase 3b
DNMT3L	DNA methyltransferase 3-like
DOP-PCR	degenerate oligonucleotide primed PCR
DSB	double strand break
EC	euchromatin
EDMD	Emery-Dreifuss muscular dystrophy
ER	endoplasmatic reticulum
ESC	embryonic stem cells

fHC	facultative heterochromatin
FISH	fluorescence in situ hybridisation
fLADs	facultative LADs
G	guanine
G1	Gap 1 phase of the cell cycle
G2	Gap 2 phase of the cell cycle
G9a	histone methyltransferase for H3K9
GCL	ganglion cell layer
GCL	germ-cell-less
GFP	green fluorescent protein
h	hours
H3	histone 3
H3K27me3	lysine 27 trimethylated histone 3, repressive mark
H3K36me3	lysine 36 trimethylated histone 3, euchromatic mark
H3K4me3	lysine 4 trimethylated histone 3, euchromatic mark
H3K9me2	lysine 9 dimethylated histone 3, repressive mark
H3K9me3	lysine 9 trimethylated histone 3, repressive mark
H3S10P	histone 3 serine 10 phosphorylation
H4	histone 4
H4K20m3	lysine 24 trimethylated histone 4, repressive mark
HAT	histone acetyltransferase
HC	heterochromatin
HDAC	histone deacetylase
HeH	helix-extension-helix
HGPS	Hutchinson-Gilford progeria syndrome
HMT	histone methyltransferase
HP1	heterochromatin protein 1
Ig	Immunoglobulin
INL	inner nuclear layer
INM	inner nuclear membrane
IPL	inner plexiform layer
KASH	Klarsicht/ANC-1/SYNE homology
kb	kilo base
kDa	kilo Dalton
KMTase	histone lysine methyltransferase
KO	knock-out
L1	abundant mouse LINE repeat family
LAD	Lamina-associating domain
LAP	Lamina-associated polypeptide
LAP2	Lamina-associated polypeptide 2
LB1	Lamin B1
LBR	Lamin B receptor
LEM	LAP/emerin/MAN1
LINC	linker of nucleoskeleton and cytoskeleton
LINE	long interspersed nuclear element
LmA	Lamin A
LmA/C	Lamin A/C

LmC	Lamin C
m6A	adenine methylated at position C6
Mb	mega base
MBD	methylcytosine binding domain
MeCP2	methyl-CpG binding protein 2
min	minutes
MSC	MAN1/Src1p/C-terminal
MSR	major satellite repeat
NAD	Nucleolus-associated domain
NE	nuclear envelope
NET	nuclear envelope transmembrane protein
NL	nuclear lamina
NLS	nuclear localization signal
nm	nano meter
NPC	nuclear pore complex
NTD	N-terminal domain
N-terminal	amino-terminal
ONM	outer nuclear membrane
OPL	Outer plexiform layer
OR	olfactory receptor
OSN	olfactory senory neuron
P	day of postembryonic development
PCR	polymerase chain reaction
PMT	post translational modification
rDNA	ribosomal DNA
RFP	red fluorescent protein
RNA	ribonucleic acid
RNA Pol-II CTDx	non-phosphorylated carboxy-terminal domain of RNA polymerase II
RNA Pol-II Ser2ph	phosphorylated serine 2 of heptapeptide repeat on carboxy-terminal domain of RNA polymerase II
RNA Pol-II Ser5ph	phosphorylated serine 5 of heptapeptide repeat on carboxy-terminal domain of RNA polymerase II
RPOII	RNA polymerase II
RRM	RNA recognition motif
RT-PCR	real time PCR
SAMP1	spindle associated membrane protein 1
SCA-7	spinocerebellar ataxia type 7
SEM	scanning electron microscopy
SINE	short interspersed nuclear element
S-Phase	synthesis phase of the cell cycle
SUN	Sad1p, Unc-84
Suv	suppressor of variegation
Suv39h1	histone methyltransferase for H3K9me3
Suv39h2	histone methyltransferase for H3K9me3
Suv40h1	histone methyltransferase for H4K20me3
Suv40h2	histone methyltransferase for H4K20me3
T	thymidine

TAD	topologically associated domain
TEM	transmission electron microscopy
Tet	ten eleven translocation
TF	transcritpion factor
TGF β	transforming growth factor β
TM	transmembrane
TMD	transmembrane domain
TSS	transcriptional start site
Xa	X active chromosome
Xi	X inactive chromosome
Xist	X inactive specific transcript
ZF	zinc finger
ZFP	zinc finger proteins
µm	micro meter

4.3 List of publications

1. **<u>Song C,</u>** Feodorova Y, Guy J, Peichl L, Jost KL, Kimura H, Cardoso MC, Bird A, Leonhardt H, Joffe B, Solovei I. DNA methylation reader MECP2: cell type- and differentiation stage-specific protein distribution. Epigenetics Chromatin. 2014 Aug 3;7:17. doi: 10.1186/1756-8935-7-17. eCollection 2014.

2. Katharina Thanisch*, **<u>Congdi Song*,</u>** Dieter Engelkamp, Einar Hallberg, Roland Foisner, Colin Stewart, Heinrich Leonhardt, Boris Joffe, Irina Solovei. Lemd2 likely mediates lamin A/C-dependent peripheral heterochromatin tethering. Manuscript in preparation.
* Equally contributing authors

3. Eberhart A, Feodorova Y, **<u>Song C</u>**, Wanner G, Kiseleva E, Furukawa T, Kimura H, Schotta G, Leonhardt H, Joffe B, Solovei I. Epigenetics of eu- and heterochromatin in inverted and conventional nuclei from mouse retina. Chromosome Res. 2013 Aug;21(5):535-54. doi: 10.1007/s10577-013-9375-7. Epub 2013 Aug 31.

4.4 Contributions

Declaration of contributions to "*DNA methylation reader MECP2: cell type- and differentiation stage-specific protein distribution*"

I dissected the tissues from mice, fixed and embedded the tissues in the Jung freezing medium, prepared the cryosections. I performed the thorough immunostainings of MECP2 in 60 cell types of 16 mouse neuronal and non-neuronal tissues. I took images from the confocal microscopy. I extracted RNA from cells and tissues, performed RT as well as Realtime PCR experiments and analyzed the data. I read and approved the final manuscript before submission and during revision.

Declaration of contributions to "*Lemd2 likely mediates lamin A/C-dependent peripheral heterochromatin tethering*"

I performed the thorough immunostainings of the studied INM proteins in mice tissue. I took images from the confocal microscopy. I summarized and organized the data to Figure 3, 4, Table 3, supplementary figure 1, supplementary figure 2. I cloned the genes encoding INM proteins, including *Lemd2, Man1, Lap2β* and *Lap1b*. I made the Lemd2-2A-LmC and Lemd2 single construct and prepared the DNA of all three constructs used for microinjection. I optimized the pcr system for the transgenic mice screening and run the first round of LEM2 single transgenic mice screening. I performed the immunostaining of INM proteins in *Lmna*-null cells. I contributed to the first version of the manuscript.

Declaration of contributions to "*Epigenetics of eu- and heterochromatin in inverted and conventional nuclei from mouse retina*"

I performed the immunostaining and contributed to the figure 4, 7 and 9. I read and approved the final manuscript before submission and during revision.

4.5 Declaration

Eidesstattliche Erklärung

Ich versichere hiermit an Eides statt, dass die vorgelegte Dissertation von mir selbständig und ohne unerlaubte Hilfe angefertigt ist.

München, den ....

Erklärung

Hiermit erkläre ich, *

☐ dass die Dissertation nicht ganz oder in wesentlichen Teilen einer anderen Prüfungskommission vorgelegt worden ist.

☐ dass ich mich anderweitig einer Doktorprüfung ohne Erfolg **nicht** unterzogen habe.

☐ dass ich mich mit Erfolg der Doktorprüfung im Hauptfach ....

und in den Nebenfächern ....

bei der Fakultät für .... der ....

(Hochschule/Universität)

unterzogen habe.

☐ dass ich ohne Erfolg versucht habe, eine Dissertation einzureichen oder mich der Doktorprüfung zu unterziehen.

München, den.............................   ....
(Unterschrift)

*) Nichtzutreffendes streichen

4.6 Acknowledgements

First of all, I would like to gratefully and sincerely thank my doctor father and supervisor Prof. Dr. Heinrich Leonhardt. I am very grateful that you gave me the opportunity to do my PhD in your group. Heinrich, your strong leadership and smart ideas make the group full of academic atmosphere. I enjoyed so much in our group. Thanks for encouraging and supporting me when I was struggled in the experiment.

I especially thank Dr. Irina Solovei for her guidance, understanding, patience, and most importantly, her friendship during my PhD studies. She encouraged me to not only grow as an experimentalist and a biologist but also as an instructor and an independent thinker. Irina, I will cherish the happy hours we spent together in the confocal microscopy room, under the epifluorescence microscope, in the Histology practical course. For everything you've done for me, Irina, I thank you. Great thanks to Boris Joffe, a talented scientist. His passion for science was paramount in providing a well rounded experience consistent my long-term career goals.

I am very grateful to the China Scholarship Council (CSC) for the finance support.

A big thanks go to Dr. Yana Feodorova, Dr. Katharina Thanisch, Anja Eberhart for the productive collaborations.

A very big thanks goes to all members of the Leonhardt group Andreas, Christina, Christopher, Daniela, Elisabeth, Hartmann, Heinrich, Hsin-Yi, Joel, Jonas, Kamila, Katharina, Martha, Michael, Nan, Patricia, Pin, Sebastian, Stephanie, Svenja, Tobias, Weihua, Wen, Udo, Yolanda. Thank you for the supportive and cheering atmospheres, making the lab such a wonderful place to work.

I would also like to thank Susanne for her kind help.

Thanks Joel for correcting my PhD thesis.

A big thanks goes to my friends in Munich. Thanks for accompanying me in the weekends and holidays. Thanks for traveling with me and seeing beautiful world together. Thank you, Lichao, for teaching me to be in peace and in my powers.

I especially thank my "neighbors" and friends, Weihua, Wen, Nan, Hsin-Yi and Pin. Thank you for the big help and happy hours in the past four years. I would never forget all the chats

and beautiful moments I shared with you. Thank you, Wen, for showing me the beauty of images and how to present the images in perfect color combination. Thank you, Hsin-Yi, for showing me a new interpretation of life. Thank you, Nan, for everything you've done for me in the daily life. Thank you, Pin. I wish you enjoy working in the lab and have productive publications. Especially thanks to Weihua. I thank you, Weihua, for encouraging me and giving me confidence when I went through my hard time. I feel so lucky to meet you as my friend and sister.

Finally, and most importantly, I would like to thank my parents for their faith in me and allowing me to be as ambitious as I wanted. Mom and Dad, you are wonderful parents and wonderful friends. I thank my sisters for their support, encouragement and unconditional love. I could not ask for a better sister. To all of you, thanks for always being there for me.

谢谢爸爸妈妈，这些年对我无条件的支持和爱，乌鸦反哺，羔羊跪乳，以后你们的生活，由我来照顾。感谢我的姐妹，这些年一直鼓励我支持我，你们对爸妈的悉心照顾让我能安心去做自己喜欢的事情，以后我们相亲相爱，一起开心生活。

5 Curriculum Vitae

CONGDI SONG

Telephone: +49 89 2180 74223

Email: song@bio.lmu.de

Personal Information

Name	Congdi Song
Date of birth	21.02.1984
Place of birth	Baoding, China
Nationality	Chinese
Current work address	Ludwig Maximilians University of Munich
	Department of Biology II, LMU Biocenter
	Großhaderner Str. 2, 82152, Planegg-Martinsried, Germany

Education

09/2011 - present	PhD student in Biology
	Ludwig Maximilians University, Munich, Germany
	Department of Biology II
	Human Biology & Bioimaging
09/2008 – 07/2011	Master student in Genetics
	Northeast Normal University, Changchun, China
	School of Life Science
	Key Laboratory of Molecular Epigenetics of the Ministry of Education
09/2004 – 07/2008	Bachelor student in Agriculture
	Jilin University, Changchun, China
	College of Plant Science